Miniaturized High-Q Tunable RF Filters

Dissertation

for the degree of Doctor of Engineering
(Dr.-Ing.)

Submitted to the Department of Electrical and Information
Engineering of Kiel University

by

Abdulrahman Widaa

Kiel University, 2023

1^{st} Referee: Prof Dr.-Ing. Michael Höft
2^{nd} Referee: Prof. Cristiano Tomassoni

Date of oral examination: May $26^{th}, 2023$

ABSTRACT

This dissertation focuses on the investigation and development of novel efficient tuning techniques and the design of miniaturized high-Q tunable RF filters for high-performance reconfigurable systems and applications. First, a detailed survey of the available tuning concepts and state-of-art tunable filters is provided. Then, a novel so-called *inset resonator* configuration is presented for the applications of fixed and tunable coaxial filters. The design procedure of frequency tunable filters with constant absolute bandwidth (CABW) is described, and various tunable inset filters are implemented, offering many desirable merits, including the wide tuning range and stable high-Q with minimum variation. For wide octave frequency tuning ranges with CABW, a second novel concept is presented using so-called *re-entrant caps* tuners. Beside simplicity and compactness, this technique also features enhanced spurious performance and wider tuning capabilities than the conventional means. Also, in this dissertation, various miniaturized reconfigurable dual-band/dual-mode bandpass filters and diplexers are presented using compact dual-mode high-Q TM-mode dielectric resonators. Furthermore, a novel microfluidic-based ultra-wide frequency tuning technique for TM_{010}-mode dielectric resonators and filters is introduced in this dissertation. In addition to the very wide tuning window, this mechanism has key advantages of low-cost, simplicity, and intrinsic *switch-off*. Lastly, the dissertation includes a novel bandwidth reconfiguration concept with multi-octave tuning using a single element for coaxial bandpass filters. This mechanism brings many features including the fast tuning, constant high-Q, intrinsic *switch-off*, and wide BW-reconfiguration.

Zusammenfassung

Diese Dissertation befasst sich mit der Untersuchung und Entwicklung neuer effizienter Abstimmverfahren und dem Entwurf miniaturisierter abstimmbarer HF-Filter mit hohem Qualitätsfaktor für rekonfigurierbare Systeme und Anwendungen mit hoher Leistung. Zunächst wird ein detaillierter Überblick über die verfügbaren Abstimmkonzepte und abstimmbaren Filter nach dem Stand der Technik gegeben. Dann wird eine neuartige sogenannte Inset-Resonator-Konfiguration für die Anwendung von festen und abstimmbaren Koaxialfiltern vorgestellt. Das Entwurfsverfahren für frequenzabstimmbare Filter mit konstanter absoluter Bandbreite wird beschrieben, und es werden verschiedene abstimmbare Inset-Filter implementiert, die viele wünschenswerte Vorzüge bieten, einschließlich eines großen Abstimmbereichs und eines stabilen hohen Qualitätsfaktors mit minimaler Abweichung. Für breite Oktav-Frequenzabstimmbereiche mit konstanter absoluter Bandbreite wird ein zweites neuartiges Konzept vorgestellt, das so genannte "re-entrant caps tuners" verwendet. Diese Technik ist nicht nur einfach und kompakt, sondern zeichnet sich auch durch ein verbessertes Störmodenverhalten und einen größeren Abstimmbereich als die herkömmlichen Mittel aus. Außerdem werden in dieser Dissertation verschiedene miniaturisierte rekonfigurierbare Dual-Band- und Dual-Mode-Bandpassfilter und Diplexer vorgestellt, die kompakte dielektrische Dual-Mode-TM-Resonatoren mit hohem Qualitätsfaktor verwenden. Darüber hinaus wird in dieser Dissertation eine neuartige, auf Mikrofluidik basierende, ultrabreite Frequenzabstimmungstechnik für dielektrische TM_{010}-Mode-Resonatoren und -Filter vorgestellt. Neben dem sehr breiten Abstimmfenster hat dieser Mechanismus die entscheidenden Vorteile der geringen Kosten, der Einfachheit und der intrinsischen Abschaltung. Schließlich beinhaltet die Dissertation ein neuartiges Konzept zur Rekonfiguration der Bandbreite mit einer Abstimmung über mehrere Oktaven mit einem einzigen Element für koaxiale Bandpassfilter. Dieser Mechanismus zeichnet sich durch zahlreiche Merkmale aus, darunter schnelle Abstimmung, konstant hoher Qualitätsfaktor, intrinsische Abschaltung und Rekonfiguration einer großen Bandbreite.

DECLARATION

I hereby declare that I have written this dissertation entitled

Miniaturized High-Q Tunable RF Filters

independently and without improper external assistance and that I have identified all quotations of other authors. Furthermore, this thesis has not been, partially or completely, submitted to any other university or institute in the context of an examination procedure. Parts of the content of the work have already been published in my scientific publications and is stated accordingly. I declare that the following work has been written in compliance with the rules of good scientific practice established by the German Research Foundation. No academic degree has ever been withdrawn.

Place, Date

Abdulrahman Widaa

PREFACE

The contents of Chapter 2 have been communicated in part as A. Widaa, “Comparison of Tuning Means," Report, 2020.

Also, the contents of Chapter 3 have been communicated in part as A. Widaa, C. Bartlett and M. Höft, “Inset Resonators and Their Applications in Fixed/Reconfigura ble Microwave Filters," *IEEE/MTT-S International Microwave Symposium (IMS)*, 2022, pp. 172-175, **and** A. Widaa, C. Bartlett and M. Höft, "Tunable Coaxial Bandpass Filters Based on Inset Resonators," *IEEE Transactions on Microwave Theory and Techniques*, vol. 71, no. 1, pp. 285-295, Jan. 2023, **and** A. Widaa, C. Bartlett and M. Höft, "Design of Compact Quasi-Elliptic Bandpass Filters Based on Coaxial Inset Resonators," *IEEE Access*, vol. 11, pp. 18739-18749, Feb. 2023.

Furthermore, the contents of Chapter 4 have been communicated in part as A. Widaa and M. Höft, "Widely Tunable TM-Mode Dielectric Filters With Constant Absolute Bandwidth Using Re-Entrant Caps," *IEEE Journal of Microwaves*, Feb. 2023.

Additionally, the contents of Chapter 5 have been communicated in part as A. Widaa and M. Höft, "Miniaturized Dual-Band Dual-Mode TM-Mode Dielectric Filter in Planar Configuration," *IEEE Journal of Microwaves*, vol. 2, no. 2, pp. 326-336, Apr. 2022, **and** A. Widaa, C. Bartlett and M. Höft, “Miniaturized All-Reconfigurable Dual-Mode Dielectric Filter Using Piezomotors for Future Satellite Communications," *51st European Microwave Conference (EuMC)*, 2022, pp. 107-110, **and** A. Widaa and M. Höft, "Miniaturized Dual-Band TM-Mode Dielectric Filter and Its Reconfiguration Capabilities," *2022 IEEE/MTT-S International Microwave Symposium - IMS 2022*, Denver, CO, USA, 2022, pp. 344-347, **and** A. Widaa and M. Höft, "Very Compact Diplexer Based on Dual-Mode Dielectric TM-Mode Resonators," *IEEE Microwave and Wireless Technology Letters*, vol. 33, no. 4, pp. 387-390, April 2023.

Moreover, the contents of Chapter 6 have been communicated in part as A. Widaa and M. Höft, "Microfluidic-Based Ultra-Wide Tuning Technique for TM_{010} Mode Dielectric Resonators and Filters," *2021 IEEE MTT-S International Microwave Filter Workshop (IMFW), Perugia, Italy*, 2021, pp. 343-346.

Finally, the contents of Chapter 7 have been communicated in part as A. Widaa, A. Sharma, C. Bartlett, S. Cogollos, V.E. Boria, M. Guglielmi, and M. Höft, “Bandwidth-Reconfigurable Coaxial Bandpass Filter With Multioctave Tuning Using a Single Element," *IEEE Microwave and Wireless Technology Letters*, Apr. 2023.

Contents

ACKNOWLEDGEMENTS

First, I would like to express my thanks and gratitude to my advisor Prof. Dr.-Ing. **Michael Höft** for his role as a mentor and for all of the support and encouragement, in addition to providing the space for trying and exploring new ideas during my doctoral research.

I also sincerely thank all of my colleagues in the Filter team: **Daniel Miek, Fynn-Lasse Kamrath, Patrick Boe, Chad Bartlett**, and all other colleagues in the Chair of Microwave Engineering for the great help and support during my research. My thanks also go to the European Union's Horizon 2020 research and innovation consortium and the Marie Skłodowska-Curie Actions programme for funding my research within **TESLA** project under grant agreement No. 811232.

I extend my thanks also to all members of **TESLA** project, with much appreciation to Prof. **Cristiano Tomassoni, Fabrizio Cacciamani, Luca Pelliccia, Paolo Vallerotonda, Abdul Rehman,** Prof. **Vincente E. Boria, Abhishek Sharma, and El Mehdi Messaoudi.** Also, many thanks go to my home university in **Sudan**: **Gezira University**, and to my colleagues in the Electronics Engineering Department.

My deepest appreciation goes to my father "**Hassan**", my mother "**Aisha**", my brother "**Abdalla**", my sister "**Alhumaira**", and to all of my family members and friends. Most importantly, all of my thanks and gratefulness to the **Almighty Allah** for all the blessings he provided me that helped me in achieving my goals.

DEDICATION

To the two persons from whom I learnt *empathy, dedication, and persistence*:
grandfather **"Tineer Mohammed"** and uncle **"Mohammed Widaa"**.
May blessings come upon your pure souls

Chapter 1

Introduction

1.1 Dissertation Motivation

With the current massive explosion in data and information, the contribution of telecommunication industry and its associated services to the existence and future development of humankind is continuously being more vital in all life aspects, starting from internet and cellular communications, monitoring and navigation, to satellites and space exploration. A great increase in the frequency spectrum utilization is therefore essential to provide more channels, wider bandwidths, and higher data rates for this broad range of expanding telecommunication services and applications. However, as the frequency spectrum is a very-valuable limited natural resource, new technologies and design techniques are required to guarantee the optimal use of frequency resources. For example, one of the key issues is that each telecommunication service/user has a fixed allocated frequency band/channel which the other services/users cannot use even if it is free, resulting-in more pressure on the limited spectrum. Therefore, it is crucial to introduce more adaptive (i.e., smarter) telecommunication services and components that are capable of sensing the available surrounding resources, and tuning their operating frequencies whenever it is needed for optimal usage.

In the same context, the development of adaptive RF Front-End (RFFE) units and components, including RF filter, is essential for future flexible communication systems. These applications include multi-band transceivers, cognitive radio (CR) systems, next-generation cellular communications, wideband RADARs and satellite payloads, and flexible radio systems like software-defined radios (SDR). Generally speaking, in view of performance and specification requirements, these classes of ap-

plications require low loss, better frequency spectrum utilization, more functionality, smaller mass and volume, more efficient power consumption, and lower implementation cost. Moreover, in addition to all of these requirements, it is now a key trend in RF front-end systems to integrate multi-band/multi-standard operations and technologies in a single-board structure. Unfortunately, these requirements are usually contradicting each other and cannot all be maintained simultaneously without experiencing some performance deterioration.

Considering the aforementioned ever-stringent requirements, it can be clearly seen that future reconfigurable RF front-end units have a difficult-awaiting tasks to provide high-performance capabilities. Similarly, as a key element of every RFFE unit, tunable RF filters are expected to play a pivotal role in improving the capabilities of a broad range of major current and future communication systems. Consequently, the need to employ compact high-Q resonators, and more efficient tuning mechanisms is essential to meet those challenging characteristics more efficiently.

1.2 Research Objectives

The main goal of this PhD research is to investigate new tuning solutions and develop tunable RF bandpass filters suitable for high-performance reconfigurable communication systems, employing novel high-Q compact coaxial and dielectric resonators (single and multi-mode). Defining that the vast majority of the available state-of-art tunable filter designs suffer from several drawbacks including the high loss, limited tuning capabilities, bulky structures, and Q-factor deterioration with tuning, this dissertation aims to:

• Develop miniaturized high-Q tunable bandpass filters.

• Propose simple, efficient novel tuning techniques that offer wide and extended tuning ranges.

• Realize efficient tuning with minimal deterioration of high-Q reconfigurable RF filters.

1.3 Dissertation Outline

The dissertation is organized into eight main chapters as follows:

Chapter 1 states the motivation and objectives of the work in this thesis. The outline of the thesis is included in this chapter as well.

Chapter 2 presents a detailed overview and literature survey of the common tuning techniques and methods of microwave bandpass filters.

In chapter 3, a novel coaxial inset resonator configuration is presented, and its application to fixed/reconfigurable microwave filters is detailed. The first part of the chapter describes the design procedure of the inset resonator, and present realizations of quasi-elliptic fixed filters based on planar and inline longitudinal coupling configurations. In the second part of chapter 3, the employment of the inset resonators in tunable filters design with constant absolute bandwidth (CABW) is discussed, and various prototypes are implemented.

In chapter 4, widely tunable CABW dielectric combline bandpass filters are presented using a novel tuning technique of re-entrant caps.

Chapter 5 presents several miniaturized reconfigurable bandpass filters and diplexers based on dual-mode TM-mode dielectric resonators. First, dual-band dual-mode filters are developed, and their tuning capabilities are investigated. Then, very compact diplexers are presented with the key feature of independent and simultaneous frequency and bandwidth tuning of transmission and reception channels. In the last part of this chapter, compact dual-mode reconfigurable filters are implemented with constant ABW responses, having a reduced number of tuning elements using accurate piezomotors for tuning.

Chapter 6 describes a novel microfluidic-based ultra-wide tuning technique for TM_{010}-mode dielectric resonators and filters. Single resonator and second-order filter examples are developed for proof and to verify the proposed concept.

In chapter 7, a novel bandwidth tuning technique for coaxial and dielectric filters is presented with the merits of wide multi-octave tuning capabilities, stable high-Q with minimum variation, and using a single element. Various design examples are provided and discussed.

Finally, chapter 8 summarizes the obtained results and contributions of the dissertation work, and provides an outlook to the future research directions based on the current achievements.

Chapter 2

Literature Survey

This chapter includes a comprehensive review on the different tuning techniques and means of microwave filters. First, the major tuning techniques (mechanical, electrical, and magnetic-based) are explained in terms of operation mechanisms, advantages, and limitations. Also, the different concepts and means utilized in the realization of the available state-of-the-art tunable filters are provided focusing on tunable waveguide filters, including tunable dielectric resonator (DR) filters, due to their more desirable features and specifications for high-performance applications. Then, some of the new and promising tuning components and methods are also considered in the last part of this chapter including ferroelectric components and resonators, liquid crystal-based tuning, and microfluidically reconfigurable filters.

2.1 Tuning Means

2.1.1 Mechanical-Based Tuning

The mechanical-based tuning technique is known as the earliest and most straightforward method for the implementation of tunable 3-D filters. In this mechanism, the resonant frequency is tuned by changing the field distribution in the filters' cavities using physically adjustable elements (e.g., screws, discs, side-walls). The mechanical adjustment of the elements can be done either manually or using any electro-mechanical transducing mechanism (e.g., stepper/piezo motors, piezo/MEMS actuators). Mechanically-tuned hollow-waveguide filters have many advantages in comparison with the other structures including the low insertion loss, high unloaded quality factors (Q_u), and also the capability of high-power handling. However, they

are burdened by the bulky size, high complexity, relatively high cost, and low speed of tuning. All of the above are in addition to the very small and limited tuning ranges. Despite that the required specifications of the various current and future communication systems include the compact size and fast tuning speed, mechanically tunable filters still attract attention due to their unbeatable power handling capabilities and high-quality factors. The following subsection reviews and compares the mechanically tunable filter designs presented in previous literature with different tuning approaches.

Mechanically Tunable Filters

Mechanical tuning techniques have been realized in different 3-D filter structures including evanescent-cavity and waveguide-based configurations [1, 2, 3, 4, 5, 6, 7, 8, 9, 10, 11, 12, 13, 14, 15, 16, 17, 18, 19, 20, 21, 22, 23, 24, 25, 26, 27, 28]. Various tunable hybrid evanescent-cavity filters were reported based on capacitively-loaded structures by changing the gap between the inner post and a flexible top cavity as in [1] and [2]. A second-order tunable filter is realized in [1] using a piezoelectric actuator mounted on a flexible substrate to change the parasitic capacitance and tune the resonant frequency. Similarly, in [2], thin MEMS-actuated diaphragms are used for frequency tuning. Despite the good tuning capabilities, such structures require very sensitive and accurate micro-tuning and have limited Q-factor and power performance. Therefore, the application of evanescent-mode cavity configurations in high-performance and high-power flexible systems is not favorable.

On the other hand, tunable filters based on waveguide structure have received an increasing attention due to their desirable features for next-generation agile telecommunication systems. High-power and high-performance mechanically reconfigurable waveguide filters were presented previously in different empty-cavity, coaxial-, and dielectric-loaded structures. In its simplest configuration, tunable waveguide filters are realized using metallic plungers [3]. Unfortunately, more efficient tuning means are needed as such screw-based designs suffer from significant performance deterioration. Therefore, a couple of high-Q mechanically reconfigurable waveguide filters were introduced with special tuning mechanisms to minimize the Q-factor degradation while tuning, as in [7]-[15]. A high-Q manually reconfigurable K-band dual-mode waveguide filter was introduced in [7]. The proposed filter is a fifth-order Chebyshev with 3.5% tunability at 26 GHz center frequency and an extreme narrowband of just 0.1%

fractional bandwidth (FBW). Adjustable sidewall cavities are utilized for frequency reconfiguration with enhanced Q-factor measures in comparison to the conventional screws-based tuning method. The extracted effective Q-factor of the proposed reconfigurable filter is 11200. A bellow-mounted technique was presented in [8] on waveguide cavities bringing the advantages of low-loss and stable tuning responses. A thin flexible copper bellows are mounted on the cavity to control the frequency using a manual micrometer driver. The filter has a tuning window of 527 MHz at 11.95 GHz with low loss < 2 dB and a stable 3.5% bandwidth variation. Similarly, in [9], a movable metallic-end cap was employed for frequency tuning to offer less degradation across the whole tuning band and also a wide spurious-free range. The presented filter operates at 20 GHz K-band frequency with a stable 500 MHz tuning band, and high unloaded Q-factor (15500 – 16000). An additional feature of 40 – 160 MHz bandwidth tuning was also introduced through two cascaded pseudo-highpass and pseudo-lowpass tunable filters.

In [10], a screw-based manually frequency and bandwidth reconfigurable waveguide filter was proposed using a tunable coupling resonator configuration. The fabricated filter has 200 MHz tunability at center frequency 19.8 GHz and 54 – 72 MHz of bandwidth tuning. Another tuning mechanism based on the use of rotating dielectric perturbations to change the resonant frequency inside the cavity was demonstrated in [11] and [12]. The key advantage of this configuration is that there is no requirement of electrical grounding as in the other tuning techniques, therefore, attributing a reduced complexity and stable performance. In [11], the measured frequency tuning range is 9.92 – 10.12 GHz with a Q-factor of 1400 – 2150, while the filter in [12] operates at 19.36 – 19.7 GHz with a Q-factor between 2600 – 3100. Also, to offer more design flexibility, reconfigurable filters using contactless tuning elements were presented in [13]-[15]. In [13], a motorized special corrugated tuning plunger is designed to maintain high-Q levels. The filter has a tuning window of 19 – 19.48 GHz with a constant absolute bandwidth of 54.5 ± 2.5 MHz and a high extracted unloaded Q-factor of 9080. Another tuning approach was introduced in [14] using a single tunable sidewall to reduce the tuning complexity. A Ku band reconfigurable filter is implemented with a constant 2% narrow bandwidth and 15% tunability. Recently, Basavarajappa and Mansour presented a fourth-order reconfigurable dual-mode filter at 11.5 GHz with a constant narrow bandwidth of 50 MHz and 3.3% tunability using a single linearly-displaced metallic tuning element [15].

Mechanically tunable coaxial filters were reported in [16]-[19]. A refined manually

tunable coaxial filter was presented in [16]. The capacitive loading is changed through a simplified tuning mechanism composed of rotating cams controlled by a single common driving shaft covering a tuning range of 0.95 – 2.05 GHz and having a return loss less than 11 dB. A tunable high-Q narrowband combline filter was proposed in [17] with a 70 MHz tuning range from 2.565 GHz to 2.635 GHz with a high Q-factor of 2252 - 2914. Vertically-positioned tuning posts are utilized for frequency control in upward and downward movement using piezomotor actuators. In [18], an angular technique using rectangular tuning shafts was introduced to maintain high-Q measures in comparison with the conventional vertical tuning mechanism. The frequency is tuned by changing the angle of the rectangular shafts using a miniature piezomotor mechanism. A tuning range of 11.9% is achieved at 3.6 GHz with low insertion loss better than 0.32 dB and nearly constant high-Q. A tunable high-Q coaxial filter was introduced using a reduced-complexity tuning mechanism in [19]. The tuning concept is based on the rotational displacement of the coaxial resonators inside elliptically-shaped cavities using a common single motorized tuning post. The measured results show a 20% tunable low-loss filter at 2.5 GHz with a small bandwidth variation of ±10 MHz.

Dielectric resonators are broadly used in communication systems and components due to their superior performance over other resonators. They offer a high unloaded-Q and have excellent temperature stability. The frequency tuning of dielectric resonator filters was presented few-decades ago by Gil and Martínez in [20]. Also, Chen et al. presented a temperature compensated manually reconfigurable four-pole hybrid-mode HEH_{11} dielectric filter in [21]. A detailed temperature sensitivity optimization is performed to the filter structure to obtain the proper dimensions for best tuning with the least temperature variation. Double-resonator tuning configuration is employed to eliminate the problem of severe Q-factor degradation caused by the conductor-dielectric interface in the conventional tuning mechanisms. The measured tuning range is 4.6 – 4.8 GHz with low insertion loss and high unloaded Q-factors of 5200 and 4700, respectively. A tunable dielectric-loaded filter was presented in [23] with a dielectric plug as a tuning element. A relatively-wide tuning range is achieved while other features of the resonator are maintained over the whole range. The filter can be tuned from 1930 to 1990 MHz and has an unloaded Q-factor of 22000 - 23000. The DR tunable bandpass filter presented in [23] has displayed good tuning properties in terms of the filter size and tuning range, but, the filter's tuning speed is very slow due to the large travel distance of the tuning element in the screw-like configuration.

Piezoelectric-based tuning technique was reported in [24]–[26] with various dielectric resonator configurations. The operation concept is based on the movement of a resonator/plate attached to an electrically-induced piezoelectric element. First, the concept was presented in [24] where a piezoelectric frequency adjusting unit is attached in different configurations to double dielectric resonators. The frequency is tuned due to the change in the space between the resonator and the part attached to the piezoelectric unit. Similarly, in [25], a piezoelectric-based tunable dielectric dual-mode HEM_{11} mode filter was introduced with a piezoelectric bimorph connected to the metallic tuning discs to control its movement for frequency tuning. The filter is designed with a tuning range of 2.24 – 2.45 GHz with 0.5% FBW and insertion loss less than 1 dB. Another filter was also presented in [26] where a piezoelectric transducer is used to control the movement of a flexible sidewall to change the resonant frequency of the cavity. A fourth-order dielectric TME mode filter is implemented with a frequency range of 4.97 – 5.22 GHz with an extracted Q-factor of 550.

Due to its desirable features, Micro Electro Mechanical Systems (MEMS) have gained an increasing attention in a wide range of RF applications including filters. Yan et al. in [27], introduced a mechanically tunable TE_{01} mode dielectric filter using MEMS-based actuators. Similar to the piezoelectric-based tuning technique, the proposed concept of tuning used MEMS thermal actuators to control the displacement of the tuning discs.

In summary, despite the advantages of obtaining high Q-factors and high-power handling capabilities, mechanically tunable filters still suffer from one or more key limitations as the narrow tuning window, large size, slow speed of tuning, high complexity, and the high cost of implementation. Accordingly, the need for fast and more efficient tuning techniques is fundamental.

2.1.2 Electrical-Based Tuning

Electrical-based tuning is known as the most common technique all over the available state-of-the-art tunable filters because of its highly desirable and competitive features in comparison with the other tuning approaches. These advantages include the high tuning speed, low power consumption, low cost, and compact size. In addition to all, it can be easily integrated and mounted on the different printed-circuit boards (PCBs). Therefore, it has been widely employed in the realization of tunable planar and nonplanar structures [17, 29, 30, 31, 32, 33, 34, 35, 36, 37, 38, 39, 40, 41, 42, 43, 44,

45, 46, 47, 48, 49, 50, 51, 52, 53, 54, 55, 56, 57, 58, 59, 60, 61, 62, 63, 64, 65, 66, 67, 68]

The operation concept of electrical tuning means is based on loading the resonator structure with lumped switching/tuning circuits to change the electrical field distribution, and thereby, tune the resonant frequency. Generally, electrically tunable filters can be categorized into two main groups: discretely-switched filters where in which the frequency is reconfigured between separated predefined individual tuning states, and continuously tunable varactor-loaded filters where the filter can be tuned freely at any frequency across a specified span. The following parts of this section discuss various electrically-tunable filter designs realized based on various means of both groups in different planar, hybrid, and waveguide structures.

Electrically Tunable Filters

Switched Reconfigurable Filters

With the increasing development in various multi-standard and multi-band communication systems, the conventional fixed filters became an un-efficient solution. Therefore, switch-based reconfiguration techniques were introduced to provide more efficient and flexible front-end units. The centre frequency is controlled through a switched loading element/network (e.g., transmission line, capacitor). Various electrical switches were used to implement switched filters with different reconfiguration responses [27]-[29]. The most common switching-elements used in reconfigurable filters design are solid-state RF PIN diodes due to their advantages of wide market-availability, low cost, and easy fabrication and integration. The use of PIN switches in reconfigurable filters applications was firstly presented in [29] and expanded widely in various designs introducing many desirable switching functions as can be seen in [30]-[32]. In [30], for instance, a switchable WiFi/UMTS microstrip bandpass filter was presented. Six microstrip sections are switched by PIN diodes to reconfigure the two frequency bands.

In spite of the various advantages of the PIN switches, their application in high-performance frequency-agile filters is still faced with major challenges especially at higher frequencies > 2 GHz including the increasing losses, relatively high power consumption, and increasing nonlinearities. Therefore, the introduction of more efficient RF switching solutions is highly required.

In recent years, MEMS switches got an increasing attention against PINs especially at higher bands because of the advantages of high Q factor, low loss, and very

low power consumption [33]-[43]. In [34], a tunable coplanar-waveguide (CPW) filter was proposed using high-Q capacitors connected in series with MEMS switches. Similar planar and hybrid RF MEMS switched filters were also introduced on microstrip, SIW, High-Temperature Superconductors (HTS), and evanescent-mode cavities [35]-[38].

RF MEMS switches were also integrated with the different waveguide structures to introduce high-Q tunable filters [17], [39]–[42]. Chan et al., introduced an ON/OFF switchable iris waveguide BPF using an RF MEMS switchable planar resonator placed inside the waveguide cavity. When the MEMS switch is turned on, the planar resonator resonates a suppressing notch frequency to the waveguide passband [39]. On the other hand, the embedded tuning circuit will have a small impact on the waveguide resonant frequency when the MEMS switch is turned off. Also, [40] presented a Ku-band two-channel reconfigurable waveguide filter using the same MEMS-based detuning concept. Four operation states (dual-band, the lower band only, the upper band only, and all-rejects) were successfully obtained through the MEMS switching mechanism. The fabricated channel aggregation filter operates at 14.25 and 16.5 GHz channels with an insertion loss of less than 2 dB and a Q-factor > 800.

Another MEMS tunable waveguide filters were introduced by Pelliccia et al. with three different configurations in [41]. In the first approach, the MEMS switches are employed as current perturbation elements to control the distribution of the electromagnetic field. A two-pole K-band filter is designed with 160 MHz bandwidth and Q-factor of 1000 and 500 for ON and OFF states, respectively. In the second configuration, the cavity sidewall is made virtually movable to change the resonant frequency. MEMS switched conductive lines were utilized to create virtual change in the cavity. The fabricated fourth-order filter showed 3.2% tunability with a Q-factor of 500 at the ON states and 650 at the OFF-states. Switchable strips are loaded in an E-plane waveguide cavity for frequency tuning in the third implementation. The simulation results demonstrated a 4th-order filter with 1.6% frequency tuning and an expected Q of the order of 1000.

Another high-Q MEMS reconfigurable BPF was successfully proposed using coaxial combline resonators in [17], where the tuning disks are loaded by MEMS capacitor banks for frequency tuning. A second-order tunable filter is fabricated with a 2.503 – 2.393 GHz frequency range and 1.32 dB insertion loss. Also, a sixth-order filter is implemented with a tuning frequency of 2.59 – 2.63 GHz and an insertion loss of 2.5 – 4.25 dB.

In [43], RF-MEMS were also employed in two different configurations with dielectric resonators to design high-Q tunable filters. In the first mechanism, MEMS-switched conductive strips are placed in the inner hole of the dielectric resonator to control the resonant frequency. When the MEMS is turned on, the effective length of conductive strips will increase, and then the frequency will shift due to the change in the current distribution. The implemented second-order filter is designed at 4.72 GHz with a 160 MHz tuning window and Q-factor from 510 to 1200. In the second configuration, the MEMS-switched conductive strips were replaced by MEMS capacitor banks. This approach has a wider tuning range from 5.02 to 5.20 GHz with a Q-factor of 550 – 800.

In recent years, RF switches based on Phase Change Materials (PCM) were also introduced in a couple of tunable planar and hybrid filters based on Vanadium Dioxide (VO_2) and germanium telluride (GeTe) switches [44]-[47]. Nevertheless, the performance of these switching solutions must be enhanced to qualify the requirements of low-loss and high-performance switchable filters.

Overall, switchable filters offer many advantages and functions in comparison with the conventional fixed configurations as the reduced circuit size, lower cost, and more flexible passbands. However, some limiting drawbacks also clearly appear in contrast, including the slow tuning speed, increased complexity and loss, limited Q and power handling capabilities.

Varactor-Based Tunable Filters

For many of the current and future frequency-agile systems, it is required to have a compact, low-cost and reduced-complexity tuning circuitry with high tuning speeds $>$ 1 GHz/microseconds. To meet these fundamental requirements, varactor tuning configurations are quite popular in various microwave applications. Varactor diode is defined as a special kind of PN–junction diode in which its capacitance is varied with the applied reverse voltage. As the applied reverse-biasing voltage increases, the PN junction gets narrower and the junction capacitance then decreases, and vice-versa. A more detailed explanation of the varactor diodes operation can be found in [49].

Semiconductor varactor diodes are widely commercially available in a broad range of specifications and packages. It is available in two main types: abrupt and hyper-abrupt junction varactors which are constructed based on either silicon or Gallium Arsenide (GaAs) materials. Generally, silicon varactor diodes have a relatively larger capacitance range but suffer from lower Q-factors. Due to that, they are only used at low microwave frequencies up to a few GHz at max. While the GaAs varactors have

less capacitances, they have higher Q and can be applied at higher frequency bands.

Extensive research has been made on the design of varactor-tuned microwave filters including the designs presented in [48]-[68], where various degrees of tuning have been achieved with different structures. Notably, most of those varactor-tuned implementations are of low-Q planar and hybrid bandpass filters [48]-[62], while the conducted research on high-Q waveguide structures is very limited [63]-[68].

In general, research in tunable bandpass filters has been mainly focusing on the realization of frequency tunable filters with some effort towards bandwidth control and other tuning functions (e.g., input-output coupling, transmission zeros). Among the different structures, planar microstrip filters are the most broadly presented in the literature as in [48]-[58] due to their desirable advantages of low-cost, simple fabrication, and easy integration of lumped tuning components. For example, compact frequency tunable varactor-loaded microstrip filters with the feature of constant absolute bandwidth (CABW) were presented using dual-mode resonators [50], miniaturized corrugated transmission lines [51], and shorted folded resonators with improved linearity [52]. Some papers had also proposed additional features of bandwidth and external Q-factor tuning [53], and transmission zeros reconfiguration [54]. Also, more advanced tunable dual-band filters with independently tunable passbands were proposed [55].

Most varactor-tunable filters employ commercially available semiconductor varactors, however, these varactors suffer from limited linearity performance and not suitable for high power applications. Therefore, other promising alternatives as ferroelectric and MEMS varactors were successfully presented in many tunable filter designs as in [58] and [59].

Due to the limited Q-factor of the microstrip structures, higher-Q filters were introduced using Substrate Integrate Waveguides (SIW) [60]-[61], and hybrid evanescent cavities [62]. [61] introduced a compact tunable varactor-loaded SIW filter with the advantage of wide stopbands. A hybrid 3-D printed varactor-based tunable evanescent-cavity BPF was presented in [62] with flexibly tunable center frequency and bandwidth.

In regards to varactor-tuned waveguide filters, only few publications based on coaxial and dielectric resonators were reported [63]-[68]. Xu et al. reported a high-Q tunable coaxial bandpass filter with constant absolute bandwidth and wide tuning range in [63]. Three high-Q GaAs varactors are mounted in parallel to offer larger loading capacitance and also to minimize the overall parasitic resistance. The mea-

sured frequency tuning range is 30.7% at 700 – 960 MHz with 1.58 – 3.97 dB insertion loss and a Q-factor of 173 – 418.

Couple configurations of tunable varactor-loaded dielectric resonators and filters were introduced in the previous literature [64]-[68]. The first implementation was proposed in [64] where two tuning varactors connected using semi-circuited patches and positioned on top of the DR with low-loss quartz spacer in between. The measurements showed a 0.75% tuning range with a Q-factor maintained above 1000. Following in [65], a similar varactor PCB was placed in a different position beneath a TE_{01} mode resonator device. This configuration achieved 1.7% tunability and a high Q-factor up to 8000. Although that high-Q factors are obtained, those configurations have a major drawback of a very narrow tuning range. This is because that the tuning circuits just control the available field around the DR, while most of the field is focused inside the resonator body. Accordingly, [66] proposed an invasive tuning technique in which the varactor is directly embedded on a customized slot in a TE_{01} mode resonator structure. The measured tuning window is 7.1% at 4.7 GHz center frequency with a comparable Q-factor due to the direct integration of the tuning varactor on the dielectric resonator. Varactor-tuned TME mode dielectric filters were also introduced in [67] and [68]. In [67], a tuning structure composed of a varactor-loaded conductive strip is placed in the inner hole of the disk resonator to change the field distribution and tune the resonant frequency. The measurements demonstrate a tuning range of 4.87 – 4.97 GHz with 170 – 660 of Q-factor. While in [68], a TME mode resonator was connected in series with a top-positioned tuning varactor circuit. The filter is implemented with a 4.98 – 5.28 GHz frequency tuning range and Q-factor from from 303 to 576.

2.1.3 Magnetically-Based Tuning

In spite of the large complex structures, magnetic-based tuning is still favorable in some military and commercial applications due to its advantages of low insertion loss and high-power handling capabilities. The magnetic tuning operation principle is based on changing the magnetic field distribution in the filter structure using ferrite materials to tune the resonant frequency. Yttrium iron garnets (YIG) are the most common ferrites used in tunable microwave and high-frequency devices because of their low magnetic and dielectric losses, and moderate saturation magnetization values.

Magnetically Tunable Filters

Many tunable planar filters were reported using YIG ferrites in different configurations [69, 70, 71, 72, 73, 74, 75, 76, 77]. An example of a magnetically tunable bandpass filter designed with yttrium iron garnet films was presented in [69]. The design is based on a T-shaped microwave transducer with a compact coupling structure to reduce the insertion loss. Then, a YIG film is buried on another substrate of gadolinium gallium garnet (GCG). The whole structure acts as a BPF filter whose ferromagnetic resonance is tuned via a biased magnetic field. Another tunable low temperature co-fired ceramics (LTCC) BPF using partially magnetized ferrite was introduced in [77]. The proposed filter brought the benefits of size miniaturization and low biasing requirements due to the use of partially magnetized YIG ferrites.

Ferromagnetic tuning techniques were also limitedly presented in the waveguide, coaxial, and dielectric-loaded filter structures [78, 79, 80]. A ferrite-loaded low-loss tunable X-band waveguide bandpass filter was introduced in [78]. A magnetized ferrite slab is placed inside TE_{102} mode waveguide cavity using truncated pyramid-shaped metallic inserts to tune the resonant frequency by changing the magnetic field distribution. The implemented second-order filter operates at 8.74–9.63 GHz with 9.7% tunability and unloaded Q-factor of 380 – 396. Acar et al. introduced a low-loss ferrite-loaded continuously tunable coaxial filter with high-power handling capabilities in [79]. Magnetically-biased ferrite insert was loaded on the combline resonators to change the magnetic field distribution and tune the frequency. The fabricated two-pole filter exhibited a tuning range of 41% from 744 MHz to 1024 MHz with a low insertion loss of less than 3 dB and a high-Q factor of 1223 – 2425. Additionally, the proposed filter has the merit of handling high levels of power rated up to 800 Watts.

In [80], two second-order magnetically tunable dielectric filters were introduced using magnetized ferrites in axial and circumferential configurations. The implemented filter with the axially magnetized ferrites demonstrated a 20 MHz bandwidth tuning at 2.22 GHz center frequency with insertion loss less than 1.5 dB and a high Q-factor above 2500. While in the circumferentially magnetized ferrites configuration, the filter operated at 2.35 GHz with 28 MHz tunability and a Q-factor higher than 3500.

2.1.4 Other Tuning Means of Microwave Filters

In addition to the above three common tuning techniques, there are few other means reported for the design and realization of tunable filters [81, 82, 83, 84, 85, 86, 87,

88, 89, 90, 91, 92, 93, 94, 95, 96, 97, 98, 99, 100, 101, 102]. In the following, three increasingly interesting tuning approaches are briefly introduced: ferroelectric-based tuning, microfluidic-based tuning, and liquid crystal-based tuning.

Ferroelectric Tunable Filters

The application of ferroelectric materials in various emerging reconfigurable radios applications is catching an increasing attention because of their highly desirable and promising properties [81]. These features include the high-power handling capabilities, good Q-factor, and the realization of a wide variety of compact variable components. Ferroelectrics are employed either as tuning elements (varactors, variable capacitors), as discussed earlier, or as intrinsically-tunable bulk resonators and filters [81]-[86]. The operating concept of self-tuned ferroelectric resonators is based on the direct tuning of the resonator by applying a DC electric field to change the ferroelectric material properties including the relative permittivity which accordingly shifts the resonant frequency.

Two tunable ferroelectric filters were reported in the previous literature using disc-shaped ferroelectric resonators [85], [86]. In [85], a tunable narrow-band BPF was introduced using TM_{110} dual-mode ferroelectric strontium titanate (STO) resonators. The experimental results showed 8% tunability at 0.5 GHz center frequency with 2% fractional bandwidth (FBW). The filter suffered from the increasing losses and drastically decreasing Q-factor with the increase in the DC biasing field, which is a common drawback in ferroelectric materials. The second tunable ferroelectric filter was presented in [86] using a potassium titanate (KTO) resonator coated with a high superconductive layer to increase the Q-factor. The fabricated filter operates at 0.5 GHz center frequency with 1.5% fractional bandwidth and a 5% tuning span.

As can be seen, those filters suffer from the high losses which are mainly related to the ferroelectric material properties and also to the additionally induced losses under the DC biasing. Therefore, such applications of ferroelectrics cannot be expanded further without reducing the material losses. Another additional drawback is that a very high DC field is required for tuning (up to 1 kV) which is impractical for tuning applications. A more promising application of ferroelectrics is in thin-film and thick-film components as the loss effect is minimized and the required biasing is enormously reduced [81].

Liquid Crystal Tunable Filters

Liquid crystal polymers (LCP) are other functional materials that have recently received increasing attention in tunable filter applications to overcome the high loss limitation in the conventional ferroelectrics, especially at high frequencies above 10 GHz [87]-[92]. The tuning principle is based on applying external biasing fields to change the orientation and the relative permittivity of the liquid crystal molecules which will cause a change in the resonant frequency. Various liquid crystal-based tunable planar microstrip and SIW BPFs were presented where an intermediate LC layer is inserted to change the effective relative permittivity and tune the resonant frequency as shown in [87]-[90]. Also, tunable waveguide liquid crystal filters were successfully introduced in [91] and [92]. Liquid crystal containers were placed into the cavity to change the orientation of the fields inside the filter and tune the frequency. A 20 GHz tunable liquid crystal filter was introduced in [91] using a conventional waveguide structure with 2.3% tunability and insertion loss of 6 dB. In [92], a 60 GHz filter was realized using an open nonradiative dielectric waveguide structure to provide more space for the integration of the biasing electrodes. The fabricated three-pole Chebyshev filter has a 2.5% tuning range with 96 - 141 of Q-factor and an insertion loss of 4.9 - 6.2 dB.

Fluidic-Based Tunable Filters

Recently, various micro-fluidics have been explored as promising switching and reconfiguration candidates [93]-[102], mainly because of their linear properties, low loss, and high-power handling capabilities. Many fluidic-based planar and nonplanar reconfigurable/tunable filters were introduced using different fluids [94]-[102]. Various tunable microstrip filters were proposed using intermediate or top-placed microfluidic tubes (e.g., distilled water, dielectric liquids, metallic liquids) for frequency and bandwidth control [95]-[99]. For example, [95] introduced a microfluidic frequency and bandwidth tunable microstrip filter using microfluidically movable surface metalized plates (SMPs). Also in [98], water-filled tubes were placed beneath the microstrip resonator to tune the resonant frequency by changing the overall effective dielectric constant (ϵ_r).

Another fluidic tuning approach was introduced with both planar and 3-D cavity structures by filling the inner posts with fluids to reconfigure the resonant frequency [100]-[102]. Sara, et el., reported a switchable dual-band C-band SIW filter using liquid metal actuation through reconfiguring the inner posts [100]. The proposed

filter works in four different reconfiguration states: all-pass, lower passband, upper passband, and all-reject. Also, in [102], a rectangular waveguide filter was loaded by water-filled tuning posts to control the resonant frequency. Additionally, tunable tri-band filters were presented with independent passband reconfiguration on $TE_{101}/TE_{011}/TM_{011}$ modes with less than 3% tunability in all three bands and a low Q-factor of less than 30.

2.2 Summary

This chapter provided a comprehensive review of different state-of-the-art tuning means of microwave filters. The major tuning techniques: mechanical tuning, electrical tuning, and magnetic tuning, were investigated and discussed in various aspects including the operation concepts, features and specifications, advantages and limitations. The different implementation methods of tunable filters under each of these tuning groups were also discussed. The chapter also highlighted some of the new and promising tuning components and means as the PCM switches, ferroelectric capacitors and resonators, LCP and microfluidic-based tuning.

Chapter 3

Inset Resonators and Their Applications in Fixed/Reconfigurable Microwave Filters

In this chapter, a novel so-called "inset" resonator configuration is presented for fixed and tunable coaxial microwave filter applications. The proposed configuration has many attractive advantages in comparison with conventional structures, including miniaturized size, enhanced spurious performance, and wide tuning capabilities with the least deterioration in unloaded quality factor throughout the tuning window. In the first section of this chapter, the design and analysis of the inset resonator are discussed in detail and accurately modeled as a capacitively-loaded stepped-impedance half-wavelength resonator featuring more compactness, high quality factor, and enhanced spurious responses in comparison with conventional half-wavelength and combline resonators. Additionally, the operating frequency can be tuned intrinsically through the displacement of the coaxial resonator, eliminating the need for any additional tuning elements and maintaining a stable quality factor. For validation, various prototypes are implemented including two quasi-elliptic inset resonator type filters in planar and longitudinal coupling configurations, respectively. The first takes the form of a folded four-pole 2.93 GHz filter with two symmetrical transmission zeros. The fabricated filter has a compact structure of 29.76 cm^3, a midband insertion loss better than 0.73 dB, a return loss higher than 18 dB, and a wide spurious-free band up to $3.5 \cdot f_0$. The second inset-type quasi-elliptic filter is realized in a longitudinal inline arrangement. An example of a 2.53 GHz three-pole filter is presented with

a closely-positioned transmission zero, wide spurious-free band ($\approx 3 \cdot f_0$), and a very compact structure of 55.7×33×33 mm^3.

In the second half of this chapter, a new class of compact, high-Q, tunable coaxial filters is presented based on the novel inset resonator structure. The tuning concept is based on the displacement of movable resonators inside a properly modified metallic housing which features wide tuning capabilities and stable high Q-factor performance with minimum variation throughout the tuning window. Various prototypes are designed and implemented to demonstrate and validate the proposed concept. A single tunable inset resonator is first designed and measured showing distinctive results of a 43% tuning range, stable high-Q of 4100±4%, spurious-free band up to $3.8 \cdot f_0$, and volume-saving up to 50% when compared to the conventional combline and half-wavelength structures. The design procedure for constant absolute bandwidth (CABW) tunable filters is then presented, and two different tunable inset filters are designed and implemented. Firstly, a manually tunable four-pole filter is demonstrated with the merits of a wide 39.3% tuning range, while maintaining a constant bandwidth of 116 MHz±6%, and a stable high-Q of 1820±6%. Next, an automatically tunable 3rd-order inset filter is designed and measured using high-accuracy piezomotors. Similarly, the measured results exhibit a wide 1.3 GHz tuning range from 2.65 GHz - 3.95 GHz with a stable insertion loss that is less than 0.35 dB, a return loss that is better than 15 dB, and a good spurious performance up to $2.8 \cdot f_0$. To our own knowledge, the proposed tuning technique and tunable components represent state-of-the-art tuning range and stable high-Q with minimal variation when compared with similar loaded-waveguide designs.

3.1 Design of Compact Quasi-Elliptic Bandpass Filters Based on Coaxial Inset Resonators

3.1.1 Introduction

Compact coaxial microwave filters with high-Q and excellent spurious rejection performance are essential components for a broad range of evolving applications including cellular base stations and satellite payloads. In common, coaxial filters are realized using half-wavelength and combline resonators. However, from one side, the large bulky structures and poor spurious performance of the $\lambda/2$ resonators make

them an unfavorable option, except in very specific applications such as [19] and [103]. In [19], freely movable resonators were required to design a frequency-tunable coaxial filter. Whereas in [103], $\lambda/2$ dielectric resonators were employed to satisfy a high-Q requirement for satellite multiplexer applications. According to our own knowledge, these two coaxial filters are the only available examples in the literature based on $\lambda/2$ resonators. It is worth noting that both designs have bulky structures and poor spurious performance, as expected. On the other hand, combline resonators widely dominate coaxial filters research due to their compact structures with mid-high-Q and wide spurious-free bands ($>3\cdot f_0$). Similarly, as more compactness and volume-saving are always required, various miniaturized combline filters were presented with good spurious performance based on different configurations [104, 105, 106, 107, 108, 109, 110, 111, 112, 113, 114, 115]. Several of these designs have employed stepped-impedance resonators (SIRs) where the top end of the combline post is enlarged to increase capacitive loading, providing more miniaturization and increasing the band separation to the next spurious resonance [104]-[109]. However, this class of filter must take into account weak inter-resonator couplings, manufacturing complexity, and the added weight of the enlarged parts. The second group of miniaturized combline filters employs multiple interlaced compact reentrant resonators as demonstrated in [110]-[112]. These filters also have relatively complex structures, limited high-power handling capabilities, and increased losses. Recently, 3D printing was used to fabricate non-conventional geometries of compact combline filters in vertical alignments [113]-[115]. Looking at all of these aforementioned combline-based designs, we can see that there is a appreciable space for the exploration of alternative designs to enable easier manufacturing, and more flexible resonators types.

Besides miniturization and good spurious responses, coaxial filters often require transmission zeros (TZs) at one or both stopbands to meet rejection specifications. Commonly, coupling probes and folded configurations are needed to realize the cross-coupling required for TZs' creation, such as the designs in [116] and [117]. However, these probes can resonate and create unwanted spurious resonance close to the passband. Moreover, many applications require inline configurations where the input and the output are on opposite sides. Therefore, [118] and [119] presented inline cross-coupled combline filters using an orthogonal resonator arrangement without the need for any coupling probes. Here, it can be noted that the manufacturing of such orthogonal combline structures is complex and costly. Another method of introducing

TZs in inline combline filters uses strongly coupled doublets and triplets as demonstrated in [120] and [121]. Unfortunately, this mechanism has many design challenges including unwanted spurious resonances, decreased Q-factor, and limited flexibility of the TZs. Considering the above-mentioned drawbacks, we can conclude that the introduction of inline coaxial filters with easy creation and flexible control of TZs is greatly appreciated.

In this section, the design and analysis of the inset resonator are presented in detail, and various fixed coaxial inset filters are designed and implemented. The proposed inset resonator configuration provides many desirable advantages including the compact structure, good spurious performance, comparably high Q-factor, and efficient *self-tuning*. First, detailed modeling and analysis procedure of the inset-type resonator is provided, and different design parameters are investigated. Next, two possible filter setups are introduced in horizontal and vertical arrangements with flexibly controllable transmission zeros providing enhanced stopband rejection characteristics. A two-pole Chebyshev and a folded 4-pole quasi-elliptic filters are implemented in planar coupling configuration, and the measured results are reported. Furthermore, the inline longitudinal coupling configuration of the proposed resonator is presented in detail. The capability of obtaining quasi-elliptic responses with flexibly-controllable TZs is explained, and different examples are provided. The implementation feasibility is explored, and a prototype is manufactured for verification.

3.1.2 Inset Resonator Design and Analysis

Inset Resonator Structure

Fig. 3.1 depicts a 3D view of the proposed inset resonator configuration. It is comprised of a coaxial resonator inserted partially inside modified portions (sidewall caps) of a metallic housing with the aid of support elements. The resonator can be either metallic for lower cost and excellent spurious performance, or dielectric, offering higher Q and more compactness. This research work deals mainly with metallic resonators as they are more common in applications and also simpler in modeling. The support component is preferably of a low-loss dielectric material with decent strength and acceptable coefficient of thermal expansion (CTE) (e.g., Teflon, Rexolite). The resonator is centered at the middle of the structure with equal insertion inside both (symmetrical) sidewall caps. This position is for the lowest operational frequency, and it increases with either up or down displacement of the resonator, simultaneously. As

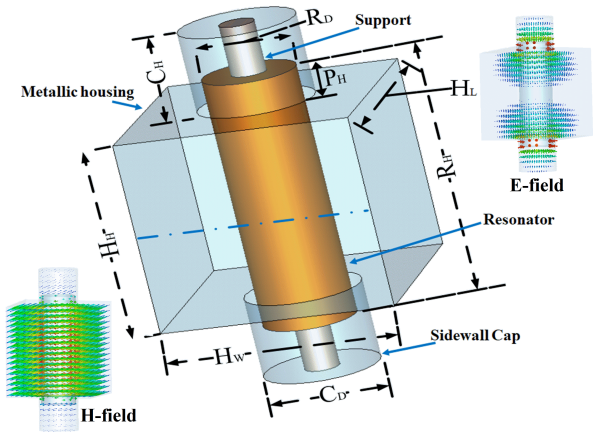

Figure 3.1: Inset resonator structure.

shown in Fig. 3.1, the operating mode is the fundamental transverse-magnetic (TM) mode where the dominant magnetic field resonates in the middle of the resonator assembly, and the electrical field propagates at the top and bottom ends of the resonator where its minima approaches zero at the middle. Hence, despite that any type of resonators can be used in the proposed inset configuration, the TM-mode resonators are particularly the most suitable ones (resonator length > resonator diameter [122]). It can be seen that the inset resonator has similar field patterns to the conventional $\lambda/2$ resonators [19], [103]. However, the inset configuration can advantageously provide substantial size miniaturization and enhanced spurious responses due to the dual capacitive loading effects at both ends of the coaxial resonator caused by the modified sidewall caps.

In comparison with the TEM combline resonators, the inset resonators can feature more compactness with comparable electrical performance. In combline resonators, the magnetic field resonates mainly at the bottom of the cavity while the electrical field is maximum at the vicinity (capacitive gap) between the combline post and the top side of the cavity. Normally, to make the combline structure more compact, the capacitive gap is reduced to increase the capacitive loading and push the resonant frequency lower. Unfortunately, this also leads to a noticeable deterioration in the quality factor due to the high intensity of the E-field in smaller areas which increases the related surface currents and losses. Furthermore, the use of tuning screws will be more critical causing additional ohmic losses and seriously affecting the power handling capabilities of the combline structure. On the contrary in the inset resonator, since the majority of the field is in the middle of the cavity, a relatively

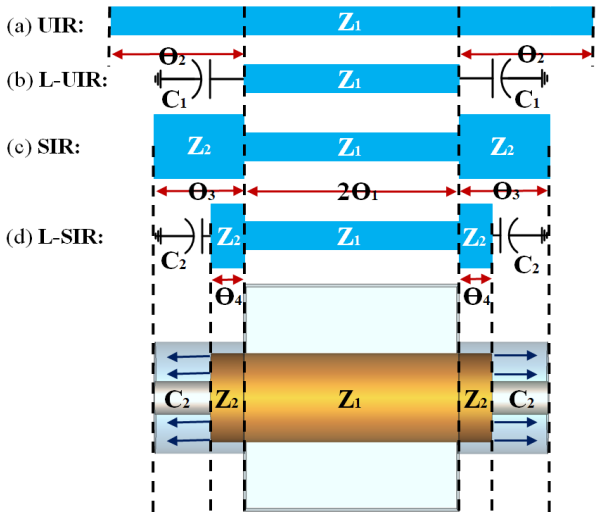

Figure 3.2: Transmission line models of the inset resonator. (a) Uniform Impedance Resonator (UIR), (b) Loaded-Uniform Impedance Resonator (L-UIR), (c) Stepped Impedance Resonator (SIR), (d) Loaded-Stepped Impedance Resonator (L-SIR).

low current density is present along the walls of the housing resulting in a higher Q-factor. Besides, the sidewall caps are properly designed to contain the lowest field densities. Accordingly, small capacitive gaps (i.e., 0.5 mm) between the caps and the inset resonator can be used, attributing more miniaturization with less sacrifice of quality factor. Here, it should be noted that in the inset resonator, similar to the other configurations, the designer should be aware that the quality factor is usually traded off for reduced mass, size, and complexity. One of the key novelties of the inset resonator structure is the efficient (intrinsic) tuning through the displacement of the coaxial resonator without the need for any auxiliary tuning elements (e.g., screws). Thus, unlike the combline structures, the quality factor remains very stable, as will be shown in the following sub-section.

Inset Resonator Model

Looking at Fig. 3.2, it can be shown that the inset resonator configuration can be accurately described as a capacitively-loaded stepped-impedance half-wavelength resonator. To extract the equivalent transmission line model, we begin with an equivalent conventional $\lambda/2$ uniform impedance resonator (UIR) as depicted in Fig. 3.2(a). The resonator has a uniform impedance Z_1 and a total electrical length $\theta_T = 2 \cdot (\theta_1 + \theta_2) = \pi$, where $2 \cdot \theta_1$ is the height of the metallic housing (H_H) and Z_1 is the characteristic impedance of the coaxial resonator structure excluding the cap sections and

can be calculated (in Ohm) using [123], [124]:

$$Z_1 = \frac{60}{\sqrt{\epsilon_r}} \cdot \ln\left(1.079 \cdot \frac{H_W/2}{R_D/2}\right) \tag{3.1}$$

where ϵ_r is the relative permittivity (equals 1 in vacuum mediums), H_W is the square metallic housing width, and R_D is the coaxial resonator diameter. The next spurious resonance of the UIRs normally appears at $2{\cdot}f_0$ (refer to upcoming equation (3.7)). Then, the length of the open-end $\lambda/2$ UIR can be shortened and the spurious performance can be enhanced using lumped-element capacitors as depicted in Fig. 3.2(b). Here, the capacitor-loaded UIR (L-UIR) is more compact than the UIR by a length equal to $2 \cdot \theta_2$. The loaded lumped-element capacitors *(C_1)* can be extracted (in Farad) thru [123]:

$$C_1 = \frac{\tan\theta_2}{Z_1 \cdot \omega_0} \tag{3.2}$$

where ω_0 is the angular resonant frequency ($= 2 \cdot \pi \cdot f_0$), and $\theta_2 = \pi/2 - \theta_1$. Here, C_1 capacitors represent the cap sections including the inserted parts of the coaxial resonator inside them, while $2 \cdot \theta_1$ and Z_1 remain unchanged. Alternatively, as the lumped-element capacitors are not convenient for frequencies above 1 GHz, they can be replaced by equivalent transmission line sections representing a stepped impedance resonator (SIR) as can be seen in Fig. 3.2(c). The SIRs are commonly favorable in a wide range of applications due to their distinct advantage of adjusting the resonator length (hence, frequency), and the spurious resonances with high flexibility and degree of freedom [123], [125]. Similarly, the inset resonator can be modeled as a SIR with two different impedances Z_1 (the metallic housing part) and Z_2 (the caps sections). Whereas Z_1 is known from (3.1) similar to the UIR and L-UIR models, Z_2 can be found (in Ohm) using [123], [124]:

$$Z_2 = \frac{60}{\sqrt{\epsilon_r}} \cdot \ln\left(\frac{C_D/2}{R_D/2}\right) \tag{3.3}$$

where C_D is the diameter of sidewall caps. From this point, the equivalent electrical length of the cap sections θ_3 (and accordingly the overall SIR length $\theta_T = 2 \cdot (\theta_1 + \theta_3)$ can be calculated based on the impedance ratio Z_R *(Z_2/Z_1)*, and θ_1 as follows:

$$\tan\theta_3 = \frac{Z_R}{\tan\theta_1} \tag{3.4}$$

Also, the SIR total length θ_T can be extracted from [125]:

$$\tan\frac{\theta_T}{2} = \frac{1}{1-Z_R}\cdot\left(\frac{Z_R}{\tan\theta_1} + \tan\theta_1\right) \tag{3.5}$$

From this equation, it can be seen clearly the dependence of resonator length on the impedance ratio. When $Z_R = 1$, this is the UIR case where $\theta_T = \pi$. Then, the smaller the impedance ratio than 1 ($Z_2 < Z_1$), the shorter will be the resonator. In addition to the SIR model, the inset resonator can be represented more thoroughly as a loaded SIR (Fig. 3.2(d)) where the caps sections and the inserted parts of the coaxial resonator can be regarded as a capacitively-loaded combline posts. Accordingly, the capacitance gap at both ends (C_2) shortens the inset resonator further by a length of $2\cdot(\theta_3 - \theta_4)$ where θ_3 is known from (4), and θ_4 is the length of the inserted part of the coaxial resonator inside the sidewall caps ($(R_H - H_H)/2$). Similar to (3.2), C_2 (in Farad unit) can be expressed as:

$$C_2 = \frac{\tan(\theta_3 - \theta_4)}{Z_2\cdot\omega_0} \tag{3.6}$$

Besides the contribution to the inset resonator length adjustment, the impedance ratio also incorporates in controlling the frequency ratio of the first spurious (f_S/f_0) and improving the spurious performance. This relation can be seen clearly in equation (3.7) below which tells that the frequency ratio increases with the decrease of the impedance ratio [123], [125].

$$\frac{f_S}{f_0} = \frac{\pi}{2\cdot\tan^{-1}\sqrt{Z_R}} \tag{3.7}$$

The simplified equivalent electrical circuit of the inset resonator is provided in Fig. 3.3. The resonant frequency (f_0) can be found based on the cavity inductance (L_1) and the total capacitance (C_T) as follows:

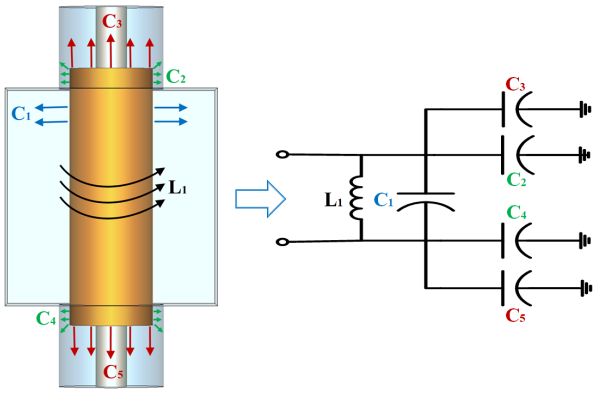

Figure 3.3: Simplified equivalent electrical circuit of the inset resonator.

$$f_0 \approx \frac{1}{2 \cdot \pi \cdot \sqrt{L_1 \cdot C_T}} \tag{3.8}$$

The inductance of the caps sections is relatively small and can be neglected, for simplification. On the other hand, the total capacitance depends on the resonator-housing capacitance (C_1) and the series loading capacitances of the two sidewall caps (C_2, C_3, C_4, C_5):

$$C_T \approx C_1 + ((C_2 + C_3) \parallel (C_4 + C_5)) \tag{3.9}$$

where C_2 and C_4 represent the resonator-cap capacitance at each side and C_3, C_5 are the loading capacitances of the gap between the resonator and the top and bottom surfaces of the caps, respectively. Then, equation (3.8) can be re-written as:

$$f_0 \approx \frac{1}{2 \cdot \pi \cdot \sqrt{L_1 \cdot (C_1 + (\frac{(C_2+C_3)\cdot(C_4+C_5)}{C_2+C_3+C_4+C_5})}} \tag{3.10}$$

For simplicity, we assume that the two cap sections are symmetrical, and accordingly, C_2=C_4, C_3=C_5. Then, the inductance (L_1), and the different capacitance components can be found (in Henry unit) as follows [123], [126]:

$$L_1 \approx \frac{1}{6 \cdot \pi \cdot 10^8} \cdot \sqrt{\frac{\mu_0}{\epsilon_0}} \cdot \ln\left(1.079 \cdot \frac{H_W/2}{R_D/2}\right) \cdot H_H \tag{3.11}$$

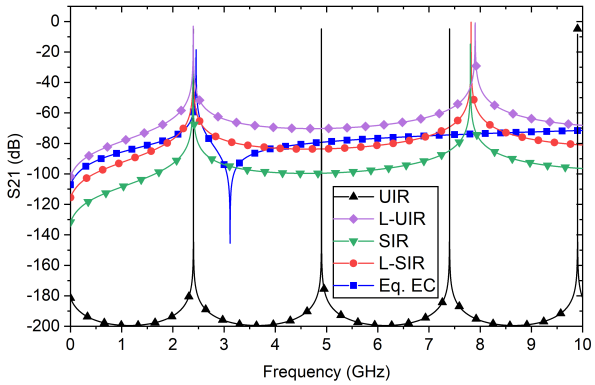

Figure 3.4: Transmission coefficient responses of various inset resonator TL models and equivalent electrical circuit at 2.5 GHz. The corresponding physical dimensions are in Table 3.1. Black line: uniform impedance resonator ($Z_1 = 59.54\ \Omega$, $\theta_1 = 63^o$, $\theta_2 = 58.5^o$). Violet line: loaded-uniform impedance resonator ($C_1 = 1.75$ pF). Green line: stepped impedance resonator ($Z_2 = 7.066\ \Omega$, $\theta_3 = 10.99^o$). Red line: loaded-stepped impedance resonator ($\theta_4 = 6^o$, $C_2 = 0.787$ pF). Blue line: equivalent electrical circuit ($L_1 = 4.153$ nH, $C_1 = 0.59$ pF, C_2, $C_4 = 0.472$ pF, C_3, $C_5 = 0.222$ pF).

$$C_1 \approx \frac{2 \cdot \pi \cdot H_H}{6 \cdot 10^8 \cdot \sqrt{\frac{\mu_0}{\epsilon_0}} \cdot \ln\left(1.079 \cdot \frac{H_W/2}{R_D/2}\right)} \tag{3.12}$$

$$C_2, C_4 \approx \frac{2 \cdot \pi \cdot P_H}{6 \cdot 10^8 \cdot \sqrt{\frac{\mu_0}{\epsilon_0}} \cdot \ln\left(\frac{H_W/2}{R_D/2}\right)} \tag{3.13}$$

$$C_3, C_5 \approx \frac{\epsilon_0 \cdot \pi \cdot (R_D/2)^2}{C_H - P_H} \tag{3.14}$$

To further validate and confirm the aforementioned conceptualization and models of the proposed inset resonator configuration, a single resonator example is designed, and its different parameters are investigated in detail. The resonator is designed to operate at a resonant frequency of 2.5 GHz. An EM-based model is built and analyzed using the Eigenmode solver in CST microwave studio, while the various transmission line (TL) models and equivalent electrical circuit are calculated using the provided equations and then implemented in ADS circuit simulation environment. The results in Fig. 3.4 show quite well agreement between the different models in both the reso-

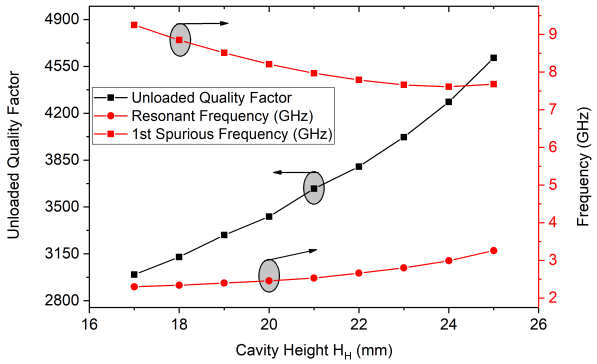

Figure 3.5: Dependence of the fundamental frequency, 1st spurious resonance, and unloaded quality factor on the height of the metallic housing (H_H). The corresponding physical dimensions are in Table 3.1.

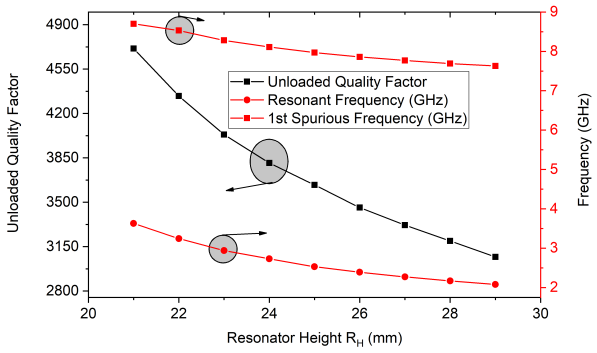

Figure 3.6: Fundamental frequency, 1st spurious resonance, and unloaded quality factor with respect to resonator height (R_H). The corresponding physical dimensions are in Table 3.1.

nant frequency at 2.5 GHz and the next spurious resonance at around 8 GHz. The inset resonator is then compared with the conventional combline (reported in [127]) and half-wavelength resonators as summarized in Table 3.1. The coaxial resonator length is 50 mm ($\approx \lambda/2$) in the half-wavelength resonator case, and 25 mm ($\approx \lambda/4$) in the combline and inset configurations. The chosen metal for all components is copper ($\sigma = 5.8{\times}10^7$ S/m). As is shown, the inset resonator yields a better spurious performance ($3.2 \cdot f_0$), up to more than 60% volume-saving, and a comparable high Q factor with the best Q_u/volume ratio. Next, the different design parameters (the housing, resonator, and sidewall caps) of the presented inset resonator are studied. Fig. 3.5 and Fig. 3.6 depict the variation in the resonant frequency, 1st spurious resonance, and unloaded Q-factor with respect to the housing height (H_H) and resonator length (R_H), respectively. When the H_H is reduced, this means more parts of the

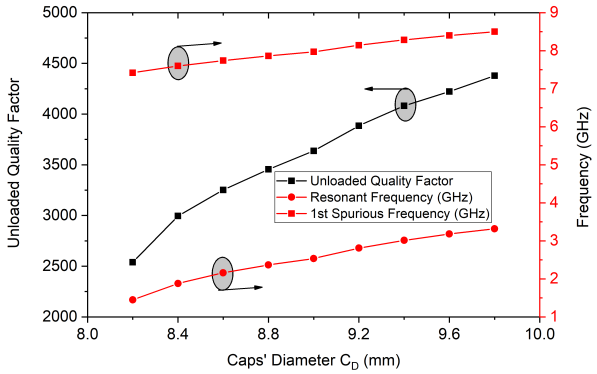

Figure 3.7: Fundamental frequency, 1st spurious resonance, and unloaded quality factor with respect to the caps' diameter (C_D).The corresponding physical dimensions are in Table 3.1.

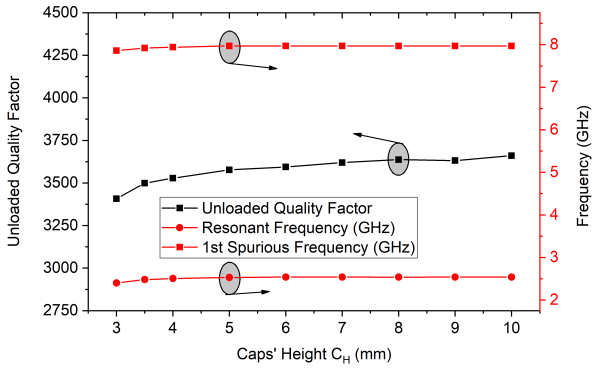

Figure 3.8: Fundamental frequency, 1st spurious resonance, and unloaded quality factor with respect to the cap's height (C_H). The corresponding physical dimensions are in Table 3.1.

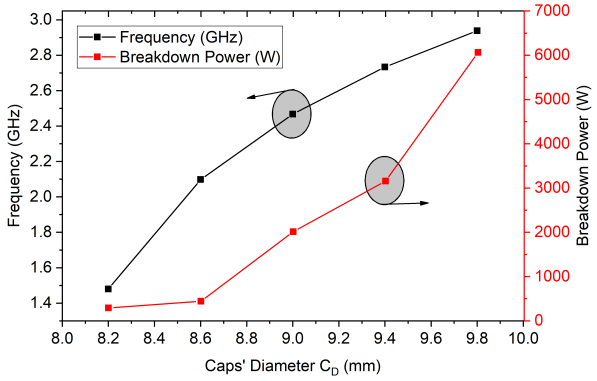

Figure 3.9: Center-frequency and power breakdown level with respect to the cap's diameter (C_D). The corresponding physical dimensions are in Table 3.1.

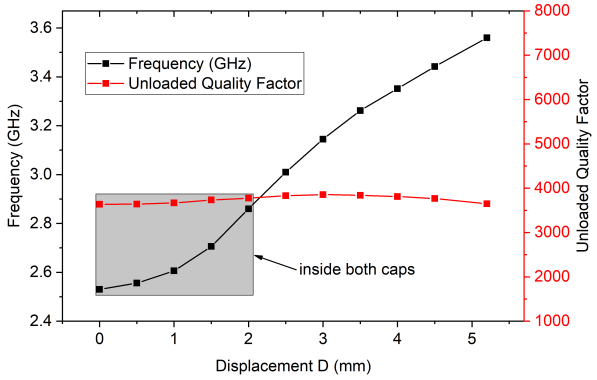

Figure 3.10: Fundamental frequency and unloaded quality factor variation with respect to inset resonator displacement. The corresponding physical dimensions are in Table 3.1 ($C_H = 8$ mm).

resonator will be inserted into the sidewall caps. Consequently, the corresponding capacitance components will increase (C_2, C_3, C_4, C_5) and move the resonant frequency lower based on equation (3.10). Besides, an improvement in the spurious separation can be noticed. The same happens when the resonator is elongated as can be seen in Fig. 3.6. In both cases, this will be accompanied by a variation in the quality factor. The sidewall caps are the most important part of the inset resonators and should be designed properly based on the desired requirements. Fig. 3.7 describes the impact of the caps' diameter (C_D) on the frequency and the Q factor. The smaller the gap between the cap and the resonator, the smaller the corresponding impedance Z_2 (refer to equation (3.3)) will be. Consequently, based on equations (3.5) and (3.7), the resonant frequency will be shifted downwards, and the spurious performance will improve. Fig. 3.8 relates the frequency and quality factor to the change in the caps' height (C_H). Since the contained fields inside the caps are relatively small, we can see that the resonant frequency and the Q-factor remain almost constant and stable. This feature is particularly useful for the design of tunable inset structures where the caps are designed based on the required room for the movable inset resonators to obtain the desired tuning, as will be explained in the second part of this chapter. Apart from that, the resonant frequency can still be decreased by further reducing the capacitive gap between the resonator and the caps, and increasing the corresponding capacitances C_3, C_5. Since relatively small gaps are needed between the resonator and the caps (i.e. 0.5 mm) for higher miniaturization, some worries might be raised regarding the power handling capabilities of the proposed inset resonator configuration. Therefore, we have investigated this using the Sparks3D tool in CST with

Table 3.1: Comparison of the inset resonator with the conventional half-wavelength and combline resonators at 2.5 GHz.

Structure	Half-wavelength	Combline	**Inset**
f_0 (GHz)	2.5	2.5	**2.5**
f_S (GHz)	5.0	7.4	**8.0**
Q_u	4733	3591	**3536**
Volume (cm^3)	24	12	**8.9**
Q_u/Volume (cm^{-3})	197.2	299.25	**397.3**

Dimensions (in mm): Half-wavelength: $H_W = 20$, $H_L = 20$, $H_H = 60$, $R_H = 50$, $R_D = 8$. Combline: $H_W = 20$, $H_L = 20$, $H_H = 30$, $R_H = 25$, $R_D = 8$. Inset: $H_W = 20$, $H_L = 20$, $H_H = 21$, $R_H = 25$, $R_D = 8$, $C_H = 4$, $C_D = 9$. The material of all metallic parts is copper.

different gaps sizes between the caps and the resonator. It is evident in Fig. 3.9 that the resonator can handle power levels of more than 2000 W while the gap size is of only 0.5 mm. It can be further improved up to 6000 W by increasing the gap size. Additionally, it was shown in [128] that lamination with a dielectric material (e.g., Teflon) can further enhance the power handling capabilities.

One of the key advantages of the inset resonator configuration is the ability to tune the resonant frequency through the displacement of the coaxial resonator without the need for any additional tuning elements. As mentioned earlier this so-called "*self-tuning*" simplifies the tuning process and is able maintain a stable Q-factor. Fig. 3.10 shows the tuning capabilities of the presented inset resonator. Here, we extended the height of the caps by 4 mm (C_H=8 mm) to offer more room for the resonator displacement and provide higher tunability. When the resonator is displaced from the center, the resonant frequency will increase due to the change in the loading capacitances at both ends (refer to Fig. 3.3, eqs. (3.9) and (3.10)). For post-tuning of microwave filters, we normally require fine-tuning elements for a small frequency range. Therefore, the designer can move the resonator slightly to adjust the resonant frequency (e.g., within the shaded gray box at Fig. 3.10, where the resonator is inside both caps). Of course, further tuning can be obtained as can be seen, which is useful for tunable filter applications as explained in the following section. The most interesting feature of this tuning mechanism is that the Q-factor remains stable with minimum variation throughout the tuning window.

For verification and validation purposes, a 2.33 GHz single inset resonator structure is implemented, assembled, and measured. The resonator dimensions (in mm unit) are: $H_H = 15$, $H_W = 30$, $H_L = 30$, $R_H = 20$, $R_D = 10$, $R_{Di} = 3$, $C_H = 8$,

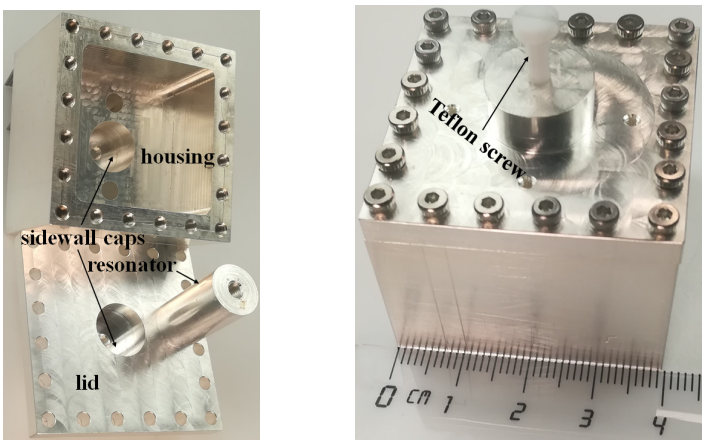

(a) (b)

Figure 3.11: The fabricated inset resonator prototype. (a) Disassembled and (b) assembled.

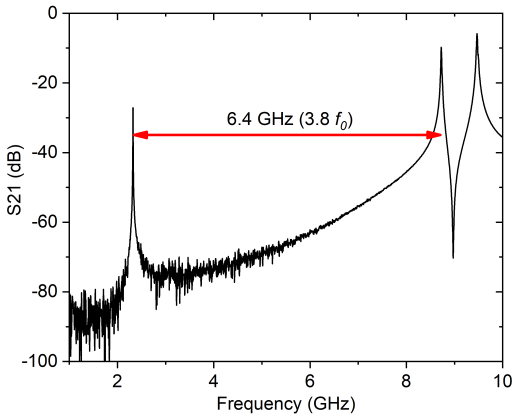

Figure 3.12: Measured S21 response.

$C_D = 11$. Both the metallic cavity and the resonator were manufactured using brass alloy and then coated with silver to achieve higher quality factor results. The fabricated prototype and the measured results are depicted in Fig. 3.11 and Fig. 3.12, respectively. The resonator operates at 2.32 GHz with a quality factor of approximately 3910 and a spurious-free band that approaches $3.8 \cdot f_0$. Also, the inset resonator structure has a compact size of 15.02 cm^3, offering up to 50% and 25% volume-saving in comparison with the conventional half-wavelength and combline resonators.

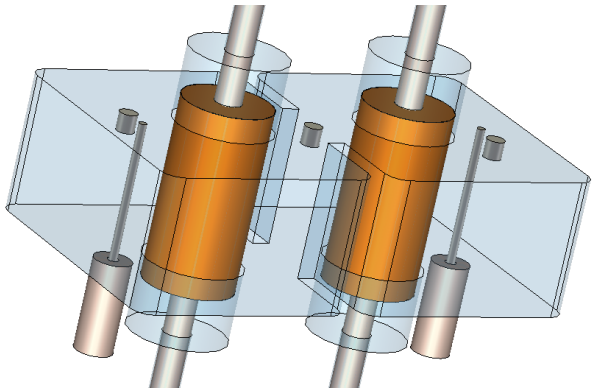

Figure 3.13: 3D view of the proposed two-pole inset BPF.

3.1.3 Inset Bandpass Filters

Inset Filters in Planar Configuration

Fig. 3.13 illustrates a 3D schematic of a two-pole bandpass filter using the proposed inset resonator. The filter is designed to have a Chebyshev response and operates at a center frequency of 2.45 GHz with an absolute bandwidth of 50 MHz. Firstly, the corresponding coupling matrix is extracted and optimized following the standard synthesis process in [129]. Then, the required physical coupling coefficients (K_{12} and external quality factor Q_{ext}) are calculated and realized. The extracted Q-factor is 3000 when considering copper metal. Photographs and measured S parameters of the implemented filter are depicted in Fig. 3.14 and Fig. 3.15, respectively. Measurements agree very well with simulations. This prototype was manufactured out of brass metal and then silver-plated to get higher Q_u. The filter prototype operates at a frequency of 2.51 GHz with 53 MHz bandwidth and extracted Q_u of ≈2000. The filter has a wide spurious-free band up to 8.63 GHz ($3.44 \cdot f_0$) as can be seen in Fig 3.15(b).

Next, a compact fourth-order coaxial inset filter is designed also in a planar coupling configuration with folded topology to realize a cross-coupling and create transmission zeros. Fig. 3.16 shows a perspective view of the quasi-elliptic four-pole filter designed to operate at 2.8 GHz with a bandwidth of 75 MHz, Q_u of 3100 (with copper), and two symmetrical transmission zeros. It is worth to remark that this filter is also designed for tunable applications, but, will not discuss it here as we are only interested in its fixed version (for tunable responses, please refer to the following section). Based on the specifications, the corresponding coupling matrix is extracted following the standard synthesis procedure [129]:

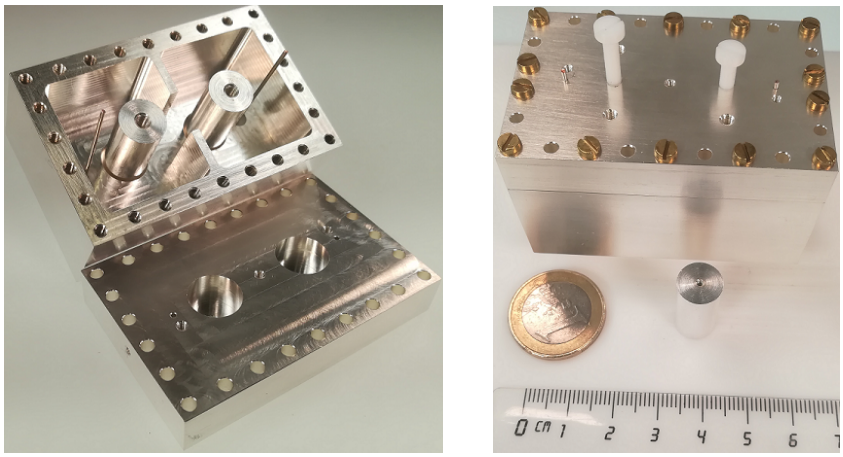

(a) (b)

Figure 3.14: The fabricated two-pole inset bandpass filter. (a) Disassembled and (b) assembled.

$$\begin{bmatrix} & S & 1 & 2 & 3 & 4 & L \\ S & 0 & 1.04 & 0 & 0 & 0 & -0.0003 \\ 1 & 1.04 & 0 & 0.91 & 0 & 0 & 0 \\ 2 & 0 & 0.91 & 0 & 0.70 & 0 & 0 \\ 3 & 0 & 0 & 0.70 & 0 & 0.91 & 0 \\ 4 & 0 & 0 & 0 & 0.91 & 0 & 1.04 \\ L & -0.0003 & 0 & 0 & 0 & 1.04 & 0 \end{bmatrix} \tag{3.15}$$

Next, the required physical input-output (IO) and inter-resonator couplings are realized. As shown in Fig. 3.16, the IO couplings are obtained using inductive coupling posts fed through Sub-Miniature version A (SMA) connectors. Similarly, the required physical inter-resonator couplings are realized by properly adjusting the dimensions of the iris sections. A capacitive coupling probe is used to realize a source-load coupling path introducing two symmetrical transmission zeros. A prototype is then manufactured and assembled as depicted in Fig. 3.17 and Fig. 3.18, respectively. The metallic housing is made of aluminum, while the coaxial resonators are milled out of brass metal. The resonators are positioned using Polyetheretherketone (PEEK) screws at one end (which are more durable than the Teflon screws) with the aid of Teflon posts at the other end. The overall volume of the filter prototype is $54\times52\times35$ mm^3.

The simulated and measured results of the proposed folded filter are presented in Fig. 3.18 with and without the capacitive coupling probe (i.e., with and without TZs). The filter is centered at 2.93 GHz with a mid-band insertion loss better than

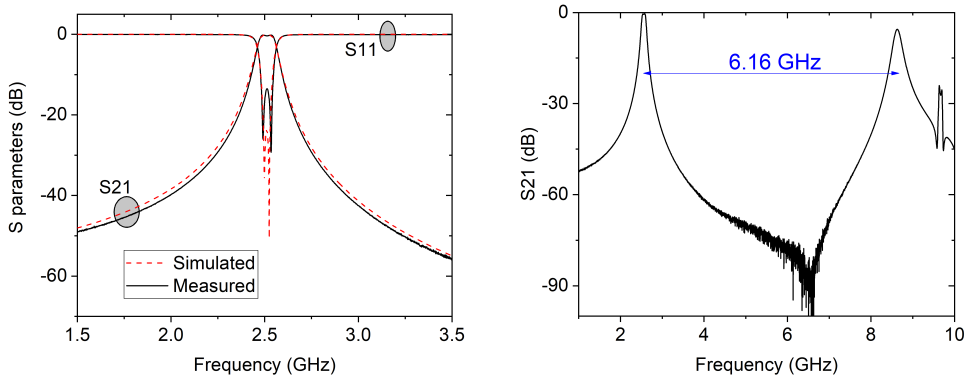

Figure 3.15: The fabricated two-pole inset bandpass filter. (a) Measured S-parameters and (b) wideband response.

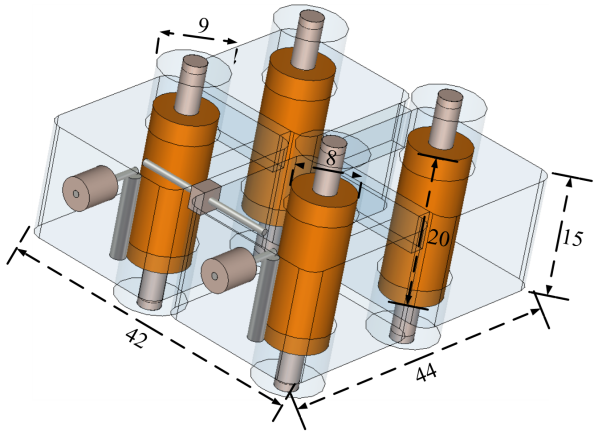

Figure 3.16: 3D structure of the proposed folded 4th-order coaxial inset filter. All dimensions are in mm unit.

0.73 dB, a return loss higher than 18 dB, and extracted quality factor of 1000. It is worth mentioning that no tuners are employed. A 4.6% increase is noticed from the simulated operating frequency (2.8 GHz). This is mainly due to manufacturing tolerances, particularly in the caps' sections which are the most sensitive parts. Hence, the simulations were optimized to resemble the measurements through decreasing the gap between the coaxial resonators and the caps by 0.08 mm. To compensate for this increase in frequency, tuning screws can be introduced, however, this is not a favorable option in many applications as discussed earlier. Alternatively, it is more convenient for designers to consider the manufacturing tolerances in advance to get an excellent agreement. For example, a second version of this filter can be designed at a 4.6% lower frequency ($\approx$ 2.67 GHz). Then, if a further up-tuning is required, the resonators can

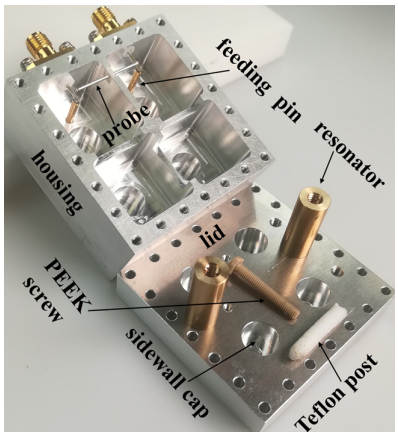

Figure 3.17: The fabricated folded four-pole inset filter (disassembled).

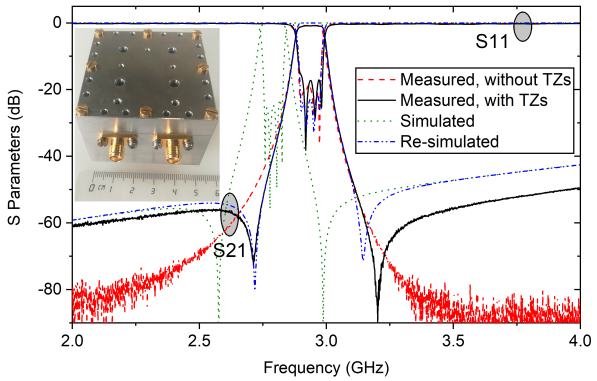

Figure 3.18: Simulated and measured results of the folded 4th-order inset filter.

be displaced accordingly. In this manner, the need for additional tuning screws (to decrease the resonant frequency) can be eliminated. Another possible option since that the coaxial resonators are separated components, they can be simply replaced by longer ones (could save cost and time). The wideband response of the implemented filter is demonstrated in Fig. 3.19. The next spurious frequency is at $3.5 \cdot f_0$, while the iris resonances can be noticed at $\approx 3 \cdot f_0$, which can be redesigned to suppress their unwanted resonances.

Inset Filters in Longitudinal Configuration

As we earlier discussed, there is a fundamental need for inline coaxial filter configurations that are able to introduce TZs with flexible positioning. With regard to this, another possible setup of the inset resonator filters is the inline longitudinal configuration. Besides to the more compact structures, compared with the aforementioned

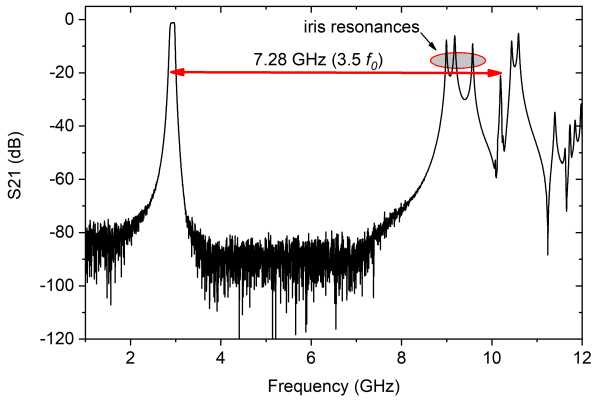

Figure 3.19: Wideband response of the four-pole inset filter.

planar topology, the longitudinal inset configuration has the capability of obtaining quasi-elliptic responses in inline arrangements. For instance, Fig. 3.20 illustrates a 3rd-order inset filter that operates at 3.08 GHz with a bandwidth of 56 MHz and unloaded quality factor about 2720 (with copper). The couplings between the adjacent resonators (inter-resonator couplings) are magnetic-based (inductive) couplings. In addition, there is a transmission zero that can be seen relatively far away from the passband at 2.55 GHz. This TZ is created through a relatively weak electrically dominant (capacitive) coupling path between the nonadjacent resonators (1 and 3). This TZ can be moved closer to the passband by increasing the electrical coupling strength between the resonators. Referring to Fig. 3.1, we know that the E-field is mainly focused at the ends of the inset resonators. Consequently, the E-field coupling strength can be increased effectively by: 1) making central openings in the irises, so, the adjacent resonators' ends face each other directly, and then, 2) moving the resonators closer. Simultaneously, the irises and the resonant frequency of each cavity must be re-optimised to provide the same operating frequency and bandwidth. Fig. 3.21(a) presents a design example which has similar passband specifications to the above filter (i.e., f_0=3.08 GHz, BW=56 MHz), but, the TZ is moved and positioned very close to the passband at 2.98 GHz. Additionally, the TZ can be flexibly shifted to the upper side by simply changing the sign of any inter-resonator coupling pair (m_{12} or m_{23}). This is realized by rotating the respective coupling iris by 180^o angle as can be seen in the filter-2 example in Fig. 3.21(b). This advantage of introducing flexibly controllable TZs distinguishes the proposed inset configuration from similar longitudinally-coupled loaded-waveguide filters available in the literature [113], [115], [130], [131], and [132]. While the inline coaxial filter in [113] and

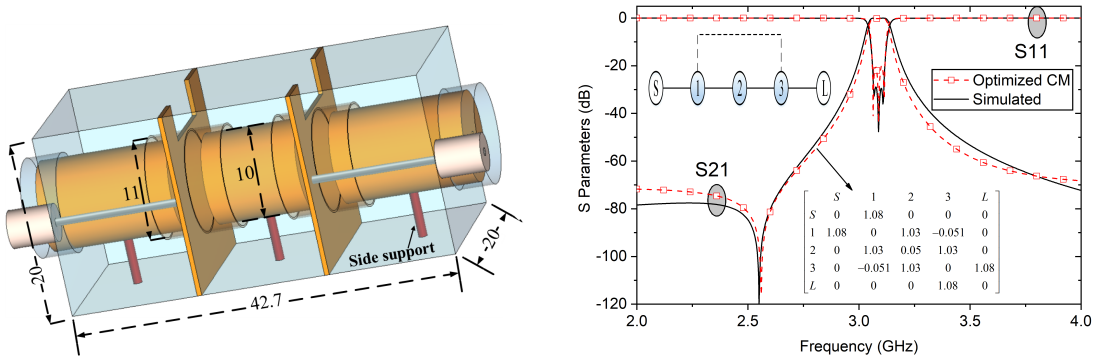

(a) (b)

Figure 3.20: Third-order inset filter in a longitudinal configuration. (a) 3D structure (in mm unit) and (b) simulated (solid black line) and optimized coupling matrix (dashed red line).

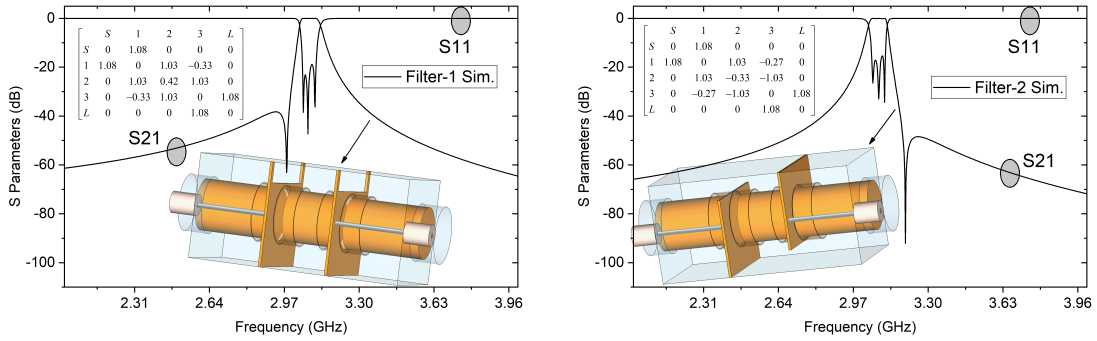

(a) (b)

Figure 3.21: Longitudinal inset filters with similar frequency and bandwidth of the previous example in Fig. 3.20. (a) Filter-1: Close transmission zero at the lower stopband. (b) Filter-2: Close transmission zero at the upper stopband.

the electrically-coupled TM-mode dielectric filters in [130]-[132] cannot introduce TZs, the TZ controllability was not demonstrated in the additively-manufactured combline filter in [115].

Regarding the realization of the longitudinal inset filters, a common dielectric support element can be used to fix all resonators in their required positions, simultaneously. Alternatively, side support elements can be used to fix each resonator independently as it shown in Fig. 3.20(a). The support element is preferably to be positioned at the middle of the resonator where the E-field is minimum (almost zero). Accordingly, the side support will have a minimum impact on the resonant frequency and the quality factor, and can be either dielectric or metallic. This could allow for monolithic additive manufacturing which helps in reducing the assembly-

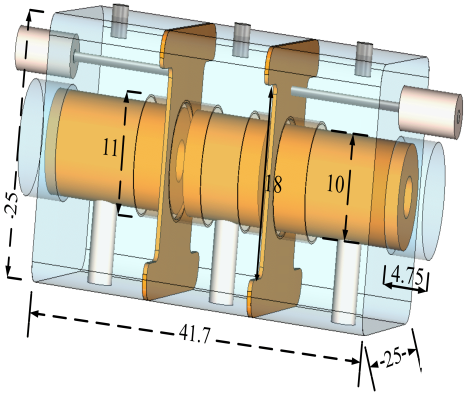

Figure 3.22: 3D structure of the proposed longitudinal three-pole coaxial inset filter at 2.69 GHz. All dimensions are in mm unit.

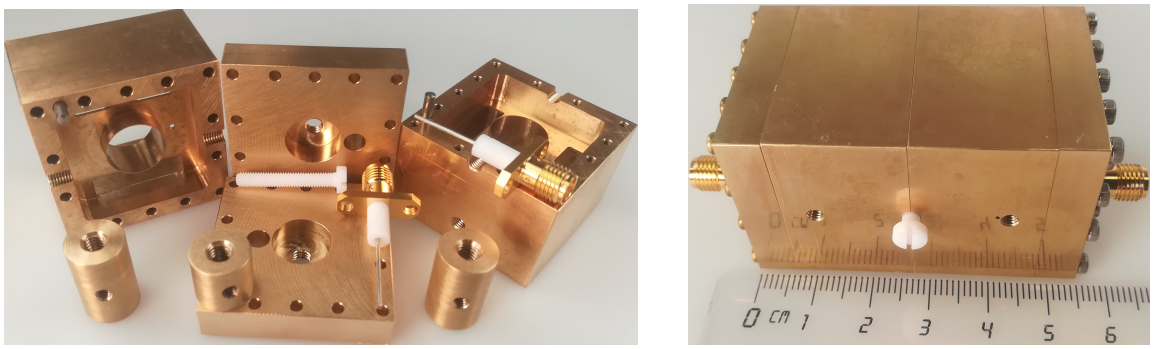

(a) (b)

Figure 3.23: The fabricated longitudinal inset filter. (a) Disassembled parts. (b) Final assembled prototype.

related errors and losses. This would be even more beneficial as frequency tuning is more challenging in longitudinal configurations than in the planar ones, because the resonators cannot be displaced independently.

To experiment the feasibility of implementing such structures using the conventional CNC machining, a 3rd-order filter is designed and manufactured. The filter shown in Fig. 3.22 is designed to operate at 2.69 GHz with a bandwidth of 81 MHz and a lower transmission zero at 2.48 GHz with a 50 dB rejection level. The simulated quality factor is around 2820 when using copper metal ($\sigma = 5.8\times10^7$ S/m) and 1470 with brass ($\sigma = 1.59\times10^7$ S/m). The resonators are fixed in their positions using M3 Teflon screws from one side, while metallic M3 screws are introduced at the other side for tuning purposes. Unlike the filter example in Fig. 3.20(a) with single-sided irises, slots are made here at two sides to increase the inter-resonator coupling strength for

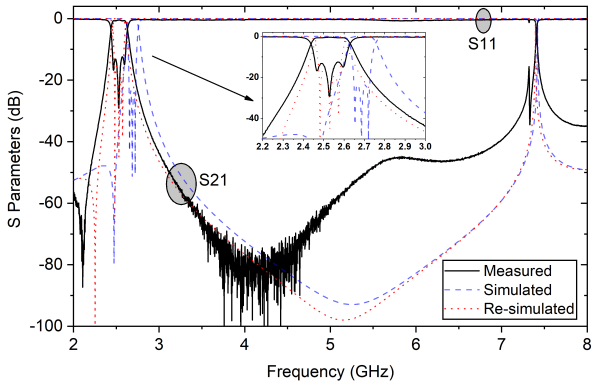

Figure 3.24: Measured vs. simulated results of the implemented three-pole inset filter.

a wider bandwidth. The filter prototype parts were manufactured using brass alloy and then assembled as exhibited in Fig. 3.23. The filter prototype has a compact volume of 55.7×33×33 mm^3. The measured results in Fig. 3.24 show that the filter is centered at 2.53 GHz with a BW of 120 MHz, a midband insertion loss better than 0.45 dB, and a return loss higher than 12.5 dB. The estimated unloaded quality factor is around 800 (54% of simulated-Q). Also, a 60 dB lower stopband transmission zero is introduced at ≈ 2.11 GHz. A 160 MHz frequency decrease from simulated results is noticed due to the manufacturing and assembly tolerances, mainly at the caps sections (re-simulations estimate caps' radii smaller by 0.09 mm). As result, the electrical coupling decreases (hence, the TZ is pushed further), and the inter-resonator (magnetic) couplings increase (thus, the BW becomes wider). The response can be conveniently recovered similar to the earlier prototype in the above sub-section. Besides, silver-plated M3 screws were added to provide additional tuning. The next spurious resonance frequency is noticed at 7.43 GHz (≈3·f_0); it can be suppressed further up to 8.89 GHz (≈3.5·f_0) with proper design procedure.

A comparison between the proposed inset filters and similar quasi-elliptic coaxial BPFs is summarized in Table 3.2. As apparent, the inset-based designs provide the merits of volume miniaturization and enhanced spurious performance, in addition to the capability of obtaining flexibly controllable quasi-elliptic responses. The first planar configuration follows the common folded topology to realize a cross-coupling and create TZs, similar to [108], [112], [116]. Also, as the inline structure is favourable in many applications, [118] and [119] used orthogonal combline resonators to introduce TZs. Nevertheless, these designs are complex in manufacturing and have a degraded spurious performance. Whereas in [115], the compact vertical combline structure

Table 3.2:
Comparison of the Proposed Quasi-Elliptic Inset Filters with Similar State-of-The-Art Designs.

Ref.	**Configuration**	f_0 **(GHz)**	**Order**	**BW (MHz)**	**TZs**	**IL (dB)**	**Q-factor**	f_S (GHz)	**Size** (λ_g^3)
[108]	folded SIR combline	2.58	4	98	3	0.25	2900	NA	0.012
[112]	folded re-entrant combline	1.54	6	49	2	0.86	NA	$2.34f_0$	0.105
[115]	inline longitudinal combline	3.51	3	235	1	$\geq$0.09	2461	$3.13f_0$	NA
[116]	folded combline	2.0175	4	15	2	0.65	NA	NA	0.074
[118]	inline orthogonal combline	1.54	6	48.8	2	NA	4400	$2.7f_0$	0.039
[119]	inline orthogonal combline	2.14	6	60	2	NA	NA	$2.2f_0$	0.043
This work-1	**folded inset**	**2.93**	**4**	**82**	**2**	**0.73**	**1000**	$\mathbf{3.5}f_0$	**0.029**
This work-2	**inline longitudinal inset**	**2.53**	**3**	**120**	**1**	**0.45**	**800**	$\mathbf{3}f_0$	**0.016**

Ref.= reference, f_0= resonant frequency, IL= insertion loss, f_S= spurious frequency, λ_g= guided wavelength at the operating frequency.

allowed the cross-coupling between the non-adjacent resonators to happen and generate a single TZ. However, it has a major limitation in controlling the TZ position. Contrary, in the presented longitudinal inline configuration of the inset filters, transmission zeros can be adjusted flexibly and effectively.

3.2 Tunable Coaxial Bandpass Filters Based on Inset Resonators

3.2.1 Introduction

Propelled by the exponential development in the telecommunication industry and the escalating demand for more efficient and adaptable multi-channel multi-standard systems, tunable microwave filters are constantly gaining ground as they are playing a pivotal role in frequency-agile RF front-ends and payloads. The tunable filter market is expected to have an annual growth of more than 10%, crossing USD 148 million by

2025 [133], driven mainly by major industrial sectors including RADAR systems, test and measurement instruments, and software-defined radios. These evolving applications have stringent requirements for high-performance tunable filters with regard to volume and mass, high unloaded quality factor (Q_u), and wide tuning capabilities with efficient tuning mechanisms. Looking in the available literature, tunable filters have been realized in planar and 3-dimensional structures using a variety of different electrical, magnetic, and mechanical tuning means [134]. While the majority of research is based on simple, compact, and low-cost planar tunable microstrip filters which utilize fast electrical tuning elements (e.g., varactor diodes) [135], their high losses and poor power performance hinder their employment in high-performance applications. On the other hand, the use of waveguide filters, despite their high Q-factor and ability to handle high power levels, usually have bulky structures, as well as slow and narrow tuning capabilities (i.e., <5% tuning) [28], making hollow waveguide tunable filters an unfavorable solution; especially at lower frequency bands less than 10 GHz. Considering the drawbacks of the aforementioned technologies, loaded-waveguide structures have attracted more attention in tunable filters applications due to being much more compact when compared with hollow waveguide designs, while still providing comparably high quality factors. Accordingly, various loaded-waveguide tunable filter designs were presented based on dielectric resonators, conventional metallic half-wavelength, and combline configurations using different mechanical tuning means [28, 19, 136, 5, 27, 17, 26, 16, 137, 138, 139, 140, 141, 142, 43, 63, 79]. A 2.5 GHz tunable $\lambda/2$ coaxial filter was presented in [19] with a 20% tuning range by using a common element which rotates all of the resonators simultaneously inside an elliptical cavity, providing a means of tuning the operation frequency. However, this mechanism of tuning has limited tuning capabilities since it functions only within a specific range of the cavity (0° - 90°). Furthermore, the filter experiences a noticeable deterioration in the Q-factor (≈20%) when the resonators are rotated closer to the cavity, which ultimately increases the losses. The large size, and degraded spurious responses are further drawbacks of this half-wavelength configuration. According to the authors' knowledge, this is the only tunable filter available in the literature based on the conventional $\lambda/2$ resonators. On the other hand, several combline-based tunable filters were presented using different tuning elements and means [136, 5, 27, 17, 26, 16, 137, 138, 43, 63, 79]. A straightforward approach is by using mechanically, vertically movable tuning screws, disks, or sidewalls in the vicinity between the combline resonators and the top part of the metallic cav-

ity [136, 5, 27, 17, 26]. For example, [5] introduced an 18% reconfigurable S-band combline filter using dielectric tuning posts controlled by a common tuning plate. Also in [17], a 2.6 GHz $\lambda/4$ tunable coaxial combline filter was implemented using metallic tuning discs controlled by individual piezomotors with a very small tuning range ($\approx$70 MHz). A third example employing a piezoelectrically-actuated flexible sidewall was presented in [26]. A four-pole C-band tunable dielectric combline filter is implemented with 4% tunability and unloaded Q-factor of less than 550. In this regard, it is clear that this category of vertically movable tuning elements suffers from severe deterioration in the Q_u as the tuning elements approach closer to the combline resonators, with additionally risking the possibility of generating unwanted spurious resonances. Excellent electrical contact must be guaranteed between the top part of the cavity and the tuning elements (i.e., using nuts), otherwise, the Q-factor will be impacted negatively and the tuning range will decrease. Besides, the volume of such filters is relatively large since the height of the cavity must be increased to provide room for the tuning screws/disks inside of the housing. Another group of tunable coaxial combline filters is employing horizontally sliding and/or rotational metallic or dielectric elements mounted on a common tuning post [16, 137, 138]. For instance, an L-band tunable $\lambda/4$ combline filter was introduced in [137] with an 11% tuning range using rotational elliptical metallic loadings. In comparison with the aforementioned group of vertically movable tuning elements, this configuration features an easier tuning process. However, the frequency tuning windows of these means are very narrow since less EM-field can be perturbed. Hence, larger elements must be used to increase the tuning capabilities. Unfortunately, this increases the size and weight of the filter and also unwanted spurious resonances might appear. Recently, we presented tuning concepts based on TM-mode dielectric resonators featuring compact structures and wide tuning capabilities >90% [139, 140, 141, 142]. Unfortunately, they also experience noticeable deterioration in the Q_u with the tuning process. Besides the above mechanical-based tuning technique which is the most favorable, couple of loaded-waveguide filters were introduced using electrical and magnetic tuning elements to attribute fast tuning speed [43, 63, 79]. For example, the authors in [43] presented reconfigurable 2nd-order dielectric filters using tuning circuits loaded with MEMS and GaAs varactors. The filters show tuning windows up to 3.5% with an unloaded quality factor ranging from 170 to 1220. Similarly in [63], 30% varactor-tuned combline filters were implemented with a quality factor of 173 to 418. Also, a two-pole L-band ferrite-loaded tunable combline filter was introduced in [79] with

41% tunability and a Q_u varies from 1223 to 2425. It can be shortly said that both electrical and magnetic tuning means still need more development to be employed effectively in tunable waveguide filters and compete with the mechanical-based tuning techniques. Many major challenges must be addressed further including the losses, power handling capabilities, and integration complexity.

Given all these aforementioned limitations and challenges of the various state-of-the-art designs, the introduction of more efficient tuning mechanisms and tunable filter structures is thoroughly required. This section presents new tunable filter designs based on our novel *inset* resonator configuration. In addition to their earlier-discussed merits, inset resonators can be employed effectively in designing tunable filters and components with wide, extended frequency tuning capabilities while maintaining a stable Q_u that have only minimal deterioration over the specified tuning range.

In the following, the tunable inset resonator configuration is first introduced and detailed. Then, the design procedure of tunable filters with constant absolute bandwidth (CABW) is discussed, and tunable inset filters are designed and implemented using different realization setups. Measurements are discussed and a detailed comparison with similar state-of-the-art tunable filters is provided with a discussion and followed by a conclusion.

3.2.2 Tunable Inset Resonator Configuration and Operating Principle

Structure and Setup

The inset resonator setup is depicted in Fig. 3.25. It comprises a metallic or dielectric resonator inserted partially inside a metallic housing with modified sidewalls (caps). The resonator is positioned within the cavity using a support made of a low-loss material (e.g., Teflon, Rexolite) and has neither electrical nor mechanical contact with the metallic housing. As shown in earlier, the inset resonator configuration has highly desirable advantages in comparison with the conventional half-wavelength and combline structures, including more compactness, better spurious performance, and comparably high Q-factor with the best Q_u/volume ratio. As can be seen in Fig. 3.26, the inset resonator initially operates using the fundamental TM-mode with a half-wave field distribution similar to the conventional $\lambda/2$ structures. Here, due to the capacitive load at both cap-ends, the length of the resonator can be shortened substantially (i.e., >50%). The dominant magnetic field is mainly resonating in the

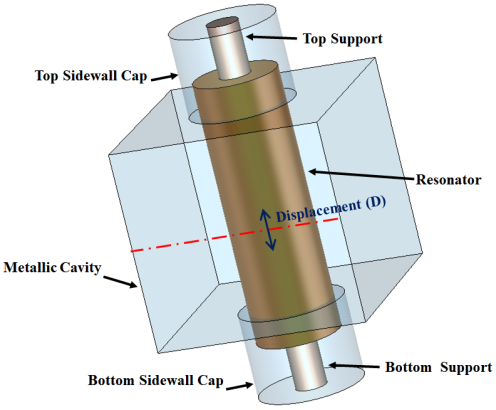

Figure 3.25: Perspective view of the inset resonator configuration. Tunable responses are obtained through the displacement of the movable resonator inside modified parts of the cavity (caps). The resonant frequency is the lowest when the resonator in centred (D=0) and increases gradually when $|D| > 0$.

middle, while the electric field is maximum at the ends of the resonator and minimum in the middle. Accordingly, the current density is minimum at the ends of the resonator and a relatively low current density is present along the housing sidewalls. This advantageously results in a higher Q-factor for the overall resonator assembly. Furthermore, the sidewall caps are designed to contain the lowest field intensities, therefore, the high Q-factor can be maintained even when there is a close proximity between the resonator and sidewall caps. It is also worth mentioning that in addition to the configuration in Fig. 3.25, other shapes of resonators and sidewall caps can be used (e.g., conical), and alternative arrangements can be realized following the same concept of the design but have different performance characteristics [143].

Operation Principle

By looking back at the available literature, it can be concluded that there are three major challenges that tunable filter designers are concerned with:

• how to design compact tunable structures that are able to provide wide tuning ranges,

• how to have a tunable structure without the need for auxiliary tuning elements (e.g., screws, disks),

and

• how to maintain a high, yet stable quality factor with minimum variation over a wide window of frequencies.

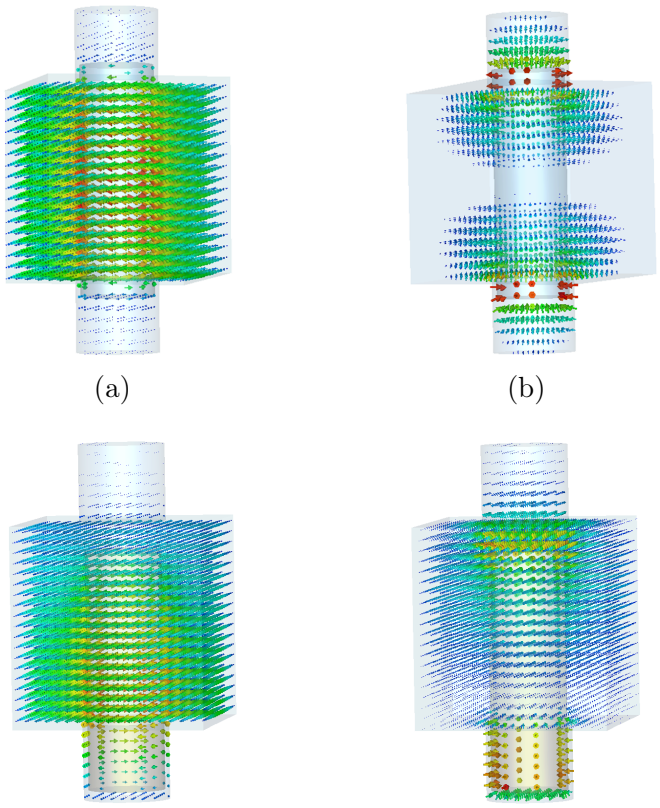

Figure 3.26: Fields distribution inside the inset resonator at the extreme ends of the tuning range. (a) H-field, (b) E-field at the lowest tuning state. (c) H-field, (d) E-field at the highest tuning state.

Through the proposal of the tunable inset resonator structure, we aim to provide a tuning mechanism that covers these stringent requirements efficiently. Fig. 3.27 shows a tunable inset resonator and its simplified equivalent circuit. The tuning principle is based on the displacement of the resonator to change the resonant frequency while maintaining high Q-factor without the need for additional tuning means. When the resonator is centered: this is the reference (fixed) case where the resonant frequency is the lowest. Here, the resonant frequency (f_r) can be calculated based on the corresponding inductance (L_{ph}) and total equivalent capacitance (C_T) using:

$$f_r \approx \frac{1}{2 \cdot \pi \cdot \sqrt{L_{ph} \cdot C_T}} \tag{3.16}$$

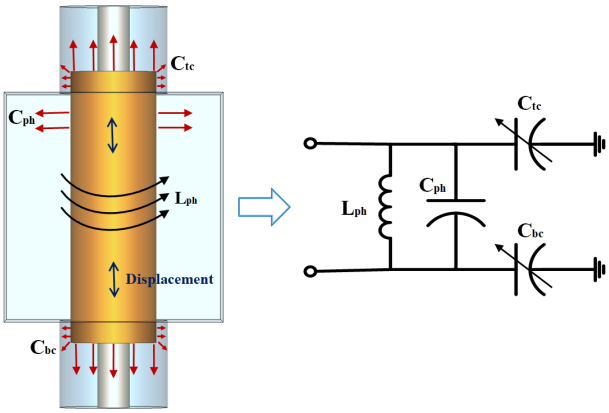

Figure 3.27: Tunable inset resonator and its simplified equivalent circuit.

Where C_T comprises three main components: the capacitance between the movable inset resonator and (a) the housing (C_{ph}), (b) the top sidewall cap (C_{tc}), and (c) the bottom sidewall cap (C_{bc}):

$$C_T \approx C_{ph} + (C_{tc} \parallel C_{bc}) \tag{3.17}$$

Then, the tunable resonant frequency of the inset resonator can be re-expressed as:

$$f_r \approx \frac{1}{2 \cdot \pi \cdot \sqrt{L_{ph} \cdot (C_{ph} + (\frac{C_{tc} \cdot C_{bc}}{C_{tc} + C_{bc}}))}} \tag{3.18}$$

Moving the resonator up or down will displace it away from one sidewall cap and closer to the other sidewall end. When the resonator moves downwards, C_{tc} will decrease and the resonant frequency will move upwards with reference to the top sidewall and also, simultaneously shift down with reference to the bottom side (C_{bc} tends to increase). In general, this is correct, but due to the fact that the contained EM fields in the sidewall caps are minimal, the up-shift in the frequency caused by the displacement away from the top sidewall (C_{tc} decrease) is larger than the frequency down-shift caused by the displacement towards the opposite side inside the bottom cap (the increase due C_{bc} is comparably small and negligible). Therefore, the net result is that the resonant frequency is always shifted upwards to higher frequencies when compared to its center (fixed) state. As previously mentioned, the sidewall caps are designed to have the lowest field densities. When considering the rapid decay of the EM fields, this allows designers to increase the inset-cap heights, providing further room for the movement of the resonators (hence, more tuning can be obtained) without causing any change

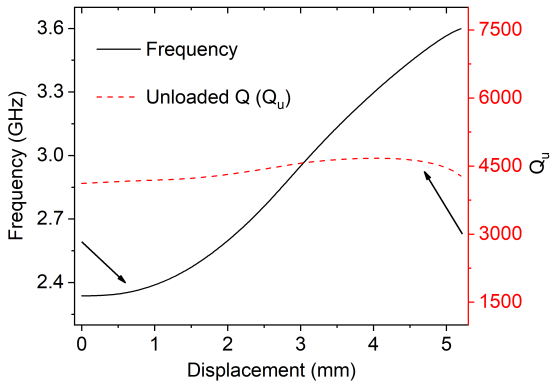

Figure 3.28: Operating frequency and unloaded Q-factor in relation to the resonator displacement over the range of D=0 mm - 5.2 mm.

in the reference (lowest) resonant frequency (C_{tc} and C_{bc} are fixed). Besides, since there are a small amount of fields in the caps' areas, this also means that the Q-factor will not be much affected by the tuning process, unlike what happens in most of the conventional tuning concepts. With reference to Fig. 3.26, the EM fields resonate as half-wavelength waves at the lower tuning states where the resonator is inserted partially at both sidewall caps. Then, the distribution of fields becomes more similar to the combline configuration at the higher tuning states where the resonator is more displaced from the first top sidewall and inserted only in the second bottom sidewall cap. Here, the electric field propagates mainly in the vicinity between the first sidewall and the resonator. In these quasi-combline cases, the Q-factor should remain stable as the resonator is not close to the top side of the housing. Another key advantage of the proposed configuration is that there is no requirement for electrical contact to the metallic cavity, contrary to the combline-based tuning concepts where excellent electrical contact is required, otherwise, both the tuning capabilities and the Q-factor will severely deteriorate.

To validate the above claims of the inset-type tuning concept, a single inset resonator example is investigated using the Eigen-mode solver in CST Microwave Studio and then manufactured and measured. Copper metal is considered in simulation for the metallic housing and resonator (electrical conductivity $\sigma = 5.8 \times 10^7$ S/m). The corresponding dimensions in (mm) are: cavity height = 15, cavity width = 30, cavity length = 30, resonator height = 20, resonator outer diameter = 10, resonator inner diameter = 3, caps height = 8, caps diameter = 11. Fig. 3.28 demonstrates the simulated frequency and unloaded Q-factor in relation to the resonator displacement. As

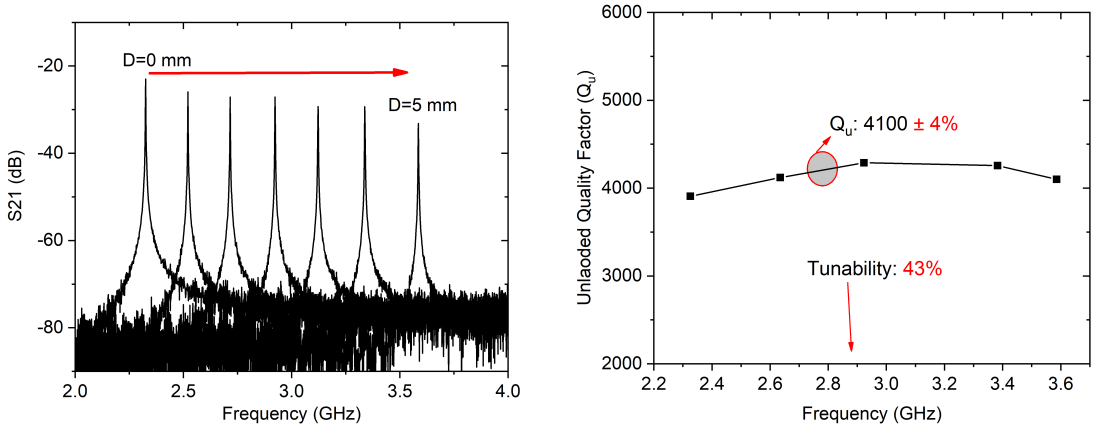

(a) (b)

Figure 3.29: Measured results of the tunable inset resonator. (a) The tuned response over D = 0 mm - 5.0 mm. and (b) Relationship between the measured Q_u of the tunable inset resonator and the tuning window of operating frequencies.

shown, the frequency is reconfigured from 2.3 GHz (D=0) to 3.6 GHz (D=5.2 mm), providing a wide tunability of 44%. Additionally, the configuration has maintained a high Q_u of 4400±6.5% with minimum variation throughout the tuning window. To confirm the concept and simulation results, the tuning capabilities of the prototype in Fig. 3.11 are measured as depicted in Fig. 3.29. The results demonstrate a wide frequency tuning range of 43% from 2.32 GHz to 3.59 GHz, and a stable Q_u of 4100±4% across the whole tuning window. These excellent results confidently validate the proposed tuning mechanism of the inset-type resonators in designing high-performance tunable filters and components. In the following subsection, the design procedure of constant bandwidth frequency tunable filters is explained, and different tunable inset filters are designed.

3.2.3 Tunable Inset Filters

Design Procedure of Tunable Filters with Constant Absolute Bandwidth

In frequency tunable filters, it is essential to maintain a constant operation bandwidth at all different frequencies within the tuning window. However, this is not easy in practice, especially when designing tunable filters with relatively wide tuning ranges (i.e., tunability >20%). To maintain a constant bandwidth response, the variation of physical inter-resonator couplings $(K_{i,j})$ and input-output couplings (Q_e) should be adjusted and balance the change in the centre frequency (f_0) as can be concluded

from:

$$K_{i,j} = \frac{ABW \cdot M_{i,j}}{f_0} \tag{3.19}$$

$$Q_e = \frac{f_0}{ABW \cdot M_{S1}^2} \tag{3.20}$$

where ABW is the absolute bandwidth, M_{S1} and $M_{i,j}$ are the normalized coupling values, which are fixed at all frequency tuning states. Accordingly, similar to [14], the design procedure of constant bandwidth tunable filters can be formulated in three main steps as follows:

a) Extract the corresponding coupling matrix using the standard synthesis method [129] based on the desired ABW and other specifications.

b) From (3.19), and taking into account that ABW and $M_{i,j}$ are fixed and known from (a), the following relation must be satisfied for the required physical inter-resonator couplings ($K_{i,j}$) at every given frequency *(f_n)* in the tuning range:

$$K_{i,j} \cdot f_n = constant = ABW \cdot M_{i,j} \tag{3.21}$$

where the required $K_{i,j}$ is realized through the iris sections between the adjacent resonators and can be calculated as described in [129] using:

$$K_{i,j} = \frac{f_2^2 - f_1^2}{f_2^2 + f_1^2} \tag{3.22}$$

c) For the required input-output couplings of the CABW tunable filter: the external quality factor *(Q_e)* can be expressed in terms of the peak reflection group delay ($T_{\mathrm{d}}(n)$) as:

$$Q_e = \frac{f_n}{ABW \cdot M_{S1}^2} = \frac{\pi \cdot f_n \cdot T_d(n)}{2} \tag{3.23}$$

We can then extract that:

$$T_d(n) = constant = \frac{2}{\pi \cdot ABW \cdot M_{S1}^2} \tag{3.24}$$

where ABW and M_{S1} are fixed for all tuning states and known from *step (a)*. Accordingly, the reflection group delay should be adjusted through the input feeding structure (can be extracted as explained in [129]) in order to obtain constant BWs at

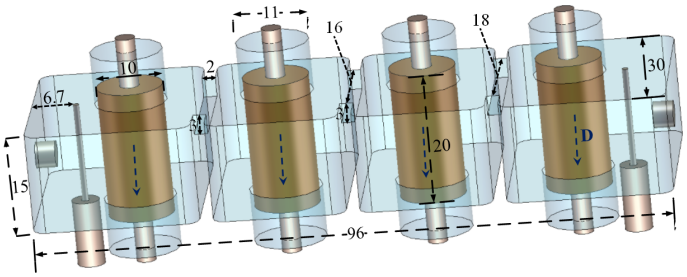

Figure 3.30: 3D view of the proposed four-pole tunable inset BPF. The direction of resonators' displacement D is downwards. All dimensions are in mm unit.

all tuning states.

In the following, two constant bandwidth tunable inset filters are designed based on this procedure and then implemented with two different possible control mechanisms; manually and automated motor-based setups.

Manually Tunable Inset Filter

Fig. 3.30 shows a perspective view of a four-pole inset filter. In this design, the required specifications include a wide tunability of 43% from 2.54 GHz to 3.94 GHz and a constant absolute bandwidth of 108 MHz. The desired coupling matrix is synthesized as:

$$\begin{bmatrix} & S & 1 & 2 & 3 & 4 & L \\ S & 0 & 1.035 & 0 & 0 & 0 & 0 \\ 1 & 1.035 & 0 & 0.91 & 0 & 0 & 0 \\ 2 & 0 & 0.91 & 0 & 0.70 & 0 & 0 \\ 3 & 0 & 0 & 0.70 & 0 & 0.91 & 0 \\ 4 & 0 & 0 & 0 & 0.91 & 0 & 1.035 \\ L & 0 & 0 & 0 & 0 & 1.035 & 0 \end{bmatrix}. \tag{3.25}$$

Then, the physical inter-resonator couplings must satisfy the following relations from (3.21) for all tuning states of frequency f_n (2.54 GHz – 3.94 GHz):

$$K_{12} \cdot f_n = ABW \cdot m_{12} = 0.108 \times 0.91 = 0.098 \tag{3.26}$$

$$K_{23} \cdot f_n = ABW \cdot m_{23} = 0.108 \times 0.7 = 0.076 \tag{3.27}$$

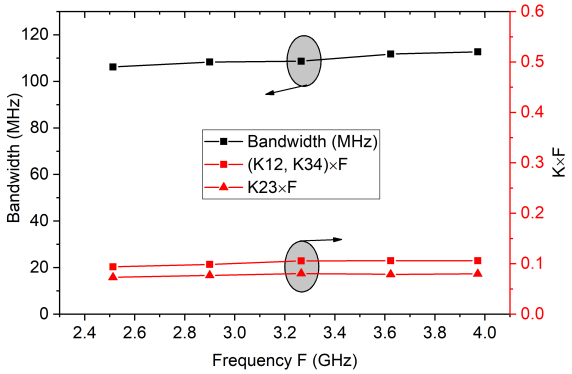

Figure 3.31: Inter-resonator couplings and bandwidth variation in relation to the frequency tuning, realized through the proposed iris structures shown in Fig. 3.30.

Even though further tuning elements can be added to obtain the required inter-resonator couplings (e.g., screws) of various states, this solution is unfavorable, especially in tunable filters, because it makes the tuning process more complex, very slow, and also increases the losses. Alternatively, a more suitable method can be employed is by properly designing the coupling irises to provide balanced inter-resonator couplings and maintain a constant bandwidth throughout [19], [137]. Similarly in this filter, rectangular irises (in Fig. 3.30) have been designed and the corresponding couplings satisfy (3.26) and (3.27), as can be seen in Fig. 3.31. When the filter is tuned to higher frequencies, this accordingly means that the inter-resonator couplings should decrease in a balancing manner to keep the bandwidth constant. Referring to Fig. 3.26, as the resonators are moving downwards, the magnetic field will tend to move towards the bottom of the cavity. Therefore, we positioned the irises at the top of the cavity, so, when the frequency is tuned up, the resonators move down, the magnetic field moves to the bottom, the inter-resonator couplings decrease, and a constant bandwidth can be obtained allover the tuning window.

Similarly, the required peak reflection group delay for a constant ABW can be calculated using (3.24) as:

$$T_d(n) = \frac{2}{\pi \cdot 0.108 \cdot 10^9 \cdot 1.035} = 5.7\ nS \tag{3.28}$$

As shown in Fig. 3.30, the input feeding structure is realized using 0.9 mm inductive wires through coaxial Sub-Miniature (SMA) connectors. Especially for designs with wide tuning ranges, it is convenient to introduce screws to adjust the input and output coupling strengths since only two elements are needed for any filter order. In

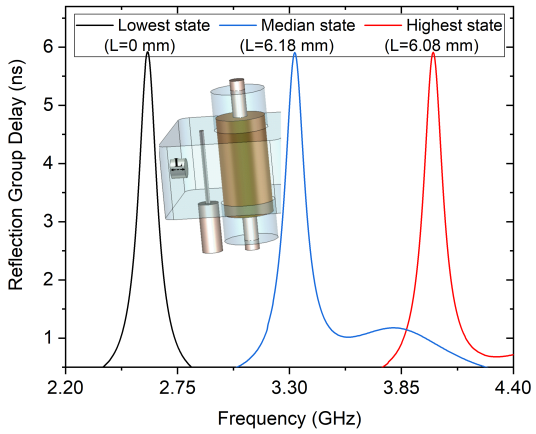

Figure 3.32: Reflection group delay at the lowest, median, and highest tuning states of the filter, realized through the proposed input-feed structure shown in Fig. 3.30.

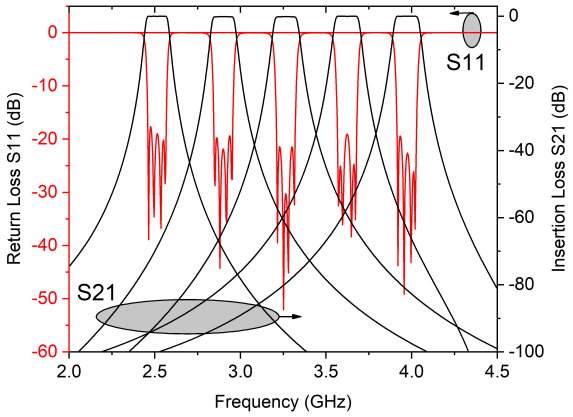

Figure 3.33: Variation of the simulated S-parameters for the 4th-order tunable inset filter. The frequency is tuned from 2.54 GHz - 3.94 GHz with a CABW of 109 MHz ± 3 MHz.

the proposed IO feeding configuration, the IO coupling strength increases with the increase in the tunable frequency (the downwards movement of the inset resonators). Hence, two metallic M3 screws are used to decrease the IO coupling strengths with tuning, and maintain a constant reflection group delay. Fig. 3.32 shows the adjusted reflection group delay at the lowest, median, and highest tuning states, effectively satisfying equation (3.28).

A model of the filter is then designed and optimized. The simulated S-parameter responses are demonstrated in Fig. 3.33 at different tuning states. As shown, the filter meets the desired specifications with a constant absolute bandwidth of 109± 3 MHz and a wide tunability of 43%.

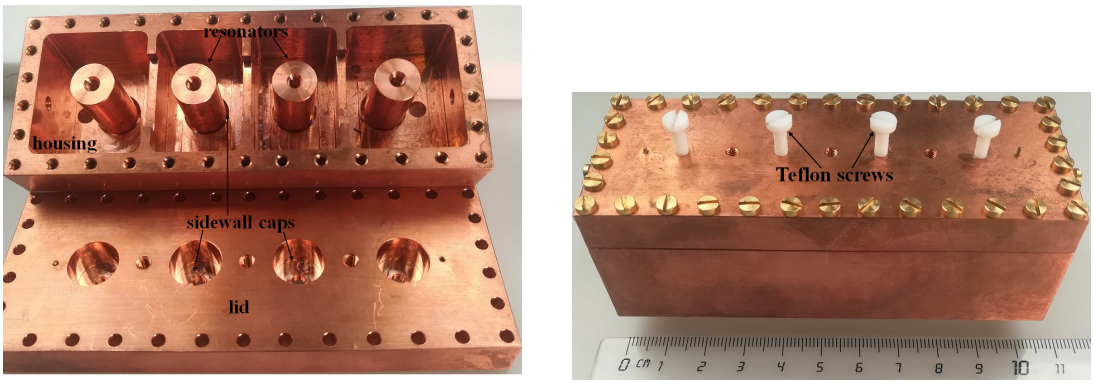

(a) (b)

Figure 3.34: The fabricated four-pole tunable inset filter. (a) Disassembled and (b) assembled.

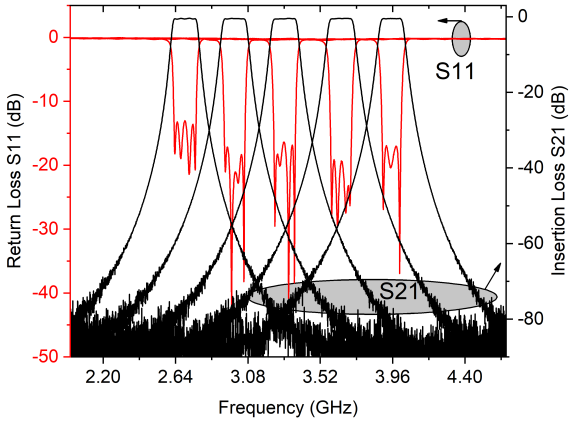

Figure 3.35: Measured S-parameter results of the implemented four-pole tunable inset filter. Frequency range: 2.66 GHz to 3.96 GHz, tunability: 39.3%.

A prototype is then manufactured and assembled as depicted in Fig. 3.34. The filter has a compact volume of 49.28 cm^3. All parts including the resonators were milled using copper metal. 20 mm M3 Teflon screws (dielectric constant = 2.1, loss tangent = 0.0002) were used to control the displacement of the resonators inside the housing. Measurements agree very well with simulations, allowing the design procedure to be verified. The measured S-parameter responses in Fig. 3.35 exhibit a 1.3 GHz frequency tuning range from 2.66 GHz to 3.96 GHz with constant bandwidth of 116 MHz±6%, return loss > 13.5 dB, and steady insertion loss averaging at 0.4 dB, as shown in Fig. 3.36. This resembles a stable Q-factor of 1820±6% throughout the 39.3% tuning window. This Q-factor corresponds to around 50% of simulated version and can be enhanced further by silver plating, similar to the earlier presented

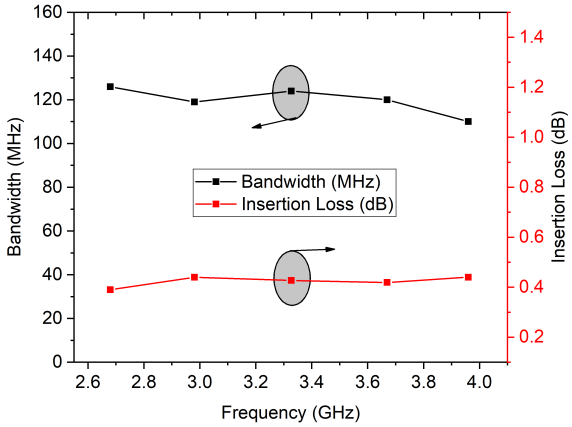

Figure 3.36: Measured bandwidth (116 MHz±6%) and insertion loss response (0.39 dB - 0.44 dB) over the frequency tuning window.

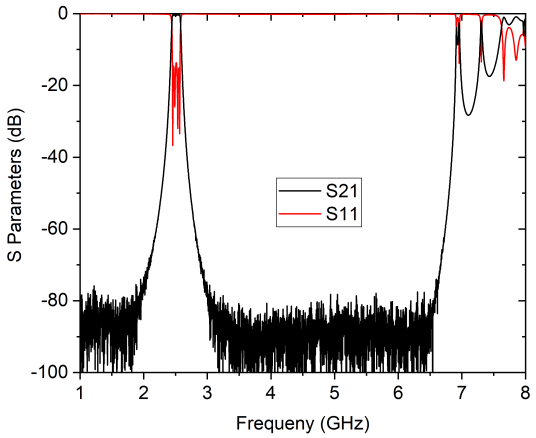

Figure 3.37: Measured wideband response of the proposed four-pole inset filter's S-parameters.

resonator prototype. Furthermore, the filter has a wide spurious-free rejection band of more than 4.3 GHz, as shown in Fig. 3.37. It can be noted that each of these responses was obtained effectively without the use of any tuning screws (including the IO tuners), advantageously featuring easier and faster tuning process which tracks across a wide frequency range.

Besides the presented inline all-pole filter, folded structures can be designed for the realization of cross-couplings which create transmission zeros that improve the rejection characteristics. For example, Fig. 3.38 demonstrates a fourth-order tunable inset filter in a quadruplet configuration with an alternative 2 mm input-feed setup to the one detailed in Fig. 3.30, and a capacitive probe between the source and the load to create two transmission zeros around the passband. The filter is designed similar to

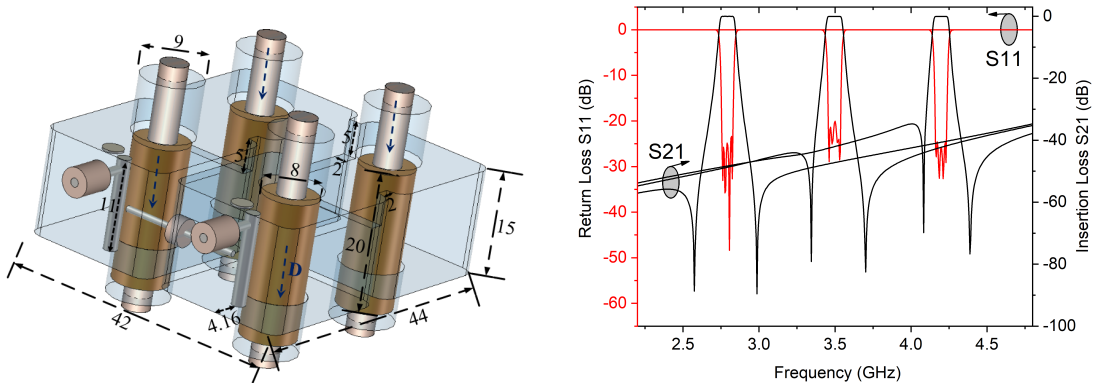

(a) (b)

Figure 3.38: (a) 3D view of a folded four-pole tunable inset BPF. The direction of resonators' displacement D is downwards. All dimensions are in mm unit. (b) Variation of the simulated S-parameters for the 4-pole tunable quadruplet inset filter. The frequency is tuned from 2.8 GHz - 4.2 GHz with a CABW of 77 MHz ± 3 MHz.

the earlier example and has a tuning range of 1.4 GHz and operates from 2.8 GHz to 4.2 GHz with a constant bandwidth of 77 MHz ±3 MHz, as exhibited in Fig. 3.38(b). The measured tunable responses of the fabricated prototype are provided in Fig. 3.39, whereas the fixed version of the filter was presented earlier in the above section (see Fig. 3.17 - Fig. 3.19).

Beside the use of metallic inset resonators, tunable inset filters can be designed also using dielectric resonator to feature higher Q-factor results. For example, Fig. 3.40 shows a tunable CABW inset filter using low-loss dielectric Alumina resonators (Dk = 9.8, loss tangent = 0.0001), with frequency tuning range from 4.6 GHz to 5.9 GHz, a CABW of 65±5% MHz, and stable high-Q of 3500±7%. It should be remarked that designers need to carefully consider the spurious resonances when using dielectric resonators, especially those with high Dk, as they might limit the tuning range if they were close to the desired tuning band.

Automatically Tunable Inset Filter

In future flexible telecommunication systems (e.g., next generation satellites), the frequency bands must be remotely and automatically adjustable. Therefore, it is important to present tunable filter designs with efficient tuning techniques suitable for remote tuning. The tuning mechanism should be stable, fast, and have a long-life of usage. Unfortunately, the available motorized screw-based tunable filters like [136] and [17] always need special arrangements for good electrical contact between the tun-

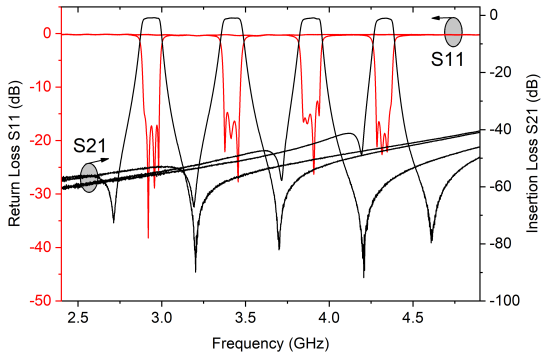

Figure 3.39: Measured S-parameter results of the fourth-order quasi-elliptic CABW tunable inset filter.

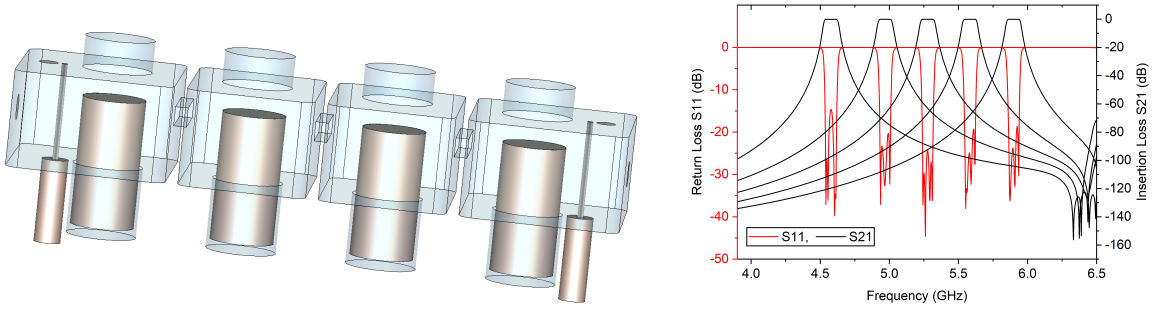

(a) (b)

Figure 3.40: (a) 3D structure, and (b) tunable responses of a 4-pole dielectric inset filter.

ing elements and metallic housing in order to reduce the loss and prevent the leakage of radiation. This results in complex and unstable structures, having a short-life with increased losses. In contrast, the proposed contact-less inset resonator tuning concept effectively overcomes all these drawbacks and can be efficiently employed in remotely tunable designs. To validate this, a 3-pole tunable inset filter (Fig. 3.41) is designed and implemented in this section using pizomotors. The filter is designed to operate from 2.54 GHz to 3.96 GHz with a CABW of 102 MHz and a tunability of 43%. The design procedure is similar to the presented four-pole example. The required $k_{12} \cdot f_{\mathrm{n}} = 0.11$ and $T_d(n) = 5.5$ nS are calculated and then realized as shown in Fig. 3.42(a) and Fig. 3.42(b), respectively. Then, the filter model is constructed and optimized to provide the required responses. Fig. 3.43 exhibits the simulated S-parameters of the filter satisfying the design specifications with a 43% tunability and a CABW varying from 102 MHz to 91 MHz. Then, a copper prototype is implemented and assembled as depicted in Fig. 3.44 using high-accuracy LL06 piezomotors from PiezoMotor [144].

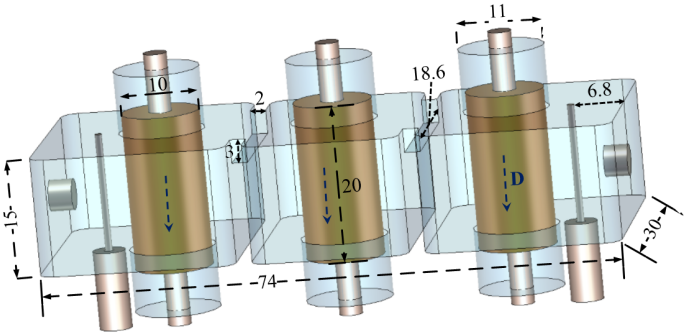

Figure 3.41: 3D view of the proposed 3rd-order tunable inset BPF. The direction of resonators' displacement D is downwards. All dimensions are in mm unit.

The filter has a compact size of 37.86 cm^3. A 3D-printed fixture is manufactured to properly hold the piezomotors. Here, the Teflon screws are used as posts which results in a smoother and faster tuning process, in addition to the longer usage life than the manual screw-based tuning where the Teflon material corrodes easily. The measured S-parameter responses of the fabricated filter are demonstrated in Fig. 3.45 with good agreement to the simulations. The filter is tuned over a 1.3 GHz window from 2.65 GHz to 3.95 GHz with a constant bandwidth of 114 MHz±8%. The filter features a return loss > 15 dB, and a stable insertion loss from 0.26 dB to 0.35 dB as presented in Fig. 3.46. Furthermore, the proposed filter has a good spurious performance better than $2.8 \cdot f_0$ as shown in Fig. 3.47.

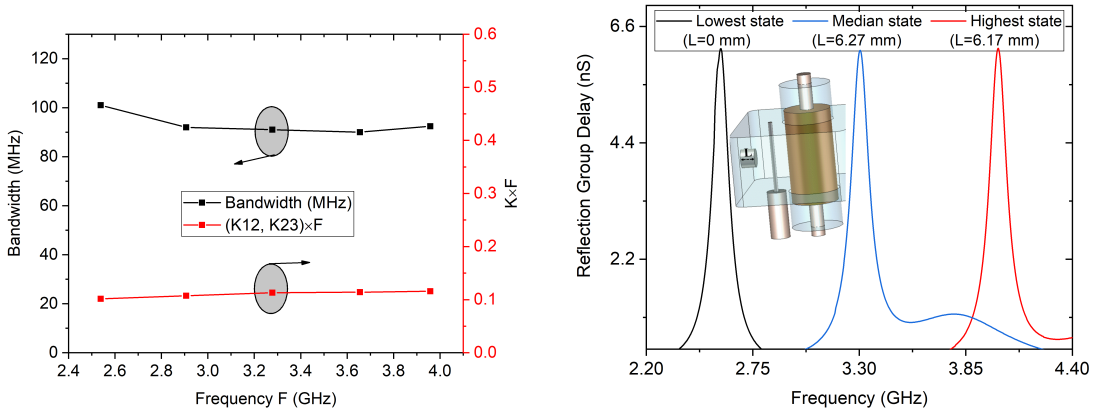

(a) (b)

Figure 3.42: (a) Inter-resonator couplings and bandwidth variation in relation to the frequency tuning, realized through the proposed iris structures in Fig. 3.41. (b) Reflection group delay at the lowest, median, and highest tuning states of the filter, realized through the proposed input-feed structure shown in Fig. 3.41.

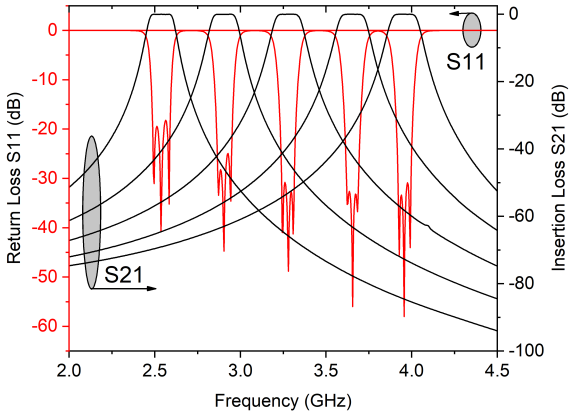

Figure 3.43: Variation of the simulated S-parameters for the three-pole tunable inset filter. The frequency is tuned from 2.54 GHz - 3.96 GHz with a CABW of 96.5 MHz ± 5.7%.

3.2.4 State-of-the-art Comparison

Table 3.3 summarizes a comparison of the presented tunable inset structures with similar CABW tunable loaded-waveguide filters available in the literature. As can be seen, the tunable inset components show very competitive results including the distinctive wider tuning ranges than the other designs, and demonstrate high-Q measurements with stable performance throughout the window of tuning. In addition to these highly desirable merits, the inset components also offer more volume-saving and enhanced spurious performance (up to $3.8 \cdot f_0$). The proposed inset filters eliminate the need for any auxiliary tuning components which advantageously increases the tuning speed, reduces the losses, weight, cost, and the complexity of the tuning process. The filters have N tuning elements (which are the movable coaxial inset resonators) with two (optional) tuning elements for adjusting the IO coupling. Additionally, a mechanism of tuning using a single element can be adopted effectively using similar setups to [145] and [146], with more design effort needed for the required IO coupling, and maybe sacrificing some of the tuning range. With regard to the number of tuning elements, while we can see that the majority of designs need N independent tuning elements, the filters of [19], [5], and [137], interestingly, have a single tuning element. This provides a fast tuning feature at one side, but on the other hand, it is challenging to sustain stable and well-matched responses for the different states

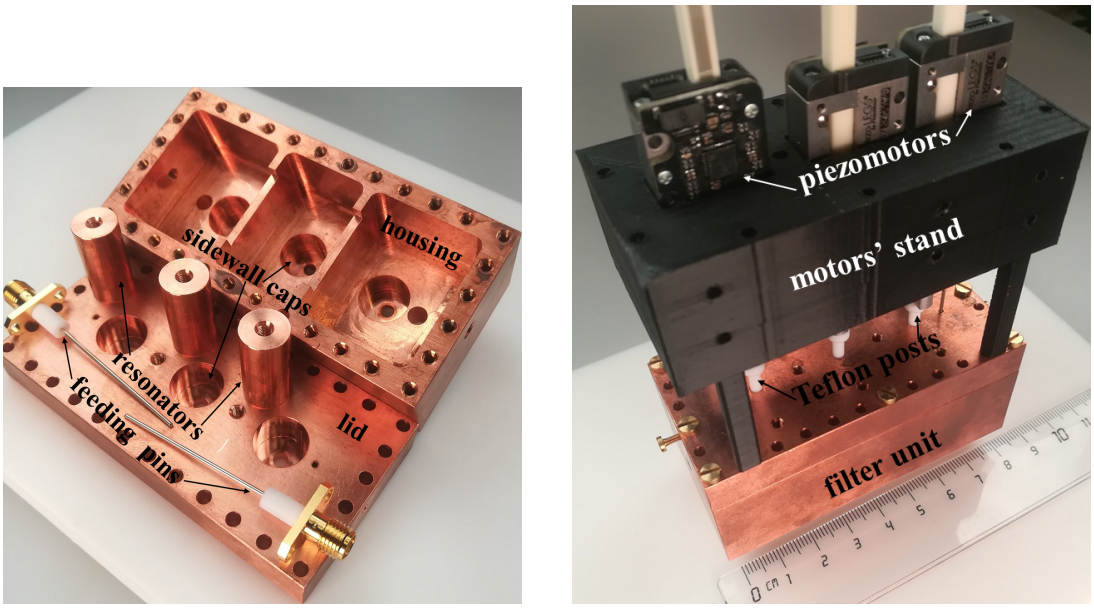

(a) (b)

Figure 3.44: The fabricated four-pole tunable inset filter. (a) Disassembled, and (b) assembled.

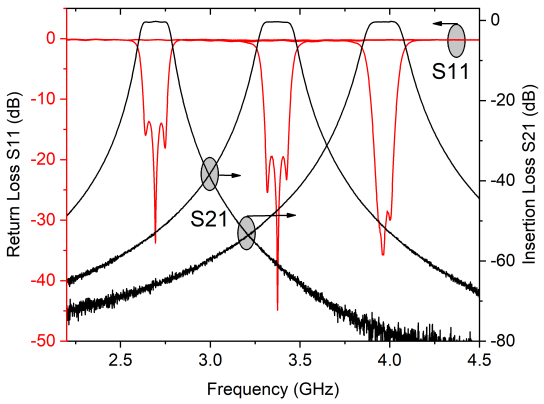

Figure 3.45: Measured S-parameter results of the third-order tunable inset filter. Frequency range: 2.65 GHz to 3.95 GHz, tunability: 39.4%.

in the tuning window. Therefore, for practical applications, many designers would prefer to have independent frequency tuning elements (N), unless there is a specific need for a faster tuning process. Another comparison aspect between the different state-of-the-art designs is the tuning mechanism. For many of the mechanically tunable filters as [136] and [17], it is crucial to have a good electrical contact between the movable tuning elements and the filter cavity. Therefore, additional components are needed (e.g., nuts, elastomer, conductive ball bearings), which results in a re-

duced usage-life, slower tuning speed, and higher loss. Whereas the authors in [5] utilized dielectric tuners to avoid these issues, the proposed inset tuning mechanism uses freely movable contact-less resonators, similar to [19], having no requirement of any electrical contact with the cavity. It can also be noted that dielectric resonators can be used instead of metallic ones, providing more volume-saving and enhanced quality factor (see Fig. 3.40 example). This is a currently on-going research activity and will published in a future-coming article.

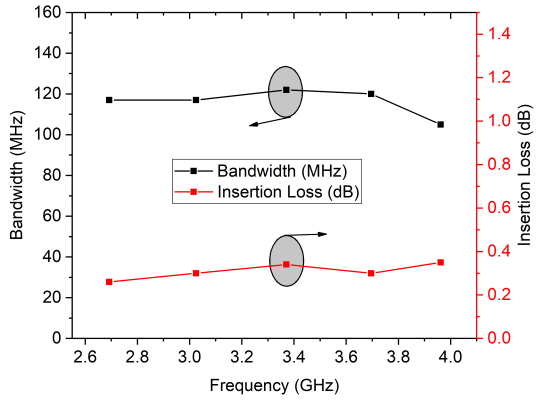

Figure 3.46: Measured bandwidth (114 MHz±8%) and insertion loss response (0.26 dB - 0.35 dB) over the frequency tuning window.

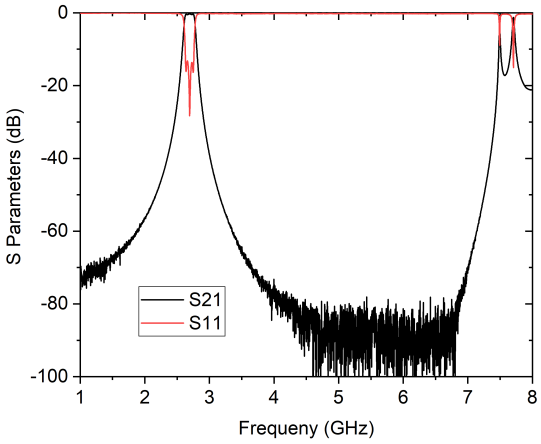

Figure 3.47: Measured wideband response of the propose 3rd-order inset filter's S-parameters.

Table 3.3:
Comparison of the Proposed Tunable Inset Filters with Similar State-of-The-Art Designs.

Ref.	**Structure**	**f (GHz)**	**Order**	**Tunability (%)**	**ABW (MHz)**	**IL (dB)**	**Q-factor**	**Volume (cm^3)**	**Q-factor/ Volume (cm^{-3})**	#
[19]	Half-wavelength	2.275-2.775	4	19.8%	106.5±9%	< 0.4	$> 4850^{\ddagger}$	275.65	$> 17.6^{\ddagger}$	1
[136]	Combline-dual-post	9.15-10.87	4	17.2%	230±3.9%	< 0.6	1500	NA	NA	2N
[5]	Combline	1.81-2.17	5	18.1%	25	< 1.8	2000-2500	NA	NA	1
[27]	Dielectric-TE	15.6-16	3	2.5%	150	1.5-4.5	$421\text{-}1630^{\dagger}$	NA	NA	N
[17]	Combline	2.565-2.634	6	2.7%	NA	0.9-2.3	$2252\text{-}2914^{\dagger}$	NA	NA	N
[26]	Dielectric-combline	4.97-5.22	4	4.9%	66±1.5%	3.3-4.9	536-548	NA	NA	N
[137]	Combline	0.68-0.76	4	11.1%	11.2±8.9%	0.8-0.9	$> 5800^{\ddagger}$	2291.625	$> 2.53^{\ddagger}$	1
[141]	Dual-mode dielectric-TM	4.72-5.51	2	15.4%	50±10%	0.2-0.9	540-1100	3.456	318.29	N/2
[63]	Combline	0.707-0.963	3	30.7%	27.5±2.5%	1.58-3.97	173-418	94.067	4.44	N
This work-1	Inset	2.32-3.59	-	43%	-	-	4100±4%	15.02	283.89	-
This work-2	Inset	2.65-3.95	3	39.4%	114±8%	0.26-0.35	1660±6.6%	37.86	46.74	N+2
This work-3	Inset	2.66-3.96	4	39.3%	116±6%	0.39-0.44	1820±6%	49.28	39.15	N+2

‡Based on simulated Q-factor. †Based on the measurements of a single-cavity resonator. N represents the filter order. #: Number of tuning elements.

3.3 Summary

• The design and analysis of a novel inset resonator configuration are presented in the first section of this chapter for coaxial filter applications. The inset configuration has several desirable characteristics including the miniaturized size, high-quality factor, ability to handle relatively high levels of power, and very good spurious performance ($>3\cdot f_0$). Furthermore, the inset resonator structure has a distinct feature of *self-tuning* without the need for any auxiliary tuning elements, attributing stable high-Q performance with minimum variation. Different coaxial inset filters are reported using planar and longitudinal coupling configurations with the capability of obtaining quasi-elliptic responses in inline structures and flexible control of transmission zeros.

All these competitive merits promote the new inset configuration in a wide range of coaxial filter applications (e.g., cellular base stations and tunable filters).

• This chapter also presented in its second part a new tuning technique and several tunable coaxial filters based on novel compact inset resonators. The operation principle is explained and a tunable inset resonator structure is implemented for proof-of-concept. The measured results demonstrate a wide tuning range of 43% with a stable Q-factor of 4100±4% and a wide spurious-free band up to $3.8 \cdot f_0$. A design procedure for constant bandwidth tunable filters was introduced, and two widely tunable inset filters were designed, manufactured, and measured. A manually tunable four-pole inset filter was presented featuring a frequency tuning range of 39.3%, a CABW of 116 MHz±6%, and a Q-factor of 1820±6%. Also, an automatically tunable three-pole inset filter was built to incorporate piezomotors for highly accurate and remote tuning. Similarly, the filter is demonstrated with a 1.3 GHz tuning window over the range of 2.65 GHz to 3.95 GHz with a CABW of 114 MHz±8% and a stable Q-factor of 1660±6.6% throughout the tuning window. In comparison with all available state-of-the-art loaded-waveguide CABW tunable filters demonstrated in the literature, the presented tunable inset filters provide the widest tuning ranges and the most stable performance in Q-factor. These distinctive advantages, in addition to the added benefit of compact structures and excellent spurious performance, strongly promote the proposed tuning concept for a wide range of high-performance tunable filter applications.

Chapter 4

Widely Tunable TM-Mode Dielectric Filters With Constant Absolute Bandwidth Using Re-Entrant Caps

This chapter reports on octave tunable dielectric combline bandpass filters with constant absolute bandwidth (CABW) using a novel *re-entrant cap* tuning technique. The resonant frequency is tuned by a hollow re-entrant cap penetrating into the filter cavity as an envelope around the dielectric resonator. This mechanism of tuning provides wider tuning capabilities and better spurious performance than the conventional screw-based tuning. Also, the cap tuners can be employed effectively to tune the input-output and inter-resonator couplings simultaneously with the frequency reconfiguration, enabling a CABW over a wide frequency tuning window. For proof of concept purposes, a single widely tunable resonator is presented with octave tuning ratio of 2.64:1, high quality factor from 1705 to 5480, and spurious-free band up to $3.44 \cdot f_0$. Afterwards, two octave tunable re-entrant cap filters are designed, fabricated, and tested. The first filter is a 78% widely tunable two-pole filter with a CABW of 43.5±12% MHz, low insertion loss equals to 0.28±0.03 dB, and a compact volume of 39 cm^3. The second design is a four-pole octave tunable bandpass filter from 2.96 GHz to 1.36 GHz with a constant 69±13% MHz bandwidth, low insertion loss better than 0.6 dB, return loss higher than 16 dB, and a compact 62 cm^3 structure. According to our own knowledge, thanks to the proposed tuning mechanism, the presented designs are the first CABW octave tunable high-Q waveguide-based filters, having the widest tuning ranges over all similar state-of-the-art-designs.

4.1 Introduction

Tunable RF filters are expected to play a crucial role in many evolving frequency-agile applications including multi-band cellular base stations and flexible satellite payloads [147, 16, 148, 28]. However, to replace the current fixed filter banks, tunable filters must provide similar capabilities fulfilling the stringent requirements of the various frequency-adaptable applications. With regard to this, the achievable tuning range and the ability to maintain a constant absolute bandwidth are two challenging characteristics of frequency tunable filters in addition to the high quality factor. While many widely tunable planar and evanescent-mode cavity filters were reported in the open literature as [149, 1, 150, 151, 152, 124, 153, 154, 155, 156, 157, 101, 158, 159], few of them were able to maintain constant ABW responses [160, 161, 162, 163, 164, 165, 166, 167, 168, 169]. For example, the authors in [161] introduced a two-pole 25 MHz constant ABW tunable evanescent-mode filter with a 56.5% tuning window and a relatively low quality factor varies from 310 to 225. Also, [164] presented a second-order L-band varactor-tuned microstrip filter with a constant 3-dB bandwidth over a wide 54.2% tuning range. The majority of these designs are based on low-order filters (i.e., 2nd-order). This implies that for higher-order filters, the design of constant ABW will more complicated, and the tuning mechanism associated losses will increase. Consequently, the achievable tuning range will be impacted. Furthermore, planar and evanescent-mode structures are not suitable for high-performance applications of tunable filters due to their low quality factor and limited high-power handling capabilities. On the other hand, CABW reconfigurable filters based on hollow-waveguides suffer from bulky structures and very narrow tuning windows (i.e., $< 5\%$) despite their superior Q-factor and ability to handle high levels of power [28]. For instance, a 4-pole 180 MHz K-band reconfigurable TE_{311} waveguide filter was presented in [12] with 1.74% of frequency tuning and a Q-factor from 3100 to 2600 using dielectric plates. To this end, coaxial and dielectric-loaded waveguides have gained more interest in many tunable filter applications due to their advantages of miniaturized structures, high-Q, and good power handling capabilities [148, 5, 170, 17, 171, 18, 19, 63, 137, 172, 173, 136, 174, 175, 21, 23, 27, 176, 26, 43, 141]. For example, a CABW tunable coaxial filter was reported in [148] for future agile 5G Base Transceiver Stations (BTSs). The filter operates from 942.5 MHz to 737.5 MHz (24.4%) with a CABW of 23 MHz$\pm$8% and a quality factor ranges from 2900 to 2300. Also in [174] and [175], our group recently presented 40% tunable CABW coaxial fil-

ters with the least variation of Q-factor over the tuning window using inset resonators. To provide more compactness and a higher-Q factor than the coaxial filters, a couple of tunable dielectric resonator (DR) filters were proposed [21, 23, 27, 176, 26, 43, 141]. A four-pole 65 MHz C-band tunable dielectric combline filter was reported in [26] with a tuning window of 4.9% and a Q-factor of 548 to 536. Also, [141] introduced a compact tunable dual-mode C-band filter based on TM-mode dielectric resonators. The filter has a tuning range of 15.4% with a CABW of 50 MHz±10% and a Q-factor varies from 1100 to 500. Despite that this group of loaded-waveguide constant ABW tunable filters features good tuning capabilities of up to 40%, the introduction of new designs that cover wider octave tunable ranges and maintain a CABW is still highly desirable.

In [140], we introduced a novel tuning technique for TM-mode dielectric resonators using *re-entrant caps*. In this chapter, widely octave-tunable TM-mode DR filters with constant absolute bandwidth are presented based on re-entrant caps. The proposed tuning mechanism has the key advantages of simple configuration, high-Q, improved spurious performance, and the ability to achieve wide tuning ranges while maintaining constant ABW responses. First, the design requirements of octave tunable CABW filters are discussed. Then, the unique employment of re-entrant caps in widely tunable CABW filters design is detailed and compared with the conventional tuning mechanism using screws. Finally, two BPF examples are designed, implemented, and compared with similar state-of-the-art filters.

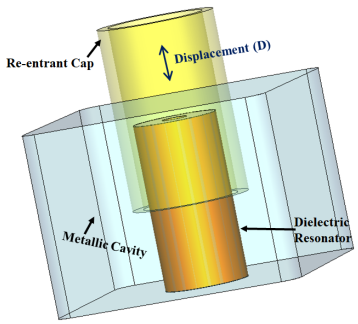

Figure 4.1: Tunable dielectric combline resonator with a re-entrant cap.

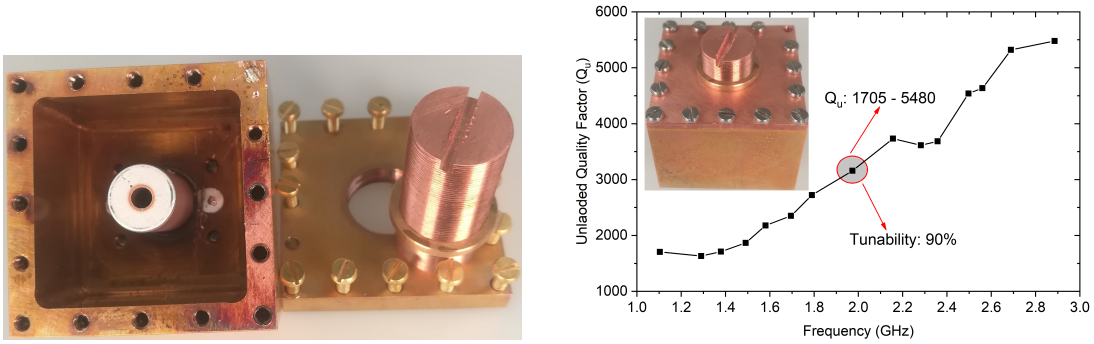

(a) (b)

Figure 4.2: Tunable resonator prototype. (a) Disassembled parts. (b) Measured tunability and unloaded quality factor.

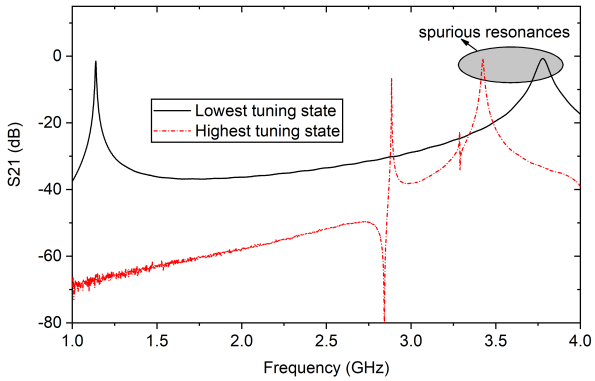

Figure 4.3: Spurious measurements at the lowest and highest tuning frequencies.

4.2 Tuning Concept and Design Principles

4.2.1 Tunable TM-Mode Dielectric Resonator

Fig. 4.1 illustrates a perspective view of TM-mode dielectric resonator with a re-entrant cap for frequency tuning. The chosen configuration is the dielectric combline resonator, which has high quality factor and good spurious performance, combining the merits of the dielectric-loaded resonators and metallic coaxial resonators [129]. The operation mode is the fundamental TM-mode $TM_{01\delta}$ where the E-field is focused in the middle of the resonator and the H-field resonates mainly in the DR surroundings [140]. The movable re-entrant cap tunes the resonant frequency by two means, simultaneously: 1) the part which intrudes the cavity around the DR, and 2) the part outside the cavity which functions as a movable sidewall. As result, wider tuning ranges (i.e., $> 90\%$) can be obtained in comparison with the traditional screw-

based tuning [140]. Besides, the proposed technique has the advantage of improved spurious performance over tuning [140], unlike in the other screw/disk-based designs where unwanted spurious resonances could appear at lower states due to the tuning elements. To verify the aforementioned features, a single resonator prototype is implemented and measured as depicted in Fig. 4.2 and Fig. 4.3, respectively. The TM-mode dielectric resonator (length= 20 mm, inner diameter= 3 mm, outer diameter= 10 mm) has a dielectric constant of 44, and a loss tangent of 4×10^{-5} @ 3.5 GHz. The metallic housing ($30 \times 30 \times 22$ mm^3) and re-entrant cap (length= 21 mm, inner diameter= 11 mm, outer diameter= 14 mm) were milled from copper metal. The DR is soldered in the metallic cavity, and the resonator prototype is then assembled and tested. As can be seen in Fig. 4.2(b), the resonator has a wide 90% octave-tuning window from 2.9 GHz to 1.1 GHz with a high unloaded quality factor ranging from 5480 to 1705. Also, the resonator has a good spurious-free band of 520 MHz at the highest tuning frequency, and improves gradually up to $3.44 \cdot f_0$ at the lowest tuning state, as shown in Fig. 4.3. It is worth mentioning that excellent electrical contact is always needed between the re-entrant cap and the cavity (e.g., using nuts), similar to the screw/disk-based designs. Besides, it is advised to have a relatively thin contact area to reduce the related losses (e.g., the chosen lid thickness here is 2 mm). Alternatively, the designer can use dielectric caps where no electrical contact is required, however, at the cost of narrower tuning ranges.

4.2.2 Design Guidelines of Octave Tunable Filters With Constant Absolute Bandwidth

It is known from chapter 3 ([175]) that the physical inter-resonator (IR) and input-output (IO) couplings should also change with the frequency tuning to maintain a constant ABW and a stable return loss level. In practice, keeping this harmony is a very challenging task, especially for broad tuning ranges. This is mainly because the design process and IR/IO tuning elements' capabilities (e.g., varactor diode capacitance, tuning screw penetration) cannot cover such wide ranges of required coupling variations. For this reason, we can see that the majority of CABW tunable filters cannot provide octave tunable ranges (tuning ratio $\geq$ 2:1), while the few reported octave tunable filters are not able to maintain a CABW allover the operation frequencies. To overcome these limitations and enable octave frequency tuning with CABW, the solution is by employing the frequency tuning elements to also tune the

IR and IO couplings in a way that the required IR and IO couplings to maintain a CABW can be obtained with (or without) the IR and IO tuning elements. In most of the available tuning techniques, when the frequency is tuned downwards, the IR and IO couplings will either decrease or remain fixed. Therefore, the IR and IO tuners cannot provide the required coupling over a wide range, and the ABW becomes narrower with the frequency tuning as can be noticed in [151] and [157], for example. Contrary, in the proposed re-entrant cap tuning technique, when the caps intrude the filter housing, they mainly cut the E-field in the area around the resonators (close to the irises and IO feeding structure), resulting in an increase in the (magnetic) IO and IR couplings. This advantageously reduces the required coupling adjustment for a CABW, allowing the desired IR and IO couplings to be obtained effectively over a wide tuning window. In the following section, a second-order CABW octave-tunable BPF is designed using the proposed tuning mechanism, and compared with another design using the conventional tuning screws.

4.3 Tunable CABW Two-Pole Bandpass Filter: Re-Entrant Caps Vs. Tuning Screws

To validate to proposed tuning concept, a two-pole bandpass filter is designed and tuned over a wide frequency span using re-entrant caps and tuning screws for comparison, as presented in Fig. 4.4 and Fig. 4.5, respectively. First, both filters are designed at 2.67 GHz with 20-dB bandwidth of 42.3 MHz. The required physical inter-resonator coupling (K_{12}) for both filters is realized using a simple inductive iris,

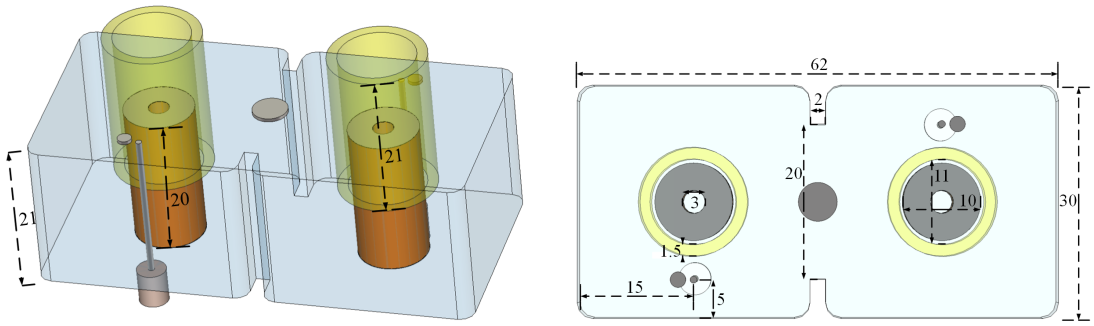

(a) (b)

Figure 4.4: Second-order tunable dielectric combline filter using re-entrant caps. (a) Perspective view. (b) Top view. All dimensions in mm unit.

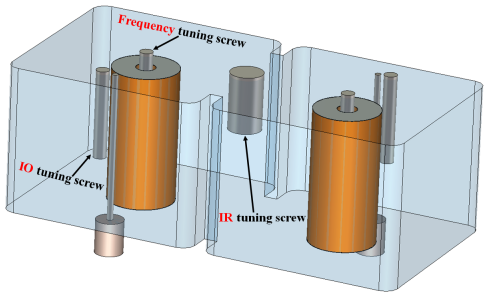

Figure 4.5: Second-order tunable dielectric combline filter using tuning screws. All dimensions are similar to the first filter except the cavity height= 22.1 mm, and iris width= 19.7 mm.

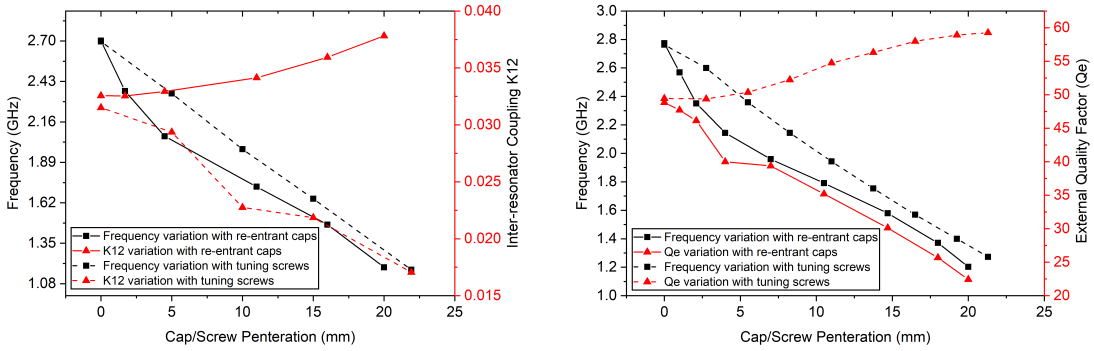

(a) (b)

Figure 4.6: Resonant frequency and (a) physical inter-resonator coupling variation, (b) external quality factor change of the presented two-pole filters with respect to the frequency tuning elements displacement.

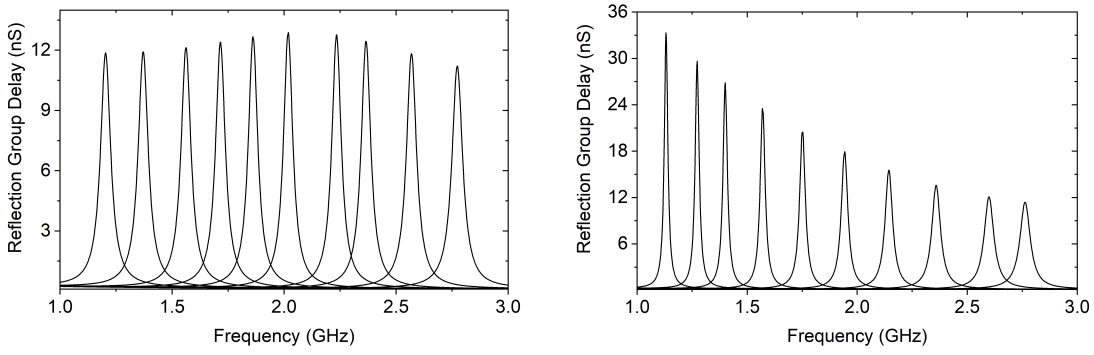

(a) (b)

Figure 4.7: Peak reflection group delay over the frequency tuning window of the designed two-pole tunable filters: (a) With re-entrant cap tuners, (b) with tuning screws.

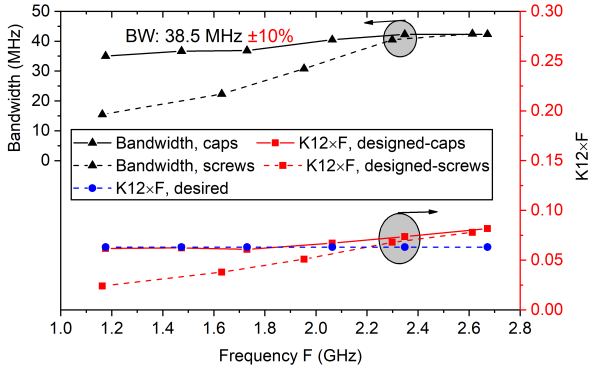

Figure 4.8: Inter-resonator couplings and bandwidth variation in relation to the frequency tuning for the two-pole tunable filter with re-entrant caps (Fig. 4.4) and tuning screws (Fig. 4.5).

while the IO feeding is obtained using an inductive loop wire. Initially, we investigated the variation in the IR and IO couplings due to the frequency tuning elements of both designs (caps and screws) as depicted in Fig. 4.6(a) and Fig. 4.6(b), respectively. As can be seen in Fig. 4.6(a), the IR coupling (K_{12}) increases with the frequency decrease when using re-entrant cap tuners, whereas it decreases with frequency when using screws to tune the operation frequency. Similarly, in Fig. 4.6(b), we can see that the IO coupling strength (represented in form of external quality factor) increases with the frequency tuning in the re-entrant cap example, while it decreases with the frequency decrease in the tuning screws design. These observations of the IR and IO couplings confirm the proposed tuning mechanism and allow the design

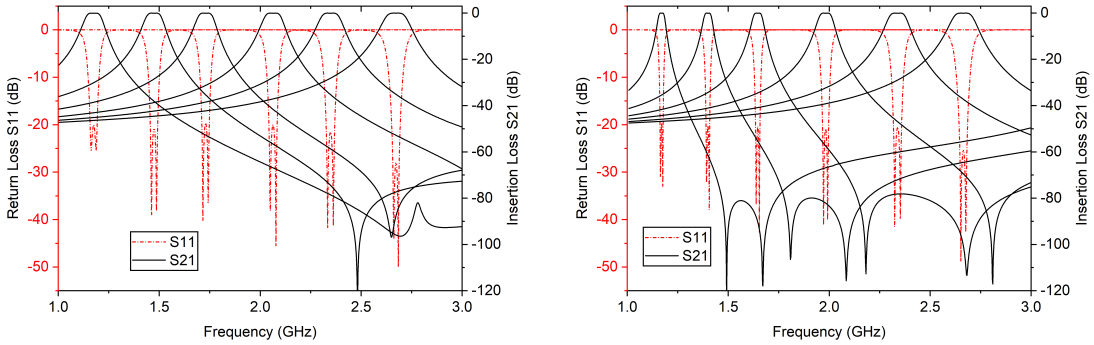

Figure 4.9: (a) Simulated S-parameters of the two-pole re-entrant cap widely tunable BPF. Tuning ratio: 2.28:1, 20-dB CABW: 38.5 MHz±10%. (b) Simulated results of the two-pole screws-based tunable filter. Tuning ratio: 2.28:1, 20-dB BW: varies from 42.3 MHz to 15.5 MHz.

of re-entrant cap frequency tunable filters while maintaining a CABW over a wider tuning range than the conventional tuning screws. It is also worth to remark that tuning disks generally behave similarly to the tuning screws. Also, they are not a favorable option as more vicinity is needed inside the cavity to obtain more tuning which results in large, bulky structures. Then, in this part, we explore the tuning capabilities of the two presented filters. The desired design is an octave tunable filter from 2.67 GHz to 1.17 GHz (tuning ratio 2.28:1) with a constant 20-dB bandwidth of 38 MHz. Following the design procedure of CABW tunable filters detailed in chapter 3, the required $K_{12}\times f$ product and reflection group delay are calculated as 0.063 and 11.2 nS, respectively. Then, one M5 tuning screw and two M2 tuning screws were introduced at both filters to obtain the desired IR and IO couplings, respectively. As can be seen in Fig. 4.7, the reflection group delay is stable over the tuning window (the IO coupling is increasing with frequency tuning) in the re-entrant filter, while it increases noticeably in the screw-based design (the IO coupling is decreasing with frequency tuning). This tells that the M2 screws can effectively adjust the IO coupling in the re-entrant cap filter, and will not be able to obtain the desired IO coupling in the screws-tuned filter. Also, Fig. 4.8 shows that the re-entrant cap design, with the aid of the M5 tuning screw, fulfills the required IR coupling requirement, while the screw-tuned filter cannot provide the required IR coupling, even with the M5 tuning screw. The simulated S-parameter responses of the two tunable filters are exhibited in Fig. 4.9(a) and Fig. 4.9(b), respectively. It can be seen clearly that the re-entrant cap filter maintains a CABW response of 38.5 MHz$\pm$10%, while the bandwidth de-

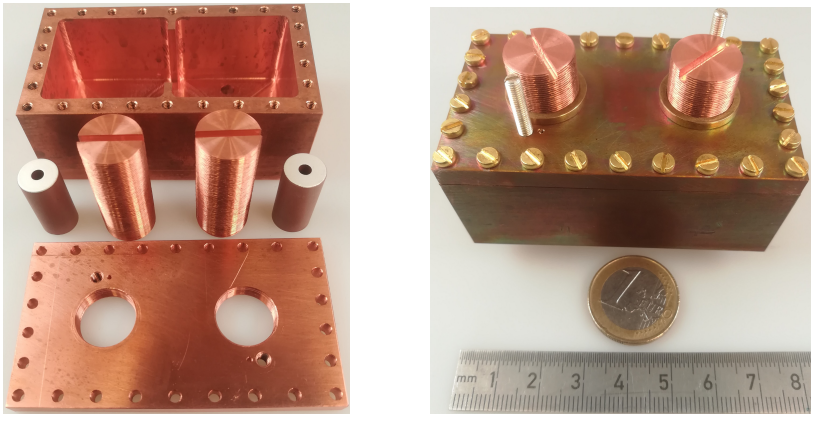

(a) (b)

Figure 4.10: The fabricated second-order tunable dielectric filter with re-entrant caps. (a) Disassembled parts. (b) Assembled prototype.

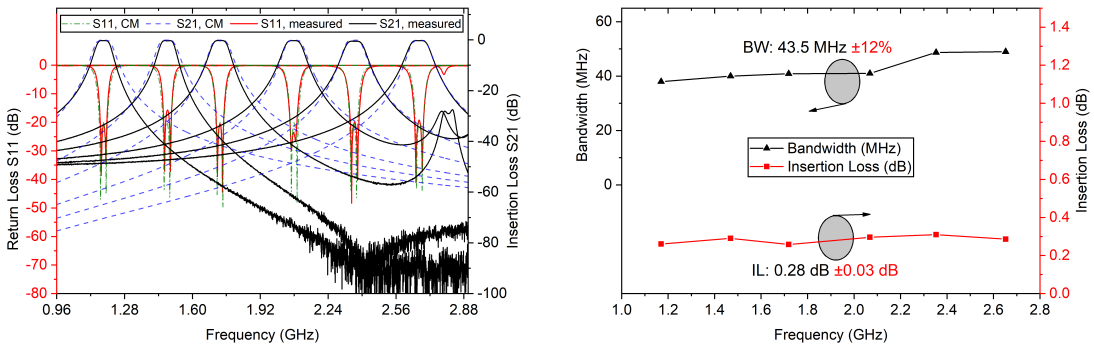

(a) (b)

Figure 4.11: Measured results of the implemented two-pole CABW octave tunable filter. (a) S-parameter responses compared to their associated coupling matrices (20-dB BW = 38 MHz, Q_u = 4000): frequency tuning range: 2.67 GHz to 1.17 GHz, tunability: 78.13%. (b) Bandwidth and insertion loss variation over the tuning window.

creases significantly in the screw-based design from 42.3 MHz at 2.67 GHz to only 15.5 MHz at 1.17 GHz and cannot be recovered. Then, a prototype is manufactured and measured to validate the designed octave-tunable CABW re-entrant cap filter. The disassembled parts and the final prototype, made of copper metal, are depicted in Fig. 4.10. The measurements in Fig. 4.11 show that the filter can be tuned over a wide range of 78.13% from 2.67 GHz to 1.17 GHz with a constant ABW of 43.5 MHz±12% (at S11 = -15 dB), low insertion loss of 0.28 dB ±0.03 dB, and return loss higher than 15.6 dB. The estimated unloaded quality factor varies from 1350 to 850.

4.4 Tunable CABW Four-Pole Bandpass Filter

Fig. 4.12 depicts a 3-D structure of a fourth-order octave tunable BPF with constant ABW. The filter is designed to operate from 2.86 GHz to 1.34 GHz with a constant 20-dB bandwidth of 71 MHz. Similar to the previous example, the design procedure begins from the desired reflection group delay (8.3 nS) and IR couplings ($K_{(12,34)}\times f$= 0.066, $K_{23}\times f$= 0.05) calculation based on [175]. Next, the required reflection group delay is realized through the IO feeding structure with the aid of two M3 tuning screws as shown in Fig. 4.13(a). As can be seen, the IO tuning screws are used at the lower tuning states to decrease the IO coupling strength and maintain the reflection group delay at the desired peak. For the design of the inter-resonator irises, one can use simple inductive irises with tuning screws similar to the earlier

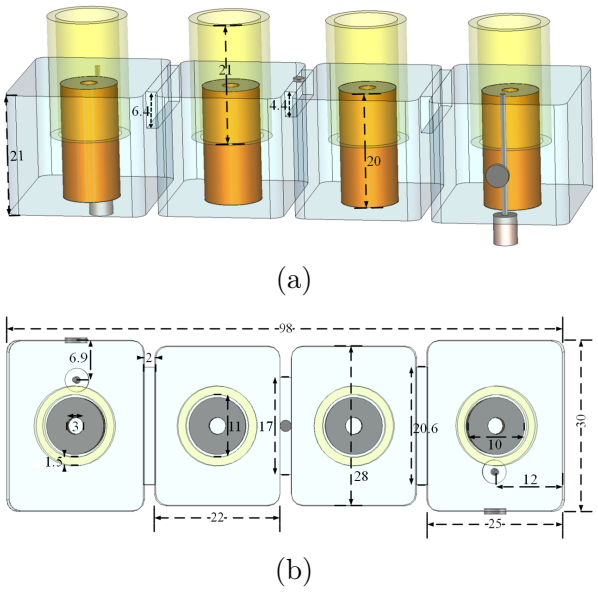

Figure 4.12: Fourth-order CABW tunable dielectric combline filter using re-entrant caps. (a) Perspective view. (b) Top view. All dimensions in mm unit.

two-pole design. However, another way is used here by optimizing the position and dimensions of the iris to provide the required coupling variation for a CABW over the tuning range, eliminating the need for the IR tuning screws, as explained in [19] and [175]. Therefore, we can see that the used IR coupling layout here is distinct from the conventional inductive iris in Fig. 4.4 filter. However, due to the wide tuning window, one M3 tuning screw is still needed to tune K_{23} at a couple of states. As shown in

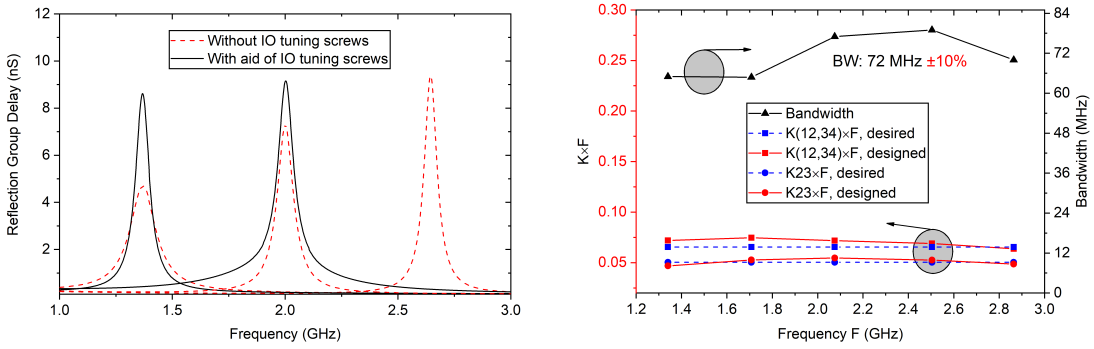

Figure 4.13: (a) Peak reflection group delay over the frequency tuning window of the designed four-pole octave tunable filter. (b) Inter-resonator couplings and bandwidth variation in relation to the frequency tuning in the proposed four-pole octave tunable filter.

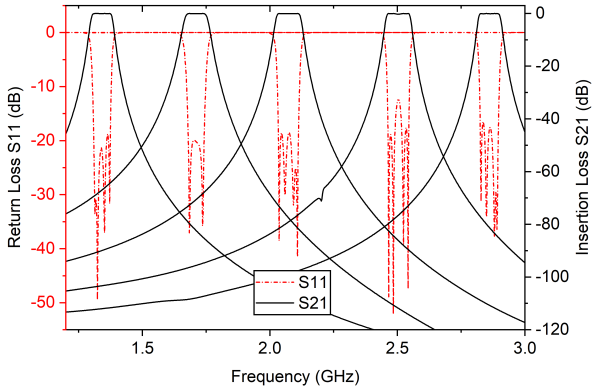

Figure 4.14: Simulated S-parameters of the designed four-pole re-entrant cap octave tunable BPF. Tuning ratio: 2.13:1, 20-dB CABW: 72 MHz±10%.

Fig. 4.13(b), the designed irises successfully provide the required IR couplings of the different states within the tuning range. The simulated S-parameter responses are demonstrated in Fig. 4.14 with a CABW of 72 MHz±10% over a wide tuning range of 1.52 GHz (tuning ratio 2.13:1). The simulated unloaded quality factor ranges from 5900 to 1670 using copper metal. A prototype is then fabricated and tested as depicted in Fig 4.15 and Fig. 4.16, respectively. The filter has a wide 74% tuning window from 2.96 GHz to 1.36 GHz with a CABW of 69 MHz±13%, low insertion loss of 0.5 dB ± 0.08 dB, and return loss better than 16 dB. The extracted unloaded quality factor varies from 2000 to 750, where degradation can be noticed compared with simulations, which could be due to the metal properties and imperfect contact between the caps and the metallic housing. It is worth noting here that despite the IO tuning screws were considered in the prototype, they were not employed in obtaining

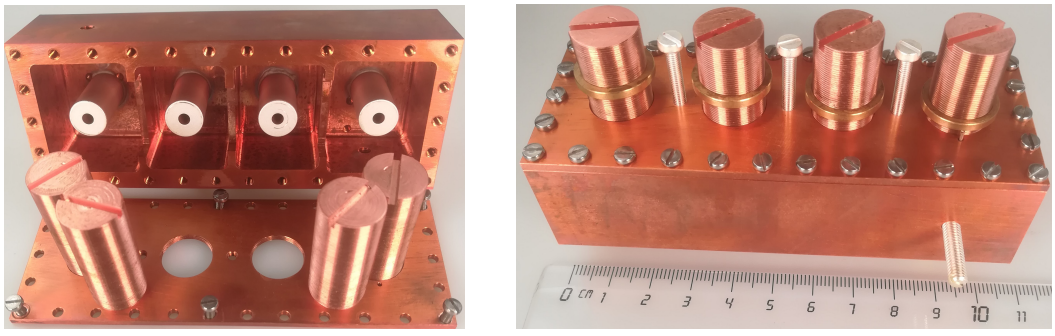

(a) (b)

Figure 4.15: The fabricated four-pole octave tunable dielectric combline filter. (a) Disassembled and (b) assembled.

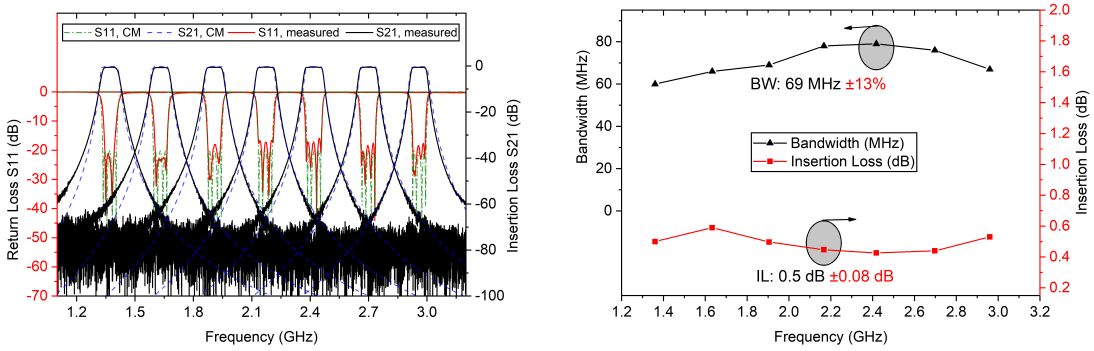

(a) (b)

Figure 4.16: Measured results of the implemented four-pole CABW widely tunable filter. (a) S-parameter responses compared to their associated coupling matrices (20-dB BW = 72 MHz, Q_u = 4000): frequency tuning range: 2.96 GHz to 1.36 GHz, tunability: 74%. (b) Bandwidth and insertion loss variation over the tuning window.

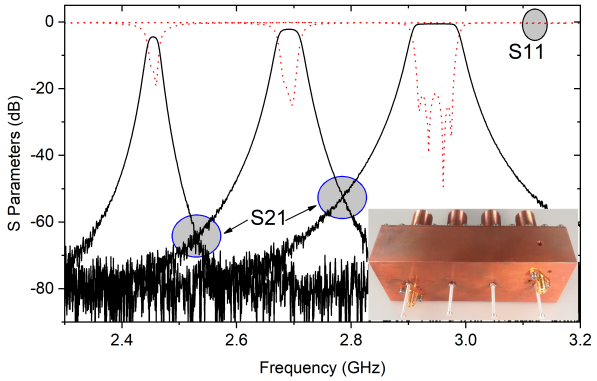

Figure 4.17: Measured results of the proposed filter using screws to tune the operation frequency instead of re-entrant caps (caps are fixed at the lid of filter cavity).

the measured results. For curiosity, the filter is tuned with silver-plated M2 tuning screws instead of the re-entrant caps as exhibited in Fig. 4.17. As expected, there is an obvious variation in the absolute bandwidth, confirming the advantage of the presented tuning technique. The wideband response of the implemented filter using re-entrant caps and tuning screws is provided in Fig. 4.18, at the lowest and highest tuning states. As shown, the spurious performance is being improved with frequency tuning in the re-entrant caps filter up to 4.5 GHz at the lowest tuning state, while it remains fixed at around 3.4 GHz when using tuning screws.

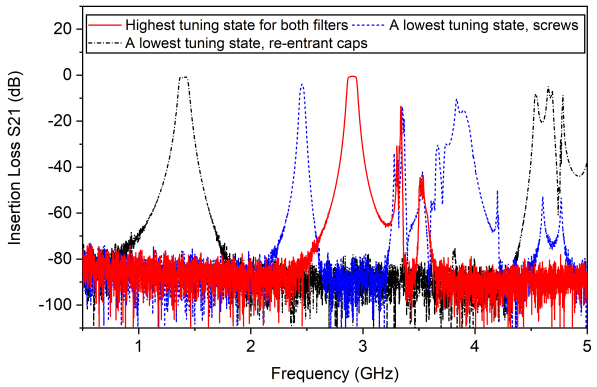

Figure 4.18: Wideband response of the fabricated 4th-order tunable filter with re-entrant caps (Fig. 4.15 filter) and tuning screws (Fig. 4.17 filter) at the extreme ends of tuning window.

4.5 State-of-the-art Comparison

Table 4.1 provides a comparison between the proposed re-entrant cap tunable filters and similar state-of-the-art designs with constant absolute bandwidth. As evident, the re-entrant cap designs have the widest tuning capabilities providing up to 90% of tunability and octave 2.64:1 tuning ratio with a high-Q up to 5480. Besides, they feature a stable return loss level better than 15.5 dB and low insertion loss with a maximum ± 0.08 dB of variation allover the broad band of tuning. All these advantages are added to the compact structures, simple tuning configuration, and improved spurious performance over tuning. Concerning the number of tuning elements, the proposed technique requires a least N tuning elements (N is the filter order), which must be in excellent electrical and mechanical contact with the cavity. Accordingly, this attributes a slower tuning speed than the designs which use a single tuning mechanism as [5], or contactless tuning like [174]. Hence, further research and unconventional solutions that enable faster tuning processes are still needed.

Table 4.1:
Comparison of the Proposed Octave CABW Tunable Filters with Similar State-of-The-Art Designs.

Ref.	**Structure (tuning mechanism)**	***f* (GHz)**	**Order**	**Tunability (%)**	**ABW (MHz)**	**IL (dB)**	**RL (dB)**	**Q-factor**	**Volume (cm^3)**	#
[161]	Evanescent-mode (E)	0.8-1.43	2	56.5%	25±0.27%	1.6-3.1	> 10	225-310	NA	6
[164]	Microstrip (E)	0.78-1.36	2	54.2%	103±5.8%	1.68-2.9	> 13	NA	2.032	2
[12]	Hollow waveguide (M)	19.36-19.7	4	1.74%	181±1.66%	< 1.8	> 11	2600-3100	NA	4
[5]	Combline (M)	1.81-2.17	5	18.1%	25	< 1.8	> 14	2000-2500	NA	1
[17]	Combline (M)	2.565-2.634	6	2.7%	NA	0.9-2.3	> 16.2	2252-2914†	NA	6
[19]	Half-wavelength (M)	2.275-2.775	4	19.8%	106.5±9%	< 0.4	> 7.5	> 4850‡	275.65	1
[63]	Combline (E)	0.707-0.963	3	30.7%	27.5±2.5%	1.58-3.97	> 14	173-418	94.067	3
[137]	Combline (M)	0.68-0.76	4	11.1%	11.2±8.9%	0.8-0.9	> 12	> 5800‡	2291.625	1
[136]	Combline-dual-post (M)	9.15-10.87	4	17.2%	230±3.9%	< 0.6	> 12	1500	NA	8
[175]	Inset (M)	2.66-3.96	4	39.3%	116±6%	0.39-0.44	> 13.5	1820±6%	49.28	4
[27]	Dielectric-TE (M)	15.6-16	3	2.5%	150	1.5-4.5	> 8	421-1630†	NA	3
[26]	Dielectric-combline (M)	4.97-5.22	4	4.9%	66±1.5%	3.9-4.4	> 10	536-548†	NA	4
[141]	Dual-mode dielectric-TM (M)	4.72-5.51	2	15.4%	50±10%	0.2-0.9	> 18	540-1100	3.456	2
This work-1	Dielectric-combline (M)	1.1-2.9	-	90%	-	-	-	1705-5480	19.8	-
This work-2	Dielectric-combline (M)	1.17-2.67	2	78.13%	43.5±12%	0.28±0.03	> 15.6	850-1350	39.06	5
This work-3	Dielectric-combline (M)	1.36-2.96	4	74%	69±13%	0.5±0.08	> 16	750-2000	62.034	5

‡Based on simulated Q-factor. †Based on the measurements of a single-cavity resonator. #: Number of tuning elements. E: Electrical tuning. M: Mechanical tuning.

4.6 Summary

Octave CABW frequency tunable TM-mode dielectric filters were presented in this chapter using a novel re-entrant cap tuning technique. First, a single resonator is implemented providing a wide 90% tuning range from 2.9 GHz to 1.1 GHz and a spurious-free band up to $3.44 \cdot f_0$. Then, the design guidelines of widely tunable BPFs with CABW are discussed, and octave tunable filters are designed, manufactured, and measured. The fabricated filters have the merits of wide tuning ranges (tuning ratio $>$ 2:1), high-Q, compact structure, good spurious performance, and simple tuning mechanism. All these highly desirable features strongly promote the proposed tuning technique and tunable components in a wide range of frequency-agile systems and applications.

Chapter 5

Compact and Reconfigurable Bandpass Filtering Components Using Dual-Mode TM-Mode Dielectric Resonators

In this chapter, a new class of compact inline dual-band bandpass filters using TM-mode dielectric resonators in planar configuration is first presented for tunable filters applications. Thanks to the employment of the dielectric-loaded TM-mode waveguide configuration and the dual-mode TM_{120} and TM_{210} resonances, substantial size miniaturization and volume saving ($> 70\%$) can be obtained in comparison with conventional waveguide technology. Additionally, the planar topology of the presented concept offers highly desirable advantages for industry and mass production including the ease of manufacturing, assembly, and tuning. Furthermore, the resonating doublets and the nonresonating TM_{110} mode are effectively utilized to introduce and control both inter-band and outer-band transmission zeros, advantageously increasing the isolation between the two passbands and enhancing the outer-band rejection regions. The general design procedure of the proposed filter is discussed in detail. Two-pole and three-pole dual-band dual-mode TM dielectric filters are designed, implemented, and measured with the investigation of their tuning capabilities.

A very compact in-line C-band diplexer is reported in section 5.2 based on dual-mode dielectric TM-mode resonators in planar coupling configuration. In addition to the advantages of substantial volume-saving and easy assembly, the proposed diplexer

features high quality factor, enhanced spurious performance, high-power handling, and efficient tuning process with independent control of each passband. For verification purposes, a C-band diplexer is designed, implemented, and tested. The final assembled diplexer unit has a compact overall volume of $43\times40\times15.9$ mm^3. It operates at 4.73 GHz and 5.03 GHz with same bandwidth of 24 MHz, an insertion loss better than 0.9 dB, and a return loss higher than 21 dB. Additionally, high-power breakdown analysis shows that the introduced diplexer can handle high levels of input power up to 5200 watts. Furthermore, the reconfiguration capabilities of the fabricated diplexer are reported, and a 3rd-order tunable diplexer design example is presented using a single tuning element.

In the final part of this chapter, compact reconfigurable C-band pseudo-elliptic bandpass filters for the applications of next-generation flexible satellite systems are introduced. The first is a fully-reconfigurable 2nd-order filter realized using a dual-mode TM-mode dielectric resonator, attributing ultra-high miniaturization and volume saving $> 70\%$. A wide 790 MHz tuning window is obtained from $4.72 - 5.51$ GHz with a constant bandwidth of 50 MHz. Additionally, two independently reconfigurable transmissions zeros are introduced through the use of a doublet configuration and non-resonating modes. A piezomotor-based fixture is utilized for accurate fine-tuning. The measured results show good agreement with simulations. The prototype filter has demonstrated high-Q measurements across the whole tuning band (> 500) while maintaining a low insertion loss of less than 1 dB and return loss higher than 18 dB. Similarly, the second design is a 4th-order compact reconfigurable quasi-elliptic filter using a single tuning element with stable TZs positioning.

5.1 Miniaturized Dual-Band Dual-Mode TM-Mode Dielectric Filters in Planar Configuration

5.1.1 Introduction

The current rapid development of multi-channel/multi-standard RF and satellite communications have urged the demand for more efficient, compact, and lightweight multi-band payloads and subsequent filtering units. Often, those essential requirements cannot be effectively fulfilled using the conventional single-band filter structures, and more efficient multi-band designs are needed [177]. Accordingly, various

dual-band bandpass filters were introduced in the literature using different technologies and configurations [178, 179, 180, 181, 182, 183, 184, 185, 186, 187, 188]. Whereas the majority of the presented dual-band bandpass filters are developed using compact planar microstrip and SIW structures as presented in [178] and [179], they are not favorable in satellite and high-performance communications due to the high losses and limited power handling capabilities. Therefore, high-Q and high-power compatible waveguide cavities have gained more interest in the implementation of dual-band BPFs [180]-[182]. For example, [180] introduced a new class of waveguide dual-band bandpass filters in an in-line configuration using dual-mode TE_{101}/TE_{011} modes for size reduction. However, a special milling machining is required to realize such structures, and cross-couplings cannot be introduced to generate additional transmission zeros (TZs). Folded side-coupled dual-band dual-mode TE_{11m} mode elliptical cavity filters were presented in [181] to facilitate the cross-coupling and TZs' creation. Nevertheless, the proposed filters suffer from many unwanted spurious resonances and inflexibility in controlling the transmission zeros' positions. In addition to the aforementioned limitations of empty-cavity waveguide dual-band filters, more size reduction and lighter weight are still required. This motivated the introduction of more compact dual-band coaxial and dielectric-loaded waveguide filters [183]-[188]. Work performed by [185] presented a 3rd-order dual-band filter using an open-circuited-stub-loaded quarter-wavelength coaxial resonator. The bandpass filter operates at 0.9 GHz and 2 GHz bands with a single uncontrolled inter-band transmission zero. A third-order dual-band filter was introduced in [186] using dielectric resonators to offer a more compact size and higher Q_u than the other configurations. However, specially customized dielectric resonators and assembly processes are needed to implement the filter. Besides, the filter suffers from close spurious modes and limited selectivity due to the difficulty in the introduction and control of transmission zeros. All of these drawbacks limit the extension of the proposed dual-band DR filter to higher orders and also to use in industry.

TM mode dielectric resonators are particularly favorable in filter applications due to their substantial size miniaturization, mechanical stability, high Q_u, and wider spurious-free band [189]. To take the advantage of all these desirable features with considering the limitations of the aforementioned dual-band filter structures, the authors in [187] introduced a new highly compact dual-band dual-mode TM mode dielectric filter with more than 90% reduced volume than the conventional waveguide structures. The dual-band response is realized through properly modifying the trans-

verse doublet structure. Additionally, the coupling scheme is adjusted to move at least one transmission zero between the two passbands to enhance the inter-band isolation. However, this transversal configuration has many drawbacks including difficult tuning, sensitivity to TZs locations, and precise selection of iris locations. Additionally, since the filter is built out of separated transversal blocks, this leads to more assembly time and cost, and can also increase the related losses. Therefore, alternative dual-band TM-mode dielectric-loaded configurations are required to benefit from the TM mode DR advantages and overcome the challenges of the transversal topology.

A new miniaturized C-band dual-band dual-mode TM-mode dielectric filter is presented in this section. The filter is designed in planar coupling configuration for the purposes of easy tuning, manufacturing, and assembly. Additionally, enhanced inter-band isolation and outer-band rejection are achieved through flexibly positioned transmission zeros. The following subsections discuss the design procedure of the proposed topology and report the measured results of a three-pole dual-band dual-mode TM-mode dielectric resonator filter.

5.1.2 Concept and Design

Dual-Response Dual-Mode TM-Mode Dielectric Resonator

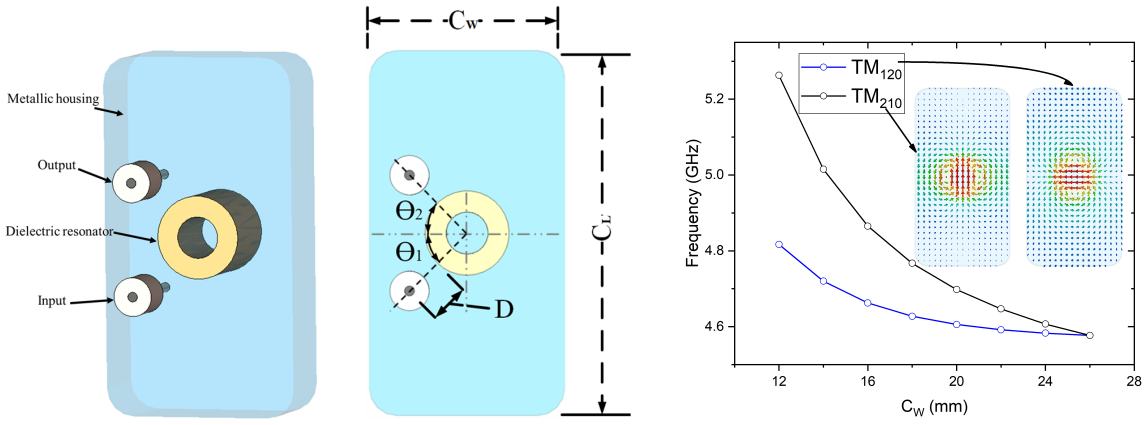

(a) (b)

Figure 5.1: Dual-band TM-mode DR cavity. (a) Perspective view and top view. Both modes TM_{120}, TM_{210} are excited equally through input probe with angle $\theta_1 = 45^o$ and output probe with angle $\theta_2 = -45^o$. (b) f_{TM120}, f_{TM210} change in relation to the change in the cavity width (C_W) while the cavity length is kept unchanged (C_L = 26 mm). The TM-mode dielectric resonator has outer diameter D = 8 mm, inner diameter d = 4 mm, height = 6 mm, and dielectric constant $\epsilon_r = 45$.

The basic doublet block was introduced earlier in [190] and employed to design a dual-mode dielectric filter using TE-mode dielectric resonators in [191]. Similarly, dual-mode TM-mode DR configurations were introduced in planar topology for miniaturized single-band fixed and tunable filters applications. For instance, in [192], a dual-mode filter is designed using the two orthogonal degenerate modes TM_{120} and TM_{210} in a single resonator structure. The resonant frequencies of the orthogonal modes are adjusted primarily through the cavity length (C_L) and width (C_W) where each mode is mainly propagating and more sensitive in a corresponding dimension. Herein, the cavity length and width are set equal in order to obtain the desired dual-mode passband ($C_L \approx C_W$). Alternatively, the dual-mode configuration can be altered to a dual-passband response by shifting any of the degenerate resonant frequencies away from the other one as depicted in Fig. 5.1. This is basically done by changing the respective dimension of any of the resonant modes ($C_L \neq C_W$). As can be seen in Fig. 5.1(b), both TM_{120} and TM_{210} resonate at the same central frequency (4.58 GHz) when $C_L = C_W = 26$ mm, while f_{TM210} increases and moves away from f_{TM120} with the reduction of the cavity width creating a dual-band response. The separation of the two passbands is proportionally related to the ratio between the cavity length and width (C_L/C_W). Similar to conventional doublet configurations [191], the input and output feeding probes are rotated to excite both modes with angles $\theta_1 = 45^o$ and $\theta_2 = -45^o$, respectively. If the rotation equals to 45^o, then the IO probes are coupled to both orthogonal TM_{120} and TM_{210} modes equally. If θ is less than 45^o, then the IO probes are more coupled to TM_{210} while in contrary, they will be more coupled to TM_{120} when θ is larger than 45^o. θ_1 and θ_2 are related to the coupling coefficients using:

$$\tan\theta_1 = \frac{M_{S1}}{M_{S2}}, \quad \tan\theta_2 = \frac{M_{1L}}{M_{2L}} \tag{5.1}$$

The angular distance between the dielectric resonator and the IO probes (D) controls the coupling strength to both modes. Fig. 5.2 demonstrates a dual-response cavity using a dual-mode TM-mode dielectric resonator with three different coupling routes and S parameter responses. The H-fields of the resonating TM_{120}, TM_{210}, and nonresonating TM_{110} modes are also included. The cavity length is set larger than the width to move f_{TM210} away from f_{TM120}, therefore, creating a dual-band response at 4.98 GHz and 4.66 GHz, respectively. Based on (5.1), the input probe is positioned at an angle $\theta_1 = 45^o$ ($M_{S2} = M_{S1}$), and the output pin is rotated to an angle $\theta_2 = -45^o$

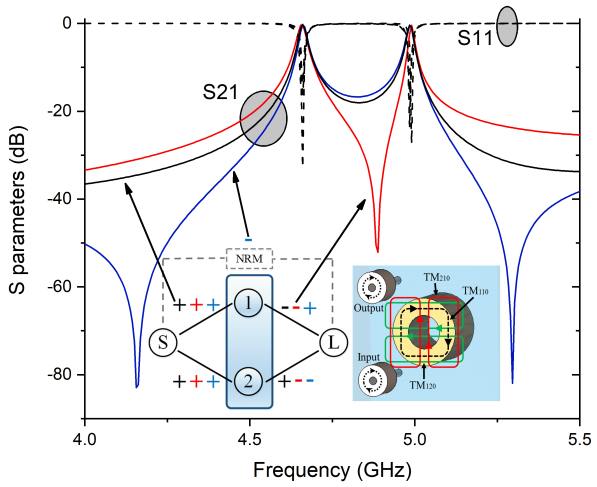

Figure 5.2: S-parameter responses of three different dual-band configurations and their corresponding coupling routes (black, red, blue) realized by proper excitation and orientation of the IO feedings. Dual-band response is obtained through $C_W \neq C_L$ ($f_{TM120} = 4.66$ GHz, $f_{TM210} = 4.98$ GHz). Blackline: Chebyshev responses ($M_{S2} = M_{S1}$, $M_{1L} = -M_{S1}$, $M_{2L} = M_{S2}$, $M_{SL} = 0$). Redline: inter-band TZ is introduced (sign change of M_{2L} causing a phase reversal at the output with respect to the input). Blueline: 2 TZs are introduced by the mean of the nonresonating TM_{110} mode bypass source-load coupling (NRM) ($M_{SL} < 0$). The TM-mode dielectric resonator has outer diameter D = 8 mm, inner diameter d = 4 mm, height = 6 mm, and dielectric constant ϵ_r = 45. C_W = 14 mm, C_L = 26 mm.

($M_{2L} = -M_{1L}$). The first path S-1-L corresponds to the lower channel (f_{TM120}) and the second route S-2-L represents the upper band (f_{TM210}). The blackline represents the basic dual-response configuration with Chebyshev characteristics ($M_{S2} = M_{S1}$, $M_{1L} = -M_{S1}$, $M_{2L} = M_{S2}$, $M_{SL} = 0$). Also, both inter-band and outer-band TZs can be easily introduced and flexibly controlled which provides high isolation between the two bands and also improves the out-of-band rejection level. The appearance of an inter-band transmission zero in the second case (redline) is due to phase reversal of the orthogonal modes at the output port with respect to the input side ($M_{S2} = M_{S1}$, $M_{1L} = -M_{S1}$, $M_{2L} = -M_{S2}$, and $M_{SL} = 0$). This is realized by rotating the output probe to an angle $\theta_2 = -135^o$ to change the sign of M_{2L}. While in the third case (blueline), the bypass coupling caused by the nonresonating mode (NRM) TM_{110} mode creates a pair of outer-band transmission zeros ($M_{S2} = M_{S1}$, $M_{1L} = M_{S1}$, $M_{2L} = -M_{S2}$, $M_{SL} < 0$) [187], [190]. In this case, the output pin is rotated to an angle $\theta_2 = -225^o$. All of these interesting capabilities of the proposed concept can be effectively applied to filter's configurations and will be discussed in the following sub-section.

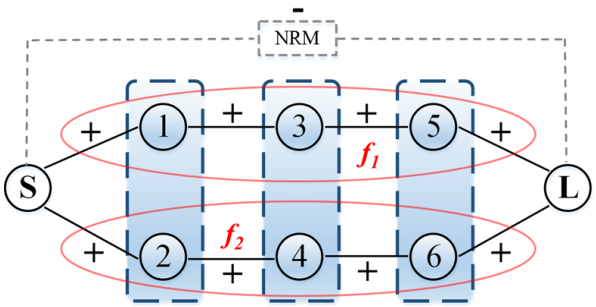

Figure 5.3: Generalized coupling scheme of the proposed dual-band dual-mode TM mode DR filters. N corresponds to the filters' orders. Each orthogonal degenerate mode creates an individual channel (f_1, f_2). In some cases, the nonresonating TM_{110} mode (NRM) is excited and creates a S-L coupling path introducing outer-band transmission zeros.

Dual-Band Dual-Mode TM-Mode Dielectric Filters

The generalized coupling mechanism of the proposed miniaturized dual-band dual-mode TM-mode DR filters is depicted in Fig. 5.3. It is comprised of two coupling paths that are composed of directly coupled doublet blocks. Each doublet block exhibits two orthogonally resonating modes (TM_{120}, TM_{210}) at two different frequencies which create a dual-passband response. Also, in particular configurations, the nonresonating fundamental TM_{110} mode is employed to create a bypass source-load coupling path that introduces additional transmission zeros [193]. The general design procedure begins with the synthesis and extraction of the corresponding coupling scheme and parameters of each passband individually which has been then optimized and applied to the overall dual-band response and any additional transmission zeros [194]. The coupling matrices in this paper are extracted following simple steps:

• A good start point is by using the standard synthesis method to extract the coupling matrix of every single passband individually (f_1, ABW_1), (f_2, ABW_2) with an order of N/2 for each band.

• Normalize both channels to a single-band N-order filter using the pre-synthesized values from the first step. The 1, 2, 3,....N/2 resonators from the first and second single-band filters represent 1, 3, 5,.....N-1 path and 2, 4, 6,....N channel, respectively, and constitute the initial coupling coefficients of the overall matrix (Mi, j_0). The chosen channel has a centre frequency $f_0 = (f_1+f_2)/2$, and an absolute bandwidth $ABW_0 = ABW_1$. Note that f_0, ABW_0, and normalized coupling coefficients can also be chosen arbitrarily [194]. The mutual and self-couplings are calculated using:

$$M_{i,i} = -\frac{f_0}{ABW_0} \times (\frac{f_1}{f_0} - \frac{f_0}{f_1}), \quad i = 1, 3, ..., N-1 \tag{5.2}$$

$$M_{i+1,i+1} = -\frac{f_0}{ABW_0} \times (\frac{f_2}{f_0} - \frac{f_0}{f_2}), \quad i = 1, 3, ..., N-1 \tag{5.3}$$

$$M_{i,j} = M_{i,j\_0} \times \frac{f_0}{f_1} \times \frac{ABW_1}{ABW_0}, \quad i = 1, 3, ..., N-3, \quad j = i+2 \tag{5.4}$$

$$M_{i+1,j+1} = M_{i+1,j+1\_0} \times \frac{f_0}{f_2} \times \frac{ABW_2}{ABW_0}, \quad i = 1, 3, ..., N-3, \quad j = i+2 \tag{5.5}$$

$$M_{S1} = \sqrt{\frac{f_0}{Q_{ext\_1} \times ABW_0}}, \quad M_{S2} = \sqrt{\frac{f_0}{Q_{ext\_2} \times ABW_0}} \tag{5.6}$$

Where $Q_{\text{ext\_1}}$ and $Q_{\text{ext\_2}}$ are the calculated external quality factors from the coupling matrices of the single-band filters from the first step. Next, the required physical coupling coefficients (K) and external quality factors (Q_{ext}) for the lower passband (f_1) and higher passband (f_2) are calculated using the corresponding f_0 and bandwidth (ABW_0) as follows:

$$K_{i,j} = \frac{ABW_0 \times M_i, j}{f_0}, \quad i = 1, 3, ..., N-3, \quad j = i+2 \tag{5.7}$$

$$K_{i+1,j+1} = \frac{ABW_0 \times M_{i+1,j+1}}{f_0}, \quad i = 1, 3, ..., N-3, \quad j = i+2 \tag{5.8}$$

$$Q_{ext\_1} = \frac{f_0}{ABW_0 \times {M_{S1}}^2}, \quad Q_{ext\_2} = \frac{f_0}{ABW_0 \times {M_{S2}}^2} \tag{5.9}$$

Afterward, the dual-band bandpass filter is realized using the presented dual-mode TM-mode dielectric resonators. Figures 5.4 to 5.16 show two design examples of second and third-order dual-band TM mode DR filters based on the proposed planar topology, respectively. SMA connectors are used for the I/O feeding and a compact TM mode DR (outer diameter = 8 mm, inner diameter = 4 mm, height = 6 mm) is also employed with a high dielectric constant of 45 to provide more volume reduction. Considering the fields' coupling nature of the two orthogonal modes, the

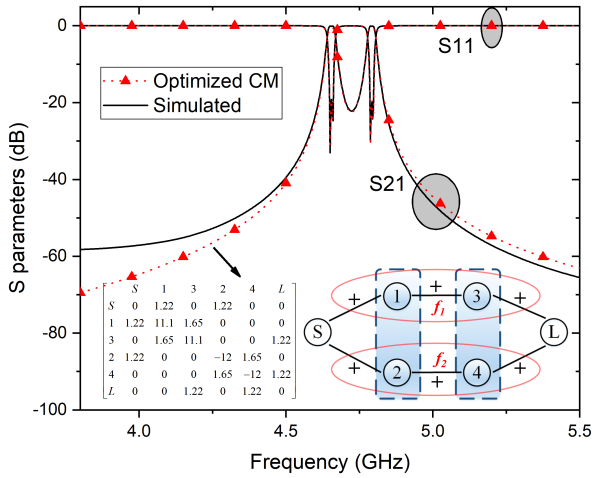

Figure 5.4: Coupling scheme, optimized coupling matrix (redline), and simulted S-parameters (blackline) of the proposed 2nd-order dual-band dual-mode TM-mode DR filter in aligned IO configuration.

required dual-band response cannot be obtained with conventional coupling irises configurations because they cannot provide the required isolation between the two modes. Therefore, inductive rectangular posts are effectively employed to obtain the required inter-resonator couplings and provide bands' isolation and separation. The IO feedings are rotated to excite both orthogonal modes at the same time as discussed earlier. Fig. 5.4 and Fig. 5.5 demonstrate a 2nd-order dual-band filter of the proposed structure operates at 4.65 GHz and 4.79 GHz with a narrow bandwidth of 12 MHz at both passbands. The coupling topology and optimized matrix are provided in Fig. 5.4 following the aforementioned procedure. The simulated S-parameter responses are also included in Fig. 5.4 with excellent agreement with the required

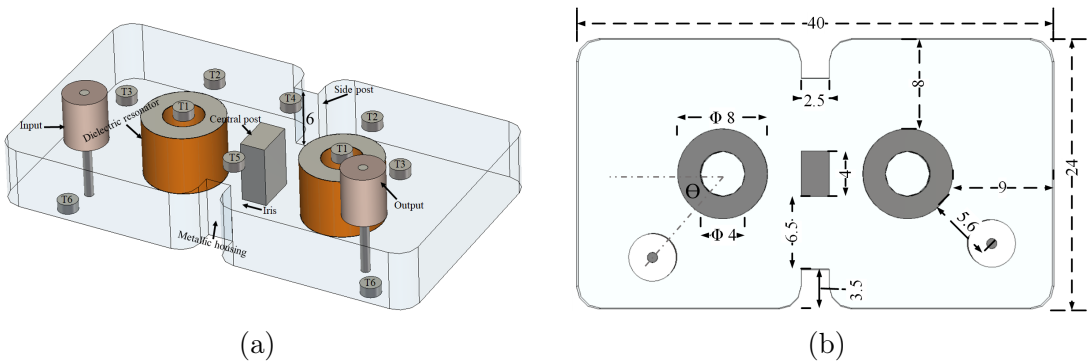

(a) (b)

Figure 5.5: Second-order dual-band dual-mode TM-mode DR filter in aligned IO configuration. (a) Perspective view. (b) Top view. All dimensions in mm unit.

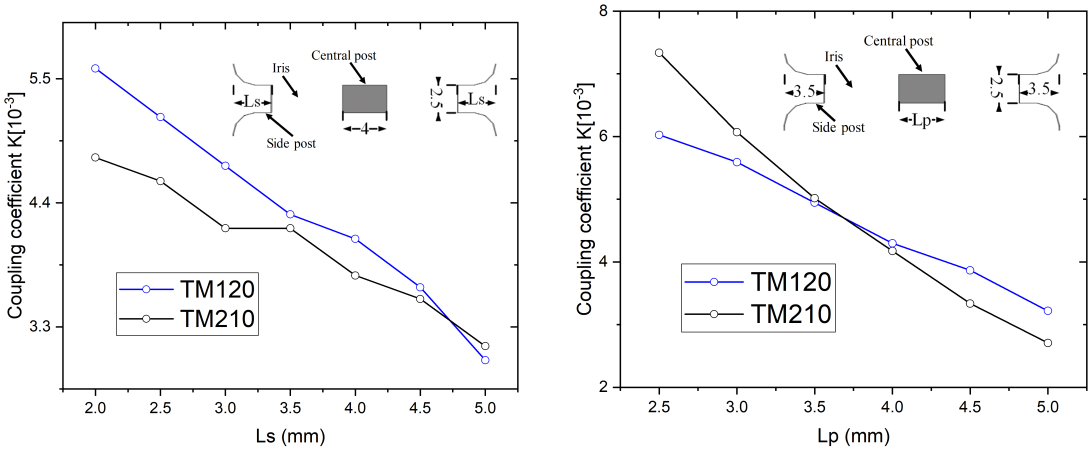

Figure 5.6: Relationship between the physical coupling coefficients of TM_{120} and TM_{210} modes and (a) side posts length L_{S}, and (b) central post length L_{P}.

specifications. The simulated Q_{u} for the first passband is 3440 and 3330 for the higher band. Fig. 5.5 shows the realized dual-band BPF using dual-mode TM-mode DR in planar configurations. The TM_{120} mode constructs the lower passband (f_1) while the higher channel (f_2) is formed by the orthogonal TM_{210} mode. As shown earlier, the separation between the resonant frequencies of the two modes is mainly controlled by the cavity length/width ratio. In this example, the two channels are closely-spaced with 140 MHz separation. The required inter-resonator couplings of both passbands (K_{13}, K_{24}) are realized using common inductive irises with side and central inductive posts. The relation between the coupling coefficients (K) of TM_{120} (K_{13}), TM_{210} (K_{24}) channels and the central and side posts is depicted in Fig. 5.6. The inter-resonator coupling of the first passband is more controlled by the side posts (L_{S}) since the TM_{120} mode resonates mainly in sides and it is less distributed in the centre of the cavity (see Fig. 5.1(b)). In contrast, the coupling bandwidth of the upper passband is more related to the central post (L_{P}) as the TM_{210} mode is more distributed in the centre of the cavity than the sides. Furthermore, as the central post is located close to the maximum of the TM_{210} mode, the post width (W_{P}) can be altered to push the TM_{210} channel further away from the TM_{120} mode passband as can be seen in Fig. 5.7. All these capabilities advantageously provide a more relaxed degree-of-freedom to the designers towards getting different/similar bandwidths at the two passbands with extended spacing. Tuning screws can be introduced easily and utilized effectively in this planar structure to compensate for various tolerances

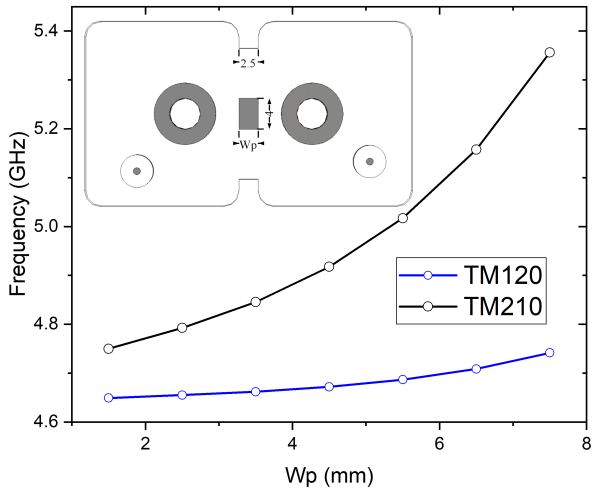

Figure 5.7: Dependence of f_{TM120} and f_{TM210} on the central post width W_{P}.

and retain the required response. The inter-resonator couplings of both passbands can be tuned through T4 and T5, while T1 is used to tune the resonant frequency of both bands at the same time (frequencies will move up with tuning [141]). Furthermore, T2 and T3 can be employed to tune the lower (TM_{120}) and upper (TM_{210}) bands independently (frequencies will decrease with tuning). Similarly, T6 can be added to control the IO coupling.

The desired external quality factors Q_{ext_1} (TM_{120}), Q_{ext_2} (TM_{210}) are realized using inductive probes rotated with an angle θ. The dependence of Q_{ext_1} and Q_{ext_2} on the rotation angle of the IO probe is presented in Fig. 5.8. As shown, Q_{ext_1} of TM_{120} increases with smaller angles whereas Q_{ext_2} of TM_{210} is decreasing, and vice versa.

The introduced dual-band filter has Chebyshev outer-band response and inter-band isolation at 22 dB level. These two aspects need to be enhanced for high-performance applications. Therefore, the introduction of inter-band and outer-band TZs is importantly needed to improve the isolation between the two channels and the outer-band selectivity. [195] presented a detailed overview of the TZs' generation in multi-path coupling structures. Similarly, [196] showed that a TZ can be created between the passbands through the proper orientation of the feeding waveguides to cause a phase reversal between the signals traveling through different paths. The same concept can be employed effectively and more flexibly in the proposed dual-band TM-mode DR filter configuration. In the original structure in Fig. 5.5, the input and output probes are in aligned configuration with the same angle ($\theta_2 = \theta_1$). The phase

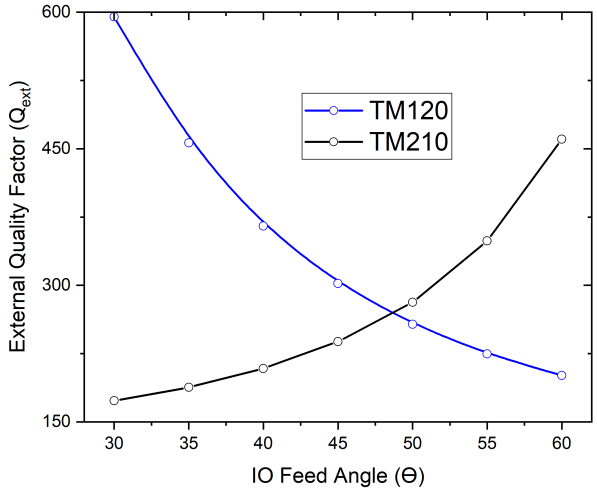

Figure 5.8: External quality factors of TM_{120} and TM_{210} modes in relation to the rotation of the IO probe.

change diagram of the presented filter is demonstrated in Fig. 5.9. All couplings are inductive with reference to the corresponding coupling topology in Fig. 5.4. As can be seen in Table 5.1, the signals of both bands are in-phase to each other, hence, no inter-band transmission zero can be introduced. An inter-band TZ is generated if the output probe is rotated by 90^o for phase reversal between the two modes. Fig. 5.10 depicts the phase-reversed IO configuration of the presented filter with its corresponding coupling route and simulated S parameters. As can be seen, inter-band transmission zero is effectively generated. As the output probe is rotated by 90^o, the sign of M_{3L} changes to negative causing the two channels to be coupled out-of-phase as shown in Table 5.1. Thus, a transmission zero is introduced between the two passbands enhancing the isolation to more than 50 dB. In addition to the creation of the inter-band transmission zero, the 90^o rotation of the output probe also excites

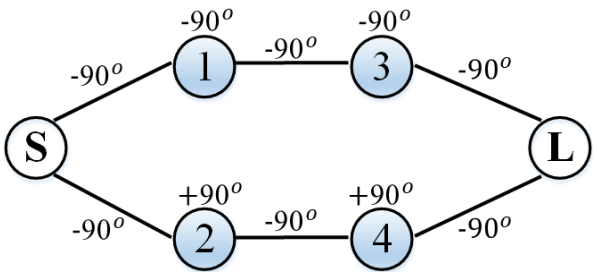

Figure 5.9: Phase shift diagram of the presented two-pole dual-band dual-mode filter in in-phase configuration (Fig. 5.4).

the non-resonating fundamental TM_{110} mode creating a source-load (S-L) coupling path (M_{SL} = -0.0004) introducing two asymmetrical transmission zeros below and above the filter passbands at 4.1 GHz and 5.1 GHz, respectively. The introduction and control process of the transmission zeros due to the nonresonating modes are well explained in [197] at transversal TM-mode structures. In principle, multiple inter-band and outer-band transmission zeros can be introduced and controlled in the proposed planar configurations. However, this is practically challenging since the IO probes will need to be rotated close to/inside the coupling irises unlike the transversal configurations [187] where the IO feedings can be rotated freely 360^o. This limits the flexibility of controlling the outer-band transmission zeros in the presented filter. Fig. 5.11 shows the dependence of the transmissions zeros on the feeding angle (θ). As can be seen, both transmission zeros are controlled towards the same direction [197]. Referring also to Fig. 5.8, when θ decreases, M_{S1}/M_{SL} increases and M_{S2}/M_{SL} decreases resulting-in a decrease in the zeros' frequencies and vice versa. To locate both TZs closer to the passbands, the transferred energy through the nonresonating TM_{110} mode should increase with respect to the coupling of the resonating TM_{120}, TM_{210} modes [193]. A possible straight-forward option is by pushing the nonresonating TM_{110} mode to a higher frequency closer to the resonating TM_{120}, TM_{210} modes. This can be done at the first design steps with the selection of the DR and its dimensions.

Another design example of a three-pole dual-band TM-mode DR filter is demon-

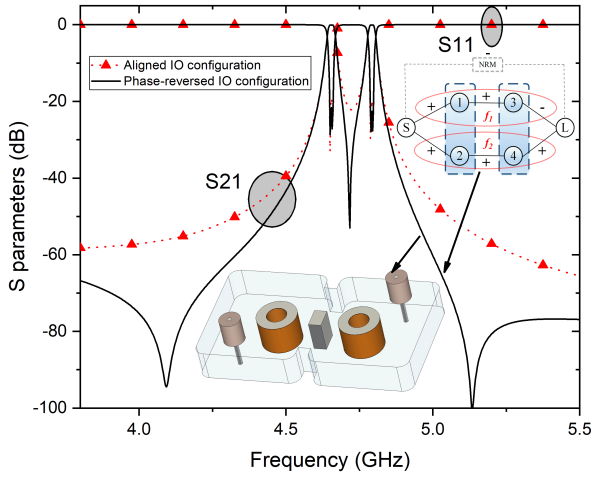

Figure 5.10: Second-order dual-band dual-mode TM-mode DR filter in phase-reversed configuration. Inter-band transmission zero is introduced (M_{3L} = -M_{S1}, M_{4L} = M_{S2}), and outer-band transmission zeros are created ($M_{SL} < 0$ = -0.0004).

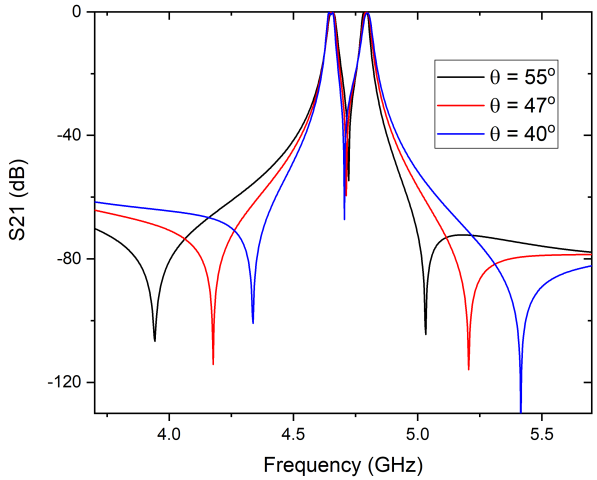

Figure 5.11: Outer-band transmission zeros relation to the IO feeding angle.

Table 5.1: Total Phase Shifts for the Two Paths of the Two-Pole Dual-Band Filters.

Filter		**Phase shift at the transmission zero's frequency**
1st filter with no inter-band TZ	Lower passband (Resonators 1, 3)	-90°-90°-90°-90°-90° =**-90°**
	Upper passband (Resonators 2, 4)	-90°+90°-90°+90°-90° =**-90°**
	Result	**In-phase**
2nd filter with inter-band TZ	Lower passband (Resonators 1, 3)	-90°-90°-90°-90°**+90°** =**-270°**
	Upper passband (Resonators 2, 4)	-90°+90°-90°+90°-90° =**-90°**
	Result	**Out-of-phase**

strated in Fig. 5.12 to Fig. 5.16. The filter here is designed to operate at 4.77 GHz and 5.11 GHz with fractional bandwidths of 1.1% and 1.3%, respectively. The generalized corresponding coupling matrix is stated below in (5.10).

$$\begin{bmatrix} & S & 1 & 3 & 5 & 2 & 4 & 6 & L \\ S & 0 & 1.08 & 0 & 0 & 1.25 & 0 & 0 & 0 \\ 1 & 1.08 & 7.0 & 1.03 & 0 & 0 & 0 & 0 & 0 \\ 3 & 0 & 1.03 & 6.87 & 1.03 & 0 & 0 & 0 & 0 \\ 5 & 0 & 0 & 1.03 & 7.0 & 0 & 0 & 0 & 1.08 \\ 2 & 1.25 & 0 & 0 & 0 & -6.5 & 1.37 & 0 & 0 \\ 4 & 0 & 0 & 0 & 0 & 1.37 & -6.37 & 1.37 & 0 \\ 6 & 0 & 0 & 0 & 0 & 0 & 1.37 & -6.5 & 1.25 \\ L & 0 & 0 & 0 & 1.08 & 0 & 0 & 1.25 & 0 \end{bmatrix} \tag{5.10}$$

Structures and corresponding responses of the phase-reversed and in-phase configurations are demonstrated in Fig. 5.13 and Fig. 5.15, respectively. Here in these

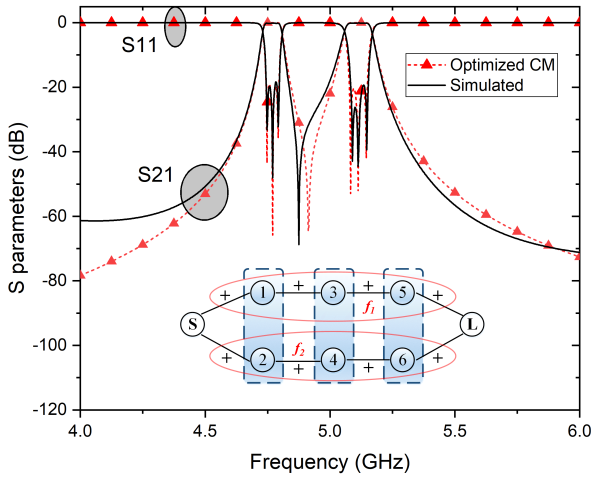

Figure 5.12: Coupling scheme, optimized coupling matrix (redline), and simulted S-parameters (blackline) of the proposed third-order dual-band dual-mode TM-mode DR filter in aligned IO configuration with an inter-band transmission zero ($M_{5L} = M_{S1}$, $M_{6L} = M_{S2}$), and no outer-band transmission zero ($M_{SL} = 0$).

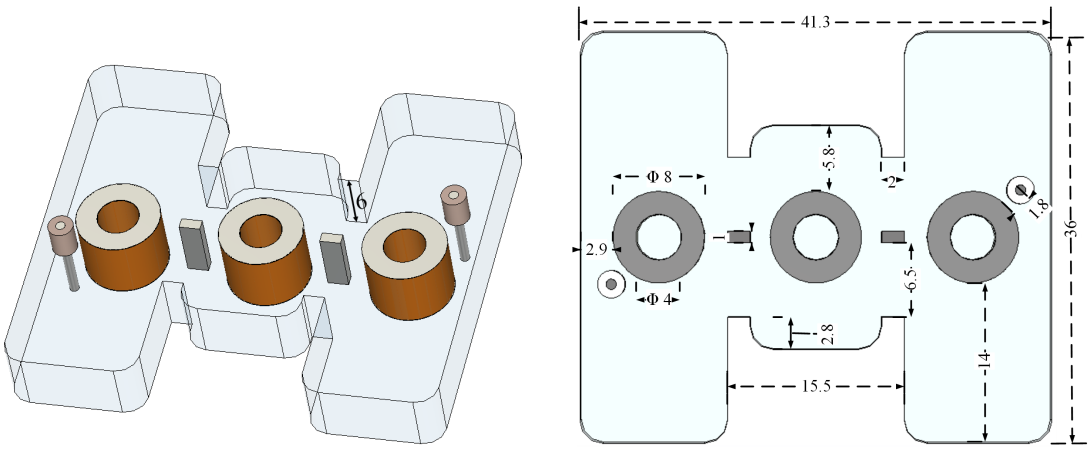

(a) (b)

Figure 5.13: Third-order dual-band dual-mode TM-mode DR filter in aligned IO configuration. (a) Perspective view. (b) Top view. All dimensions in mm unit.

designs, the cavity length/width ratio is set larger than in the previous two-pole examples to obtain wider spacing between the two passbands (350 MHz). The simulated unloaded-Q for the lower passband is 3200, while in the upper passband is 3000. Similar to the two-pole designs, inter-band and outer-band TZs can be positioned effectively by controlling the I/O orientation. Fig. 5.13 depicts one configuration of the proposed third-order dual-band filter with an inter-band transmission zero having a high isolation level $>$ 70 dB. As discussed earlier, the appearance of this TZ is due

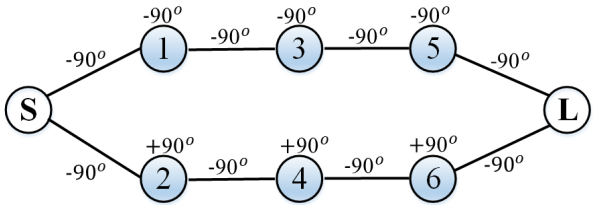

Figure 5.14: Phase shift diagram of the presented 3rd-order dual-band filter in phase-reversed configuration (Fig. 5.12).

Table 5.2: Total Phase Shifts for the Two Paths of the Three-Pole Dual-Band Filters.

Filter		Phase shift at the transmission zero's frequency
1st filter with inter-band TZ	Lower passband (Resonators 1, 3, 5)	90°-90°-90°-90°-90°-90°-90° =**-270°**
	Upper passband (Resonators 2, 4, 6)	-90°+90°-90°+90°-90°+90°-90° =**-90°**
	Result	**Out-of-phase**
2nd filter with no inter-band TZ	Lower passband (Resonators 1, 3, 5)	-90°-90°-90°-90°-90°-90°**+90°** =**-90°**
	Upper passband (Resonators 2, 4, 6)	-90°+90°-90°+90°-90°+90°-90° =**-90°**
	Result	**In-phase**

to the phase reversal between the two paths of the filter as can be seen from the phase shift diagram in Fig. 5.14 and Table 5.2. Since each cavity causes a 180^o phase shift to the signals (3×180^o), the output probe is rotated 90^o to keep the sign of M_{5L} positive. Consequently, the NRM bypass coupling is not excited and no outer-band

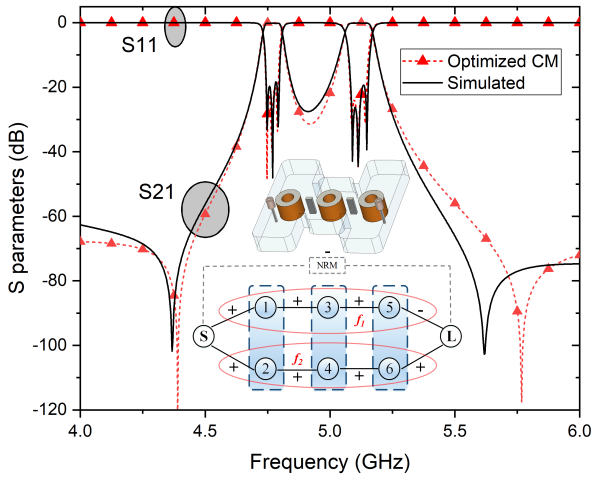

Figure 5.15: 3D structure, simulated S-parameters and optimized coupling matrix (CM) of the proposed third-order dual-band dual-mode TM-mode DR filter in aligned IO configuration. No inter-band transmission zero (M_{5L} = -M_{S1}, M_{6L} = M_{S2}), and outer-band transmission zeros are created (M_{SL} < 0 = -0.00021).

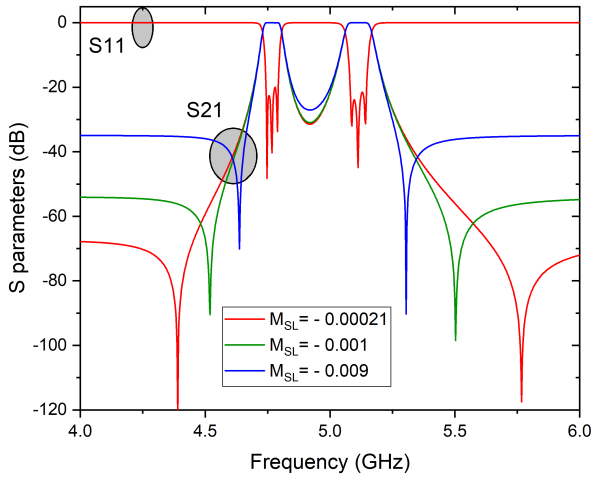

Figure 5.16: Optimized coupling matrix (CM) of the proposed third-order dual-band dual-mode TM-mode DR filter in aligned IO configuration with different S-L couplings.

TZs are obtained ($M_{\mathrm{SL}} = 0$). The case is the opposite in the second dual-band filter example shown in Fig. 5.15. When the input and output ports are aligned, the sign of M_{5L} changes to negative and both signals become in-phase. As a result, the inter-band transmission zero cannot be introduced. On the other hand, the NRM bypass coupling is excited and creates two asymmetrical TZs at both edges ($M_{\mathrm{SL}} < 0$ = - 0.00021). Conceptually, the source-load coupling strength can be changed to control the positions of the TZs as can be seen in Fig. 5.16. Here, good isolation $>$ 30 dB is obtained between the two passbands but with no inter-band TZ. It should be noted that the design procedure and control process of the TZs of the presented 2nd and 3rd order filters extend and apply the same to all other multiples of even and odd cavities. Also, the proposed planar configuration can be utilized effectively to implement other miniaturized TM-mode DR components (e.g., diplexers, tunable filters). For example, a 3-pole ultra-compact TM-mode diplexer can be introduced by just modifying the output feeding mechanism of the proposed 3-pole dual-band dual-mode DR filter. All dimensions and passbands' specifications are the same as the dual-band filter. The only adjustment needed here is to modify the output structure to receive each channel separately unlike in the dual-band configuration. This can be done easily since the TM_{120}, TM_{210} modes are orthogonally distributed. Then, as shown in Fig. 5.17, the input probe (port 1) is positioned with 45^o angle to excite both modes. On the other side, port 2 is positioned at an angle ($\theta = 0^o$) to only excite the TM_{120} mode and receive only one channel corresponding to the lower passband of

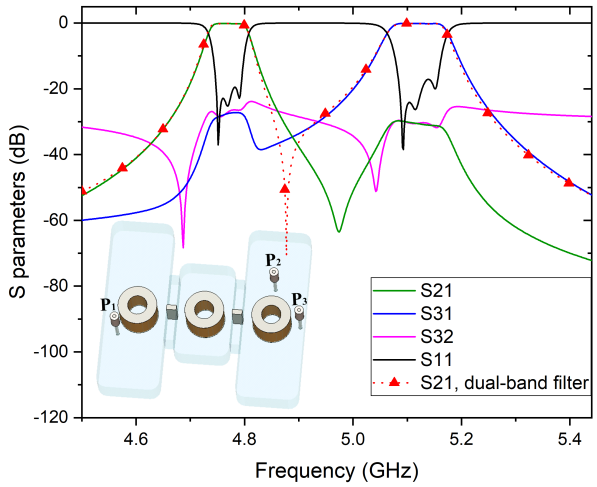

Figure 5.17: 3D structure and simulated S-parameters of a highly-miniaturized 3-pole diplexer using the proposed planar dual-mode TM-mode DR configuration. The structure dimensions and channels specifications are the same as the presented three-pole dual-band BPF examples. Input port (P_1) excites both orthogonal modes TM_{120}, TM_{210}. Unlike the dual-mode configurations, each degenerate mode is excited separately at the output side. Port 2 (P_2) excites only TM_{120} mode constructing the RX channel. Port 3 (P_3) excites only TM_{210} mode forming the TX channel.

the dual-band filter. Similarly, port 3 is positioned orthogonally at 90^o angle to only excite the TM_{210} mode and receive just the upper channel of the dual-band filter. As can be seen in Fig. 5.17, the passbands' specifications of the ultra-compact diplexer are ideally identical to the dual-band channels.

Experimental Results and Comparison

A three-pole C-band dual-band TM-mode dielectric resonator filter is manufactured and measured to validate the concept of the proposed planar configuration. A photograph of the implemented filter is shown in Fig. 5.18. The TM-mode dielectric resonator that has been used is an E6045 ($\epsilon_r = 45$, $Q_u = 8000$ @ 5 GHz) from EXXELIA [198] with the same dimensions stated in the above section. The TM-mode dielectric resonators are then soldered in a compact metallic housing milled out of copper. Fig. 5.19 and Fig. 5.20 depict the measured responses of both the in-phase and phase-reversed configurations. Measurement results generally agree with simulations in the bandwidth specifications and the transmission zeros that have been created and controlled. A shift in the passband frequencies from simulated ones is noticed mainly due to the tuning process and uncertainty of the dielectric constant

of the DRs (100 MHz in the first passband, and 190 MHz in the upper band). The frequencies in simulations were then re-optimized to resemble the measured results. Fig. 5.19 shows the measured S parameter responses in comparison with the optimized simulations. The first passband operates at a centre frequency of 4.86 GHz with a 53.5 MHz of bandwidth compared to a bandwidth of 53.8 MHz in the simulated one (both at -15 dB level of S11). The measured insertion loss is $\leq$ 1.1 dB and the return loss is better than 19 dB. The upper band has a central frequency of 5.3 GHz with 77.2 MHz BW compared to 78.2 MHz of the simulated one. The mid-band insertion loss is lower than 0.9 dB and the return loss is better than 17 dB. Measurements and simulations have a good agreement in the lower passband frequency, while the measured higher passband has a slight shift of 50 MHz from simulations. This could be due to the sensitivity of this band (TM_{210}) to the central post as aforementioned, especially since the resonators are positioned very close to the central post and the cavity. Fig. 5.20 depicts the measurements of the implemented filter in both in-phase and out-of-phase configurations obtained by the rotation of the output probe. As can be seen, an inter-band TZ provides high isolation between the two passbands up to 60 dB in the out-of-phase case, while two outer-band TZs are introduced in the in-phase configuration. Silver-plated tuning screws (shown or located where the empty holes in Fig. 5.18) were added similar to those in Fig. 5.5 to tune both frequencies or each one independently, inter-resonator couplings, and the IO couplings.

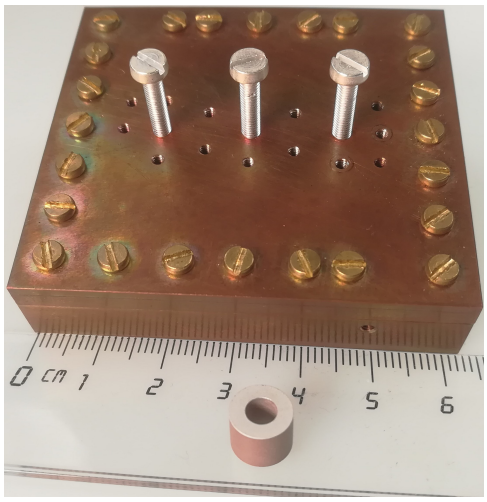

Figure 5.18: Photograph of the manufactured 3-pole dual-band dual-mode TM-mode DR filter. The used TM-mode dielectric resonator and some of the tuning screws are also included.

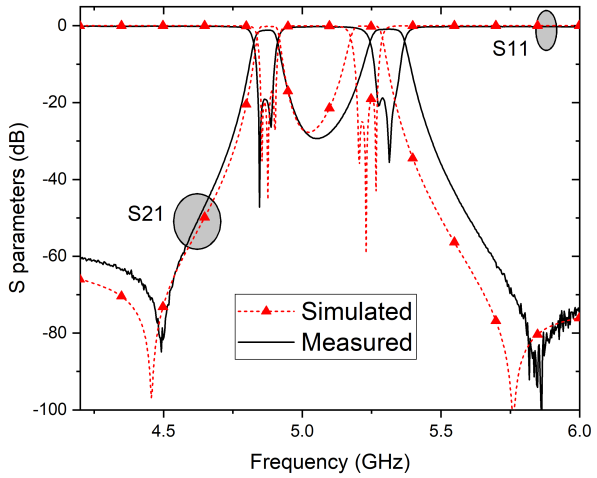

Figure 5.19: Simulated and measured S parameters of the implemented 3-pole dual-band dual-mode TM-mode DR filter in aligned IO configuration.

The extracted unloaded Q-factor is better than 1040 ($\approx$ 35% of the simulated ones). Silver-plating and larger dielectric resonators can be considered to increase the Q_{u} up to 3000. The filter has a compact size of 41.3×36×5.9 mm^3 offering more than 70% volume reduction than the conventional waveguide structure. Fig. 5.21 exhibits the measured wideband response of the implemented filter. As shown, the filter has a good spurious-free band of 1.5 GHz at the lower side, 1.7 GHz to the next higher unwanted spurious frequency. Table 5.3 summarizes a comparison between the proposed compact inline dual-band dual-mode TM mode BPF and similar designs. The filter has a good spurious-free band 1.5 GHz which is better than the other configurations. Also, the proposed filter offers the advantage of effective introduction and control of inter-band and outer-band transmission zeros. Despite that the transversal configuration in [187] is able to introduce multiple inter-band and outer-band TZs, those TZs are sensitive to many parameters and cannot be effectively controlled. Contrary, the generated inter-band TZ in the proposed planar configuration is controlled just through the phase shift between the two signal paths and it is not affected by any other parameters. Additionally, whereas the structure must be folded in [181] to introduce both inter-band and outer-band TZs at both sides, out-of-band rejection characteristics of the inline filters in [186] and [187] need to be improved either at one or both edges. While the presented configuration has shown the capability of obtaining and controlling inter-band and outer-band TZs at both edges to provide higher out-of-band rejections. Nevertheless, it should be mentioned that the positioning of the outer-band TZs closer to the passband is not easy and the coupling ratio

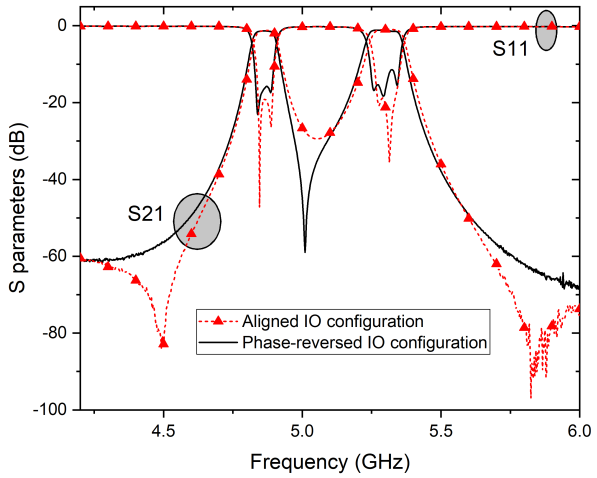

Figure 5.20: Measured results of the manufactured 3-pole dual-band dual-mode TM-mode DR filter in both aligned and phase-reversed IO configurations.

of the nonresonating TM_{110} mode should be considered carefully. Another attractive advantage of the proposed planar topology is that it makes the assembly and tuning process easier and more feasible than the transversal configurations resulting-in better responses and less implementation effort. Post-tuning is even more important in such designs where each of the two signals needs to properly couple and excited in the same single cavity with the same IO feedings. Advantageously, the introduced planar configuration allows the designer to introduce tuning screws to efficiently control all resonant frequencies, bandwidths, and IO couplings.

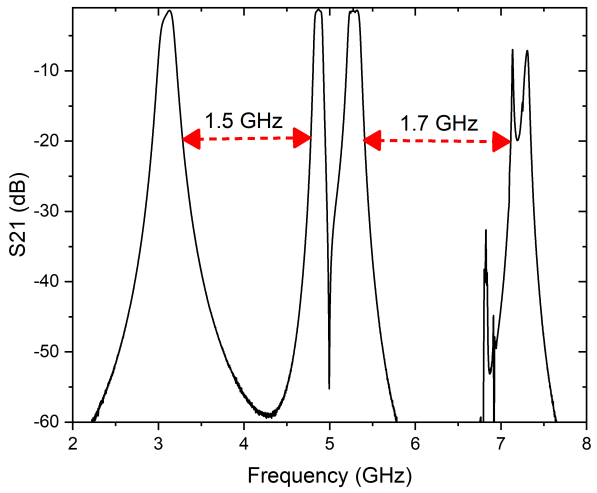

Figure 5.21: Wideband response of the presented 3-pole dual-band dual-mode TM-mode DR filter.

Table 5.3:
Comparison With Other Reported Dual-Band Filters.

Ref.	**Technology**	f_1/f_2 **(GHz)**	**FBW (%)**	**IL (dB)**	**Spurious-free band (GHz)**	**Controllable TZs**
[181]	folded waveguide	3.4/3.6	1.77/1.67	0.15/0.22	0.18	No
[186]	customized DR	2.6/3.5	0.7/1.1	0.45/0.4	0.5	No
[187]	transversal TM DR	4.25/4.55	1.5/1.5	1.3/1.15	NA	No
This work	**planar TM DR**	**4.86/5.3**	**1.1/1.46**	**1.1/0.9**	**$\geq$ 1.5**	**Yes**

5.1.3 Reconfigurable Miniaturized Dual-Band Filters

Introduction

As discussed earlier, dual-band bandpass filters (DBBPFs) have received growing demand in recent years with the exponential development in multi-standard, multi-band communication systems [199]. In the same context, the proposal of tunable dual-band bandpass filters is of focal importance for future frequency-agile and software-defined radios [200]. Those applications have strict requirements of high-performance, low-loss, and compact dual-band filter structures with reconfigurable frequency plans. Unfortunately, despite planar dual-band filters are easy to design and offer very compact structures, they suffer from high losses and limited power handling capabilities. On the other side, empty-waveguide structures have key features of high unloaded quality factor (Q_u) and high-power performance. Nevertheless, their large, bulky size makes them an unfavourable solution for the design of miniaturized fixed/tunable dual-band filters. Considering the above drawbacks of planar and waveguide configurations, dual-band dielectric bandpass filters are getting increasing attention because of their desirable advantages of high Q_u, compact size, and compatibility with high-power levels. Couple of dual-band dielectric filters were presented in the open literature using different types of dielectric resonators (DRs) with fixed passbands [186, 201, 202, 187, 203]. Among all, TM-mode dielectric resonators offer more compactness, better spurious performance, and mechanically-stable structures. To benefit from these attractive features, [187] presented a highly miniaturized, high-Q DBBPF using dual-mode TM-mode dielectric resonators in a transversal configuration. Unfortunately, this structure is not suitable for the realization of tunable filters since the resonant frequency and inter-resonator coupling cannot be tuned efficiently because the resonators cannot be accessed due to the transversal topology. Therefore,

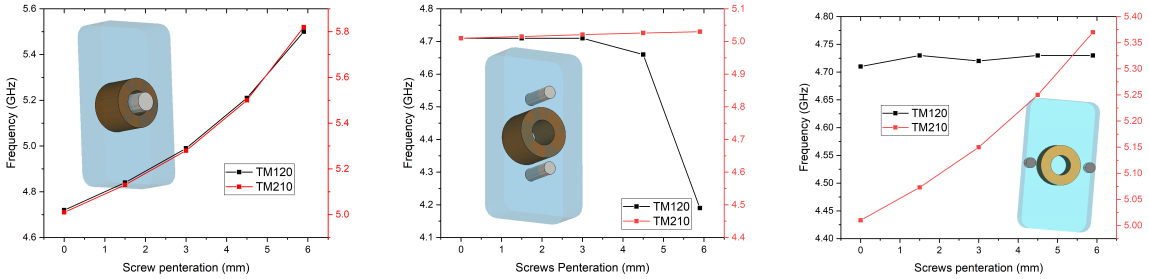

(a) (b) (c)

Figure 5.22: Relation between TM_{120}, TM_{210} modes and tuning screws at different locations. (a) A single tuning screw in the centre. (b) Two longitudinally-positioned screws. (c) Two laterally-positioned screws.

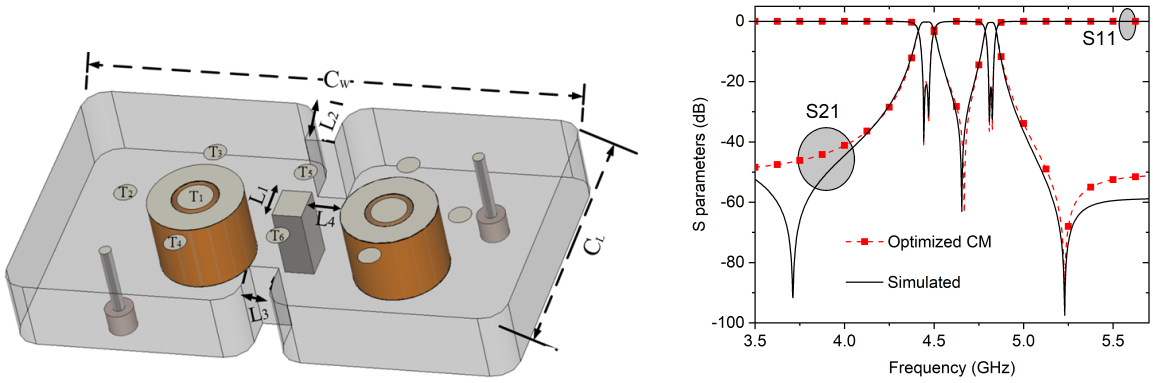

(a) (b)

Figure 5.23: (a) 3D view of the proposed two-pole dual-band dual-mode TM mode DR filter. Dimensions (in mm): C_W = 40.5, C_L = 26, L_1 = 3, L_2 = 3, L_3 = 2.5, L_4 = 3. (b) Simulated S parameters and optimized coupling matrix (CM).

there is an essential need for alternative compact TM-mode DBBPFs suitable for reconfigurable filter designs. This subsection introduces miniaturized reconfigurable dual-band dual-mode TM-mode dielectric filters based on the above-presented planar topology ([203]). The tuning capabilities of the proposed dual-band filters are explored for the application of tunable filters.

Reconfigurable Second-Order Dual-Band Filter With Simultaneous and Independent Passbands Tuning

Originally, TM-mode DR filters are designed using the fundamental TM_{110} (TM_{010}) mode. Recently, the orthogonal degenerate modes TM_{120} and TM_{210} were utilized to design highly miniaturized dual-mode TM-mode dielectric filters in [192]. Similarly,

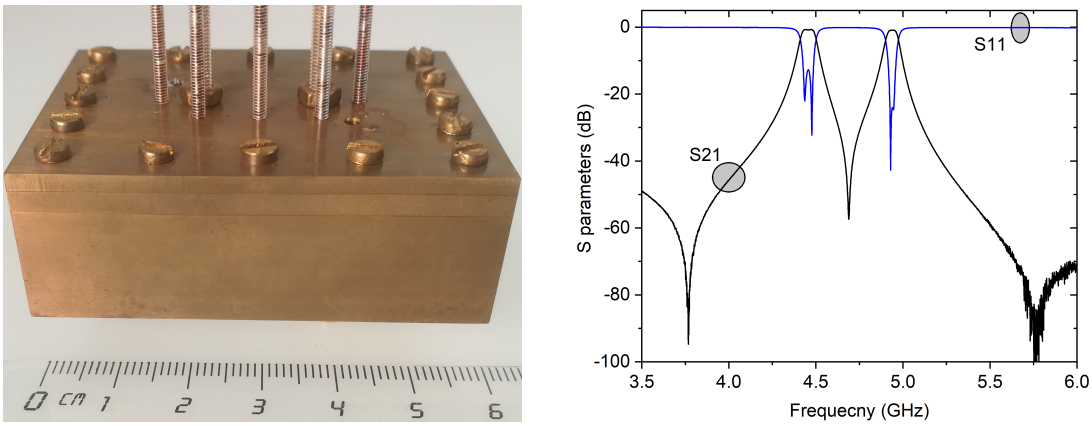

(a) (b)

Figure 5.24: (a) Photograph, and (b) measured results of the two-pole dual-band dual-mode TM-mode dielectric filter.

the dual-mode response can be changed to a dual-band response by moving any of the orthogonal modes away from the other one. With reference to Fig. 5.1, each of the orthogonal modes is propagating mainly along one axis of the cavity (TM_{120} along the length axis (C_{L}), TM_{210} along the width axis (C_{W})). Consequently, dual-band response can be realized by reducing the width of the metallic cavity (C_{W}) pushing TM_{210} to a higher frequency. The coupling topology of the dual-band response is represented similar to the conventional doublet structures [190] as shown earlier in Fig. 5.2. Also, the nonresonating TM_{110} mode (NRM) is employed to create a source-load (S-L) coupling path generating two transmission zeros [193]. The IO feeding is realized using SMA probes. The IO feedings are positioned at an angle (θ) of 45^o to excite both modes equally. If $\theta < 45^o$, then the IO pins are more coupled to TM_{210}, while they will be more coupled to TM_{120} in case of $\theta > 45^o$. The coupling strength is adjusted through the angular distance between the resonator and the feeding pin (D). Interestingly, the orthogonal distribution nature of the fields inside the dual-mode cavity features more frequency tuning flexibility. As can be seen in Fig. 5.22, tuning screws can be properly positioned to control either both modes simultaneously, or individual modes separately.

Similarly, the above dual-response cavity can be expanded to introduce reconfigurable dual-band dual-mode TM-mode filters in planar configuration. For example, this subsection introduces a two-pole dual-band bandpass filter. The design process begins by defining the required specifications of each band (f_1, f_2) individually, and extracting the corresponding matrices using the standard synthesis procedure [129].

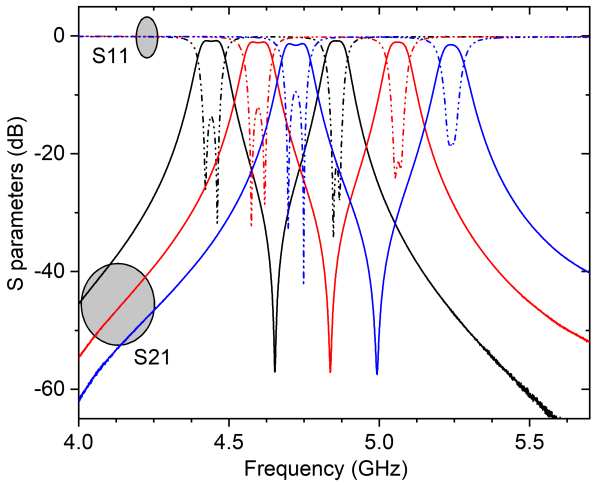

Figure 5.25: Measured reconfigurable responses of the 2nd-order dual-band dual-mode TM mode filter with both passbands tuning.

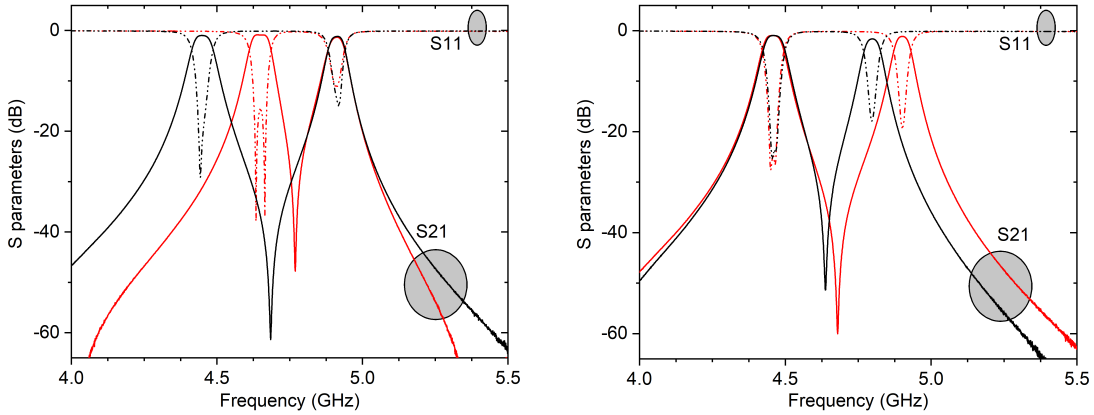

Figure 5.26: Measured reconfigurable responses of the 2nd-order dual-band dual-mode TM-mode filter with independent tuning: (a) Lower-passband only. (b) Higher-passband only.

Then, the overall matrix is optimized with the inclusion of any additional transmission zeros [193], [203]. Afterwards, the required external quality factors (Q_{ext_1}, Q_{ext_2}) and physical coupling coefficients ($K_{1,3}$, $K_{2,4}$) are calculated using equations (5.7)-(5.9), where ABW_1 and ABW_2 are the absolute bandwidth of the first (lower) and second (upper) bands, respectively. The dual-band BPF is designed to operate at 4.46 GHz with absolute bandwidth (ABW_1) of 38 MHz, and 4.82 GHz with 26 MHz of bandwidth (ABW_1). Both inter-band and out-band transmission zeros (TZs) are introduced to increase the isolation between the two channels and improve

the out-of-band rejection characteristics. The inter-band TZ is realized by inducing a phase reversal between the two modes at the output side (M_{S2}=M_{4L}, M_{S1}=-M_{3L}). Whereas the nonresonating TM_{110} mode is employed effectively to introduce two asymmetrical TZs at both sides of the dual-band filter without the need for any further cross-coupling setups.

In the next step, the designed dual-band bandpass filter is realized using the proposed planar dual-mode TM mode configuration as shown in Fig. 5.23. The both orthogonal modes TM_{120} and TM_{210} are excited simultaneously through inductive feeding pins positioned with an angle $\theta = 45^o$ and angular distance = 8 mm. The lower passband is constructed by the resonating TM_{120} mode, while the upper channel is built through the degenerate TM_{210} mode. The required inter-resonator couplings $K_{1,3}$ and $K_{2,4}$ are obtained using inductive irises with a central inductive post. $K_{1,3}$ is more controlled by L_2 since the TM_{120} is more distributed on the sides, while the post length (L_1) mainly controls the $K_{2,4}$ since it is located at the peak of the TM_{210} fields. This indicates also that the central post is also used to adjust the resonant frequency of the upper channel. Both inter-band and out-band TZs are successfully created. The required change in the sign of M_3L to introduce inter-band TZ is obtained by positioning the output feeding pin opposite to the input pin (180^o phase change of TM_{120}). Similarly, this 180^o in the output side creates a negative S-L coupling path through the nonresonating TM_{110} mode generating two asymmetrical TZs.

One of the key motivations behind the proposal of the above planar topology of dual-band TM mode filters is to ease the tuning process for reconfigurable filters applications. It is worth reminding that tuning is more feasible in TM-mode DR components than in others. Simple screws/rods (see Fig. 5.23) can be used to tune both the resonant frequency and bandwidth. T_1 screw is used to tune the resonant frequency of both passbands at the same time. Here, unlike TM_{110} (TM_{010}) mode, H-field is the maximum in the centre of the DR while E-field is stronger in the surrounding (refer to Fig. 5.1). This means that the frequency will be shifted up with the intrusion of the tuning element (T_1). Also, considering that the TM_{120} and TM_{210} modes propagate orthogonally to each other, T_3 and T_4 are used to check the independent reconfiguration of the lower passband (TM_{120}), and T_2 is utilized to tune the upper passband (TM_{210}). In these cases, the frequency will decrease with the insertion of the tuning screw since the E-field is maximum, as mentioned earlier. T_5, T_6 can be used to tune the inter-resonator couplings.

A two-pole dual-band dual-mode TM-mode dielectric filter is implemented and

measured to verify the proposed planar configuration and investigate its tuning capabilities. An E6045 TM-mode dielectric resonator from EXXELIA is used (dielectric constant = 45, Q-factor = 8000 @ 5 GHz) with outer diameter = 8 mm, inner diameter = 4 mm, height = 6 mm. The filter parts are assembled and the dielectric resonators are soldered to a copper metallic housing. The filter has a very compact structure of 40.5×26×5.9 mm^3 providing > 70% volume saving in comparison with the conventional waveguide technology. A photograph and the measured S parameter responses of the implemented DBBPF are depicted in Fig. 5.24. The first passband is centred at 4.46 GHz with fractional bandwidth (FBW) of 1.05% and Q_u of 1000. While the higher passband operates at 4.94 GHz with FBW of 0.57% and Q_u equals 950. As can be seen, high inter-band isolation and out-of-band rejections are obtained. An Inter-band transmission zero is introduced providing a high 60 dB isolation between the two passbands. Two asymmetrical TZs are generated below and above the filter passbands at 3.75 GHz and 5.75 GHz, respectively. Also, the frequency tuning capabilities of the fabricated dual-band filter are demonstrated in Fig. 5.25 and Fig. 5.26. Firstly, both passbands are reconfigured at the same time (Fig. 5.25) showing a 260 MHz tuning band from 4.46 GHz to 4.72 GHz at the lower channel and from 4.85 GHz to 5.24 GHz at the upper passband with a tuning window of 390 MHz. Furthermore, each passband is reconfigured independently. Fig. 5.26(a) demonstrates a 200 MHz tuning band at the lower passband from 4.65 GHz – 4.45 GHz, while the upper channel remains fixed at 4.92 GHz. Contrary, in Fig. 5.26(b), the lower channel stays at 4.46 GHz, while the upper passband is tuned over 100 MHz window from 4.90 GHz to 4.80 GHz.

Reconfigurable Third-Order Dual-Band Filter

Fig. 5.27 demonstrates the tunable responses of the implemented three-pole dual-band filter in the previous section. The lower passband is tuned from 4.86 GHz to 5.3 GHz, while the upper channel is tuned from 5.3 GHz to 5.8 GHz. Interestingly, one can see that insertion loss deterioration in such dual-mode-based design (i.e., TM_{120}, TM_{210}) is minimized than what normally noticed in the conventional single-mode-based (i.e., TM_{110}) designs. This is mainly because here the tuners work on magnetic-dominant areas (less E-field, then, less losses), and also due to the less number of used tuners (i.e., half). Another observed feature from the measurements is that the filter maintained a constant absolute bandwidth through the different tuning states at

both channels without following a specific design process, which significantly eases the designers job. Considering the design procedure of tunable filters with CABW provided in chapter 3, this tells us that the required inter-resonator (IR) coupling adjustment in such upward frequency tuning designs (IR coupling should decrease with frequency increase) is less than what is required in the conventional downward frequency tuning designs where the IR coupling should increase with the decrease in the operating frequency.

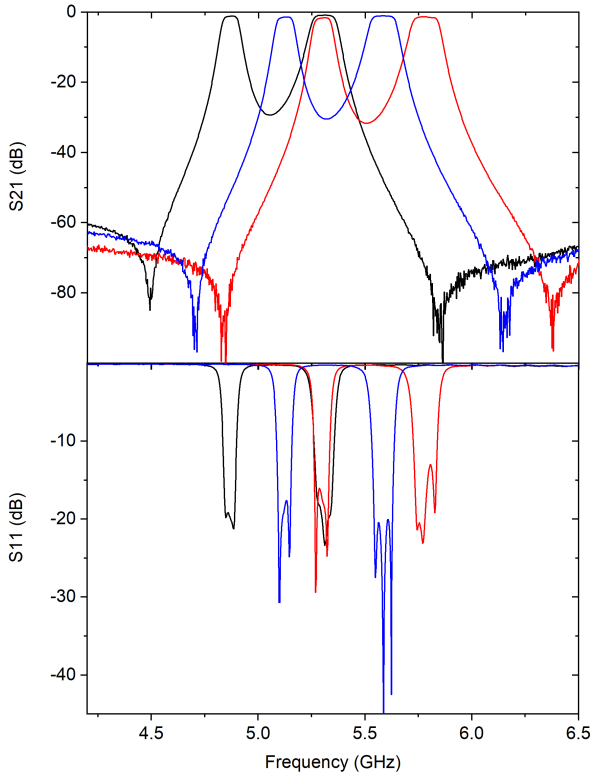

Figure 5.27: Measured reconfigurable responses of the implemented third-order dual-band dual-mode TM-mode filter.

5.2 Very Compact Diplexers Based on Dual-Mode Dielectric TM-Mode Resonators

5.2.1 Introduction

High-Q, compact, and high-power diplexers are an essential component of every multi-band transceiver in a broad range of high-performance evolving applications, including

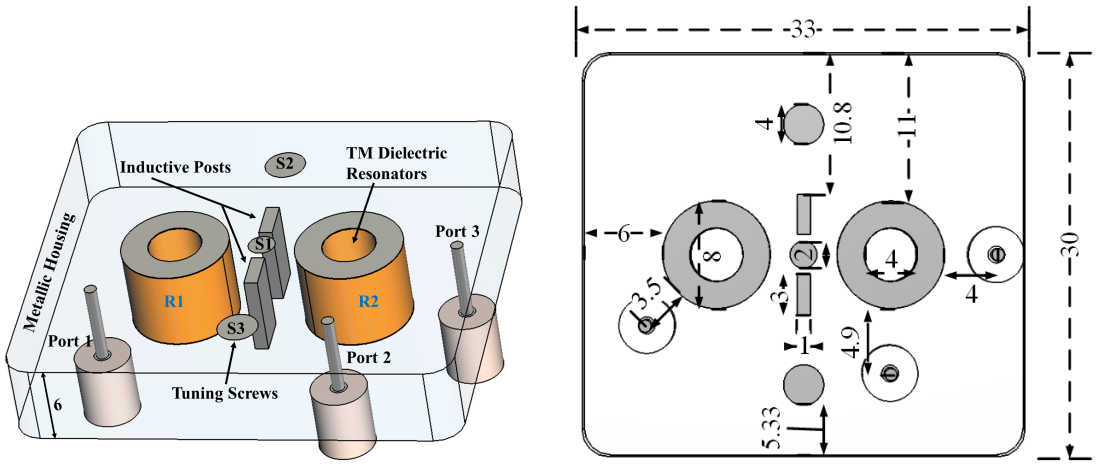

(a) (b)

Figure 5.28: Second-order compact dielectric TM-mode diplexer. (a) Perspective view and (b) top view. All dimensions are in mm unit.

cellular base stations and satellite payloads. Accordingly, many diplexers were presented in the open literature based on various planar and waveguide technologies. In particular, loaded-waveguide diplexers have gained an increasing amount of attention because of their desirable features of more size miniaturization, high-Q, and good power handling capabilities [204, 205, 136, 206, 207, 208, 209, 210, 211]. For example, [204] presented an L-band combline diplexer for space applications with input power up to 1800 watts. Also, a couple of dielectric diplexers were introduced to offer more size compactness and lower losses than coaxial ones based on triple-mode resonators [207], customized corner-cut [208], oval [209] dual-mode HE resonators, and TM_{010} mode resonators [210], [211]. Among all, TM_{010} dielectric resonators have highly desirable advantages of substantial volume-saving, mechanical stability, enhanced high-power performance, and wider spurious-free bands. Hence, they were employed successfully in high-performance terrestrial and satellite filtering components as in [210, 211, 212, 213]. The authors in [210] and [211] recently introduced compact L-band TM_{010} dielectric diplexers for high-power space applications up to 768 W. Also, besides the single-mode TM_{010} mode, the orthogonal modes TM_{120} and TM_{210} were utilized to design very compact dual-mode and dual-band filters [214, 141, 203, 142]. For instance, we recently introduced a miniaturized in-line TM-mode dual-band filter in a planar configuration suitable for mass production [203]. Similarly, diplexers can be designed to benefit from these highly desirable merits.

In this subsection, very compact C-band diplexers based on dual-mode TM-mode

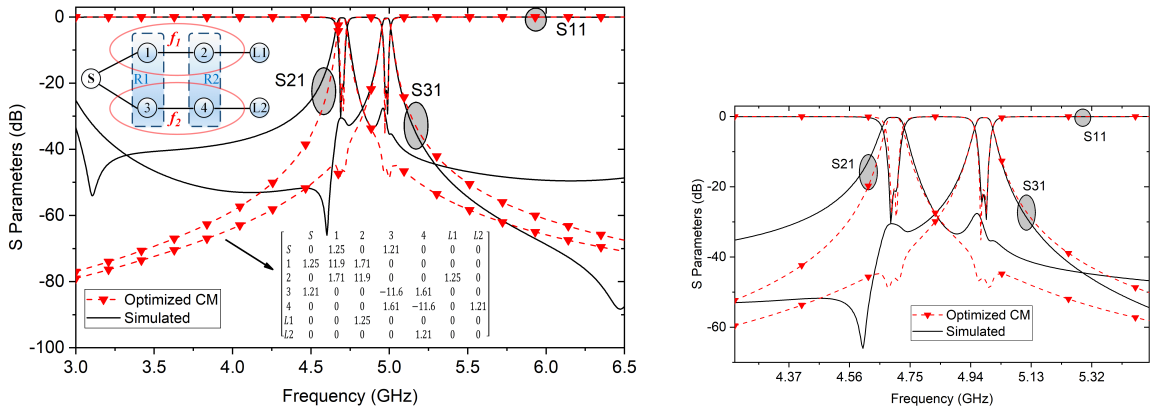

Figure 5.29: (a) Coupling scheme, optimized coupling matrix (redline), and CST EM simulated S-parameters (blackline) of the two-pole diplexer over a wider range. (b) S-parameters over a narrower window.

dielectric resonators are presented. The use of high dielectric constant (Dk) dual-mode TM-mode dielectric resonators attributes a substantial volume saving in comparison with conventional waveguide technology. Also, the proposed diplexer structure eliminates the need for coupling junctions featuring more compactness, handling of higher power levels, and a simpler design procedure. Furthermore, the diplexers are designed in an in-line planar coupling configuration that advantageously provides easy tuning and assembly. Thanks to the planar topology and the properly designed inter-resonator (IR) coupling irises, all the input-output couplings, resonant frequencies, and inter-resonator couplings can be controlled effectively and independently. First, a second-order diplexer is implemented, and its reconfiguration capabilities are reported. Then, another design example of a reconfigurable three-pole diplexer is introduced using a single tuning element.

5.2.2 Second-Order Diplexer

Specifications and Configuration

The configuration, coupling topology, and CST EM simulations of the proposed compact dielectric TM-mode diplexer are depicted in Fig. 5.28 and Fig. 5.29, respectively. The design is based on second-order filters operating at 4.7 GHz (f_1) and 4.98 GHz (f_2) with similar 20 dB bandwidth of 24 MHz. The design procedure begins with the synthesis and optimization of the corresponding coupling matrix based on the

required specifications following the method detailed in [203]. Then, the required inter-resonator couplings and input-output couplings are calculated (K_{12}= 0.009, K_{34}= 0.008, Q_{e1}= 129, Q_{e2}= 137.7). The receiver (RX) and transmitter (TX) channels (f_1, f_2) are realized using the two orthogonal modes TM_{120} and TM_{210} [12], respectively. At the input side (port 1), the feeding pin is positioned at an angle of 45° to couple with both modes simultaneously. Then, two orthogonal outputs (port 2, port 3) are used to couple the RX (TM_{120}) and TX (TM_{210}) channels separately and independently. Two inductive posts are used the realize the required inter-resonator couplings for each channel.

Input-Output Couplings

The input and outputs feedings are realized using inductive wires (grounded at the top side of the housing) soldered on SMA (Sub-Miniature) connectors as shown in Fig. 5.28. The input feeding (port 1) is firstly positioned at a 45° angle to be coupled to both orthogonal modes (TM_{120}, TM_{210}). Then, the coupling strengths are adjusted through the angular spacing between the first resonator and the input feeding (L_1) as depicted in Fig. 5.30(a). At the output side, two perpendicularly positioned feeding probes are used to couple each of the orthogonal modes separately. The first output (port 2) is used to feed only the receiver channel (TM_{120}) and the second output (port 3) is used to couple the transmitter channel (TM_{210}). The corresponding coupling strengths are controlled through the gap between the second resonator and the feeding pins (L_2 for TM_{120} channel, and L_3 for TM_{210} passband) as can be seen in

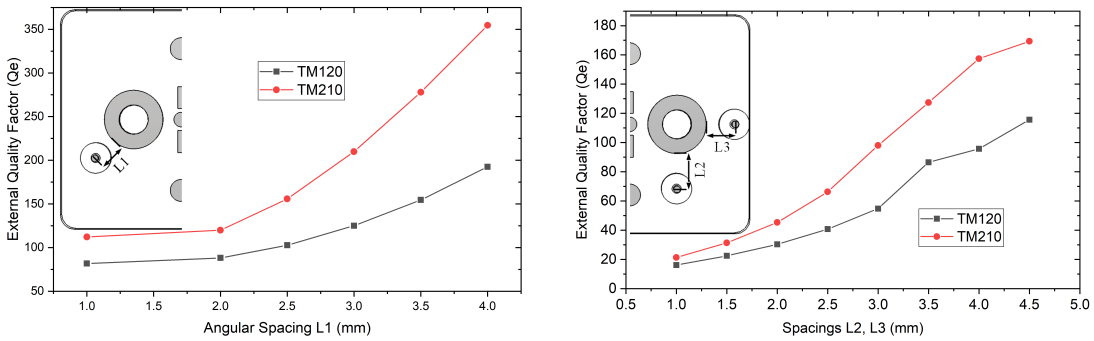

(a) (b)

Figure 5.30: External quality factor of TM_{120} and TM_{210} modes in relation to the IO feeding probes. (a) The dependence of both modes on the angular spacing L_1. (b) TM_{120} and spacing L_2, TM_{210} and spacing L_3. All dimensions are in mm unit.

Fig. 5.30(b).

Inter-Resonator Couplings

It was shown earlier in this chapter that a single central inductive post is employed to obtain the required couplings for dual channels at the same time. Here, we alternatively propose two inductive posts instead of the single central post to provide more flexibility and degree of freedom in realizing the required inter-resonator couplings for both modes more independently. As shown in Fig. 5.31, the required IR couplings are obtained by adjusting the gap between the two posts (D_1) and the distance between the posts and the sidewalls of the cavity (D_2). The IR coupling of TX channel (TM_{210}) is mainly controlled by D_1 (see Fig. 5.31(a)) since the TM_{210} mode resonates in the middle of the cavity. On the other hand, as the TM_{120} mode propagates mainly at the sides, the coupling of the RX channel (TM_{120}) is adjusted using D_2 as exhibited in Fig. 5.31(b).

Especially for such multi-mode designs, tuning screws might be essential to obtain the required responses and compensate for any assembly and fabrication tolerances. It was demonstrated in [142] (refer to the previous section) that such planar TM-mode-based configurations allow efficient tuning of resonant frequencies either simultaneously or independently. Additionally, and thanks to the proposed two-post iris structure here, tuning screws (S1, S2, and S3 in Fig. 5.28) can be added to control the inter-resonator coupling of each channel independently as can be seen in Fig. 5.32.

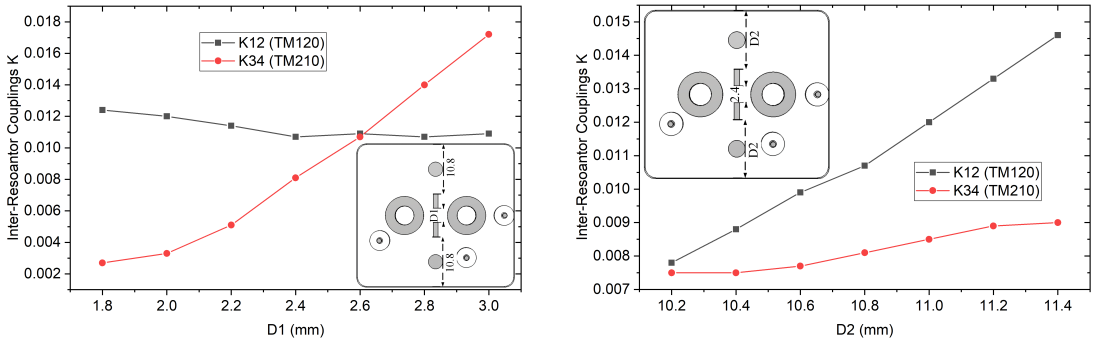

(a) (b)

Figure 5.31: Relationship between the physical coupling coefficients of TM_{120} and TM_{210} modes and (a) the gap between the two posts (D_1), and (b) the distance between the posts and the sidewalls of the cavity (D_2). All dimensions are in mm unit.

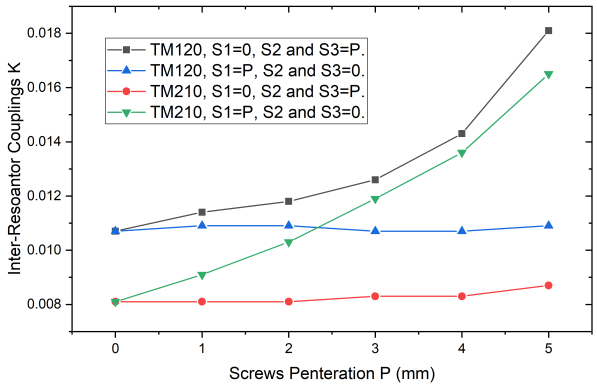

Figure 5.32: Inter-resonator couplings relation to the tuning screws' (S1, S2, S3) penetration (refer to Fig. 5.28).

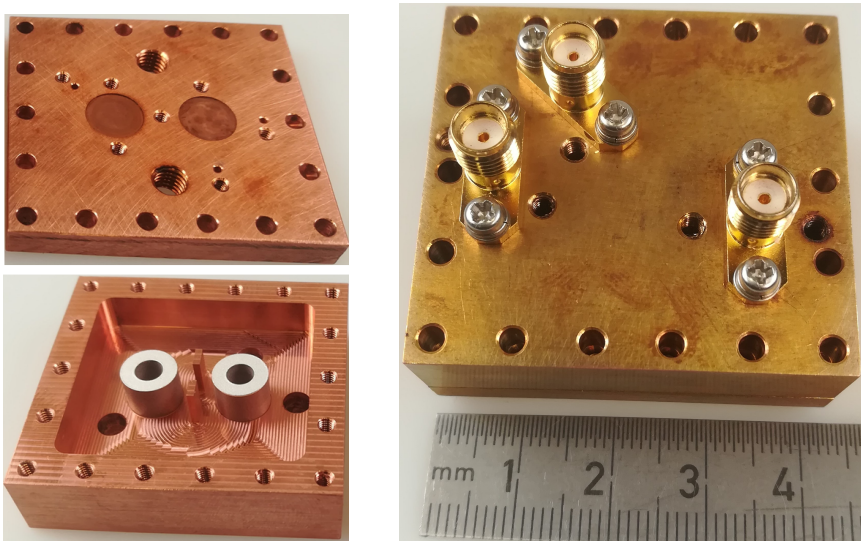

(a) (b)

Figure 5.33: Diplexer prototype. (a) Disassembled parts. (b) Assembled.

This is a key advantage of the proposed structure. It is worth also to note that higher-order diplexers can be designed further effectively following the same design procedure.

Experimental Results

A prototype is manufactured, assembled, and measured to verify the proposed very compact diplexer design. The disassembled components and the final assembled diplexer are exhibited in Fig. 5.33. The TM-mode dielectric resonators are E6045 (Dk = 45, Q-factor = 8000 @ 5 GHz) from EXXELIA [198] with outer diameter =

8 mm, inner diameter = 4 mm, and length = 6 mm. The metallic housing and lid were manufactured using copper metal. The diplexer is then assembled and the DRs were soldered with the metallic cavities using a silver paste. The diplexer prototype has a compact overall volume of 43×40×15.9 mm^3 offering a substantial volume-saving in comparison with the conventional empty-waveguide structures. Fig. 5.34 illustrates the measured S-parameter responses of the implemented compact diplexer showing a good agreement with the re-optimized simulations considering the dielectric constant uncertainty (Dk≈44.2) and assembly tolerances. The first channel (f_1) operates at 4.73 GHz with an insertion loss better than 0.7 dB, while the second passband (f_2) is centered at 5.03 GHz, with an insertion loss of less than 0.9 dB. Both passbands have similar BW of 24 MHz with a return loss better than 21 dB. The estimated quality factor of the manufactured prototype is 1500 (≈50% of simulation), and the isolation between the two channels is higher than 31 dB. Tuning screws were considered in the manufactured prototype, but were not used as the frequency shift is small (less than 1%) and we also do not want to introduce additional losses. Also, the high-power handling capabilities of the introduced diplexer were evaluated using the Spark3D tool. The diplexer has no multipactor discharge breakdowns up to 4700 W at the RX channel and 5200 W at the TX channel. Here, it should be noted that hardware limitations (e.g., SMA connectors) and thermal tests are still needed for complete high-power analysis, especially due to the instability issues of such TM-mode structures over temperature [211]. Table 5.4 summarizes a comparison between the proposed diplexer and similar designs, featuring a very compact structure, higher quality factor, spurious-free band better than 1.9 GHz (lower spurious 2.82 GHz, upper spurious 7.07 GHz), and high power levels up to 5200 W. Furthermore, the

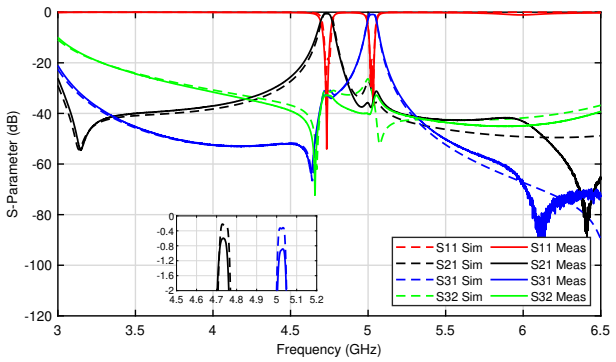

Figure 5.34: Measured results of the proposed very compact TM-mode DR diplexer.

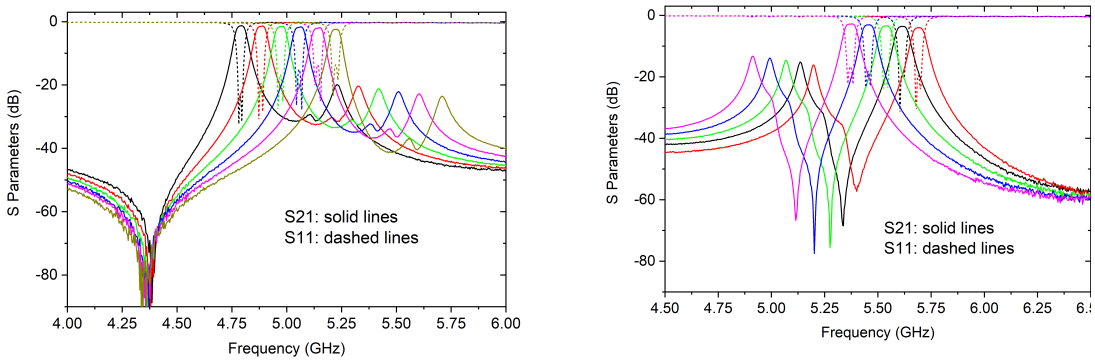

Figure 5.35: Reconfiguration capabilities of a fabricated two-pole diplexer: (a) Lower channel (TM_{120}), and (b) higher channel (TM_{210}).

planar coupling configuration of the presented diplexer brings highly desirable advantages of easy assembly, integration, and tuning, where the operating frequencies and inter-resonator couplings of the diplexer channels can be tuned independently. The isolation of the diplexer prototype is higher than 31 dB which is better than [207] and comparably similar to [208] and [210]. Alternatively, single-mode resonators can be added at the outputs to enhance the isolation similar to [205].

The measured reconfiguration capabilities of a two-pole TM-mode DR diplexer are presented in Fig. 5.35. The RX channel it tuned from 4.79 GHz to 5.22 GHz with insertion loss from 1.3 dB - 2.4 dB, and return loss higher than 13.5 dB. Whereas the TX passband is tuned from 5.37 GHz to 5.69 GHz, with insertion loss varies from 2.75 dB to 3.99 dB, and return loss higher than 16.5 dB. In both passbands, CABW responses are obtained with aid of inter-resonator coupling tuning screws positioned as shown in Fig 5.28. It should be remarked that the increase loss is mainly due to imperfect soldering process. Also, for the same reason, the other-channel suppression is not good, the simultaneous reconfiguration of both channels was not possible as there is an up-shift in one of the TX resonances, and the response cannot be recovered without affecting the other passband.

Table 5.4: Comparison of the Two-Pole Diplexer Prototype with Similar Coaxial/Dielectric-Loaded Waveguide Diplexer Designs.

Ref.	[205]	[207]	[208]	[210]	**This work**
f_0 **(GHz)**	1/1.8	2.55/2.66	1.52/1.64	1.54/1.65	**4.73/5.03**
Order	4/4	3/3	2/2	3/3	**2/2**
FBW (%)	16/6	3.8/3.5	0.85/1.1	2.74/2.96	**0.51/0.48**
IL (dB)	0.72/0.55	0.63/1.1	0.8/0.5	0.17/0.31	**0.7/0.9**
Isolation (dB)	> 50	20	33	≥ 30	$>$ **31**
Size ($\lambda_g{}^3$)	0.0383	0.2653	0.01344	0.0633†	**0.021**
$\mathbf{Q_u}$	190/650	1080/670	810/1050	2000	**1500**
Vol. ($\mathbf{cm^3}$)	1035.26	432	106.24	468†	**5.94**
$\mathbf{Q_u}$**/Vol.** ($\mathbf{cm^{-3}}$)	0.63	2.5	9.88	4.27	**252.53**

(Ref.= Reference, λ_g= Guided wavelength at the lower operation channel, Vol.= Volume).
†Metallic wall thickness included.

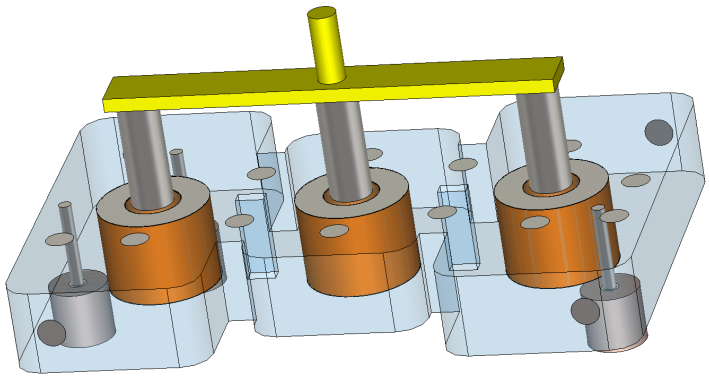

Figure 5.36: 3D structure of a reconfigurable 3-pole dual-mode TM-mode DR diplexer.

5.2.3 Reconfigurable Third-Order Diplexer With a Single Element

A design example of a three-pole dual-mode TM-mode DR diplexer is presented in Fig. 5.36 using a single tuning element. As shown in Fig. 5.37, the lower channel is tuned from 4.76 GHz to 5.56 GHz, while the upper passband is controlled from

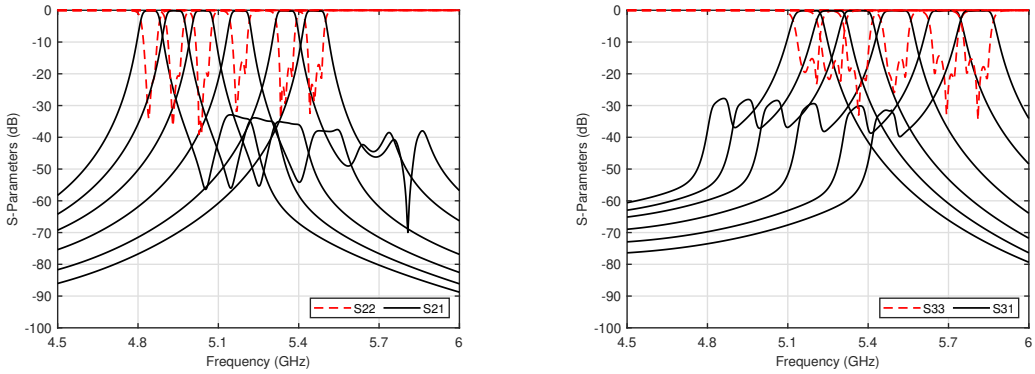

(a) (b)

Figure 5.37: Simulated S-parameter responses of the proposed 3-pole reconfigurable dual-mode TM-mode DR diplexer.

5.09 GHz to 5.81 GHz. The frequency is tuned using a common single element connected to three M3 tuning screws with equal-penetration into the TM-mode resonators. As can be seen, constant ABW responses are obtained effectively, without any further need for other tuning screws.

5.3 Miniaturized Reconfigurable Dual-Mode Dielectric Filters Using Piezomotors for Future Satellite Communications

5.3.1 Introduction

Filter units represent a fundamental part of every RF front-end subsystem including satellite payloads which require compact filters with high unloaded Q-factors (> 500) and high-power handling capabilities. Similarly, high-performance reconfigurable filters are major components in next-generation flexible satellite systems. Various high-Q reconfigurable waveguide filters were presented in the open literature with low-loss and high-power capabilities in [215, 10, 28, 17, 26]. For example, [215] introduced a second-order frequency and bandwidth reconfigurable filter using a dual-mode TE_{311} waveguide cavity for High Throughput Satellite systems (HTS). The frequency is tuned from 11.125 GHz to 11.275 GHz with a constant 52 MHz bandwidth using a stepper motor mechanism. Another output filter for satellite payloads based on an

air-filled waveguide structure was also presented in [10]. The fabricated filter has 200 MHz tunability at a center frequency of 19.8 GHz and 54 – 72 MHz of bandwidth tuning. Also in [17], a frequency reconfigurable combline filter was presented using piezomotors with a 2.7% tuning window. Another tunable dielectric combline filter was also introduced in [26] where a piezoelectric transducer is used to control the movement of a flexible sidewall to change the resonant frequency of the cavity. A fourth-order TEM mode reconfigurable filter is implemented with a frequency range of 4.97 – 5.22 GHz and extracted Q-factor of 550. However, the integration of those filters in future satellites is still burdened by their bulky structures, limited tuning functionalities, and poor spurious-mode responses. Therefore, the introduction of more efficient tunable structures is thoroughly required. In recent years, TM-mode dielectric resonators have attracted an increasing amount of attention in satellite filter applications due to their miniaturized size and better spurious-free ranges, while also being able to exhibit decent unloaded Q-factor values [213, 216, 214, 139]. For instance, a miniaturized L-band TM_{010} mode DR input filter was introduced in [216] for mobile satellite services (MSS) providing a 50% volume reduction with enhanced rejection levels. Also in [214], two degenerate dual-mode TM-mode DRs were employed in transversal configuration to implement a highly compact C-band filter. Additionally, another desirable feature of TM-mode DR filters, especially for the implementation of tunable filters, is that tuning is more feasible than in the other waveguide structures [139]. Therefore, all of the aforementioned advantages strongly promote the employment of TM-mode DR filters for the next-generation of flexible satellite systems.

In this subsection, highly miniaturized reconfigurable dual-mode TM-mode dielectric bandpass filters are introduced for the next generation of flexible satellite payloads. First, a two-pole BPF is presented where all of its parameters including frequency, bandwidth, and TZs can be effectively and flexibly reconfigured. Advantageously, due to this high degree of freedom, frequency tuning can be obtained over a wide frequency range with constant absolute bandwidth responses. Also, two transmission zeros are positioned below and above the passband offering very good out-of-band rejection characteristics. Then, a 4th-order quasi-elliptic filter is introduced with constant absolute bandwidth, using a single tuning element. The closely-positioned transmission zeros are created in in-line configuration, and have a fixed spacing allover the tuning window. To meet the remote control requirement, a piezomotor tuning mechanism is utilized providing an accurate fine-tuning in both filters.

5.3.2 All-Reconfigurable Two-Pole Dual-Mode Filter

Filter Design

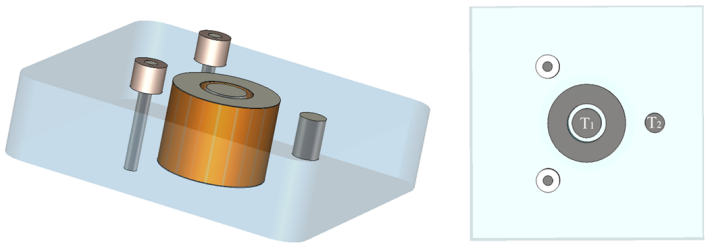

Figure 5.38: 3D (left) and top view (right) of the proposed miniaturized reconfigurable dual-mode TM-mode DR filter.

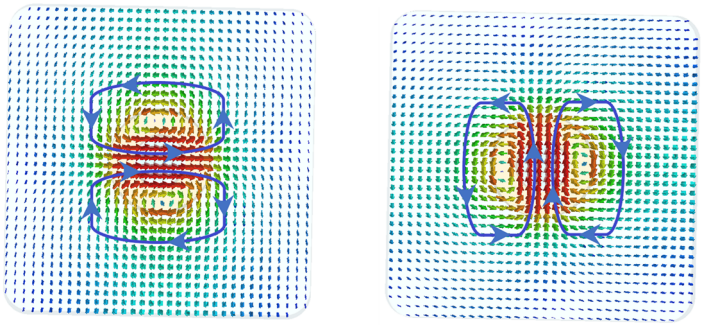

Figure 5.39: Top view of the proposed dual-mode filter showing H-field distribution at the two degenerate modes: TM_{120} (left) and TM_{210} (right).

The proposed pseudo-elliptic C-band dual-mode TM-mode dielectric resonator filter is depicted in Fig. 5.38. The 2nd-order filter is designed using two orthogonal degenerate modes, namely TM_{120} and TM_{210}, in a single resonator structure as shown in Fig. 5.39. The resonator dimensions are carefully chosen in order to assure adequate separation between the operating modes and the other unwanted lower and upper spurious modes. The selected TM-mode resonator has a dielectric constant (Dk) of 45 with an 8 mm outer diameter (D), 4 mm inner diameter (d), and a height of 6 mm. It is also worth mentioning that as the TM operating modes are independent of Z-axis; the resonator height is chosen based on the desired unloaded-Q, structure compactness, and the spurious modes separation.

The corresponding S-parameter responses of the proposed miniaturized two-pole dual-mode TM-mode filter are shown in Fig. 5.40(a). The two degenerate modes (TM_{120}, TM_{210}) constitute a doublet operating at 4.74 GHz with a bandwidth of

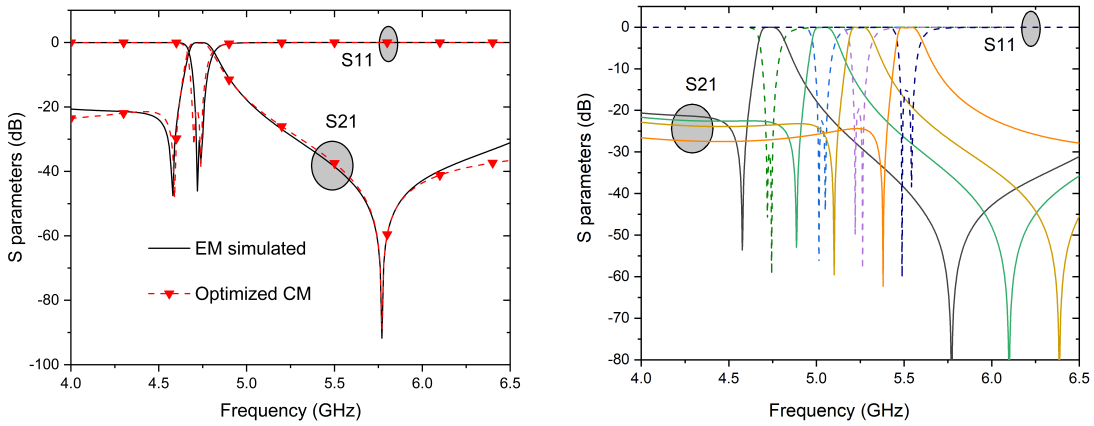

Figure 5.40: (a) EM simulated S-parameter responses and optimized coupling matrix (CM). (b) Simulated S-parameter responses of the proposed all-reconfigurable dual-mode TM-mode DR filter with CABW.

50 MHz. The filter is designed to obtain a high-selectivity pseudo-elliptic response by introducing two independent transmission zeros in the lower and upper stopband regions. The doublet configuration introduces one TZ on the left side of the passband while the fundamental TM_{110} non-resonating mode (NRM) creates a source-load by-pass path ($-M_{SL}$) to introduce another TZ on the right side. The first transmission zero is located closely at 4.57 GHz while the second TZ is positioned at a frequency of 5.76 GHz. Sub-miniature connectors (SMA) are used for input-output feeding through grounded inductively-coupled pins as shown in Fig. 5.38 The IO feedings are

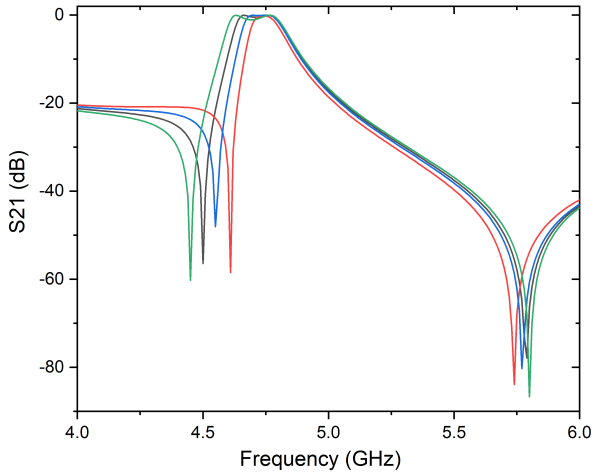

Figure 5.41: Bandwidth reconfiguration of the proposed all-reconfigurable dual-mode TM-mode DR filter.

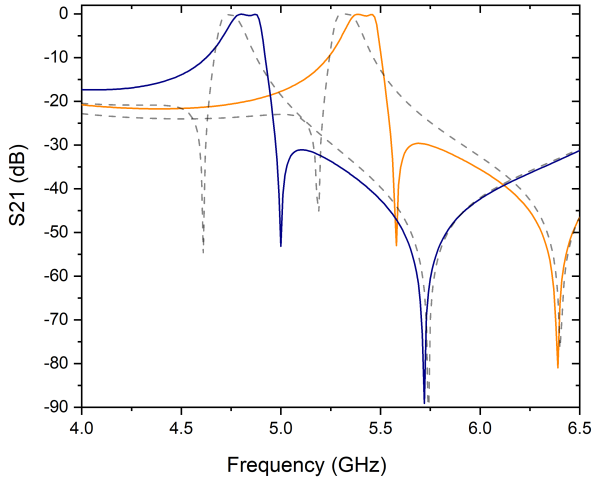

Figure 5.42: An example of the doublet's TZ reconfiguration at the lowest and highest tuning states: TZ at the left side where $f_{120} < f_{210}$ (dashed line), and TZ shifted to the right side after M_{11} sign changes where $f_{120} > f_{210}$ (solid line).

aligned angularly in mirror configuration in order to excite both orthogonal modes simultaneously. Next, following the above design specifications, the corresponding coupling matrix [M] can be synthesized by extracting the different coupling components following the procedure stated in [217] for the doublet configuration and [218] for the non-resonating mode representation. The final optimized coupling matrix is:

It should be noted that, unlike the transversal configuration presented in [214], the proposed dual-mode TM-mode filter here is designed in a planar configuration for the purpose of easier and more flexible tuning from the top side as it's highly favorable for the implementation of reconfigurable filters.

Next, a fully and flexibly reconfigurable filter is designed using the presented dual-mode TM-mode DR filter. All filter parameters including the frequency, bandwidth, and transmission zeros can be effectively reconfigured using just two metallic tuning pins (T_1, T_2). The resonant frequencies of both modes are reconfigured simultaneously using the T_1 through the inner hole of the TM-mode resonator. In the TM_{120} and TM_{210} modes, unlike the fundamental TM_{110} mode where the max E-field is focused in the centre of the resonator and H-field is rotating in the surroundings, the max H-field is primarily located in the centre of the resonator (see Fig. 5.39). Thus, the frequency shifts upwards as the T_1 tuning pin is introduced into the resonator body. Since there is no intracavity coupling between the two orthogonal modes ($M_{12} = M_{21} = 0$), the filter bandwidth can be controlled by tuning each mode separately. The bandwidth, however, is reconfigured by tuning the TM_{120}

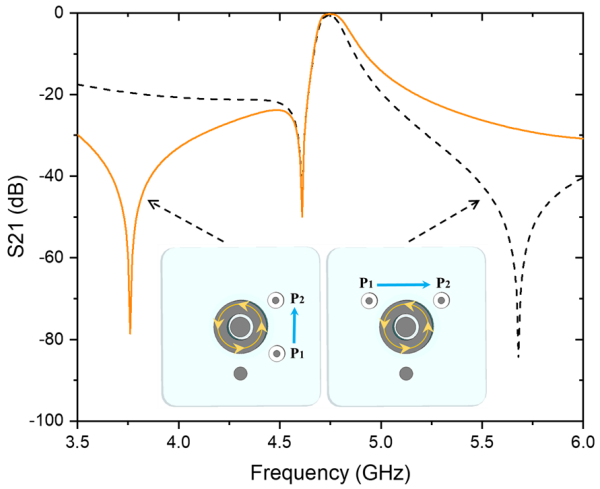

Figure 5.43: An example of the TM_{110} non-resonating mode TZ reconfiguration at the lowest tuning state: TZ positioned at the left side where source (P_1) – load (P_2) is in the same direction of TM_{110} H-field (M_{SL}) (solid line), and TZ shifted to the right side where S-L is in opposite direction to TM_{110} propagation (- M_{SL}) (dashed line).

mode using the tuning pin T_2. This advantage of flexibility in BW tuning remarkably contributes to the implementation of reconfigurable filters with constant passband responses throughout the tuning band. Fig. 5.40(b) shows the simulated results of the presented reconfigurable dual-mode TM-mode DR filter with constant absolute bandwidth responses of 50 MHz. The filter is tuned from 4.74 GHz to 5.51 GHz providing 15% of frequency tuning. Also, bandwidth reconfiguration capability is demonstrated in Fig. 5.41 with more than one-octave of BW tuning.

In addition to the frequency and bandwidth reconfiguration functions of the proposed pseudo-elliptic filter, the positions of the two transmission zeros are also independently controllable. One of the unique features of the generalized doublet configuration is the introduction of a TZ on one side of the passband without the need for any auxiliary cross-coupling/extracted-pole configurations. Furthermore, the TZ can be easily configured to either side of the passband by just changing the self-coupling sign of the operating degenerate modes [217]. This can be seen in Fig. 5.42 wherein which the TZ that is produced through the bypass coupling remains fixed while the doublet TZ is shifted to the right side of the passband by changing the self-coupling sign of the first mode TM_{120} using T_2 pin. On the other hand, the position of the TZ produced through the bypass coupling can also reconfigured independently by the I/O feeding arrangement and the control of the coupling ratio between the reso-

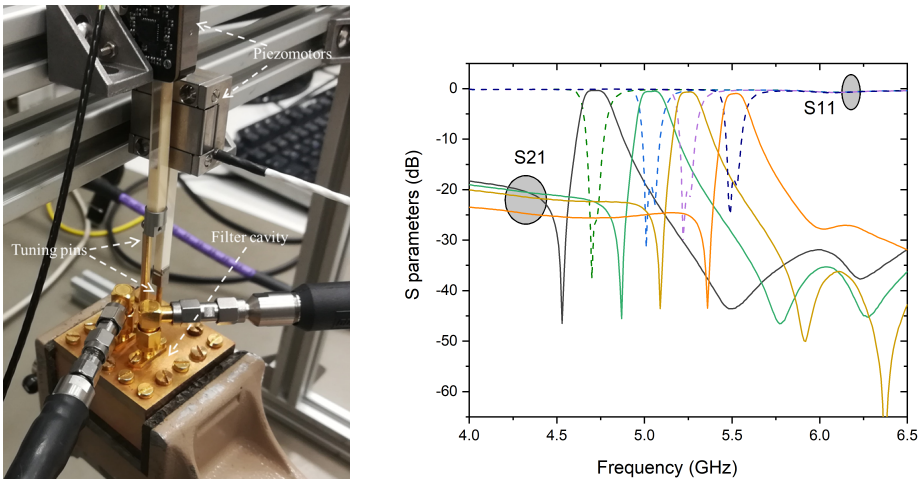

(a) (b)

Figure 5.44: (a) Photograph, and (b) measured S-parameter responses of the proposed reconfigurable dual-mode TM-mode DR filter.

nant orthogonal TM-modes and the TM_{110} NRM as explained in [218] and shown in Fig. 5.43.

Experimental Results

For the purpose of validation and demonstration of the proposed all-reconfigurable dual-mode DR filter, a prototype filter was built and measured. The hollow TM-mode dielectric resonator that has been used is a compact E6045 (Dk = 45, Q-factor = 8000 @ 5 GHz) from EXXELIA [198]. The resonator is then metalized inside a 24×24×6 mm_3 metallic brass box. In reference to the accurate and digitally-controlled tuning requirement of future flexible satellite payloads, a dual piezomotor fixture is attached to the tuning pins T_1 and T_2. The filter setup and the measured results are shown in Fig. 5.44(a) and Fig. 5.44(b), respectively. Measurements show very good agreement with simulations. The frequency is tuned from 4.72 GHz to 5.51 GHz with a constant absolute bandwidth of 50±5 MHz. The fabricated filter has demonstrated a high unloaded Q-factor ranging from 1100 to 540 with low midband insertion loss ranging from 0.2 – 0.9 dB and return loss higher than 18 dB. The Q-factor can even be enhanced further by ensuring perfect soldering and also by silver-plating the filter cavity and the associated tuning pins.

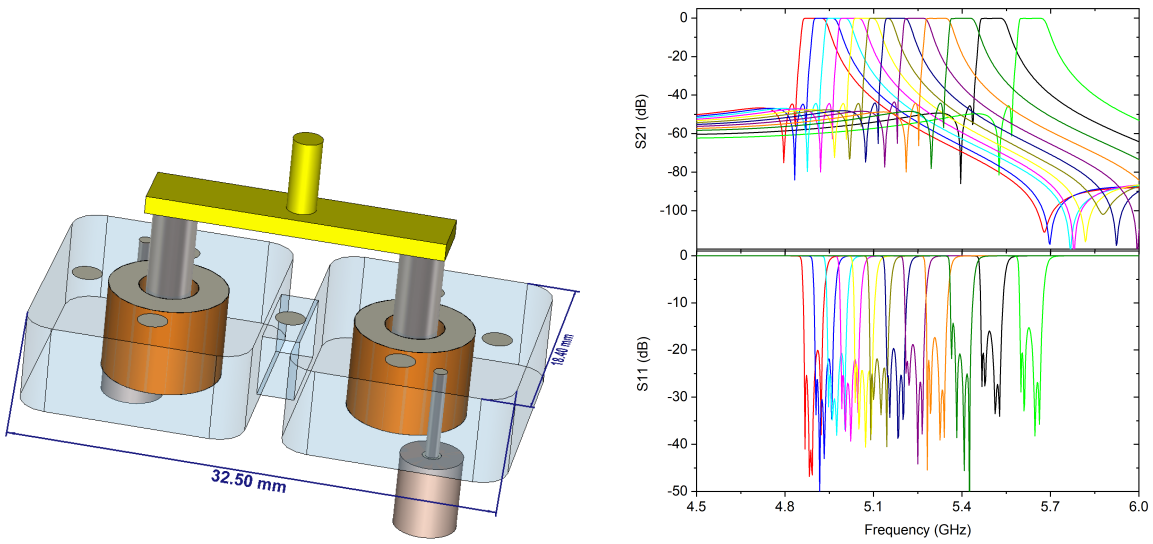

(a) (b)

Figure 5.45: (a) 3D structure, and (b) simulated S-parameter results of the proposed 4th-order reconfigurable dual-mode TM-mode DR filter.

5.3.3 Reconfigurable 4th-Order Filter With a Single Element

Fig. 5.45 depicts a compact four-pole reconfigurable dual-mode filter using a single element. Two identical M3 screws are used for tuning and controlled through a common element, for simplification and faster tuning. The filter is tuned from 4.91 GHz to 5.63 GHz with a constant absolute bandwidth of 66±4 MHz, and two closely-positioned transmission zeros with stable spacing at all tuning states. A first prototype is then implemented and assembled as shown in Fig. 5.46 using piezomotors for accurate remote-tuning, similar to the above two-pole filter. The measurements in Fig. 5.47(a) exhibit that the filter can be tuned from 4.97 GHz to 5.48 GHz with insertion loss from 1.7 dB to 2.97 dB, and return loss higher than 8 dB. This increase loss is mainly related to imperfect assembly and soldering, therefore, a second prototype is being sent for manufacturing. Nevertheless, the results still feature the constant ABW and TZs' spacing. The wideband response of the presented filter is demonstrated in Fig. 4.47(b) showing a spurious-free band wider than 1.7 GHz.

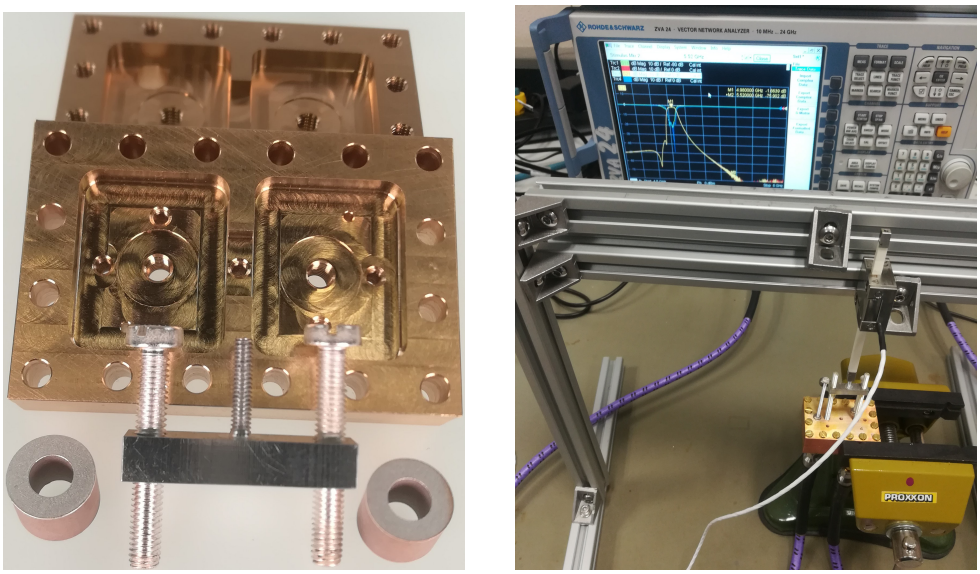

(a) (b)

Figure 5.46: Implemented 4th-order reconfigurable dual-mode filter: (a) Disassembled parts. (a) Overall setup.

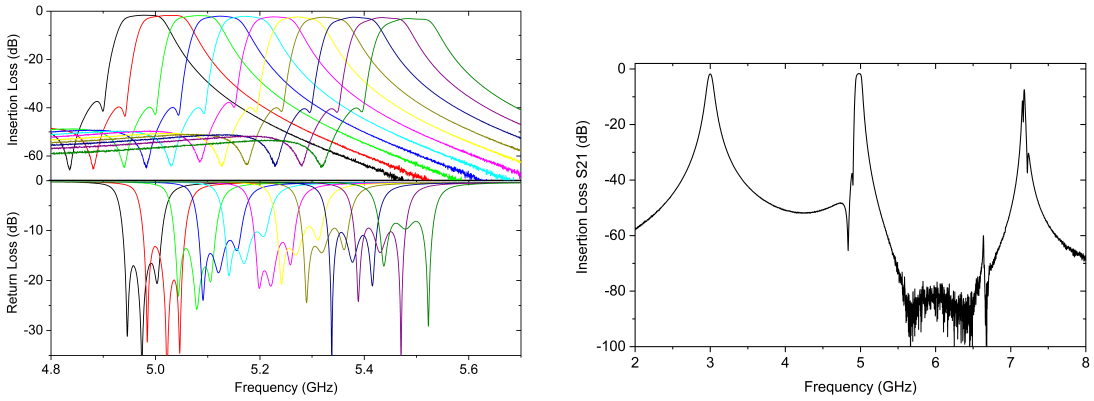

(a) (b)

Figure 5.47: Measured results of the fabricated 4th-order reconfigurable dual-mode filter: (a) Tuning window. (a) Wideband response.

5.4 Summary

This chapter presented several compact reconfigurable bandpass filters and diplexers based on dual-mode TM-mode dielectric resonators as follows:

• In section 5.1, miniaturized fixed and reconfigurable dual-band dual-mode TM-mode dielectric filters were presented in planar configuration. The use of the TM-mode DRs and the orthogonal degenerate TM_{120} and TM_{210} modes effectively provide

substantial compactness with high Q_u and good spurious-free response. Also, high inter-band isolation and outer-band rejections are obtained through the introduction of flexibly controlled transmission zeros. The proposed planar configuration brings various advantages in comparison with the transversal configuration including easier tuning, assembly, and production. All these features strongly promote the employment of the presented planar design in other ultra-compact components (e.g., tunable filters, diplexers). Various design examples and prototypes have been manufactured and the measurements allow for the design approach to be verified.

• A new class of very compact fixed and reconfigurable in-line diplexers based on dual-mode dielectric TM-mode resonators in planar coupling configuration were introduced in section 5.2. The proposed diplexers have many desirable advantages including substantial volume-saving, high quality-factor, good spurious performance, and high-power handling capabilities. Besides, thanks to the planar configuration and the proposed iris structures, the introduced diplexers feature easy assembly and efficient, independent tuning process for both transmission and reception channels.

• Section 5.3 presented highly compact reconfigurable C-band pseudo-elliptic BPFs for future flexible satellite payload applications. Thanks to the miniaturized dual-mode TM-mode dielectric resonator, the proposed filters offer a significant volume reduction of up to 75% in comparison with the conventional waveguide technologies. In a first two-pole example, both frequency and bandwidth are effectively tuned offering 15% of frequency tuning with constant absolute bandwidth and high unloaded-Q throughout the tuning window ($Q > 500$). Additionally, two independently reconfigurable transmission zeros are introduced attributing a high-selectivity and excellent out-of-band rejections. In a second design of 4th-order filter, quasi-elliptic responses with CABW were effectively obtained in inline configuration using a single tuning element. A piezoelectric motor-based tuning mechanism is employed in both filters for accurate and fine remote control. All of these attractive features strongly promote the proposed compact reconfigurable filters for the next-generation flexible satellite and other high-performance applications.

Chapter 6

Microfluidic-Based Ultra-Wide Tuning Technique for TM_{010} Mode Dielectric Resonators and Filters

This chapter introduces a new technique of designing widely frequency tunable TM_{010}-mode dielectric-loaded waveguide resonators and filters. The proposed tuning method is based on using liquid metals to tune the resonant frequency by altering the liquid level inside the resonator hollow-channel. First, a single-pole bandpass filter is designed, fabricated, and measured for proof-of-concept purposes. The realized filter demonstrated wide frequency tuning from 2.33 GHz to 0.67 GHz maintaining low insertion loss < 1 dB allover the tuning window. Furthermore, a two-pole bandpass filter is implemented and tested, exhibiting a wide octave tuning range from 2.75 GHz to 1.24 GHz with 76% of tunability. The presented results advocate the great potential of the proposed technique in high-performance widely-tunable next-generation RF systems.

6.1 Introduction

The massive evolution in the various multi-standard and multi-band communication technologies has emerged a vital demand for more efficient and flexible RF front-end components and filters to manage the increasingly crowded spectrum more effectively. High-performance frequency-agile filters are key and fundamental component of many current and next-generation communication services, including future flexible satellite

payload systems. Dielectric resonators have been introduced since the early '60s and employed widely in various microwave applications due to their compact structures and good spurious-free performance in comparison with the other waveguide configurations, in addition to the high unloaded-Q and the ability to operate at high power levels. Accordingly, a couple of tunable bandpass filters have been introduced based on dielectric resonators in different hybrid electric-magnetic modes (e.g., HEH, HEM, TME), using various tuning methods as in [21, 27, 43, 68].

Generally, the tuning methods for dielectric resonator filters presented in previous literature are distributed into two main techniques: mechanical tuning and electrical tuning. In the mechanical tuning method, the frequency is tuned using movable tuning elements (e.g., screws, discs, sidewalls) as presented in [21] and [27]. Despite the straight-forward tuning and high power handling capability, these designs are burdened by the bulky size, high complexity, high cost, and low-speed of tuning. All above is in addition to the very small and limited tuning range. On the other hand, electrical tuning elements (e.g., varactors, RF MEMS) were utilized in [43] and [68] to bring the advantages of higher tuning speed, reduced size and cost. However, such filters suffer from major limitations in terms of linearity, quality-factor, and high-power handling capability. Besides, the challenging integration of semiconductor and MEMS tuning circuits on the 3D resonator structures incorporates more losses and increases the filters' complexity. All of these drawbacks limit the capability of attaining low-loss over wide tuning ranges. [219] presented a hybrid tuning method combining both mechanical and electrical tuning techniques, proposing an electrically switchable tuning rod to improve the speed of tuning. However, it also shares the same limitations of bulky, complex structure, and small tuning range.

TM_{010} mode dielectric resonators and filters were firstly presented in [220], a few decades ago. In recent years, they have received increasing attention and employed successfully in many major high-performance applications (e.g., mobile base-stations, satellite payloads) due to their strongly desirable features in comparison with the other dielectric resonators. They offer high volume-saving and also better spurious-free stopbands, besides the improved stability against vibrations and more feasibility for tuning. All of these advantages promote the use of TM_{010} mode dielectric resonators in the implementation of high-performance tunable bandpass filters, which according to our knowledge, has never been reported in the previous literature.

Liquid metal (LM) microfluidics have recently been explored as a promising switching and reconfiguration candidate [93], mainly because of their linear properties, low-

loss, and compatibility with high-power applications. A couple of planar and hybrid reconfigurable/tunable filters were introduced using liquid microfluidic-based concepts [93, 95, 221, 101, 222]. However, the performance of such PCB-based structures is always limited by the low power handling, low Q-factor, and increasing loss, which subsequently affects the tuning capabilities. Also, a microfluidically reconfigurable TE_{01} mode rectangular waveguide (RWG) filter was presented in [222]. Despite the advantage of high-power performance of the hollow-waveguide structures, the proposed filter has shown a very small frequency reconfiguration and a relatively high insertion loss.

In this chapter, a new microfluidic-based, frequency tuning mechanism for the design of widely tunable TM_{010} mode dielectric resonators and filters is presented. The proposed tuning method is based on the actuation of liquid metals inside TM_{010} mode hollow ceramic resonators, where the inner hole of the resonators is used as a channel for the liquid metals [223]. This mechanism provides the advantage of getting the highest possible achievable frequency tuning with minimal losses and high-quality factors. Furthermore, the presented tuning technique is applied in a simple, low-cost, and efficient configuration.

6.2 Concept and Design

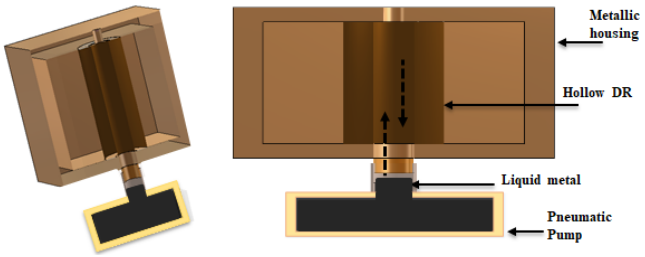

Figure 6.1: Illustration drawing (cut-away view) of the proposed widely tunable TM-mode dielectric-loaded waveguide resonator using liquid metal actuation.

An illustration drawing of the proposed liquid metal tunable TM_{010} mode resonator configuration is shown in Fig. 6.1. The proposed embodiment comprises a hollow cylindrical TM-mode dielectric resonator, a metallic housing, a liquid metal, and a pump. The operation concept is based on LM actuation inside a containing hollow resonator to tune the resonant frequency. The ceramic resonator is metalized and connected with the bottom and top walls of the metallic housing operating at

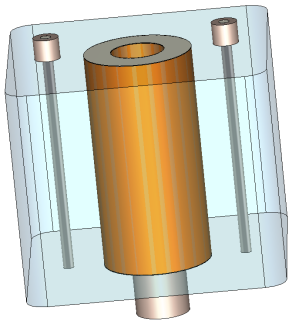

Figure 6.2: EM-based 3D model of the proposed widely tunable 1-pole BPF.

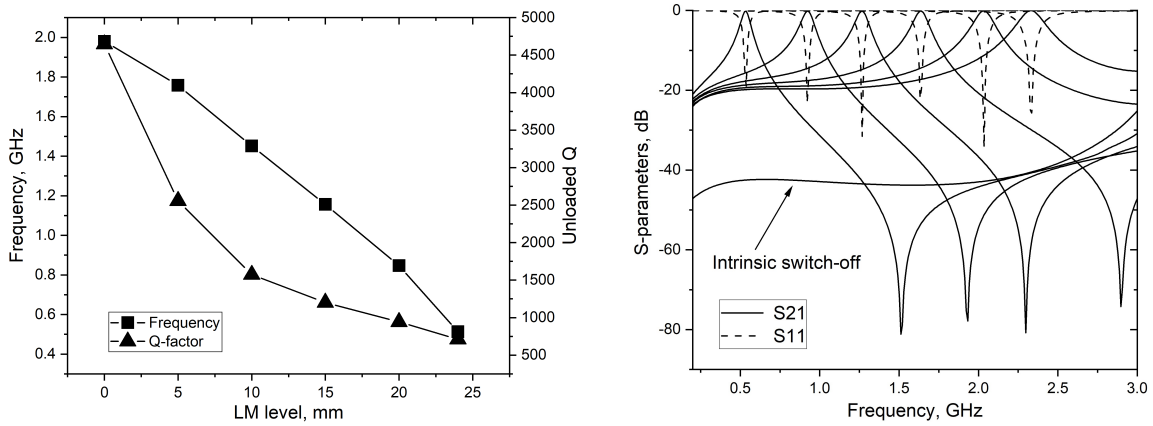

(a) (b)

Figure 6.3: Simulated filter responses: (a) Simulated frequency and unloaded Q-factor as a function of the LM level inside the resonator channel. (b) Simulated S-parameter responses with different tuning states.

TM_{010} mode. The inner hole of the dielectric hollow resonator is utilized as a containing channel for the intrusion of the liquid metal from the bottom of the metallic housing. Then, the in-going LM functionalizes as a tuning post to change the resonant frequency of the resonator. As LM level increases inside the channel, the EM field is perturbed resulting in a decrease of the resonant frequency. A microfluidic eutectic alloy of gallium, indium, and tin —commercially known as "Galinstan"— is chosen here due to its advantages of relatively higher electrical conductivity ($\sigma = 3.46 \times 10^6$ S/m) and non-toxic characteristics. The pump is used to pneumatically control the movement of the liquid metal inside the resonator channel.

In addition to its advantages stated in the previous section, the TM_{010}-mode resonator structure is particularly chosen because of two key reasons. Firstly, its configuration is ideally suitable for the proposed mechanism as the LM can be actuated

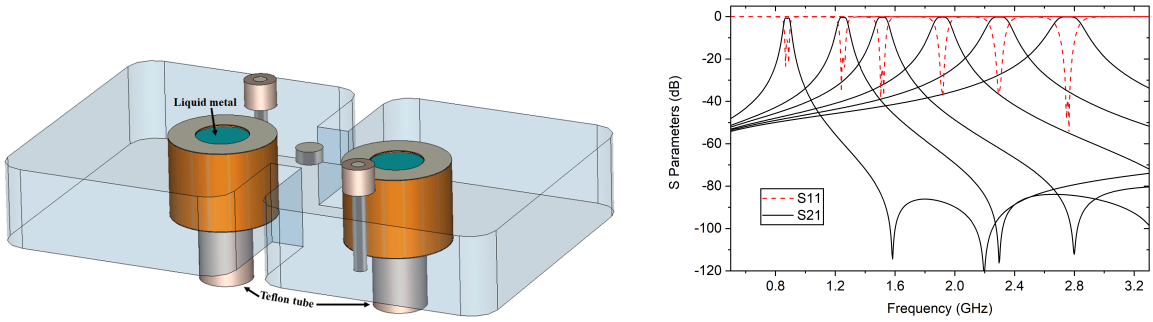

(a) (b)

Figure 6.4: Two-pole LM-tunable TM-mode DR filter: (a) 3D structure. (b) Simulated S-parameter responses with different tuning states.

simply and effectively through a direct, single path with no need for any further modifications or elements. Secondly, since the electric field of the TM_{010}-mode dielectric resonator is confined and focused at the center of the resonator where the LM is being actuated, the proposed mechanism can be applied efficiently to provide a very wide frequency tuning window.

To verify and evaluate the proposed concept of widely tunable TM_{010}-mode resonator filters, a one-pole bandpass filter is designed and investigated in terms of its performance and tuning capabilities. Fig. 6.2 demonstrates the 3D EM model of the proposed structure. It includes a metallic box surrounding a dielectric resonator with a relative dielectric constant of 44 and an unloaded quality factor equals to 20000. The filter is designed to operate at 2.33 GHz which represents the initial frequency of the tuning window. Since it is a TM-mode structure, the height of the dielectric resonator does not affect the resonant frequency, but just on the unloaded quality factor. Then, the outer and inner diameters of the resonator are adjusted to obtain the desired resonant frequency. The used resonator height is 25 mm to offer a relatively high-Q and more room for tuning, while the outer and inner diameters are chosen here as 10 mm and 5 mm, respectively. A metallic cavity ($30\times30\times25$ mm^3) is adjusted properly to attain a high Q-factor and a good spurious-free stopband.

The proposed structure is firstly investigated using Eigenmode analysis in CST microwave studio without the IO feeds to precisely evaluate the unloaded-Q. Simulations considered Copper ($\sigma = 5.8 \times 10^7$ S/m) as housing metal, and liquid metal Galinstan with electrical conductivity equals to 3.46×10^6 S/m. The simulated frequency and unloaded-Q factor responses are illustrated in Fig. 6.3(a) in relation to the LM variation inside the resonator channel. As can be seen from the graph,

wide frequency tuning is achieved with high-Q factor measures. The channel is filled gradually with Galinstan up to 24 mm and the resonant frequency shifted down accordingly, covering a wide span of frequencies ranging from 1.98 GHz to 0.51 GHz providing wide tunability of 118%. Also, a high Q-factor is maintained all over the tuning window ranging from 4600 to 710. These competitive advantages exhibit the potential of the proposed tuning technique as a promising solution for the design of high-performance and widely tunable loaded-waveguide filters.

In tunable filters, proper IO coupling is essentially required to maintain low-loss responses across the different tuning frequencies. This becomes more challenging in widely tunable filter structures and could cause a significant decrease in the tuning performance. Herein, a 1-pole bandpass filter is implemented to check the feasibility of the proposed wide tuning mechanism in TM_{010}-mode tunable filters. The RF feeding configuration is depicted in Fig. 6.2. The IO coupling is realized using strongly-coupled capacitive feeding pins to cover the whole wide tuning band effectively with low insertion loss. The simulated S-parameters of the proposed widely tunable TM_{010}-mode filter are shown in Fig. 6.3(b). The frequency is tuned over a wide range from 2.33 GHz to 0.54 GHz with a high Q-factor (> 600) and low insertion loss (< 0.3 dB). Also, an additional desirable feature of intrinsic-switching is presented, as in which the passband can be easily switched off by just filling the whole resonator channel with LM cutting all field lines of the operating TM_{010}-mode. Similarly, Fig. 6.4 presents another example of a two-pole LM-tunable bandpass filter with an ultra-wide tuning

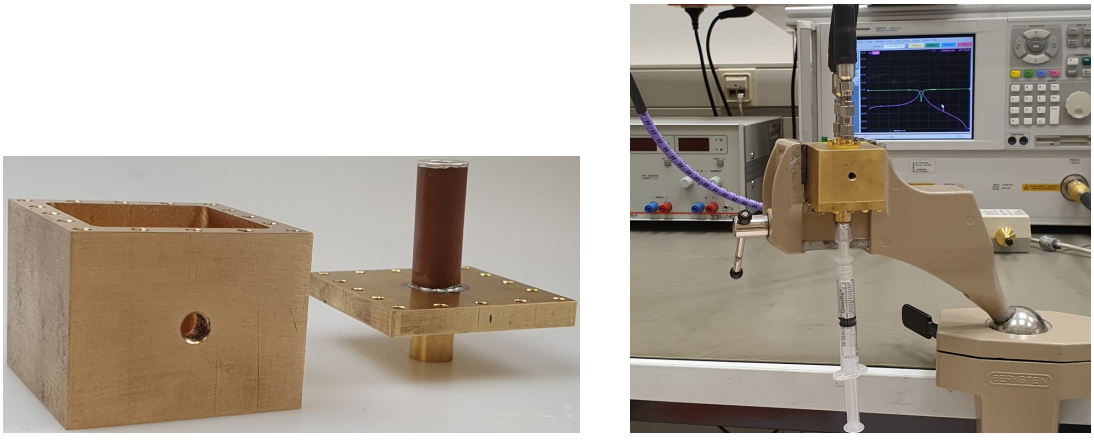

(a) (b)

Figure 6.5: Fabricated prototype of liquid metal-actuated TM_{010} dielectric resonator: (a) Disassembled, and (b) assembled.

window from 2.75 GHz to 0.88 GHz and 103% of tunability. The evaluated simulated Q-factor varies from 2230 to 500.

6.3 Experimental Results

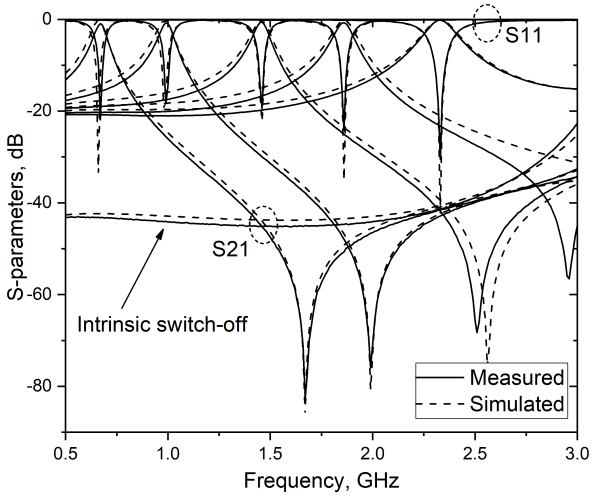

Figure 6.6: Measured and simulated S-parameters at different tuning states including the intrinsic switch-off feature.

To validate the proposed concept, 1-pole and 2nd-order liquid metal tunable TM_{010}-mode filters are fabricated, assembled, and measured. The 1-pole filter components and its measurements are depicted in Fig. 6.5 and Fig. 6.6, respectively. The dielectric resonator is firstly enclosed and well-soldered with the metallic cavities to ensure against any leakage in the liquid channel. Next, the channel is firstly cleaned with 1% NaOH electrolyte solution to facilitate the movement of LM, and then Galinstan is pneumatically actuated inside the resonator channel using a syringe. The measured S-parameter responses validates the ability to cover a wide frequency span with low losses. The passband frequency is tuned from 2.33 GHz to 0.67 GHz with wide tunability of 110%. Also, low insertion loss is maintained all over the tuning window better than 1 dB, and return loss higher than 18 dB. The filter has a wide spurious-free band up to $5f_0$. Additionally, the desirable intrinsic switching feature of the passband is effectively demonstrated. The extracted effective Q-factor varies from 1660 to 120 mainly attributed to the uncertain effective conductivity of Galinstan liquid metal and the lossy effect of NaOH. Therefore, the use of other less dispersive electrolyte solutions (e.g., Teflon solutions) is being considered in further

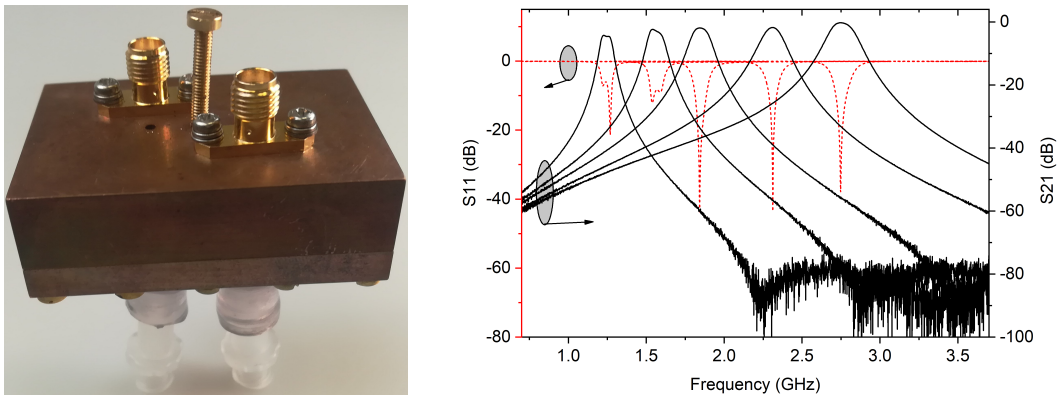

(a) (b)

Figure 6.7: Fabricated liquid metal-actuated 2nd-order TM_{010} dielectric filter. (a) Final assembled prototype. (b) Measured results.

investigations under more robust conditions to enhance the Q-factor and reduce the losses. Also, it should be noted that the Q-factor can be increased by using better electrically-conductive metals to manufacture the cavities instead of the brass metal used in the proof-of-concept prototype ($\sigma = 1.59 \times 10^7$ S/m). The Galinstan was actuated smoothly inside the ceramic channel without experiencing any absorption or stickiness issues. Nevertheless, an alternative reliable solution of micro Teflon-coating can be applied effectively to the ceramic channel if there are any such worries. For further verification, the 2nd-order BPF is also manufactured and measured as depicted in Fig. 6.7, showing a wide tuning range of 1.51 GHz from 2.75 GHz to 1.24 GHz. The measured insertion loss is 0.3 dB at the initial state with no LM, and increases with the gradual actuation of the LM inside the filter up to 4.2 dB.

The advantages of the introduced technique can be seen in comparison with the similar LM reconfigurable resonators and other tunable DRs as shown in Table 6.1. Considering the current development and improvement in the LMs properties and research, all of the aforementioned attractive and distinctive features strongly promote the proposed tuning technique in wideband, high power, and low-loss RF applications. Nevertheless, once can comment that as this is a relatively new topic, where still more development and extensive research are needed to improve the LM properties, and qualify it for high-performance and industrial applications.

Table 6.1:
Comparison of the proposed mechanism with similar LM-based tunable resonators and other DR tuning methods.

Ref.	**Structure**	**Frequency range**	**tuning (%)**	**IL (dB)**	Q_u
[221]	SIW	3.8 – 5.8	41.7%	NA	160 - 530
[222]	RWG	17.5 – 17.6	0.57%	≥ 2.8	NA
[101]	CC	2.9 – 9.9	109.4%	NA	120 - 625
[27]	DR	15.62 – 15.86	1.52%	NA	421 - 1638
This work	**DR**	**0.67 – 2.33**	**110.7%**	**< 1**	**120 - 1660**

(SIW: substrate integrated waveguide, RWG: rectangular waveguide, CC: coaxial cavity, DR: dielectric resonator).

6.4 Summary

A novel microfluidic-based mechanism for the design of widely tunable TM_{010}-mode dielectric-loaded waveguide resonators and filters was presented in this chapter. Single-pole and 2nd-order bandpass filters were designed, fabricated and measured for proof-of-concept purposes with good agreement between simulations and measurements. In addition to the wide tuning feature, the proposed method demonstrated many advantages including intrinsic switching, low-loss, simple and low-cost configuration. This new tuning technique is presented as a promising solution in future high-performance wideband frequency-agile systems and technologies.

Chapter 7

Bandwidth-Reconfigurable Coaxial Bandpass Filters With Multi-Octave Tuning Using a Single Element

Widely bandwidth tunable coaxial-loaded waveguide filters are presented in this chapter based on a novel concept using a single common tuning element. The operation principle relies on the rotation of coaxial resonators with respect to fixed iris windows to control the inter-resonator coupling strengths and tune the bandwidth. This mechanism features multi-octave tuning capabilities, while maintaining a fixed operation frequency and a stable high unloaded quality factor through only one rotary post, without the need for any additional tuning element. Additionally, the filter can be switched-off effectively through the same arrangement without the necessity for any switching components. First, a second-order design is manufactured, assembled, and measured to verify the design process of the proposed filter. The first experimental results demonstrate a wide bandwidth tunability from 12 MHz to 83 MHz (tuning ratio $>$ 6.9:1). Then, more design examples of higher-order and dielectric-loaded filters are provide to demonstrate the scalability of the proposed concept. The achieved results greatly promote the technique for many multi-standard communication systems and applications.

7.1 Introduction

Tunable filters have gained increasing attention in recent years because of their highly favorable features compared with the traditional fixed structures. In future flexible satellites, for instance, it is essential that both operation frequency and bandwidth should be remotely adjustable and can be re-defined whenever it is needed. Here, the employment of tunable filters and components enables bands' reconfiguration, and also the adoption of new technologies and plans while the satellite is in orbit, thus, remarkably decreasing the related integration and operation expenses.

Generally, the majority of the available tunable filters in both literature and the market focus on frequency reconfiguration whereas, on the other hand, bandwidth (BW) tunable filters are not so common despite their key importance in a wide range of applications. This could be mainly due to the fact that they are more challenging to design than frequency tunable ones. Most of the available BW tunable filter designs are based on planar structures using electrically-controlled varactor diodes as in [149, 224, 225]. This group suffers from major drawbacks of low unloaded quality factor (Q_u) and limited power-handling capabilities, which hinder their employment in high-performance and high-power applications. Therefore, the introduction of BW reconfigurable 3-D cavity-based filters is more desirable because of their lower loss and the ability to handle higher power levels. Accordingly, several BW tunable empty-waveguide and coaxial-loaded filters were presented [9, 10, 226, 227, 228, 141]. A cascaded lowpass filter and highpass filter configuration was used in [9] to realize a BW tunable bandpass response based on TE_{011} cavities utilizing movable metal rings. The filter operates at Ka-band and has a BW tuning range from 160 MHz to 40 MHz. Another BW reconfiguration concept, also for TE_{011} hollow-waveguide filters, was presented in [10] based on the use of coupling resonators instead of the conventional iris structures. The filter bandwidth is tuned over an 18 MHz window at Ku-band from 54 MHz to 72 MHz. A third BW tuning approach was introduced in [226] using a movable plunger on a dual-mode TE_{113} cavity. A two-pole 11 GHz filter is implemented with a BW varying from 26 MHz to 52 MHz. A fourth concept was presented in [227] at Ku-band with 35% BW tuning based on two common tuning elements. However, all these empty-cavity-based concepts suffer from various limitations including the bulky size, limited BW tuning capabilities, many individual tuning elements (2 to N+1), and increasing losses due to the employed tuning mechanism. These drawbacks are even more problematic at lower frequency bands

(e.g., C- and S-bands) since larger cavities and tuning elements are required. Therefore, more compact structures are needed with an extended tuning range and more efficient tuning mechanisms. A combline S-band BW tunable filter was reported in [228], based on the introduction of additional bandstop resonators to the passband section to reconfigure the BW through detuning the combline resonators. Also, [141] presented a fully reconfigurable compact dual-mode C-band filter using TM-mode dielectric resonators. The bandwidth reconfiguration is obtained through tuning the resonant frequency of any of the two orthogonal modes. Nevertheless, despite that these two loaded-waveguide designs feature more compactness, they still share the remaining aforementioned limitations of empty-cavity structures, and therefore, there is still an essential need for more efficient BW tuning solutions.

This chapter introduces a novel bandwidth tuning concept for coaxial-loaded waveguide filters using a single common tuning element. This concept advantageously enables very flexible bandwidth reconfiguration, from up to 10 times wider BW to a fully *switched-off* passband using a single common rod regardless of the filter order. Unlike other concepts, no further tuning components are needed, bringing the merit of a stable high quality factor with minimum variation through a simple and fast tuning process. Furthermore, the filter structure can be designed to keep the operation frequency fixed and compensate any frequency shift that could be caused by the BW tuning mechanism.

7.2 Bandwidth Tuning Concept

The structure of the proposed bandwidth reconfigurable two-pole filter is depicted in Fig. 7.1. The filter arrangement was inspired from the frequency tunable filter, with a constant absolute bandwidth, presented in [19]. However, both the purpose and the operation concept are different. Besides, we believe that this arrangement is more suitable for BW tuning than for frequency reconfiguration, as the inter-resonator couplings can be tuned broadly and easily while maintaining high quality factor with minimum variation. Contrary, beside the more complicated design procedure, the frequency reconfiguration concept of [19] has limited tuning capabilities and suffers from noticeable Q-factor degradation [175]. The proposed bandwidth tuning concept is based on the rotation of coaxial resonators with reference to a fixed iris structure, in order to change the inter-resonator (IR) coupling strength and tune the bandwidth. All resonators are rotated simultaneously using a single common rotational post with

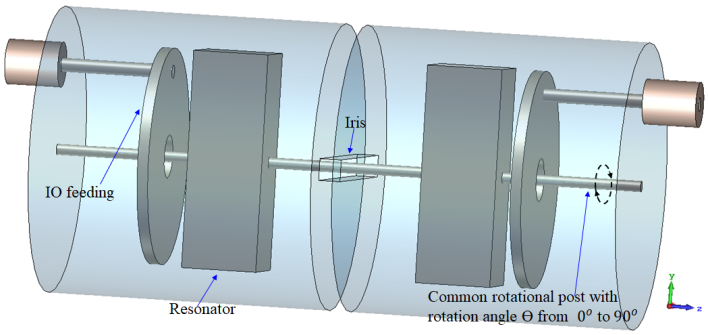

Figure 7.1: Perspective view of the proposed bandwidth tunable coaxial filter. A single common rotational element is used for tuning with an angle θ. The magnetic inter-resonator coupling is the largest when $\theta = 0°$ (the position at Fig. 7.1), and decreases gradually with the rotation of the resonators till the switch-off state at $\theta = 90°$.

an angle θ ranging from 0° to 90°. The iris structure is designed carefully based on the distribution of the fields of the operating mode. Here, our resonating mode is the fundamental TM-mode which propagates similar to the conventional half-wavelength resonators, where the magnetic field rotates mainly in the center of the structure, and the E-field is perpendicularly concentrated at the ends in the vicinity between the coaxial resonators and the cavity. Accordingly, the IR coupling is realized using a rectangular iris positioned at the center of the structure. When $\theta = 0°$ (Fig. 7.1), the (magnetic) coupling is the strongest and the BW is the largest. Then, with the rotation of the post, the inter-resonator coupling strength decreases and the BW becomes narrower. Similarly, the filter can be fully detuned and switched off through the proposed mechanism (i.e, $\theta = 90°$: $f_m \approx f_e \rightarrow K \approx 0$).

The filter cavities are chosen in circular shapes to keep the resonant frequency fixed with the rotation of the resonators. Alternatively, elliptical cavities can be used to also tune the resonant frequency (as shown in [19]) and balance any frequency shifts that might happen due to the BW tuning process.

7.3 Two-Pole BW-Reconfigurable Filter

7.3.1 Filter Specifications

The filter is a 2nd-order bandpass filter that operates at 4.19 GHz with a 20-dB reconfigurable bandwidth from 82 MHz to 8 MHz. The first design step is to synthesize

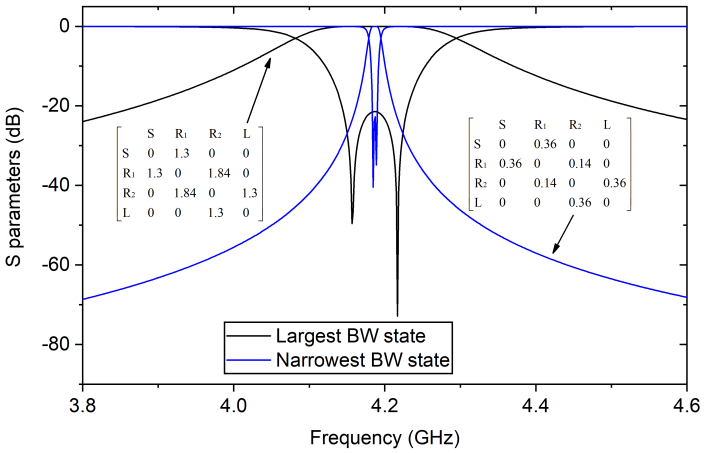

Figure 7.2: Optimized coupling matrix responses of the proposed bandwidth tunable 2nd-order filter at the largest (82 MHz) and narrowest (8 MHz) bandwidths.

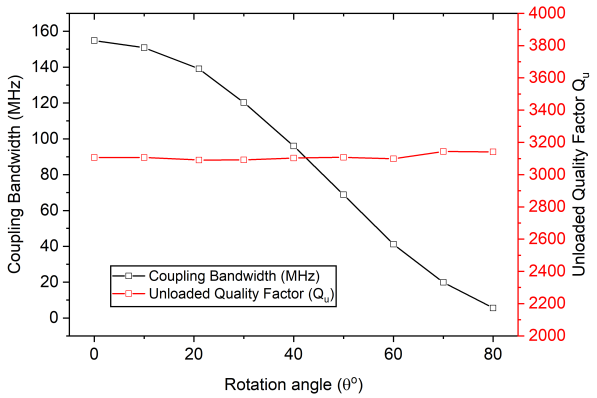

Figure 7.3: Relationship between the coupling bandwidth and unloaded quality factor with the rotation angle θ.

and extract the corresponding coupling matrices of the largest and narrowest BW states, as shown in the inset of Fig. 7.2. Here, the coupling matrix of the largest bandwidth state is firstly extracted, and then normalized and optimized again for the second coupling matrix of the narrowest tuning state. The design procedure only needs these two coupling matrices, while all the other intermediate tuning states can be then obtained without the need for any further design steps.

7.3.2 Inter-Resonator Coupling

Based on the aforementioned design specifications, the required physical inter-resonator couplings (K_{12}) for the largest and narrowest BWs can be calculated, and then realized under weak input-output (IO) excitation condition using:

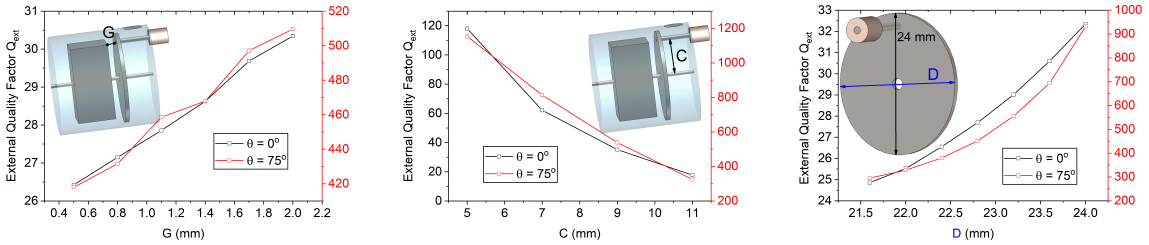

(a) (b) (c)

Figure 7.4: Relationship between the external quality factor (Q_{ext}) and (a) probe position C, (b) disk spacing from the resonator G, and (c) minor axis of the disk D.

$$K_{12} = \frac{CBW}{f_0} = \frac{f_2 - f_1}{f_0} \tag{7.1}$$

where CBW is the coupling bandwidth, f_0 is the centre frequency, f_1 and f_2 are the lower and upper frequencies, respectively. Then, the rectangular coupling iris is designed to provide the required inter-resonator couplings at the largest state ($\theta = 0°$) and narrowest state ($\theta = 75°$), simultaneously. As earlier mentioned, all other BW tuning states in-between will be realized accordingly as demonstrated in Fig. 7.3.

7.3.3 Input-Output Coupling

Similarly, the input-output feeding structure should be able to provide the required couplings at the largest and narrowest BW states. This implies that the input coupling topology should be the maximum at the largest BW case, and decreases gradually with the tuning process till the narrowest bandwidth. Based on this, the input feeding here is realized through capacitively-coupled disks fed by SMA probes as shown in Fig. 7.1. At the largest bandwidth case ($\theta = 0°$) where the coaxial resonator is in-face to the disk, the (electrical) input coupling is the highest. Then, with the rotation of the resonators, the input coupling strength will decrease as fewer E-field lines are being coupled. As shown in Fig. 7.4, the coupling strength is controlled through the gap between the disk and the resonator (G), the position of the feeding probe (C), and the shape of the feeding disk. For simplicity, the disk can be circular, and then tuning screws can be slightly introduced at the narrow BW states. Nevertheless, here we use an elliptical disk to provide the required couplings for all states without the need for any tuning screw. As can be seen in Fig. 7.4(c), the narrowest BW state at $\theta = 75°$ is very sensitive to the change in the minor diameter of the disk, whereas the

input coupling strength at the widest tuning state ($\theta = 0°$) is not much impacted.

7.3.4 Loaded-Resonant Frequency

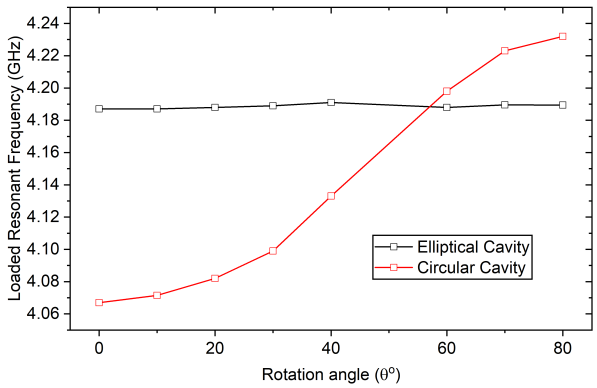

Figure 7.5: The variation of the loaded resonant frequency with elliptical (major diameter = 26.44 mm, minor diameter = 26 mm) and circular cavities (diameter = 26 mm).

When designing a BW tunable filter, it is important to keep the centre frequency fixed while the BW is changing. Here, if circular cavities are used, there will be a slight shift in the frequency when the BW is tuned. This is because only f_m will move with the tuning process while f_e remains fixed. This small change in the centre frequency can be adjusted easily by using tuning screws. However, alternatively, by using elliptical cavities instead of circular ones, the frequency can be also tuned at the same time with the BW tuning to balance any shift due to the BW tuning process, and keep the operating frequency unchanged as can be seen in Fig. 7.5.

Following the aforementioned design steps, a BW tunable filter is then realized, and its simulated S-parameters are depicted in Fig. 7.6 with various tuning states. As shown, the BW is effectively tuned from 82 MHz to 8 MHz with a fixed centre frequency at 4.19 GHz and a return loss level better than 17 dB. Also, the filter can be intrinsically switched-off at $\theta = 90°$ without the need for any auxiliary switching elements. The key feature of this filter, besides the wide BW tuning capabilities, is that the whole tuning process is done through a single element without any need for tuning screws. This advantageously results in a stable high unloaded quality factor of 3100 (with copper) all over the tuning range, as can be seen in Fig. 7.3 without any degradation, unlike the other tuning concepts.

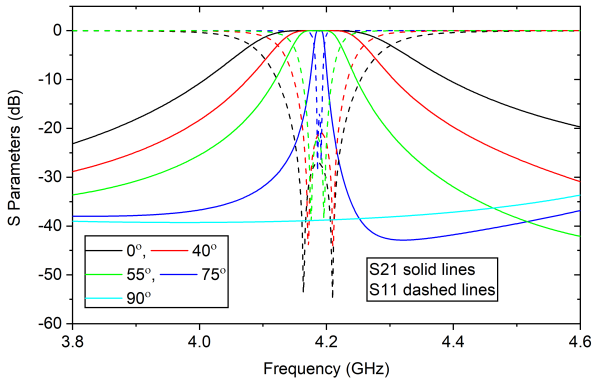

Figure 7.6: Simulated S-parameter responses at different bandwidth tuning states.

7.3.5 Experimental Results

A two-pole C-band BW tunable coaxial filter is manufactured, assembled, and tested to validate the proposed concept and design procedure. All parts of the implemented prototype were manufactured out of brass metal as depicted in Fig. 7.7,where the cavities are elliptical (major diameter = 26.44 mm, minor diameter = 26 mm). The measured results in Fig. 7.8 show that the bandwidth can be tuned effectively from 12 MHz up to 83 MHz (at S11 = -15 dB), providing a very wide multi-octave tuning ratio of 6.92:1 and additional switch-off feature. It is worth to remark here that no additional tuning elements were used. At the largest BW state, the passband is centred at 4.19 GHz with a midband insertion loss of 0.37 dB, while at the narrowest tuning sate, it operates at 4.25 GHz with a midband insertion loss of 1 dB. The increase loss is mainly due to the assembly and the imperfect input-output feeding through the disks, in addition to the related metal losses including M1 stainless-steel screws which are used to fix the resonators in their respective positions on the post. The use of other metals with higher electrical conductivity and silver-plating could be considered to enhance the unloaded quality factor. Another observation from the measured results is that there are slight shifts in the operating frequency due to the BW tuning process, and the frequency was not tuned as required. The main reason of this is that the feeding disks were not fixed at their exact positions (re-simulations estimate them at 0.7 mm closer), hence, causing this shift in the loaded resonant frequency. In comparison with the other BW reconfigurable designs and concepts in [9, 10, 226, 227, 228, 141], it can be clearly seen that the proposed technique provides the widest tuning capabilities (6.92:1) with only one single tuning element. While in the other reported works, the minimum number of tuning elements is 2

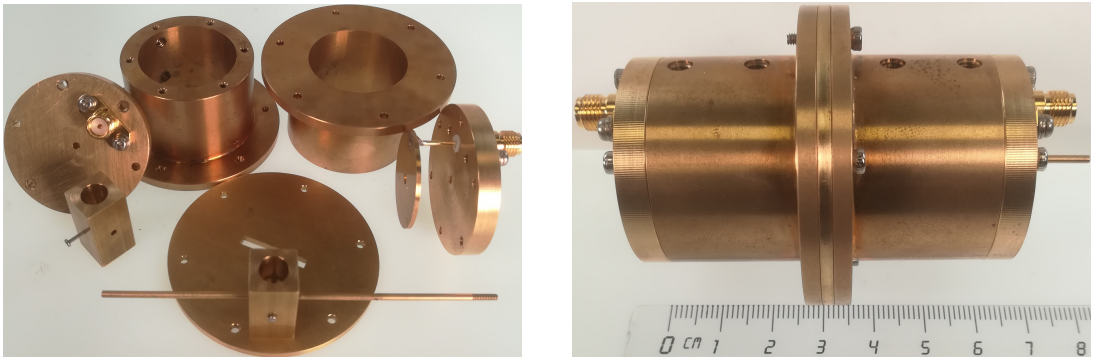

(a) (b)

Figure 7.7: The fabricated 2nd-order multi-octave BW tunable coaxial filter: (a) Disassembled, and (b) final assembled prototype.

in [227], but with only 35% of BW tuning. Also, a wide 3:1 multi-octave tuning is presented in [228], however, it needs many tuning elements, i.e. 2N+2, where N is the filter order. While introducing transmission zeros is challenging in the proposed inline configuration, a possible solution, for example, could be by using orthogonal resonators topologies to realize cross couplings similar to [118] and [119].

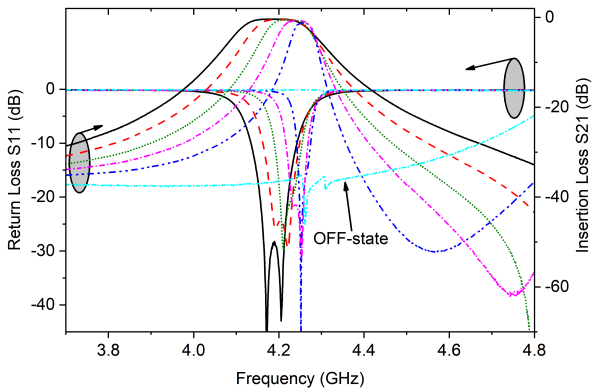

Figure 7.8: Measured S-parameter responses at different bandwidth tuning states. The BW tuning ratio is 6.92:1.

7.4 More Design Examples

7.4.1 Higher-Order BW-Reconfigurable Coaxial Filters

For further investigation, a 3-pole filter is also designed and implemented as depicted in Fig. 7.9 and Fig. 7.10, respectively. Here, the filter is designed using circular cavities

(diameter = 26 mm) instead of the elliptical ones, and tuning screws were included to tune and keep the operation frequency fixed. The simulations in Fig. 7.9(b) depict bandwidth reconfiguration from 107 MHz at 0° to 22 MHz at 64°. Fig. 7.11 shows the measurements of the filter at 4.38 GHz with two different states of 105 MHz and 61 MHz (at S11 = -15 dB), respectively. The BW reconfiguration is 72% with an insertion loss better than 1 dB, and a return loss higher than 19 dB, at both states. It is worth to note that despite this realization being able to offer more tuning flexibility, the tuning process is more time-consuming and complicated than in the first configuration. Fig. 7.12 demonstrates another example of a 4th-order BW reconfigurable filter using a single element, designed similar to the earlier-presented two-pole filter. The bandwidth is tuned effectively from 105 MHz at 0° to 24 MHz at 65°, and can also fully switched-off at 90°.

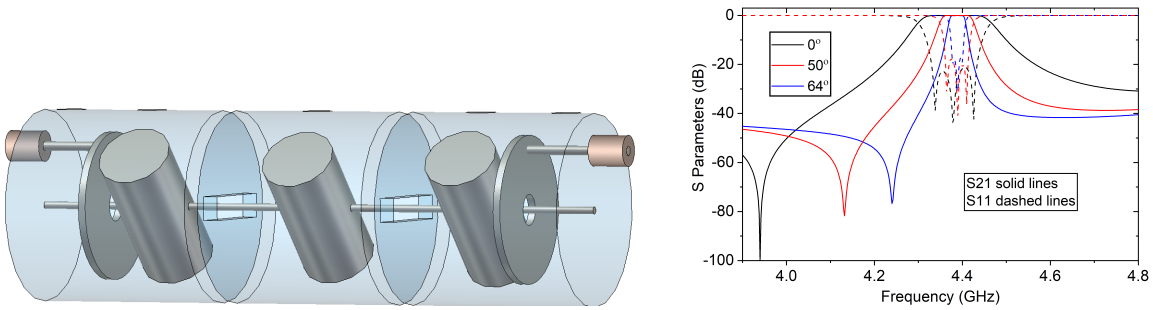

(a) (b)

Figure 7.9: Third-order multi-octave BW tunable coaxial filter: (a) 3D structure, and (b) simulated results.

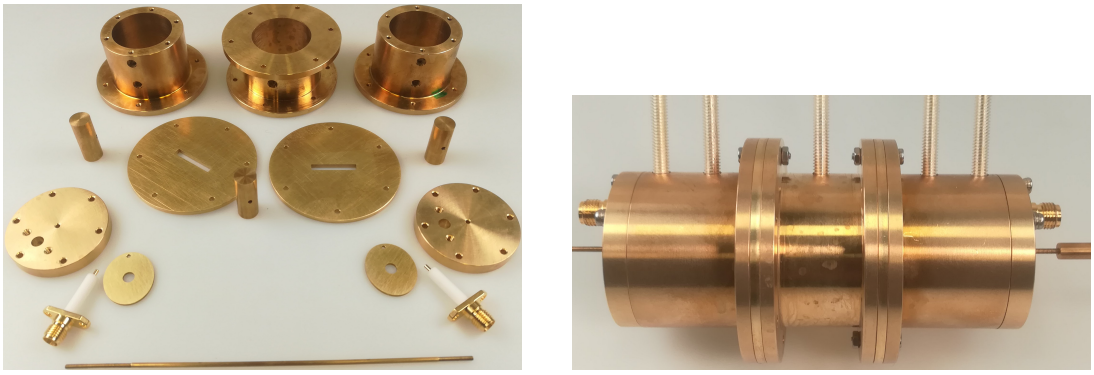

(a) (b)

Figure 7.10: The fabricated 3rd-order multi-octave BW tunable coaxial filter: (a) Disassembled, and (b) final assembled prototype.

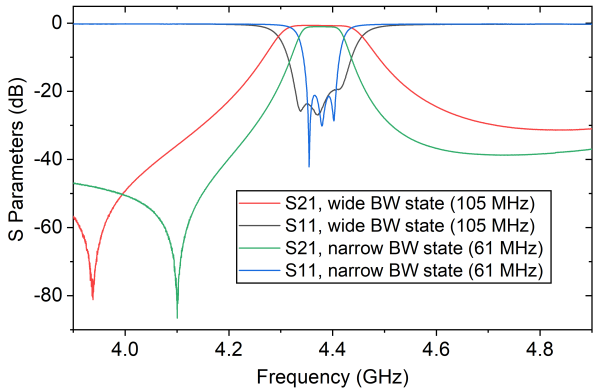

Figure 7.11: Measurements of the 3-pole filter prototype at two BW tuning states (BW tuning range is 72%).

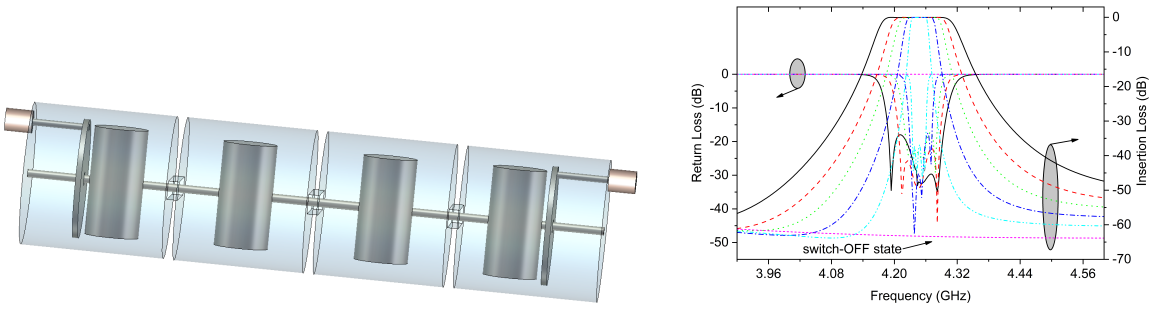

(a) (b)

Figure 7.12: Fourth-order multi-octave BW tunable coaxial filter: (a) 3D structure, and (b) simulated results.

7.4.2 BW-Reconfigurable Dielectric-Loaded Filters

The use of dielectric resonators instead of the metallic ones is more favourable in many applications as they offer higher quality factor and more stable performance with temperature variations. Therefore, to benefit from these merits and to check the feasibility, a two-pole BW-reconfigurable coaxial filter is designed as shown in Fig. 7.13 using low-loss dielectric resonators made of Alumina material (dielectric constant = 9.8 and loss tangent = 0.0001). In this example here, two screws (see Fig. 7.13) were put at fixed positions and depth to obtain the required IO coupling strengths at the narrow-BW states to maintain a stable rerun-loss level at all states. The simulated results in Fig. 7.13(b) exhibit an octave BW tuning from 97 MHz at 0° to 12 MHz at 68°, in addition to the intrinsic switch-off at 90°.

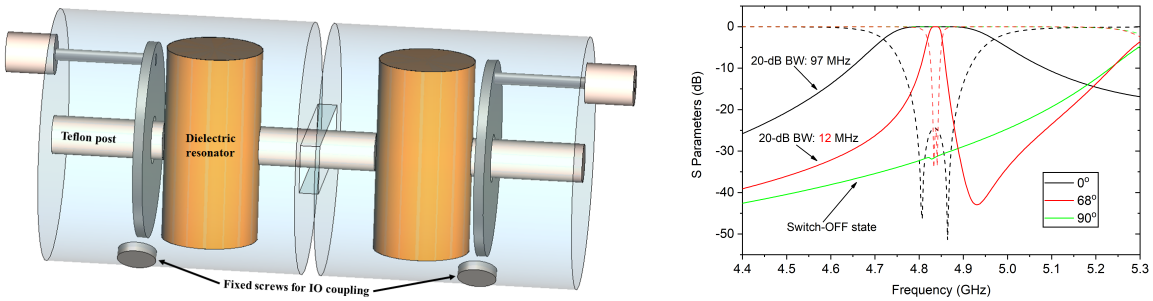

(a) (b)

Figure 7.13: Second-order multi-octave BW tunable dielectric-loaded filter: (a) 3D structure, and (b) simulated results.

7.5 Summary

A novel technique of wide bandwidth tunable coaxial-loaded waveguide filters was presented in this chapter using a single tuning element. Also, the intrinsic switch-off feature was demonstrated with no need for any further switching circuits. The filter cavities and input-output feeding were designed to keep a fixed operation frequency and provide the required input coupling at all tuning states, therefore, eliminating the need for any additional tuning element. Various design examples and prototypes were presented using both metallic and dielectric resonators. All these highly desirable advantages strongly promote the proposed configuration for tunable filter applications.

Chapter 8

Conclusion

8.1 Summary

The key objectives of this PhD research were the investigation of novel efficient tuning mechanisms and the development of high-performance frequency and bandwidth tunable bandpass filters for RF and microwave applications. In particular, the research addressed some of the key challenges surrounding the available tunable filter designs such as compactness, high-Q, tuning range, and performance degradation with tuning. In detail, the major contributions of the research presented in this thesis are summarized as below:

• In section 3.1, a novel inset resonator configuration was presented for coaxial filter applications with quasi-elliptic responses, featuring compact structures, high quality factor, and good spurious performance. The design and analysis of the inset resonator are discussed in detail, and two quasi-elliptic filters are implemented in planar and longitudinal coupling configurations, respectively. The first is a folded four-pole 2.93 GHz filter in planar topology with two symmetrical transmission zeros created using probes for cross-coupling realization. The fabricated filter has good performance characteristics and a wide spurious-free band up to $3.5 \cdot f_0$. The second inset-type quasi-elliptic filter is realized in a longitudinal inline arrangement with the advantages of more compactness and more efficient TZs creation mechanism than the first configuration. An example of a compact 2.53 GHz three-pole filter is presented with a closely-positioned transmission zero, wide spurious-free band ($\approx 3 \cdot f_0$).

• In section 3.2, a new class of compact, high-Q, tunable coaxial filters was presented based on the novel inset resonator concept. The proposed tuning technique

has the merits of wide tuning capabilities and stable high Q-factor performance with minimum variation throughout the tuning window. Single-resonator cavity, and filter prototypes are designed and implemented to demonstrate and validate the proposed concept. A single tunable inset resonator is first designed and measured showing distinctive results of a 43% tuning range with a stable high-Q of 4100±4%. Then, the design procedure for constant absolute bandwidth (CABW) tunable filters is discussed, and several tunable inset filters are presented using both metallic and dielectric resonators. The measured results of the fabricated filter examples show distinctive merits of a wide 40% tuning range, while maintaining a constant bandwidth with less than ±10% change, and a stable high-Q with minimum variation.

• In chapter 4, octave tunable dielectric combline bandpass filters with constant absolute bandwidth were presented using a novel re-entrant cap tuning technique. This mechanism of tuning provides wider tuning capabilities and better spurious performance than the conventional screw-based tuning. A single widely tunable resonator is implemented with an octave tuning ratio of 2.64:1, high quality factor from 1705 to 5480, and spurious-free band up to $3.44 \cdot f_0$. Afterwards, two octave tunable re-entrant cap filters are designed and fabricated, demonstrating octave tuning ranges wider than 70%.

• A new miniaturized C-band dual-band dual-mode TM-mode dielectric filter was presented in section 5.1. The filter is designed in planar configuration for the purposes of easy tuning, manufacturing, and assembly. Additionally, enhanced inter-band isolation and outer-band rejection are realized through flexibly positioned transmission zeros. Second and third order C-band dual-band dual-mode TM-mode dielectric filters were designed and fabricated, and their reconfiguration capabilities were investigated.

• Section 5.2 presented very compact in-line C-band diplexers based on dual-mode dielectric TM-mode resonators. In addition to the substantial volume saving in comparison with conventional waveguide technology, the proposed diplexers eliminates the need for coupling junctions featuring more compactness, handling of higher power levels, and a simpler design procedure. Furthermore, the diplexers are designed in an in-line planar coupling configuration that advantageously allows for easy tuning and assembly. Because of the planar topology and the properly designed inter-resonator coupling irises, all the input–output couplings, resonant frequencies, and IR couplings can be controlled effectively and independently.

• Miniaturized reconfigurable dual-mode dielectric TM-mode filters were presented in section 5.3 using piezomotors for high-accuracy remote tuning. First, a two-pole

fully-reconfigurable filter is presented, where all of its parameters including frequency, bandwidth, and TZs can be effectively and flexibly reconfigured. This advantageously allowed for 800 MHz of frequency tuning while maintaining a constant absolute bandwidth. Then, another design of a 4th-order tunable dual-mode TM-mode dielectric filter is introduced using a single tuning element.

• In chapter 6, a new microfluidic-based, frequency tuning mechanism for the design of widely tunable TM_{010} mode dielectric resonators and filters was presented. This mechanism provides the advantage of getting the highest possible achievable frequency tuning with minimal losses and high-quality factors. Furthermore, the presented tuning technique is applied in a simple, low-cost, and efficient configuration. Single resonator cavity and two-pole bandpass filters are implemented to verify the proposed tuning mechanism. The measured results feature wide octave tuning capabilities wider than 100%, confirming the proposed concept.

• Chapter 7 presented a novel bandwidth reconfiguration concept for coaxial and dielectric-loaded waveguide filters using a single common tuning element. This concept advantageously enables very flexible bandwidth reconfiguration, from up to 10 times wider BW to a fully *switched-off* passband using a single common rod regardless of the filter order. Unlike other concepts, no further tuning components are needed, bringing the merit of a stable high quality factor with minimum variation through a simple and fast tuning process. Furthermore, the filter structure can be designed to keep the operation frequency fixed and compensate any frequency shift that could be caused by the BW tuning mechanism.

8.2 Outlook

Based on the completed research and achieved results, there are still some aspects that need to be investigated and studied further as follows:

• Developing widely octave-tunable filters with minimum number of tuning elements (i.e., 1 tuning element).

• Exploring new techniques with fast tuning speed.

• Developing widely octave-tunable filters with high-Q, having a minimum variation allover the broad tuning window.

• Realizing tunable filters with wide spurious-free bands and quasi-elliptic responses to improve the selectivity and out-of-band rejections.

Appendix A

Publication List (as of May 2023)

A.1 Doctoral-Related Publications

This section lists the scientific contributions made during the course of the doctoral research including peer-reviewed journal articles, conference papers, reports, and patent applications.

Journal Articles:

- **A. Widaa**, A. Sharma, C. Bartlett, S. Cogollos, V.E. Boria, M. Guglielmi, and M. Höft, "Bandwidth-Reconfigurable Coaxial Bandpass Filter With Multi-Octave Tuning Using a Single Element," IEEE Microwave and Wireless Technology Letters, doi: 10.1109/LMWT.2023.3264673. ***(in special issue on "Top IMS2023 Papers" (estimated 50 papers)).***

Conceptualization	Planning	Implementation	Manuscript preparation
High	High	High	High

- **A. Widaa** and M. Höft, "Widely Tunable TM-Mode Dielectric Filters With Constant Absolute Bandwidth Using Re-Entrant Caps," IEEE Journal of Microwaves, Feb. 2023, doi: 10.1109/JMW.2023.3242689. ***(Featured MTT-S e-Newsletter Article - Mar. 2023)***.

Conceptualization	Planning	Implementation	Manuscript preparation
High	High	High	High

- **A. Widaa**, C. Bartlett and M. Höft, "Design of Compact Quasi-Elliptic Bandpass Filters Based on Coaxial Inset Resonators," IEEE Access, vol. 11, pp. 18739-18749, Feb. 2023, doi: 10.1109/ACCESS.2023.3247137.

Conceptualization	Planning	Implementation	Manuscript preparation
High	High	High	High

- **A. Widaa** and M. Höft, "Very Compact Diplexer Based on Dual-Mode Dielectric TM-Mode Resonators," IEEE Microwave and Wireless Technology Letters, vol. 33, no. 4, pp. 387-390, April 2023, doi: 10.1109/LMWT.2022.3228398.

Conceptualization	Planning	Implementation	Manuscript preparation
High	High	High	High

- **A. Widaa**, C. Bartlett and M. Höft, "Tunable Coaxial Bandpass Filters Based on Inset Resonators," IEEE Transactions on Microwave Theory and Techniques, vol. 71, no. 1, pp. 285-295, Jan. 2023, doi: 10.1109/TMTT.2022.3222321.

Conceptualization	Planning	Implementation	Manuscript preparation
High	High	High	High

- **A. Widaa** and M. Höft, "Miniaturized Dual-Band Dual-Mode TM-Mode Dielectric Filter in Planar Configuration," IEEE Journal of Microwaves, vol. 2, no. 2, pp. 326-336, Apr. 2022, doi: 10.1109/JMW.2022.3145906. ***(Featured MTT-S e-Newsletter Article - Apr. 2022)***.

Conceptualization	Planning	Implementation	Manuscript preparation
High	High	High	High

Conference Articles:

- **A. Widaa**, A. Sharma, C. Bartlett, S. Cogollos, V.E. Boria, M. Guglielmi, and M. Höft, "Bandwidth-Reconfigurable Coaxial Bandpass Filter With Multi-Octave Tuning Using a Single Element," IEEE MTT-S International Microwave Symposium (IMS), Jun. 2023, ***(selected as one of the top 50 IMS2023 papers)*, Accepted.**

Conceptualization	Planning	Implementation	Manuscript preparation
High	High	High	High

- **A. Widaa**, C. Bartlett and M. Höft, "Inset Resonators and Their Applications in Fixed/Reconfigurable Microwave Filters," IEEE/MTT-S International Microwave Symposium (IMS), 2022, pp. 172-175.
DOI: 10.1109/IMS37962.2022.9865311.

Conceptualization	Planning	Implementation	Manuscript preparation
High	High	High	High

- **A. Widaa** and M. Höft, "Miniaturized Dual-Band TM-Mode Dielectric Filter and Its Reconfiguration Capabilities," 2022 IEEE/MTT-S International Microwave Symposium - IMS 2022, Denver, CO, USA, 2022, pp. 344-347, doi: 10.1109/IMS37962.2022.9865353.

Conceptualization	Planning	Implementation	Manuscript preparation
High	High	High	High

- **A. Widaa**, C. Bartlett and M. Höft, "Miniaturized All-Reconfigurable Dual-Mode Dielectric Filter Using Piezomotors for Future Satellite Communications," 51st European Microwave Conference (EuMC), 2022, pp. 107-110.
DOI: 10.23919/EuMC50147.2022.9784226. ***(Received an extended version invitation, as a highly ranked paper, from The International Journal of Microwave and Wireless Technologies (IJMWT))***.

Conceptualization	Planning	Implementation	Manuscript preparation
High	High	High	High

- **A. Widaa** and M. Höft, "Microfluidic-Based Ultra-Wide Tuning Technique for TM_{010} Mode Dielectric Resonators and Filters," 2021 IEEE MTT-S International Microwave Filter Workshop (IMFW), Perugia, Italy, 2021, pp. 343-346, doi: 10.1109/IMFW49589.2021.9642347.

Conceptualization	Planning	Implementation	Manuscript preparation
High	High	High	High

- **A. Widaa** and M. Höft, "A novel Re-entrant Cap Tuning Technique For TM-Mode Dielectric Resonators and Filters," 2021 IEEE MTT-S International Microwave Filter Workshop (IMFW), Perugia, Italy, 2021, pp. 335-338, doi: 10.1109/IMFW49589.2021.9642354.

Conceptualization	Planning	Implementation	Manuscript preparation
High	High	High	High

Reports:

- **A. Widaa**, "Novel Multi-Mode Tunable Filter," Report, 2022, **Submitted**.

Conceptualization	Planning	Implementation	Manuscript preparation
High	High	High	High

- **A. Widaa**, "Comparison of Tuning Means," Report, 2020. [Online]. Available: `https://ec.europa.eu/research/participants/documents/downloadPublic?documentIds=080166e5d76532fe&appId=PPGMS`.

Conceptualization	Planning	Implementation	Manuscript preparation
High	High	High	High

Patent Applications:

- *Tunable Resonator Arrangement, Tunable Frequency Filter and Method of Tuning Thereof.* **A. Widaa**, C. Bartlett and M. Höft. Patent Pending, Jun. 2022.

Conceptualization	Planning	Implementation	Manuscript preparation
High	High	High	High

- *Tunable Resonator, Tunable Frequency Filter and Method of Tuning Thereof.* **A. Widaa** and M. Höft. Patent WO2022117212A1. `https://patents.google.com/patent/WO2022117212A1/`.

Conceptualization	Planning	Implementation	Manuscript preparation
High	High	High	High

A.2 Miscellaneous Publications

This section lists the scientific peer-reviewed journal and conference publications during the doctoral program, but not directly related to the dissertation topic.

Journal Articles:

- L. Robins, C. Bartlett, A. Arsanjani, **A. Widaa**, R. Teschl, M. Höft and W. Bösch, "3D-Printed Dielectric Resonators for Quasi-TE112 Mode Singlets, Doublets and Dual-Mode Filters," IEEE Access, vol. 10, pp. 130326-130338, 2022. DOI: 10.1109/ACCESS.2022.3228764.

Conceptualization	Planning	Implementation	Manuscript preparation
Medium	Low	Low	Low

Conference Articles:

- **A. Widaa**, F. Cacciamani, L. Pelliccia, C. Tomassoni, V. T. di Crestvolant and M. Höft, "Compact Ultra-Wideband Bandpass Filter Using Additively Manufactured TM - Mode Dielectric Resonators," 2022 52nd European Microwave Conference (EuMC), Milan, Italy, 2022, pp. 115-118, doi: 10.23919/EuMC54642.2022.9924504.

Conceptualization	Planning	Implementation	Manuscript preparation
Medium	Medium	Low	High

- **A. Widaa**, C. J. You and M. Awad, "High Selectivity Low-Loss Tunable Bandpass Filter with Transmission Zeros Control Using Staircase Resonators," 2021 IEEE 21st Annual Wireless and Microwave Technology Conference (WAMICON), Sand Key, FL, USA, 2021, pp. 1-4, doi: 10.1109/WAMICON47156.2021.9443594.

Conceptualization	Planning	Implementation	Manuscript preparation
High	High	High	High

- **A. Widaa**, C. J. You and M. Awad, "Compact Single/Dual-Band Bandpass Filters with Independently Controllable Passbands Using Staircase Resonators," 2020 International Conference on Computer, Control, Electrical, and Electronics Engineering (ICCCEEE), Khartoum, Sudan, 2021, pp. 1-4, doi: 10.1109/ICCCEEE49695.2021.9429611.

Conceptualization	Planning	Implementation	Manuscript preparation
High	High	High	High

Bibliography

[1] H. Joshi, H. H. Sigmarsson, D. Peroulis, and W. J. Chappell, "Highly loaded evanescent cavities for widely tunable high-Q filters," in *2007 IEEE/MTT-S International Microwave Symposium*, 2007, pp. 2133–2136.

[2] X. Liu, L. P. B. Katehi, W. J. Chappell, and D. Peroulis, "High-Q tunable microwave cavity resonators and filters using soi-based rf mems tuners," *Journal of Microelectromechanical Systems*, vol. 19, no. 4, pp. 774–784, 2010.

[3] G. L. Matthaei, L. Young, and E. M. T. Jones, *Microwave filters, impedance-matching networks, and coupling structures*. Artech house, 1980.

[4] D. Scarbrough, D. Psychogiou, D. Peroulis, and C. Goldsmith, "Low-loss, broadly-tunable cavity filter operating at UHF frequencies," in *2015 IEEE MTT-S International Microwave Symposium*, 2015, pp. 1–4.

[5] M. Höft, A. Kronberger, and O. Bartz, "Tunable bandpass filters for multi-standard applications," in *German Microwave Conference*, 2008, pp. 1–4.

[6] T. Shen, C. Wang, and K. A. Zaki, "Tunable dielectric resonators with dielectric tuning disks in rectangular enclosures," in *2000 30th European Microwave Conference*, 2000, pp. 1–4.

[7] U. Rosenberg and M. Knipp, "Novel tunable high-Q filter design for branching networks with extreme narrowband channels at mm-wave frequencies," in *2005 European Microwave Conference*, vol. 2, 2005, pp. 4 pp.–824.

[8] B. Yassini, M. Yu, D. Smith, and S. Kellett, "A Ku-band high-Q tunable filter with stable tuning response," *IEEE Transactions on Microwave Theory and Techniques*, vol. 57, no. 12, pp. 2948–2957, 2009.

[9] B. Yassini, M. Yu, and B. Keats, "A Ka-band fully tunable cavity filter," *IEEE Transactions on Microwave Theory and Techniques*, vol. 60, no. 12, pp. 4002–4012, 2012.

[10] C. Arnold, J. Parlebas, and T. Zwick, "Reconfigurable waveguide filter with variable bandwidth and center frequency," *IEEE Transactions on Microwave Theory and Techniques*, vol. 62, no. 8, pp. 1663–1670, 2014.

[11] A. Périgaud, O. Tantot, N. Delhote, S. Verdeyme, S. Bila, D. Pacaud, L. Carpentier, J. Puech, L. Lapierre, and G. Carayon, "Continuously tuned Ku-band cavity filter based on dielectric perturbers made by ceramic additive manufacturing for space applications," *Proceedings of the IEEE*, vol. 105, no. 4, pp. 677–687, 2017.

[12] S. Nam, B. Lee, C. Kwak, and J. Lee, "A new class of K-band high-Q frequency-tunable circular cavity filter," *IEEE Transactions on Microwave Theory and Techniques*, vol. 66, no. 3, pp. 1228–1237, 2018.

[13] ——, "Contactless tuning plunger and its application to K-band frequency-tunable cavity filter," *IEEE Transactions on Microwave Theory and Techniques*, vol. 67, no. 7, pp. 2713–2719, 2019.

[14] G. Basavarajappa and R. R. Mansour, "Design methodology of a tunable waveguide filter with a constant absolute bandwidth using a single tuning element," *IEEE Transactions on Microwave Theory and Techniques*, vol. 66, no. 12, pp. 5632–5639, 2018.

[15] B. Gowrish and R. R. Mansour, "A dual-mode frequency reconfigurable waveguide filter with a constant frequency spacing between transmission zeros," in *2020 IEEE/MTT-S International Microwave Symposium (IMS)*, 2020, pp. 811–814.

[16] M. Yu, B. Yassini, B. Keats, and Y. Wang, "The sound the air makes: High-performance tunable filters based on air-cavity resonators," *IEEE Microwave Magazine*, vol. 15, no. 5, pp. 83–93, 2014.

[17] S. Fouladi, F. Huang, W. D. Yan, and R. R. Mansour, "High-Q narrowband tunable combline bandpass filters using mems capacitor banks and piezomo-

tors," *IEEE Transactions on Microwave Theory and Techniques*, vol. 61, no. 1, pp. 393–402, 2013.

[18] M. A. Iskander, M. Nasresfahani, and R. R. Mansour, "A constant-Q tunable combline bandpass filter using angular tuning technique," in *2014 44th European Microwave Conference*, 2014, pp. 1103–1106.

[19] G. Basavarajappa and R. R. Mansour, "Design methodology of a high-Q tunable coaxial filter and diplexer," *IEEE Transactions on Microwave Theory and Techniques*, vol. 67, no. 12, pp. 5005–5015, 2019.

[20] F. H. Gil and J. Martinez, "Analysis of dielectric resonators with tuning screw and supporting structure," *IEEE Transactions on Microwave Theory and Techniques*, vol. 33, no. 12, pp. 1453–1457, 1985.

[21] S.-W. Chen, K. Zaki, and R. West, "Tunable, temperature-compensated dielectric resonators and filters," *IEEE Transactions on Microwave Theory and Techniques*, vol. 38, no. 8, pp. 1046–1052, 1990.

[22] T. Shen, K. Zaki, and C. Wang, "Tunable dielectric resonators with dielectric tuning disks," *IEEE Transactions on Microwave Theory and Techniques*, vol. 48, no. 12, pp. 2439–2445, 2000.

[23] C. Wang and W. Blair, "Tunable high-Q dielectric loaded resonator and filter," in *Proceedings RAWCON 2002. 2002 IEEE Radio and Wireless Conference (Cat. No.02EX573)*, 2002, pp. 249–252.

[24] N. S. P. C. Ltd., "Dielectric resonator device," Patent, Feb., 1996.

[25] S. bank university enterprise Ltd., "Tunable or reconfigurable dielectric resonator filter," Patent, Jun., 2006.

[26] F. Huang and R. R. Mansour, "Tunable compact dielectric resonator filters," in *2009 European Microwave Conference (EuMC)*, 2009, pp. 559–562.

[27] W. D. Yan and R. R. Mansour, "Tunable dielectric resonator bandpass filter with embedded MEMS tuning elements," *IEEE Transactions on Microwave Theory and Techniques*, vol. 55, no. 1, pp. 154–160, 2007.

[28] E. Laplanche, N. Delhote, A. Périgaud, O. Tantot, S. Verdeyme, S. Bila, D. Pacaud, and L. Carpentier, "Tunable filtering devices in satellite payloads: A review of recent advanced fabrication technologies and designs of tunable cavity filters and multiplexers using mechanical actuation," *IEEE Microwave Magazine*, vol. 21, no. 3, pp. 69–83, 2020.

[29] S.-F. Chao, C.-H. Wu, Z.-M. Tsai, H. Wang, and C. H. Chen, "Electronically switchable bandpass filters using loaded stepped-impedance resonators," *IEEE Transactions on Microwave Theory and Techniques*, vol. 54, no. 12, pp. 4193–4201, 2006.

[30] Z. Brito, I. Llamas, G. Navarro, J. Perruisseau, and L. Pradell, "Switchable bandpass filter for WiFi-UMTS reception standards," *Electronics Letters*, vol. 46, no. 13, pp. 1–2, 06 2010.

[31] J. Xu, "Compact switchable bandpass filter and its application to switchable diplexer design," *IEEE Microwave and Wireless Components Letters*, vol. 26, no. 1, pp. 13–15, 2016.

[32] Y.-J. Zhang, J. Cai, and J.-X. Chen, "Design of novel reconfigurable filter with simultaneously tunable and switchable passband," *IEEE Access*, vol. 7, pp. 59 708–59 715, 2019.

[33] G. M. Rebeiz, K. Entesari, I. C. Reines, S.-j. Park, M. A. El-tanani, A. Grichener, and A. R. Brown, "Tuning in to RF MEMS," *IEEE Microwave Magazine*, vol. 10, no. 6, pp. 55–72, 2009.

[34] K. Entesari and G. Rebeiz, "A 12-18-GHz three-pole RF MEMS tunable filter," *IEEE Transactions on Microwave Theory and Techniques*, vol. 53, no. 8, pp. 2566–2571, 2005.

[35] V. Sekar, M. Armendariz, and K. Entesari, "A 1.2–1.6-GHz substrate-integrated-waveguide RF MEMS tunable filter," *IEEE Transactions on Microwave Theory and Techniques*, vol. 59, no. 4, pp. 866–876, 2011.

[36] M. A. El-Tanani and G. M. Rebeiz, "High-performance 1.5–2.5-GHz RF-MEMS tunable filters for wireless applications," *IEEE Transactions on Microwave Theory and Techniques*, vol. 58, no. 6, pp. 1629–1637, 2010.

[37] E. Prophet, J. Musolf, B. Zuck, S. Jimenez, K. Kihlstrom, and B. Willemsen, "Highly-selective electronically-tunable cryogenic filters using monolithic, discretely-switchable MEMS capacitor arrays," *IEEE Transactions on Applied Superconductivity*, vol. 15, no. 2, pp. 956–959, 2005.

[38] S.-J. Park, I. Reines, C. Patel, and G. M. Rebeiz, "High-Q RF-MEMS 4–6-GHz tunable evanescent-mode cavity filter," *IEEE Transactions on Microwave Theory and Techniques*, vol. 58, no. 2, pp. 381–389, 2010.

[39] K. Y. Chan, R. Ramer, and R. R. Mansour, "A switchable iris bandpass filter using RF MEMS switchable planar resonators," *IEEE Microwave and Wireless Components Letters*, vol. 27, no. 1, pp. 34–36, 2017.

[40] ——, "Ku-band channel aggregation waveguide filters by RF MEMS-based detuning," *IEEE Transactions on Microwave Theory and Techniques*, vol. 68, no. 2, pp. 750–761, 2020.

[41] L. Pelliccia, F. Cacciamani, P. Farinelli, and R. Sorrentino, "High-Q tunable waveguide filters using ohmic RF MEMS switches," *IEEE Transactions on Microwave Theory and Techniques*, vol. 63, no. 10, pp. 3381–3390, 2015.

[42] D. Scarbrough, C. Goldsmith, J. Papapolymerou, and Y. Li, "Miniature microwave RF MEMS tunable waveguide filter," in *2009 European Microwave Integrated Circuits Conference (EuMIC)*, 2009, pp. 507–510.

[43] F. Huang, S. Fouladi, and R. R. Mansour, "High-Q tunable dielectric resonator filters using MEMS technology," *IEEE Transactions on Microwave Theory and Techniques*, vol. 59, no. 12, pp. 3401–3409, 2011.

[44] M. Agaty, A. Crunteanu, C. Dalmay, and P. Blondy, "Ku band high-Q switchable cavity filter using vanadium dioxide (VO_2) microwave disk-shaped switch," in *2018 48th European Microwave Conference (EuMC)*, 2018, pp. 483–486.

[45] S. Yang, W. Li, M. Vaseem, and A. Shamim, "Fully printed VO_2 switch based flexible and reconfigurable filter," in *2020 IEEE/MTT-S International Microwave Symposium (IMS)*, 2020, pp. 49–52.

[46] D. Bouyge, A. Crunteanu, J.-C. Orlianges, D. Passerieux, C. Champeaux, A. Catherinot, A. Velez, J. Bonache, F. Martin, and P. Blondy, "Reconfigurable

bandpass filter based on split ring resonators and vanadium dioxide (VO_2) microwave switches," in *2009 Asia Pacific Microwave Conference*, 2009, pp. 2332–2335.

[47] M. Wang, F. Lin, and M. Rais-Zadeh, "Need a change? try GeTe: A reconfigurable filter using germanium telluride phase change RF switches," *IEEE Microwave Magazine*, vol. 17, no. 12, pp. 70–79, 2016.

[48] P. W. Wong and I. Hunter, "Electronically tunable filters," *IEEE Microwave Magazine*, vol. 10, no. 6, pp. 46–54, 2009.

[49] A. S. Sedra and K. C. Smith, *Microelectronic Circuits*, 8th ed. Oxford University Press, 2019.

[50] L. Athukorala and D. Budimir, "Compact second-order highly linear varactor-tuned dual-mode filters with constant bandwidth," *IEEE Transactions on Microwave Theory and Techniques*, vol. 59, no. 9, pp. 2214–2220, 2011.

[51] M. A. El-Tanani and G. M. Rebeiz, "Corrugated microstrip coupled lines for constant absolute bandwidth tunable filters," *IEEE Transactions on Microwave Theory and Techniques*, vol. 58, no. 4, pp. 956–963, 2010.

[52] ——, "A two-pole two-zero tunable filter with improved linearity," *IEEE Transactions on Microwave Theory and Techniques*, vol. 57, no. 4, pp. 830–839, 2009.

[53] J.-R. Mao, W.-W. Choi, K.-W. Tam, W. Q. Che, and Q. Xue, "Tunable bandpass filter design based on external quality factor tuning and multiple mode resonators for wideband applications," *IEEE Transactions on Microwave Theory and Techniques*, vol. 61, no. 7, pp. 2574–2584, 2013.

[54] P.-L. Chi, T. Yang, and T.-Y. Tsai, "A fully tunable two-pole bandpass filter," *IEEE Microwave and Wireless Components Letters*, vol. 25, no. 5, pp. 292–294, 2015.

[55] J. Xu, W. Wu, and G. Wei, "Novel dual-band bandpass filter and reconfigurable filters using lumped-element dual-resonance resonators," *IEEE Transactions on Microwave Theory and Techniques*, vol. 64, no. 5, pp. 1496–1507, 2016.

[56] A. H. A. Widaa and M. A. Ahmed, "Compact tunable dual-band bandpass filter for WiFi/WiMAX applications," in *2018 International Conference on Computer, Control, Electrical, and Electronics Engineering (ICCCEEE)*, 2018, pp. 1–4.

[57] C.-F. Chen, G.-Y. Wang, and J.-J. Li, "Microstrip switchable and fully tunable bandpass filter with continuous frequency tuning range," *IEEE Microwave and Wireless Components Letters*, vol. 28, no. 6, pp. 500–502, 2018.

[58] J. Sigman, C. D. Nordquist, P. G. Clem, G. M. Kraus, and P. S. Finnegan, "Voltage-controlled Ku-band and X-band tunable combline filters using barium-strontium-titanate," *IEEE Microwave and Wireless Components Letters*, vol. 18, no. 9, pp. 593–595, 2008.

[59] R. Stefanini, J. D. Martinez, M. Chatras, A. Pothier, V. E. Boria, and P. Blondy, "Ku band high-Q tunable surface-mounted cavity resonator using RF MEMS varactors," *IEEE Microwave and Wireless Components Letters*, vol. 21, no. 5, pp. 237–239, 2011.

[60] J. Guo, B. You, and G. Q. Luo, "A miniaturized eighth-mode substrate-integrated waveguide filter with both tunable center frequency and bandwidth," *IEEE Microwave and Wireless Components Letters*, vol. 29, no. 7, pp. 450–452, 2019.

[61] A. Iqbal, A. W. Ahmad, A. Smida, and N. K. Mallat, "Tunable SIW bandpass filters with improved upper stopband performance," *IEEE Transactions on Circuits and Systems II: Express Briefs*, vol. 67, no. 7, pp. 1194–1198, 2020.

[62] D. Psychogiou and M. Deng, "High-order coaxial bandpass filters with multiple levels of transfer function tunability," *IEEE Microwave and Wireless Components Letters*, vol. 30, no. 4, pp. 367–370, 2020.

[63] J.-X. Xu, L. Yang, Y. Yang, and X. Y. Zhang, "High-Q -factor tunable bandpass filter with constant absolute bandwidth and wide tuning range based on coaxial resonators," *IEEE Transactions on Microwave Theory and Techniques*, vol. 67, no. 10, pp. 4186–4195, 2019.

[64] A. Farr, G. Blackie, and D. Williams, "Novel techniques for electronic tuning of dielectric resonators," in *1983 13th European Microwave Conference*, 1983, pp. 791–796.

[65] B. S. Virdee, "Effective technique for electronically tuning a dielectric resonator," *Electronics Letters*, vol. 33, no. 4, pp. 301–302, 2 1997.

[66] B. Virdee, A. Virdee, and L. Trinogga, "Novel invasive electronic tuning of dielectric resonators," in *IEEE MTT-S International Microwave Symposium Digest, 2003*, vol. 1, 2003, pp. 51–54 vol.1.

[67] F. Huang, S. Fouladi, and R. R. Mansour, "High-Q tunable dielectric resonator filters using MEMS technology," *IEEE Transactions on Microwave Theory and Techniques*, vol. 59, no. 12, pp. 3401–3409, 2011.

[68] F. Huang and R. Mansour, "A novel varactor tuned dielectric resonator filter," in *2013 IEEE MTT-S International Microwave Symposium Digest (MTT)*, 2013, pp. 1–3.

[69] G.-M. Yang, J. Wu, J. Lou, M. Liu, and N. X. Sun, "Low-loss magnetically tunable bandpass filters with YIG films," *IEEE Transactions on Magnetics*, vol. 49, no. 9, pp. 5063–5068, 2013.

[70] J. Wu, X. Yang, S. Beguhn, J. Lou, and N. X. Sun, "Nonreciprocal tunable low-loss bandpass filters with ultra-wideband isolation based on magnetostatic surface wave," *IEEE Transactions on Microwave Theory and Techniques*, vol. 60, no. 12, pp. 3959–3968, 2012.

[71] Z. Zhang, J. Liu, H. Ding, Z. Feng, and Y. Nie, "Microwave bandpass filters tuned by the magnetization of ferrite substrates," *IEEE Magnetics Letters*, vol. 8, pp. 1–4, 2017.

[72] M. Almalkawi, L. Zhu, and V. Devabhaktuni, "Magnetically tunable substrate integrated waveguide bandpass filters employing ferrites," in *2011 International Conference on Infrared, Millimeter, and Terahertz Waves*, 2011, pp. 1–2.

[73] S. Adhikari, S. Hemour, A. Ghiotto, and K. Wu, "Magnetically tunable ferrite-loaded half-mode substrate integrated waveguide," *IEEE Microwave and Wireless Components Letters*, vol. 25, no. 3, pp. 172–174, 2015.

[74] S. Kagita, A. Basu, and S. K. Koul, "Electrically tunable ferrite bandpass filter in X-band with wide tunability," *IEEE Transactions on Magnetics*, vol. 55, no. 7, pp. 1–4, 2019.

[75] Y. Zhu, G. Qiu, K. H. Chi, B. B. Wang, and C. S. Tsai, "A tunable X-band bandpass filter module using yig/ggg layer on rt/duroid substrate," *IEEE Transactions on Magnetics*, vol. 45, no. 10, pp. 4195–4198, 2009.

[76] X. Yang, J. Wu, S. Beguhn, T. Nan, Y. Gao, Z. Zhou, and N. X. Sun, "Tunable bandpass filter using partially magnetized ferrites with high power handling capability," *IEEE Microwave and Wireless Components Letters*, vol. 23, no. 4, pp. 184–186, 2013.

[77] E. Arabi, F. A. Ghaffar, and A. Shamim, "Tunable bandpass filter based on partially magnetized ferrite LTCC with embedded windings for sop applications," *IEEE Microwave and Wireless Components Letters*, vol. 25, no. 1, pp. 16–18, 2015.

[78] B. Belayev, K. Lemberg, and A. Serzhantov, "An X-band magnetically tunable bandpass filter based on novel waveguide cavity resonator," in *2016 Asia-Pacific Microwave Conference (APMC)*, 2016, pp. 1–4.

[79] Acar, T. K. Johansen, and V. Zhurbenko, "A high-power low-loss continuously tunable bandpass filter with transversely biased ferrite-loaded coaxial resonators," *IEEE Transactions on Microwave Theory and Techniques*, vol. 63, no. 10, pp. 3425–3432, 2015.

[80] J. Krupka, A. Abramowicz, and K. Derzakowski, "Magnetically tunable filters for cellular communication terminals," *IEEE Transactions on Microwave Theory and Techniques*, vol. 54, no. 6, pp. 2329–2335, 2006.

[81] M. Zolfagharloo Koohi and A. Mortazawi, "Reconfigurable radios employing ferroelectrics: Recent progress on reconfigurable RF acoustic devices based on thin-film ferroelectric barium strontium titanate," *IEEE Microwave Magazine*, vol. 21, no. 5, pp. 120–135, 2020.

[82] O. Vendik, E. Hollmann, A. Kozyrev, and A. Prudan, "Ferroelectric tuning of planar and bulk microwave devices," *Journal of Superconductivity*, vol. 12, pp. 325–338, 04 1999.

[83] S. Gevorgian, E. Carlsson, S. Rudner, U. Helmersson, E. Kollberg, E. Wikborg, and O. Vendik, "HTS/ferroelectric devices for microwave applications," *IEEE Transactions on Applied Superconductivity*, vol. 7, no. 2, pp. 2458–2461, 1997.

[84] A. Deleniv, A. Eriksson, and S. Gevorgian, "Design of narrow-band tunable band-pass filters based on dual mode $SrTiO_3$ disc resonators," in *2002 IEEE MTT-S International Microwave Symposium Digest (Cat. No.02CH37278)*, vol. 2, 2002, pp. 1197–1200 vol.2.

[85] ——, "Four-pole tunable band-pass filters based on two dual mode $SrTiO_3$ disc resonators," in *2002 32nd European Microwave Conference*, 2002, pp. 1–3.

[86] A. Eriksson, A. Deleniv, and S. Gevorgian, "Two-pole tunable bandpass filter based on YBCO plated single crystal KTO disk resonators," *IEEE Transactions on Applied Superconductivity*, vol. 14, no. 1, pp. 1–6, 2004.

[87] E. Economou, J. Lovejoy, I. Harward, J. Nobles, P. Kula, J. Herman, A. Glushchenko, and Z. Celinski, "Electrically tunable open-stub bandpass filters based on nematic liquid crystals," *Physical Review Applied*, vol. 8, 12 2017.

[88] D. Jiang, X. Li, Z. Fu, G. Wang, Z. Zheng, T. Zhang, and W.-Q. Wang, "Millimeter-wave broadband tunable band-pass filter based on liquid crystal materials," *IEEE Access*, vol. 8, pp. 1339–1346, 2020.

[89] A. E. Prasetiadi, "Tunable substrate integrated waveguide bandpass filter and amplitude tuner based on microwave liquid crystal technology," Ph.D. dissertation, Technische Universität, Darmstadt, June 2017.

[90] T. Franke, R. Jakoby, M. Nickel, O. Karabey, W. Hu, C. Weickhmann, M. Jost, and A. Prasetiadi, "Continuously tunable substrate integrated waveguide bandpass filter in liquid crystal technology with magnetic biasing," *Electronics Letters*, vol. 51, 09 2015.

[91] T. Franke, A. Gaebler, A. E. Prasetiadi, and R. Jakoby, "Tunable Ka-band waveguide resonators and a small band band-pass filter based on liquid crystals," in *2014 44th European Microwave Conference*, 2014, pp. 339–342.

[92] E. Polat, R. Reese, M. Jost, C. Schuster, M. Nickel, R. Jakoby, and H. Maune, "Tunable liquid crystal filter in nonradiative dielectric waveguide technology at

60 GHz," *IEEE Microwave and Wireless Components Letters*, vol. 29, no. 1, pp. 44–46, 2019.

[93] K. Entesari and A. P. Saghati, "Fluidics in microwave components," *IEEE Microwave Magazine*, vol. 17, no. 6, pp. 50–75, 2016.

[94] R. C. Gough, A. M. Morishita, J. H. Dang, W. Hu, W. A. Shiroma, and A. T. Ohta, "Continuous electrowetting of non-toxic liquid metal for RF applications," *IEEE Access*, vol. 2, pp. 874–882, 2014.

[95] E. González-Carvajal and G. Mumcu, "Frequency and bandwidth tunable mm-wave hairpin bandpass filters using microfluidic reconfiguration with integrated actuation," *IEEE Transactions on Microwave Theory and Techniques*, vol. 68, no. 9, pp. 3756–3768, 2020.

[96] J.-H. Guo, S.-W. Wong, J.-Y. Lin, Y. Li, L. Zhang, L. Zhu, Z.-M. Xie, and Y. He, "A continuously tunable bandpass filter using distilled water based on multiple-mode resonator," *IEEE Microwave and Wireless Components Letters*, vol. 30, no. 5, pp. 477–480, 2020.

[97] T. Palomo and G. Mumcu, "Microfluidically reconfigurable microstrip line combline filters with wide frequency tuning capabilities," *IEEE Transactions on Microwave Theory and Techniques*, vol. 65, no. 10, pp. 3561–3568, 2017.

[98] D. L. Diedhiou, R. Sauleau, and A. V. Boriskin, "Microfluidically tunable microstrip filters," *IEEE Transactions on Microwave Theory and Techniques*, vol. 63, no. 7, pp. 2245–2252, 2015.

[99] A. Pourghorban Saghati, J. S. Batra, J. Kameoka, and K. Entesari, "A miniaturized microfluidically reconfigurable coplanar waveguide bandpass filter with maximum power handling of 10 watts," *IEEE Transactions on Microwave Theory and Techniques*, vol. 63, no. 8, pp. 2515–2525, 2015.

[100] S. N. McClung, S. Saeedi, and H. H. Sigmarsson, "Band-reconfigurable filter with liquid metal actuation," *IEEE Transactions on Microwave Theory and Techniques*, vol. 66, no. 6, pp. 3073–3080, 2018.

[101] D. Psychogiou and K. Sadasivan, "Tunable coaxial cavity resonator-based filters using actuated liquid metal posts," *IEEE Microwave and Wireless Components Letters*, vol. 29, no. 12, pp. 763–766, 2019.

[102] R.-S. Chen, S.-W. Wong, J.-Y. Lin, Y. Yang, Y. Li, L. Zhang, Y. He, and L. Zhu, "Reconfigurable cavity bandpass filters using fluid dielectric," *IEEE Transactions on Industrial Electronics*, vol. 68, no. 9, pp. 8603–8614, 2021.

[103] M. Yu, D. Smith, and M. Ismail, "Half-wave dielectric rod resonator filter," in *2004 IEEE MTT-S International Microwave Symposium Digest (IEEE Cat. No.04CH37535)*, vol. 2, 2004, pp. 619–622 Vol.2.

[104] M. Makimoto and S. Yamashita, "Compact bandpass filters using stepped impedance resonators," *Proceedings of the IEEE*, vol. 67, no. 1, pp. 16–19, 1979.

[105] H. Wang and Q.-X. Chu, "An inline coaxial quasi-elliptic filter with controllable mixed electric and magnetic coupling," *IEEE Transactions on Microwave Theory and Techniques*, vol. 57, no. 3, pp. 667–673, 2009.

[106] H.-H. Chen, R.-C. Hsieh, Y.-T. Shih, Y.-H. Chou, and M.-H. Chen, "Coaxial combline filters using the stepped-impedance resonators," in *2010 Asia-Pacific Microwave Conference*, 2010, pp. 1724–1727.

[107] F. Gentili, L. Pelliccia, R. Sorrentino, and G. Bianchi, "High Q-factor compact filters with wide-band spurious rejection," in *2012 42nd European Microwave Conference*, 2012, pp. 160–163.

[108] X. Wang, G. Jang, B. Lee, and N. Park, "Compact quad-mode bandpass filter using modified coaxial cavity resonator with improved Q-factor," *IEEE Transactions on Microwave Theory and Techniques*, vol. 63, no. 3, pp. 965–975, 2015.

[109] C. Tomassoni, G. Venanzoni, M. Dionigi, and R. Sorrentino, "Compact quasi-elliptic filters with mushroom-shaped resonators manufactured with 3-D printer," *IEEE Transactions on Microwave Theory and Techniques*, vol. 66, no. 8, pp. 3579–3588, 2018.

[110] E. Musonda and I. C. Hunter, "Microwave bandpass filters using re-entrant resonators," *IEEE Transactions on Microwave Theory and Techniques*, vol. 63, no. 3, pp. 954–964, 2015.

[111] E. Doumanis, S. Bulja, and D. Kozlov, "Compact coaxial filters for BTS applications," *IEEE Microwave and Wireless Components Letters*, vol. 27, no. 12, pp. 1077–1079, 2017.

[112] J. Benedicto, E. Rius, J.-F. Favennec, D. Pacaud, L. Carpentier, and J. Puech, "A compact L-band bandpass filter based on SIR coaxial resonators with high multipactor threshold," *International Journal of Microwave and Wireless Technologies*, vol. 14, no. 3, p. 270–281, 2022.

[113] M. Salek, X. Shang, and M. J. Lancaster, "Compact S-band coaxial cavity resonator filter fabricated by 3-d printing," *IEEE Microwave and Wireless Components Letters*, vol. 29, no. 6, pp. 382–384, 2019.

[114] E. López-Oliver, C. Tomassoni, L. Silvestri, M. Bozzi, L. Perregrini, S. Marconi, G. Alaimo, and F. Auricchio, "3-D-printed compact bandpass filters based on conical posts," *IEEE Transactions on Microwave Theory and Techniques*, vol. 69, no. 1, pp. 616–628, 2021.

[115] K. Zhao and D. Psychogiou, "A monolithic vertical integration concept for compact coaxial-resonator-based bandpass filters using additive manufacturing," *IEEE Microwave and Wireless Components Letters*, vol. 31, no. 6, pp. 689–692, 2021.

[116] M. Höft, S. Burger, T. Magath, and O. Bartz, "Compact combline filter with improved cross coupling assembly and temperature compensation," in *2006 Asia-Pacific Microwave Conference*, 2006, pp. 781–784.

[117] M. Höft, "Tunable capacitive coupling for cavity resonator filters," in *2009 German Microwave Conference*, 2009, pp. 1–4.

[118] Y. Wang and M. Yu, "True inline cross-coupled coaxial cavity filters," *IEEE Transactions on Microwave Theory and Techniques*, vol. 57, no. 12, pp. 2958–2965, 2009.

[119] M. Höft and F. Yousif, "Orthogonal coaxial cavity filters with distributed cross-coupling," *IEEE Microwave and Wireless Components Letters*, vol. 21, no. 10, pp. 519–521, 2011.

[120] G. Macchiarella, S. Bastioli, and R. V. Snyder, "Design of in-line filters with transmission zeros using strongly coupled resonators pairs," *IEEE Transactions on Microwave Theory and Techniques*, vol. 66, no. 8, pp. 3836–3846, 2018.

[121] S. Bastioli, R. V. Snyder, and G. Macchiarella, "Design of in-line filters with strongly coupled resonator triplet," *IEEE Transactions on Microwave Theory and Techniques*, vol. 66, no. 12, pp. 5585–5592, 2018.

[122] C. Wang and K. A. Zaki, "Dielectric resonators and filters," *IEEE Microwave Magazine*, vol. 8, no. 5, pp. 115–127, 2007.

[123] M. Makimoto and S. Yamashita, *Microwave Resonators and Filters for Wireless Communication: Theory, Design and Application*, ser. Springer Series in Advanced Microelectronics. Springer Berlin Heidelberg, 2013. [Online]. Available: https://books.google.de/books?id=h-rnCAAAQBAJ

[124] A. Anand and X. Liu, "Reconfigurable planar capacitive coupling in substrate-integrated coaxial-cavity filters," *IEEE Transactions on Microwave Theory and Techniques*, vol. 64, no. 8, pp. 2548–2560, 2016.

[125] M. Makimoto and S. Yamashita, "Bandpass filters using parallel coupled stripline stepped impedance resonators," *IEEE Transactions on Microwave Theory and Techniques*, vol. 28, no. 12, pp. 1413–1417, 1980.

[126] Z. Yang, D. Psychogiou, and D. Peroulis, "Design and optimization of tunable silicon-integrated evanescent-mode bandpass filters," *IEEE Transactions on Microwave Theory and Techniques*, vol. 66, no. 4, pp. 1790–1803, 2018.

[127] D. Sh-Asanjan and R. R. Mansour, "A novel coaxial resonator for high power applications," in *2014 44th European Microwave Conference*, 2014, pp. 295–298.

[128] C. Rong, Y. Xu, and Y. Zhang, "Dielectric-loaded miniaturized cavity bandpass filter with improved power capacity," *Electronics*, vol. 11, no. 9, p. 1441, Apr 2022. [Online]. Available: http://dx.doi.org/10.3390/electronics11091441

[129] R. J. Cameron, C. M. Kudsia, and R. R. Mansour, *Microwave Filters for Communication Systems: Fundamentals Design and Applications*. Hoboken, NJ, USA : Wiley, 2018.

[130] Y. Kobayashi, K. Kojima, and S. Yoshida, "Bandpass filters using electrically-coupled TM_{010} dielectric rod resonators," *Electronics and Communications in Japan (Part I: Communications)*, vol. 66, no. 13, 1983.

[131] Y. Marchives, N. Delhote, S. Verdeyme, and P. M. Iglesias, "Wide-band dielectric filter at C-band manufactured by stereolithography," in *2014 44th European Microwave Conference*, 2014, pp. 187–190.

[132] A. Widaa, F. Cacciamani, L. Pelliccia, C. Tomassoni, V. T. di Crestvolant, and M. Höft, "Compact ultra-wideband bandpass filter using additively manufactured TM-mode dielectric resonators," in *2022 52nd European Microwave Conference (EuMC)*, 2022, pp. 115–118.

[133] MARKETSANDMARKETS, "RF tunable filter market," Accessed: 2023-03-20. [Online]. Available: https://www.marketsandmarkets.com/Market-Reports/rf-tunable-filter-market-69180206.html

[134] A. Widaa, "Comparison of tuning means," Accessed: 2023-03-20. [Online]. Available: https://ec.europa.eu/research/participants/documents/downloadPublic?documentIds=080166e5d76532fe&appId=PPGMS

[135] A. Widaa, C. J. You, and M. Awad, "High selectivity low-loss tunable bandpass filter with transmission zeros control using staircase resonators," in *2021 IEEE 21st Annual Wireless and Microwave Technology Conference (WAMICON)*, 2021, pp. 1–4.

[136] Y. Xie, F.-C. Chen, and Q.-X. Chu, "Tunable cavity filter and diplexer using in-line dual-post resonators," *IEEE Transactions on Microwave Theory and Techniques*, vol. 70, no. 6, pp. 3188–3199, 2022.

[137] G. B. and R. R. Mansour, "A tunable quarter-wavelength coaxial filter with constant absolute bandwidth using a single tuning element," *IEEE Microwave and Wireless Components Letters*, vol. 31, no. 6, pp. 658–661, 2021.

[138] N. S. P. C. Ltd., "Variable radio frequency band filter," Patent, Nov., 2010.

[139] A. Widaa and M. Höft, "Microfluidic-based ultra-wide tuning technique for TM_{010} mode dielectric resonators and filters," in *2021 IEEE MTT-S International Microwave Filter Workshop (IMFW)*, 2021, pp. 343–346.

[140] ——, "A novel re-entrant cap tuning technique for TM-mode dielectric resonators and filters," in *2021 IEEE MTT-S International Microwave Filter Workshop (IMFW)*, 2021, pp. 335–338.

[141] A. Widaa, C. Bartlett, and M. Höft, "Miniaturized all-reconfigurable dual-mode dielectric filter using piezomotors for future satellite communications," in *2021 51st European Microwave Conference (EuMC)*, 2022, pp. 107–110.

[142] A. Widaa and M. Höft, "Miniaturized dual-band TM-mode dielectric filter and its reconfiguration capabilities," in *2022 IEEE/MTT-S International Microwave Symposium - IMS 2022*, 2022, pp. 344–347.

[143] A. Widaa, C. Bartlett, and M. Höft, "Tunable resonator arrangement, tunable frequency filter and method of tuning thereof," Patent, Jun., 2022.

[144] PiezoMotor, Accessed: 2023-03-20. [Online]. Available: https://piezomotor.com

[145] K. et al., "Variable high frequency filter device and assembly," Patent, Apr., 2017.

[146] G. Macchiarella, L. Accatino, and A. Malagoli, "Design of Ka-band tunable filters in rectangular waveguide with constant bandwidth," in *2020 IEEE Asia-Pacific Microwave Conference (APMC)*, 2020, pp. 622–624.

[147] R. R. Mansour, "High-Q tunable dielectric resonator filters," *IEEE Microwave Magazine*, vol. 10, no. 6, pp. 84–98, 2009.

[148] E. Doumanis, G. Goussetis, J. Vuorio, K. Hautio, O. Amper, E. Kuusmik, and J. Pallonen, "Tunable filters for agile 5G new radio base transceiver stations [application notes]," *IEEE Microwave Magazine*, vol. 22, no. 11, pp. 26–37, 2021.

[149] M. Sanchez-Renedo, R. Gomez-Garcia, J. Alonso, and C. Briso-Rodriguez, "Tunable combline filter with continuous control of center frequency and bandwidth," *IEEE Transactions on Microwave Theory and Techniques*, vol. 53, no. 1, pp. 191–199, 2005.

[150] S. Moon, H. H. Sigmarsson, H. Joshi, and W. J. Chappell, "Substrate integrated evanescent-mode cavity filter with a 3.5 to 1 tuning ratio," *IEEE Microwave and Wireless Components Letters*, vol. 20, no. 8, pp. 450–452, 2010.

[151] A. Anand, J. Small, D. Peroulis, and X. Liu, "Theory and design of octave tunable filters with lumped tuning elements," *IEEE Transactions on Microwave Theory and Techniques*, vol. 61, no. 12, pp. 4353–4364, 2013.

[152] J.-X. Chen, Y. Ma, J. Cai, L.-H. Zhou, Z.-H. Bao, and W. Che, "Novel frequency-agile bandpass filter with wide tuning range and spurious suppression," *IEEE Transactions on Industrial Electronics*, vol. 62, no. 10, pp. 6428–6435, 2015.

[153] J. Xu and Y. Zhu, "Tunable bandpass filter using a switched tunable diplexer technique," *IEEE Transactions on Industrial Electronics*, vol. 64, no. 4, pp. 3118–3126, 2017.

[154] D. Lu, X. Tang, N. S. Barker, and Y. Feng, "Single-band and switchable dual-/single-band tunable BPFs with predefined tuning range, bandwidth, and selectivity," *IEEE Transactions on Microwave Theory and Techniques*, vol. 66, no. 3, pp. 1215–1227, 2018.

[155] L. Gao and G. M. Rebeiz, "A 0.97–1.53-GHz tunable four-pole bandpass filter with four transmission zeroes," *IEEE Microwave and Wireless Components Letters*, vol. 29, no. 3, pp. 195–197, 2019.

[156] M. Abdelfattah, R. Zhang, and D. Peroulis, "High-selectivity tunable filters with dual-mode SIW resonators in an L-shaped coupling scheme," *IEEE Transactions on Microwave Theory and Techniques*, vol. 67, no. 12, pp. 5016–5028, 2019.

[157] M. Abdelfattah and D. Peroulis, "High-Q tunable evanescent-mode cavity SIW resonators and filters with contactless tuners," *IEEE Transactions on Microwave Theory and Techniques*, vol. 67, no. 9, pp. 3661–3672, 2019.

[158] Z. Yang, R. Zhang, and D. Peroulis, "Design and optimization of bidirectional tunable MEMS all-silicon evanescent-mode cavity filter," *IEEE Transactions on Microwave Theory and Techniques*, vol. 68, no. 6, pp. 2398–2408, 2020.

[159] M. D. Sinanis, P. Adhikari, T. R. Jones, M. Abdelfattah, and D. Peroulis, "High-Q high power tunable filters manufactured with injection molding technology," *IEEE Access*, vol. 10, pp. 19 643–19 653, 2022.

[160] S.-J. Park and G. M. Rebeiz, "Low-loss two-pole tunable filters with three different predefined bandwidth characteristics," *IEEE Transactions on Microwave Theory and Techniques*, vol. 56, no. 5, pp. 1137–1148, 2008.

[161] H. Joshi, H. H. Sigmarsson, S. Moon, D. Peroulis, and W. J. Chappell, "High-Q fully reconfigurable tunable bandpass filters," *IEEE Transactions on Microwave Theory and Techniques*, vol. 57, no. 12, pp. 3525–3533, 2009.

[162] H. Guo, J. Ni, and J. Hong, "Varactor-tuned dual-mode bandpass filter with nonuniform Q distribution," *IEEE Microwave and Wireless Components Letters*, vol. 28, no. 11, pp. 1002–1004, 2018.

[163] A. C. Guyette, "Intrinsically switched varactor-tuned filters and filter banks," *IEEE Transactions on Microwave Theory and Techniques*, vol. 60, no. 4, pp. 1044–1056, 2012.

[164] C. Ge and X.-W. Zhu, "Highly-selective tunable bandpass filter with two-path mixed coupling," *IEEE Microwave and Wireless Components Letters*, vol. 24, no. 7, pp. 451–453, 2014.

[165] Z. Zhao, J. Chen, L. Yang, and K. Chen, "Three-pole tunable filters with constant bandwidth using mixed combline and split-ring resonators," *IEEE Microwave and Wireless Components Letters*, vol. 24, no. 10, pp. 671–673, 2014.

[166] N. Kumar and Y. K. Singh, "Compact constant bandwidth tunable wideband BPF with second harmonic suppression," *IEEE Microwave and Wireless Components Letters*, vol. 26, no. 11, pp. 870–872, 2016.

[167] F. Lin and M. Rais-Zadeh, "Continuously tunable 0.55–1.9-GHz bandpass filter with a constant bandwidth using switchable varactor-tuned resonators," *IEEE Transactions on Microwave Theory and Techniques*, vol. 65, no. 3, pp. 792–803, 2017.

[168] D. Tian, Q. Feng, and Q. Xiang, "Synthesis applied 4th-order constant absolute bandwidth frequency-agile bandpass filter with cross-coupling," *IEEE Access*, vol. 6, pp. 72 287–72 294, 2018.

[169] D. Lu, M. Yu, N. S. Barker, Z. Li, W. Li, and X. Tang, "Advanced synthesis of wide-tuning-range frequency-adaptive bandpass filter with constant absolute bandwidth," *IEEE Transactions on Microwave Theory and Techniques*, vol. 67, no. 11, pp. 4362–4375, 2019.

[170] P. Wang, L. Li, and Shaowei, "Design of a tunable S-band narrow-band coaxial cavity filter," in *2012 International Conference on Microwave and Millimeter Wave Technology (ICMMT)*, vol. 1, 2012, pp. 1–4.

[171] C. Kwak, M. Uhm, and I. Yom, "Feasibility study on combline filter for tunable filters," in *2013 Asia-Pacific Microwave Conference Proceedings (APMC)*, 2013, pp. 927–929.

[172] A. Sharma, S. Cogollos, V. E. Boria, and M. Guglielmi, "Analysis and design of re-configurable combline filters using dielectric tuners," in *2021 51st European Microwave Conference (EuMC)*, 2022, pp. 122–125.

[173] M. M. Fahmi, D. S. Ghadri, and R. Mansour, "A tunable filter with extended tuning range based on switched dual resonance cavities," in *2022 IEEE/MTT-S International Microwave Symposium - IMS 2022*, 2022, pp. 176–178.

[174] A. Widaa, C. Bartlett, and M. Höft, "Inset resonators and their applications in fixed/reconfigurable microwave filters," in *2022 IEEE/MTT-S International Microwave Symposium - IMS 2022*, 2022, pp. 172–175.

[175] ——, "Tunable coaxial bandpass filters based on inset resonators," *IEEE Transactions on Microwave Theory and Techniques*, vol. 71, no. 1, pp. 285–295, 2023.

[176] K. Pance and G. Rochford, "Multiple band and multiple frequency dielectric resonators tunable filters for base stations," in *2008 38th European Microwave Conference*, 2008, pp. 488–491.

[177] R. V. Snyder, A. Mortazawi, I. Hunter, S. Bastioli, G. Macchiarella, and K. Wu, "Present and future trends in filters and multiplexers," *IEEE Transactions on Microwave Theory and Techniques*, vol. 63, no. 10, pp. 3324–3360, 2015.

[178] A. Widaa, C. J. You, and M. Awad, "Compact single/dual-band bandpass filters with independently controllable passbands using staircase resonators," in *2020 International Conference on Computer, Control, Electrical, and Electronics Engineering (ICCCEEE)*, 2021, pp. 1–4.

[179] Y. Zhu and Y. Dong, "A compact dual-band quasi-elliptic filter based on hybrid SIW and microstrip technologies," *IEEE Transactions on Circuits and Systems II: Express Briefs*, vol. 69, no. 3, pp. 719–723, 2022.

[180] S. Amari and M. Bekheit, "A new class of dual-mode dual-band waveguide filters," *IEEE Transactions on Microwave Theory and Techniques*, vol. 56, no. 8, pp. 1938–1944, 2008.

[181] L. Zhu, R. R. Mansour, and M. Yu, "Quasi-elliptic waveguide dual-band bandpass filters," *IEEE Transactions on Microwave Theory and Techniques*, vol. 67, no. 12, pp. 5029–5037, 2019.

[182] ——, "Compact waveguide dual-band filters and diplexers," *IEEE Transactions on Microwave Theory and Techniques*, vol. 65, no. 5, pp. 1525–1533, 2017.

[183] J. A. Ruiz-Cruz, M. M. Fahmi, and R. R. Mansour, "Triple-conductor combline resonators for dual-band filters with enhanced guard-band selectivity," *IEEE Transactions on Microwave Theory and Techniques*, vol. 60, no. 12, pp. 3969–3979, 2012.

[184] E. Doumanis, L. Guan, G. Goussetis, and D. Ferling, "Dual-band bandpass double ground plane coaxial resonators and filters," *IEEE Transactions on Microwave Theory and Techniques*, vol. 66, no. 8, pp. 3828–3835, 2018.

[185] Y. Xie and F.-C. Chen, "Dual-band and wide stopband coaxial filters using open-circuited-stub-loaded resonators," *IEEE Transactions on Circuits and Systems II: Express Briefs*, vol. 68, no. 6, pp. 1872–1876, 2021.

[186] R. Zhang and R. R. Mansour, "Dual-band dielectric-resonator filters," *IEEE Transactions on Microwave Theory and Techniques*, vol. 57, no. 7, pp. 1760–1766, 2009.

[187] V. Nocella, L. Pelliccia, C. Tomassoni, and R. Sorrentino, "Miniaturized dual-band waveguide filter using TM dielectric-loaded dual-mode cavities," *IEEE Microwave and Wireless Components Letters*, vol. 26, no. 5, pp. 310–312, 2016.

[188] J.-X. Chen, J. Li, and J. Shi, "Miniaturized dual-band differential filter using dual-mode dielectric resonator," *IEEE Microwave and Wireless Components Letters*, vol. 28, no. 8, pp. 657–659, 2018.

[189] M. Höft, "Bandpass filter using TM-mode dielectric rod resonators with novel input coupling," in *2009 IEEE MTT-S International Microwave Symposium Digest*, 2009, pp. 1601–1604.

[190] S. Amari and U. Rosenberg, "A universal building block for advanced modular design of microwave filters," *IEEE Microwave and Wireless Components Letters*, vol. 13, no. 12, pp. 541–543, 2003.

[191] S. Amari and M. Bekheit, "New dual-mode dielectric resonator filters," *IEEE Microwave and Wireless Components Letters*, vol. 15, no. 3, pp. 162–164, 2005.

[192] H. Hu and K.-L. Wu, "A TM_{11} dual-mode dielectric resonator filter with planar coupling configuration," *IEEE Transactions on Microwave Theory and Techniques*, vol. 61, no. 1, pp. 131–138, 2013.

[193] S. Bastioli and R. V. Snyder, "Nonresonating modes do it better!: Exploiting additional modes in conjunction with operating modes to design better quality filters," *IEEE Microwave Magazine*, vol. 22, no. 1, pp. 20–45, 2021.

[194] L. Zhu, "High-Q multi-band filters," Ph.D. dissertation, University of Waterloo, Waterloo, 2019.

[195] J. Thomas, "Cross-coupling in coaxial cavity filters - a tutorial overview," *IEEE Transactions on Microwave Theory and Techniques*, vol. 51, no. 4, pp. 1368–1376, 2003.

[196] L. Zhu, R. R. Mansour, and M. Yu, "Triple-band cavity bandpass filters," *IEEE Transactions on Microwave Theory and Techniques*, vol. 66, no. 9, pp. 4057–4069, 2018.

[197] C. Tomassoni, S. Bastioli, and R. Sorrentino, "Generalized TM dual-mode cavity filters," *IEEE Transactions on Microwave Theory and Techniques*, vol. 59, no. 12, pp. 3338–3346, 2011.

[198] DIELECTRIC RESONATORS, Accessed: 2023-03-20. [Online]. Available: https://exxelia.com/uploads/PDF/e7000-v1.pdf

[199] C. Bartlett and M. Höft, "Fully inline and symmetric dual-mode dual-band bandpass filters for millimetre-wave applications," in *2021 IEEE MTT-S International Microwave Filter Workshop (IMFW)*, 2021, pp. 323–325.

[200] R. Gómez-García and A. C. Guyette, "Reconfigurable multi-band microwave filters," *IEEE Transactions on Microwave Theory and Techniques*, vol. 63, no. 4, pp. 1294–1307, 2015.

[201] M. Memarian and R. Mansour, "Dual-band half-cut dielectric resonator filters," in *2009 European Microwave Conference (EuMC)*, 2009, pp. 555–558.

[202] P. Boe, D. Miek, F. Kamrath, and M. Höft, "Dual-band filter composed of dielectric and waveguide resonators with in-band transmission zeros," in *2021 IEEE MTT-S International Microwave Filter Workshop (IMFW)*, 2021, pp. 73–75.

[203] A. Widaa and M. Höft, "Miniaturized dual-band dual-mode TM-mode dielectric filter in planar configuration," *IEEE Journal of Microwaves*, vol. 2, no. 2, pp. 326–336, 2022.

[204] K. Shamsaifar, T. Rodriguez, and J. Haas, "High-power combline diplexer for space," *IEEE Transactions on Microwave Theory and Techniques*, vol. 61, no. 5, pp. 1850–1860, 2013.

[205] Y. Xie, F.-C. Chen, Q.-X. Chu, and Q. Xue, "Dual-band coaxial filter and diplexer using stub-loaded resonators," *IEEE Transactions on Microwave Theory and Techniques*, vol. 68, no. 7, pp. 2691–2700, 2020.

[206] J.-X. Xu, M. Huang, S.-L. Song, and H.-Y. Li, "Compact multichannel filters and multiplexers based on dual-coaxial resonators," *IEEE Transactions on Circuits and Systems II: Express Briefs*, vol. 69, no. 12, pp. 4664–4668, 2022.

[207] S.-W. Wong, Z.-C. Zhang, S.-F. Feng, F.-C. Chen, L. Zhu, and Q.-X. Chu, "Triple-mode dielectric resonator diplexer for base-station applications," *IEEE Transactions on Microwave Theory and Techniques*, vol. 63, no. 12, pp. 3947–3953, 2015.

[208] L. Xu, W. Yu, and J.-X. Chen, "Unbalanced-/balanced-to-unbalanced diplexer based on dual-mode dielectric resonator," *IEEE Access*, vol. 9, pp. 53 326–53 332, 2021.

[209] D.-S. Wu, Y. Li, Q. Xue, W. Qin, and B.-J. Hu, "Balanced and unbalanced duplexers using common oval dielectric resonators," *IEEE Transactions on Circuits and Systems I: Regular Papers*, vol. 68, no. 8, pp. 3211–3221, 2021.

[210] L. Pelliccia, F. Cacciamani, A. Cazzorla, D. Tiradossi, P. Vallerotonda, R. Sorrentino, W. Steffè, F. Vitulli, E. Picchione, J. Galdeano, and P. Martìn-Igleasias,

"Compact on-board L-band dielectric-loaded diplexer for high-power applications," in *2019 49th European Microwave Conference (EuMC)*, 2019, pp. 61–64.

[211] P. Vallerotonda, F. Cacciamani, L. Pelliccia, A. Cazzorla, D. Tiradossi, W. Steffè, F. Vitulli, E. Picchione, J. Galdeano, P. Martìn-Iglesias, and et al., "Dielectric-loaded L-band filters for high-power space applications," *International Journal of Microwave and Wireless Technologies*, vol. 14, no. 3, p. 282–292, 2022.

[212] M. Höft and T. Magath, "Compact base-station filters using TM-mode dielectric resonators," 01 2006.

[213] L. Pelliccia, F. Cacciamani, F. Vitulli, W. Steffè, F. Diaferia, E. Picchione, P. M. Iglesias, and A. Jones, "On-board miniaturized L-band input filter based on TM-mode dielectric resonator for MSS applications," in *2017 47th European Microwave Conference (EuMC)*, 2017, pp. 981–984.

[214] L. Pelliccia, F. Cacciamani, C. Tomassoni, and R. Sorrentino, "Ultra-compact high-performance filters based on TM dual-mode dielectric-loaded cavities," *International Journal of Microwave and Wireless Technologies*, vol. 6, no. 2, p. 151–159, 2014.

[215] U. Rosenberg, R. Beyer, P. Krauß, T. Sieverding, A. Papanastasiou, M. Pueyo-Tolosa, P. M. Iglesias, and C. Ernst, "Reconfigurable doublet dual-mode cavity filter designs providing remote controlled center frequency and bandwidth reallocation," in *2016 46th European Microwave Conference (EuMC)*, 2016, pp. 532–535.

[216] L. Pelliccia, F. Cacciamani, P. Vallerotonda, C. Tomassoni, and R. Sorrentino, "Miniaturizating high-performance bandpass filters for satellite applications," in *2017 IEEE MTT-S International Microwave Workshop Series on Advanced Materials and Processes for RF and THz Applications (IMWS-AMP)*, 2017, pp. 1–3.

[217] U. Rosenberg and S. Amari, "Novel design possibilities for dual-mode filters without intracavity couplings," *IEEE Microwave and Wireless Components Letters*, vol. 12, no. 8, pp. 296–298, 2002.

[218] S. Bastioli, C. Tomassoni, and R. Sorrentino, "A new class of waveguide dual-mode filters using TM and nonresonating modes," *IEEE Transactions on Microwave Theory and Techniques*, vol. 58, no. 12, pp. 3909–3917, 2010.

[219] R. R. Mansour, "Rod-switched tunable filter," Patent, May, 2018.

[220] Y. Kobayashi and S. Yoshida, "Bandpass filters using TM_{010} dielectric rod resonators," in *1978 IEEE-MTT-S International Microwave Symposium Digest*, 1978, pp. 233–235.

[221] A. H. Pham, S. Saeedi, and H. H. Sigmarsson, "Continuously-tunable substrate integrated waveguide bandpass filter actuated by liquid metal," in *2019 IEEE MTT-S International Microwave Symposium (IMS)*, 2019, pp. 21–23.

[222] N. Vahabisani, S. Khan, and M. Daneshmand, "Microfluidically reconfigurable rectangular waveguide filter using liquid metal posts," *IEEE Microwave and Wireless Components Letters*, vol. 26, no. 10, pp. 801–803, 2016.

[223] A. Widaa and M. Höft, "Tunable resonator, tunable frequency filter and method of tuning thereof," Patent, Jun., 2022.

[224] X. Huang, Q. Feng, and Q. Xiang, "Bandpass filter with tunable bandwidth using quadruple-mode stub-loaded resonator," *IEEE Microwave and Wireless Components Letters*, vol. 22, no. 4, pp. 176–178, 2012.

[225] J. Ni, J. Hong, and P. M. Iglesias, "Compact bandwidth tunable IF filters for reconfigurable converters," *International Journal of Microwave and Wireless Technologies*, vol. 14, no. 3, p. 313–324, 2022.

[226] U. Rosenberg, R. Beyer, P. Krauß, T. Sieverding, A. Papanastasiou, M. Pueyo-Tolosa, P. M. Iglesias, and C. Ernst, "Novel remote controlled dual mode filter providing flexible re-allocation of center frequency and bandwidth," in *2016 IEEE MTT-S International Microwave Symposium (IMS)*, 2016, pp. 1–3.

[227] B. Gowrish and R. R. Mansour, "A novel bandwidth reconfigurable waveguide filter for aerospace applications," *IEEE Microwave and Wireless Components Letters*, vol. 30, no. 6, pp. 577–580, 2020.

[228] A. I. Abunjaileh and I. C. Hunter, "Tunable bandpass and bandstop filters based on dual-band combline structures," *IEEE Transactions on Microwave Theory and Techniques*, vol. 58, no. 12, pp. 3710–3719, 2010.